A Microfluidic Approach to the Study of Cellular Responses to Oxidative Stress

Kapiraj Chandrabalan, BSc.

Thesis submitted for the Degree of
Doctor of Philosophy

The University of Hull and the University of York

Hull York Medical School

September 2015

Abstract

The purpose of this study was to develop a method for exposing biological and chemical components to defined levels of (extracellular) oxidative stress, and to study their effects using conventional methods. Photodynamic therapy (PDT)-mimicking extracellular oxidative stress reactions (OSR); microbatch OSR (MBOSR) and microfluidic flow OSR (MFOSR) were carried out using colon carcinoma COLO320 cell line. An instrument was built and used in all the photosensitisation OSR. Several microfluidic chip configurations were designed, fabricated, studied for flow properties and used in the surface treatment reactions. Different types of photosensitisers were successfully covalently immobilised onto surfaces of the microfluidic channels, and their presence was verified using spectroscopic, colorimetric and photo-oxidation reactions. To conduct the MFOSR; syringe-, pressure- and peristaltic-pumping systems were tested to optimise the flow system and cell recovery was improved.

Initially MFOSR with immobilised porphyrin were carried out. To determine the optimum OSR conditions, MBOSR were carried out having the photosensitiser, aluminium (III) phthalocyanine tetrasulfonate ($AlPcS_4$) in solution, and the best set of photosensitisation effect inducing conditions were used in conducting the MFOSR with photosensitiser in solution. The treated samples were analysed to determine the levels of LDH released into supernatants, percentages of cells recovered, cell viability, and the modes of cellular disintegrations induced. MFOSR with immobilised photosensitiser showed high variations with no statistically significant differences, whereas MFOSR with $AlPcS_4$ in solution showed significant induction of photosensitisation effects. It was identified from the MBOSR that the induction of photosensitisation effects significantly increased with the concentration of $AlPcS_4$ or the light dose.

The MBOSR and MFOSR with photosensitiser in solution were useful in the generation of extracellular oxidative stress environment. These types of reactions mainly induced cellular disintegration through necrosis relative to apoptosis. This system can possibly be adapted to study numerous diseases where oxidative stress is involved.

Contents

Abbreviations

ACTH	Adrenocorticotropic hormone
AFM	Atomic force microscopy
ALA	Aminolevulinic acid
AlClPc	Aluminium phthalocyanine chloride
$AlPcS_4.Cl$	Aluminium(III) phthalocyanine chloride tetrasulfonic acid
$AlPcS_4$	Aluminium(III) phthalocyanine tetrasulfonate
AlSPc	Aluminium chloro sulfonated phthalocyanine
APA	Anthracene dipropionic acid
AP-1	Activator protein-1
APDMES	(3-Aminopropyl)dimethylethoxysilane
APTES	3-Amino(propyl)triethoxysilane
Ar	Aromatic
ATMPn	9-Acetoxy-2,7,12,17-tetrakis-(β-methoxyethyl)-porphycene
α	Level of significance
Balb-3T3	Mouse embryonic fibroblast cell line
Bcl-2	B-cell lymphoma 2, an integral membrane protein
C_d	Channel Depth
CDAMs	Cell death-associated molecular patterns
CD^{4+} T	Cluster of differentiation 4 T-lymphocytes
CNS	Central nervous system
COC	Cyclic olefin copolymer
COLO320, COLO321	Colon carcinoma cell line
COX-2	Cyclooxygenase-2
CTLA4	Cytotoxic T-lymphocyte-associated protein 4
DAMPs	Damage associated molecular patterns
$DCFH_2$	Dichlorodihydrofluorescein
DCF	2,7-Dichlorodihydrofluorescein
DCs	Dendritic cells
df	Degrees of freedom
DioC6(3)	3,3'-dihexyloxacarbocyanine iodide
DM	Dichroic mirror
DMPO	5,5-Dimethyl-pyrroline N-oxide
DPBF	1,3-Diphenylisobenzofuran
δ	Chemical shift
EC-SOD	Extracellular - superoxide dismutase
EFAs	Essential fatty acids
EGF	Epidermal growth factor
E_L	Illuminance
EPR	Electron paramagnetic resonance
ER	Endoplasmic reticulum
E_R	Irradiance
ESR	Electron spin resonance
FAD	Flavin adenine dinucleotide
FAs	Fatty acids
FBS	Fetal Bovine Serum
FFA	Furfuryl alcohol
FITC	Fluorescein isothiocyanate
FRET	Fluorescence resonance energy transfer
FSC	Forward scatter
GFP-LactC2	Green fluorescent protein - Lactadherin C2 domain

GPCR	G-protein coupled receptor
GPx	Glutathione peroxidase
GSH	Glutathione
GSSH	Oxidised glutathione
HC	High control
HDL	High density lipid
HeLa	Henrietta Lacks (human cervical cancer cells)
HepG2	Liver hepatocellular carcinoma cells
HIF	Hypoxia inducible factor
HNE	4-Hydroxynonenal
^{1}H NMR	Proton nuclear magnetic resonance
HPAF	Human pancreatic adenocarcinoma (cell line)
HpD	Hematoporphyrin derivative
HSD	Honestly Significant Difference
HSP40	Heat shock protein 40 kiloDalton
H_2TPPS_4- $4Na^+$	Tetra-sodium 5,10,15,20-tettrakis(4-sulfonatophenyl)porphyrin
IC	Internal conversion
ICAM-1	Intracellular adhesion molecule-1
INF- γ	Interferon-*gamma*
ISC	Intersystem crossing
LC	Low control
LDH	Lactate dehydrogenase
LDL	Low density lipid
lm	Lumens
LOO$^\bullet$	Lipid peroxyl radicals
LOOH	Lipid hydroperoxides
5-LOX	5-Lipooxygenase
M-ALA	Methyl aminolevulinate
MB	Methylene blue
MBOSR	Microbatch oxidative stress reactions
MC540	Merocyanine 540
MD	Menadione
MDA	Malondialdehyde
MFOSR	Microfluidic flow oxidative stress reactions
MiaPaCa2	Human pancreatic carcinoma (cell line)
MMPs	Matrix metalloproteinases
MPO	Myeloperoxidase
m-THPC	*meta*-Tetrahydroxyphenylchlorin
m-$TPPS_4$	Tetraphenylporphine tetrasulphonate
m-TPP	*meta*-Tetraphenylporphyrin
MTT	3-(4,5-Dimethylthiazol-2-yl)-2,5-diphenyltetrazolium bromide
NaBT	Sodium butyrate
NADPH-ox	Nicotinamide adenine dinucleotide phosphate-oxidase
NdFeB magnet	Neodymium-iron-boron magnet
NF-E2	Nuclear factor erythroid-derived 2
NF-κB	Nuclear factor κ-light-chain-enhancer of activated B cells
NOX	NAD(P)H oxidases
Nr-f2	NF-E2 related factor-2
[O]	Oxidation
8-OHdG	8-Hydroxydeoxyguanosine
8-OHG	8-Hydroxygunosine
OSR	Oxidative Stress Reactions

PABA	*para*-Aminobenzoic acid
PANC-1	Human pancreatic carcinoma - 1 (cell line)
PBN	α-Phenyl-N-tert-butylnitrone
PBS	Phosphate buffer saline
PD1	Programmed death 1
PDL1	Programmed death ligand 1
PDMS	Polydimethylsiloxane
PDT	Photodynamic therapy
p53	A tumour suppressor gene (tumour protein)
PHP	Polyhaematoporphyrin
PI	Propidium iodide
PMMA	Polymethyl methacrylate
PMT	Photomultiplier tube
PPARγ	Peroxisome proliferator-activated receptor-*gamma*
PS	Photosensitiser
PS*	Excited state photosensitiser
^{1}PS	Singlet photosensitiser
^{1}PS*	Excited singlet state photosensitiser
^{3}PS*	Excited triplet state photosensitiser
PTH	Parathyroid hormone
PUFAs	Polyunsaturated fatty acids
PVG	Porous Vycor glass
PyTPP	Pyridyltriphenylporphyrin
R$^\bullet$	Alkyl radicals
R^2	Coefficient of determination
RB	Rose Bengal
RBI	Rhodamine B Isothiocyanate
RhH_2	Dihydrorhodamine
RNI	Reactive Nitrogen Intermediate
RNS	Reactive Nitrogen Species
RO$^\bullet$	Alkoxyl radical
ROI	Reactive Oxygen Intermediate
ROO$^\bullet$	Peroxyl radical
RPMI	Roswell Park Memorial Institute
RS$^\bullet$	Thiyl radical
s.f.	Significant figures
sn	Stereospecifically numbered
Sp1	Specificity protein 1 (transcription factor)
sr	Steradian (International System of Units of solid angle)
STP	Standard Temperature and Pressure
S_V	Surface area to Volume ratio
TBHP	*tert*-Butylhydroperoxide
TDLN	Tumour-draining lymph node
TGF-*β*	Transforming growth factor-*beta*
Tj	Junction temperature
TLR	Toll like receptor
TMPO	2,5,5-Trimethyl-1-pyrroline N-oxide
TNF	Tumour-necrosis factor
$TPPS_4$	Tetraphenylsulfantoporphyrin
TPyP	5,10,15,20-Tetrakis(4-pyridyl)-21H,23H- porphyrin
uPA	urokinase Plasminogen activators
VEGF	Vascular endothelial growth factor

List of figures

List of tables

List of schemes

Acknowledgements

I like to sincerely thank my supervisors Professors Ross W Boyle, John Greenman and Nicole Pamme for their guidance, support and for offering this multidisciplinary project, which allowed me to gain immense knowledge and skills in various fields. Also I like to thank the thesis advisory panel chair, Prof. S. J. Archibald for his advice.

I am so grateful to Mr. N. Parkin and Mr. C. Lloyd for building the instrument precisely according to the author's design, Dr. S. Clark for fabricating the various chip designs provided, Dr. F. Guitini for assistance with porphyrin synthesis, Dr. L. Madden and Mrs. H. Savoie for their help and support with cell culture related work, Ms. J. Malle for making glass cell-suspension containers and Dr. H. Snelling for helping with light irradiance measurements.

Many thanks to the following members for sharing their time, expertise and valuable discussions during various positions of the project; Drs. A. Iles, R. Sturmey, C. Wiles, E. Rosca, C. Phurimsak, M. Tarn, E. Lumely and Mr. C. Randles. My sincere thanks also goes to Ms. E. Brookes for providing essential administrative support by giving appropriate information on time and Ms. R. Green for arranging all the meetings.

I would also like to thank my family members for their constant support, advice and encouragement given during all situations.

Kapiraj Chandrabalan

Author's declaration

I confirm that this work is original and that if any passage(s) or diagram(s) have been copied from academic papers, books, the internet or any other sources these are clearly identified by the use of quotation marks and the reference(s) is fully cited. I certify that, other than where indicated, this is my own work and does not breach the regulations of HYMS, the University of Hull or the University of York regarding plagiarism or academic conduct in examinations. I have read the HYMS Code of Practice on Academic Misconduct, and state that this piece of work is my own and does not contain any unacknowledged work from any other sources.

CHAPTER 1 - Introduction

This chapter is divided into five main sections (**Section 1.1** to **1.5**); the first section covers the type of reactive species, methods of detection, generation of oxidative stress environment using photosensitisation reactions, cellular oxidative stress and their effects on cellular components, methods for measuring the latter, and the function of antioxidants in reducing the effects of reactive species; the second section describes the role of oxidative stress in the development of cancer, photodynamic therapy (PDT) for treating it, the importance of inducing immune response following selective localised oxidative stress (PDT) associated damages, and some of the biological components used to study oxidative stress; the third section introduces the importance of the microfluidic approach, some of the selected microfluidic photochemical and photobiological applications, fluid dynamics, fabrication of microfluidic devices, and immobilisation of molecules of interest onto a solid support through surface treatment reactions to enable heterogeneous reactions; the fourth section highlights the research gap; and the fifth section outlines the overall aims of the project. In this thesis, the photosensitisation reactions considered together with biological cells will be referred to as "PDT-mimicking", "photodynamically sensitised", "PDT-type" or "oxidative stress" reactions.

1.1 Oxidative stress, diseases and photochemistry

Reactive species are a well-established set of chemical agents identified as mediators of useful and harmful responses within living organisms of all classes. They are used by cells as signalling agents to mediate processes such as cell proliferation.

1.1.1 Reactive chemical species and oxidative stress

Oxidative stress

The term 'oxidative stress' had been in use since1985.[1] In biology, oxidative stress could be defined as an excess production of reactive species which is not counter-balanced by protective mechanisms, such as antioxidants.[2] There are two main classes of reactive species, reactive oxygen species

(ROS) and reactive nitrogen species (RNS). Oxidative damage is the net result of oxidative stress, promoted by both ROS and RNS. Sources of oxidative stress generating free radicals include electron transport chain, phagocytosis, oxidant enzymes (e.g. xanthine oxidase), autoxidation reactions (e.g. epinephrine) and environmental sources such as ionising radiation.[3] Mitochondria undergoing mitophagy can also acts as a major source of ROS in living organisms.[2] Effects of oxidative stress from ROS include damages to genetic materials (DNA), lipid peroxidation, and inactivation of membrane bound enzymes and proteins,[3] which all have a critical role in the development of severe diseases,[2] provided in **Table 1.1**, which was adapted from reference **2** and expanded. As genetic materials are directly affected by ROS, it increases mutations during DNA replication, thereby initiating development of malignant diseases.[2, 4] Diseases such as allergy, cirrhosis, cataract, retinopathy, arthritis, macular degeneration, emphysema, asthma and hypertension are also related to oxidative stress.[3]

Table 1.1: *Diseases those are associated with oxidative stress.*

Diseases	**References**	**Diseases**	**References**
Acute respiratory distress syndrome	5	Inflammation	6
Aging	7-10	Inflammatory joint disease	11
Alzheimer's disease	12-14	Multiple sclerosis	15
Atherosclerosis (Arteriosclerosis)	16-18	Neurological disease	13
Cancer	2, 19-28	Obesity	29
Cardiovascular disease	30	Parkinson's disease	31
Chronic Hepatitis C	32	Pulmonary fibrosis	33
Diabetes	34	Vascular disease	28, 35

1.1.1.1 Classes of reactive species

Reactive nitrogen species

The amounts of RNS are comparatively lower than ROS, but they too have important roles. RNS such as peroxynitrite ($ONOO^-$) and nitric oxide ($^{\bullet}NO$) are involved in cell signalling processes.[36, 37] $ONOO^-$ and $^{\bullet}NO$ have half-lives in the ranges of 0.05 - 1.0 s and 1 - 10 s, respectively.[38] RNS accumulation can be harmful when present in excess, or when they undergo side reactions resulting in the generation of cytotoxic species. Under physiological conditions, protonated form of $ONOO^-$ decomposes to generate $^{\bullet}OH$ radical and nitrogen dioxide radical ($NO_2^{\bullet-}$). Radicals cause damage to biomolecules such as carbohydrates and DNA by promoting oxidation reactions.

Reactive oxygen species

ROS are the most common types of reactive species that is essential for vital (balanced level) cellular activities, however excess or uncontrolled levels (non-balanced) are deleterious to the biological environments.[39] Ground state molecular oxygen ($^3O_2$) is a free diradical (2p π^*, **Figure 1.1**). In biological systems, most of the $^3O_2$ diffused into an aerobic cell is reduced to water through the addition of four electrons and four hydrogen ions (**Equation 1.1**), by mitochondrial cytochrome oxidase during the process called respiration. ROS such as $O_2^{\bullet-}$, H_2O_2 and $HO^{\bullet}$ could be formed as the intermediate products, due to ineffective reduction reactions during respiration (**Scheme 1.1**). Hence in aerobic biological systems ROS are constantly being produced, and are used for various regular biochemical functions and in unusual pathological process.[25]

$$O_2 + 4H^+ + 4e^- \longrightarrow 2H_2O$$ **Equation 1.1**

There are wide varieties of actions through which ROS may be generated within biological systems, which include enzyme action, auto-oxidation or action of active oxygen by other molecules (**Scheme 1.1**).[40] Common types of ROS include superoxide radical ($O_2^{\bullet-}$), singlet molecular oxygen ($^1O_2$), hydroxyl radical ($HO^{\bullet}$), peroxyl radical ($ROO^{\bullet}$), hydrogen peroxide (H_2O_2) and hypochlorite (^-OCl) or protonated form of hypochlorite (HOCl).[3, 36, 37,

[40-42] It was also reported that plants actively produce reactive oxygen intermediate (ROI) for controlling cell functions in signal transduction pathways.[43]

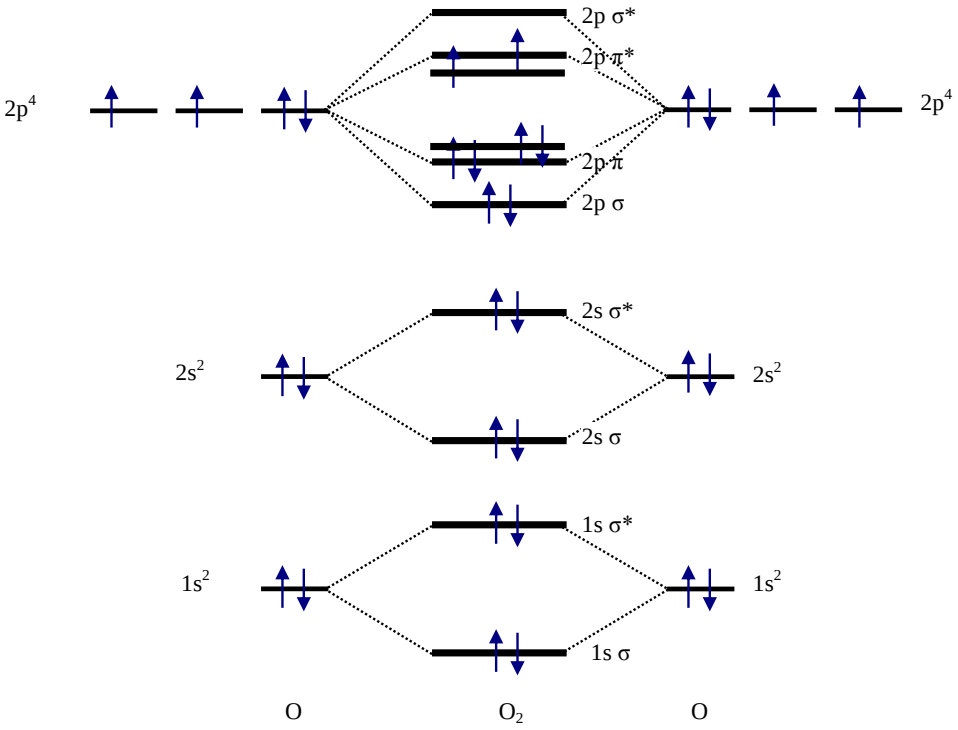

Figure 1.1: *Molecular orbital diagram of $^3O_2$.*

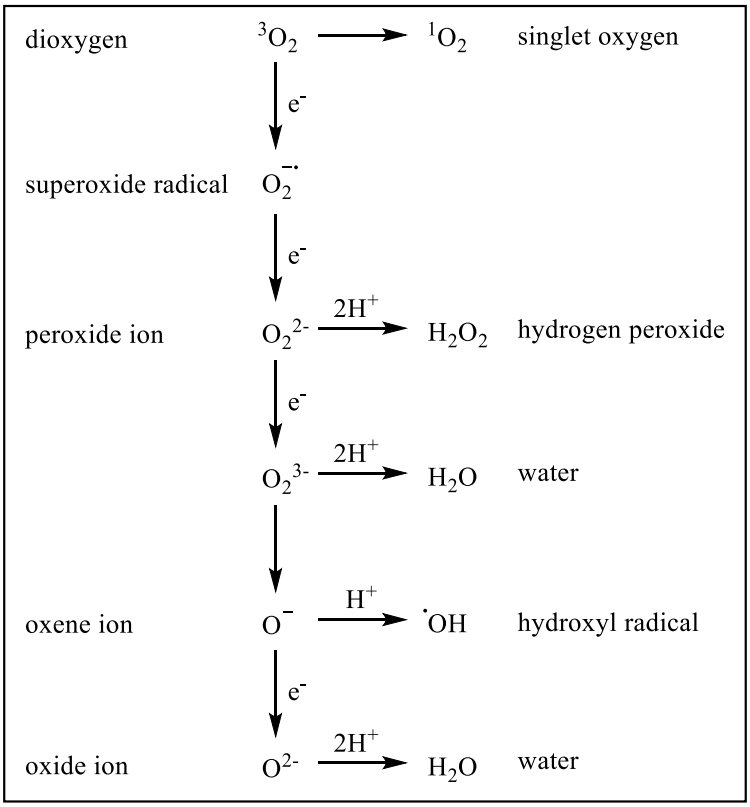

Scheme 1.1: *Reduction of O_2 and generation of ROS.*[44]

1.1.1.2 Types of reactive oxygen species (ROS)

All ROS contains one or more oxygen atom(s) which is responsible for their reactive nature.[45] Reactive oxygen species can be either radicals or non-radicals. The reactive radicals undergo one-electron reactions, and the reactive non-radicals undergo two electron reactions. Addition of an electron to a molecule produces negatively charged radical and removal of an electron from a molecule produces positively charged radical. $HO^{\bullet}$, $^1O_2$, $O_2^{\bullet-}$ and H_2O_2 are the four most common types of ROS that are important within a biological environment, their diffusion distance, reactivity and life-time are considered relative to each other in **Figure 1.2**.

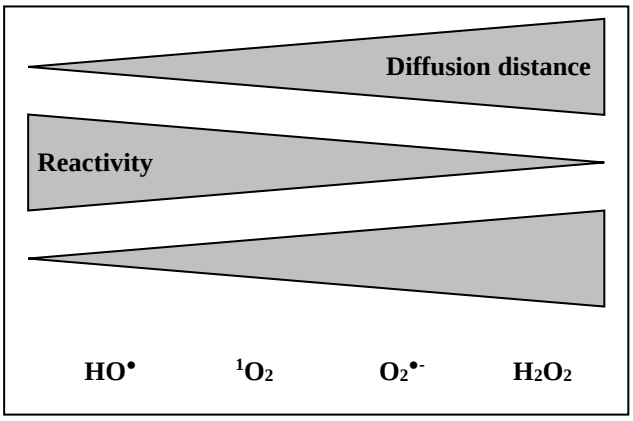

Figure 1.2: *The relation between diffusion distance, life-time and reactivity of the four most common ROS in cells.*[46]

(a) Non-radical reactive oxygen species

The oxidising strength of non-radical reactive species depends on their reduction potential, and due to the high activation energy barriers, their rate of reaction depends on kinetics. Some of the examples of non-radical ROS include $^1O_2$, H_2O_2, hydroperoxides of biomolecules, and HOCl and its related species.

Singlet Oxygen

The excited form of $^3O_2$ is called $^1O_2$, which has no unpaired electrons. The photochemical (type-II) process involved in generation of $^1O_2$ is discussed under **Section 1.1.2.1**.[47, 48] There are two forms of excited molecular oxygen (**Figure 1.3**), $^1O_2$ ($^1\Delta$) and $^1O_2$ ($^1\Sigma$), which exists at two different energy levels, where one form is more stable ($^1\Delta$) than the other ($^1\Sigma$).[48, 49] The two

different forms of $^1O_2$ arise as a result of variation in the occupancy by the paired electrons. In $^1O_2$ ($^1\Delta$), the paired electrons occupy the same antibonding orbital (π*, 2p), while in $^1O_2$ ($^1\Sigma$), the paired electrons exists in two different antibonding orbitals (π*, 2p). In both forms of $^1O_2$ ($^1\Delta$ and $^1\Sigma$), the electrons are paired and the molecules are higher in energy relative to the $^3O_2$ by 22.5 and 37.5 kcal mol^{-1}, respectively. The energy difference of 22.5 kcal mol^{-1} corresponds to the phosphorescence wavelength of 1270 nm (IR region), and the energy difference of 37.5 kcal mol^{-1} corresponds to the emission wavelength of 762 nm. The difference in energy between the two excited forms of $^1O_2$ is 15.0 kcal mol^{-1}, and it corresponds to the emission wavelength of 1910 nm.

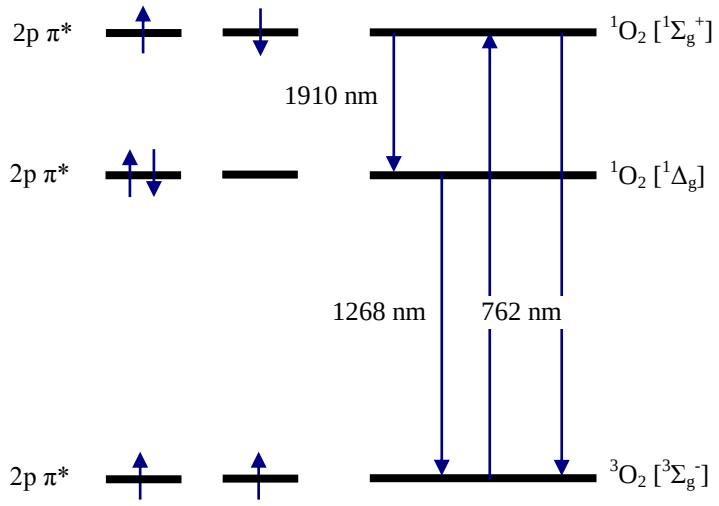

Figure 1.3: *The relative energy levels of $^3O_2$ and $^1O_2$.*

$^1O_2$ type reactions were first described in 1867 by Fritzche.[45] However, the concept of $^1O_2$ based reactions was introduced only in 1971.[40] $^3O_2$ has two unpaired electrons (**Figure 1.1**) hence it can react rapidly with similar types of atoms, ions or radicals. Hence, $^3O_2$ reacts rapidly with species that are capable of donating an electron and their reactivity is thermodynamically favoured. Organic molecules mostly have paired electrons, thus $^3O_2$ do not react readily. For $^3O_2$ to react with systems possessing paired electrons, it requires change of spin before the reaction could occur. However, due to spin selection rules (Pauli's exclusion principle) the process of spin change is said to be 'forbidden', and the reaction do not occur spontaneously. Pauli's exclusion principle predicts that no two electrons can have the same

quantum numbers, that is, no two electrons can occupy the same place at the same time, hence would not have the same energy. When $^3O_2$ is excited to produce $^1O_2$, their reactivity dramatically changes and the molecule become reactive towards the systems that it could not react otherwise when it was in its ground state.

As illustrated in **Figure 1.3**, excited forms of molecular oxygen have paired electrons, hence become reactive towards biological systems. Conjugated polymeric systems and polynuclear aromatic systems are present in abundance within living cells. $^1O_2$ ($^1\Delta$) reacts readily with conjugated polymeric systems and polynuclear aromatic systems to generate various types of ROS.[49] $^1O_2$ undergo three types of reactions with alkenes, 1,2-cycladdition, an "ene" type reaction to form hydroperoxides and 1,4-cycloaddition reaction.[50] The stereo and regio properties of the products like allylic hydroperoxide and endoperoxides, depends on steric effects, electronic effects and hydrogen bonding.[45]

Direct or indirect reactions initiated by $^1O_2$ species are of major interest in biochemistry[51] and in learning how they lead to development of diseases. In biological systems, $^1O_2$ can function as an activator of gene expression. Production of larger quantity of $^1O_2$ is toxic to cells. Immune cells like neutrophils have the potential to generate $^1O_2$ and to bind antibodies.[36] Antibodies are capable of catalysing the formation of ROS like H_2O_2 and ozone (O_3), using $^1O_2$ and H_2O.[52] It also has the potential to catalyse the formation dihydrogen trioxide (H_2O_3) and O_3, using the same starting materials, $^1O_2$ and H_2O.[53] Hence, this type of reaction is considered as the biological source of O_3. *In vivo*, oxidative stress can lead to oxidation of biological molecules like DNA, proteins and lipids.[36] The spatial resolution of the responses initiated by $^1O_2$, relative to their site of production is grouped into three levels, molecular, organelle and cellular levels. Molecular - primary oxidation of nearby molecules; organelle - initiation of organelle specific mechanism; and cellular - diffusion of mediators to initiate cellular responses.[46]

$^1O_2$ is a good oxidising agent for organic compounds and had been used in bioinorganic synthesis.[54] The average sunlight energy of 800 W m^{-2} (800000 mW m^{-2} or 80 mW cm^{-2}) is sufficient to excite photosensitisers to induce photosensitisation effects. Natural surface water could contain trace amounts of $^1O_2$, which are produced by energy transfer from excited humic and fulvic acids. Hence, $^1O_2$ is the main source of free radicals or peroxides on the Earth water surface.[55]

During oxidative stress generation using photosensitisation, triplet state photosensitisers are responsible for the production of $^1O_2$ (**Section 1.1.2.1**). However, alternative quenching pathways could deactivate triplet state photosensitisers and cause them to fluoresce, thereby prevent generation of $^1O_2$. This type of behaviour is called delayed fluorescence, and it can occur due to triplet-triplet quenching of two photosensitisers or as a result of another $^1O_2$ reacting with triplet state photosensitiser.[56] It was also observed that in the presence of molecules such as carotenoids, $^1O_2$ generated by photosensitisers such as porphyrin derivatives are rapidly quenched (**Section 1.1.4**).[57]

The type of solvent affects the half-life of triplet state photosensitiser, hence the efficiency in generation of $^1O_2$. In general, the quantum yield of $^1O_2$ ($^1\Delta$) production lies in-between 0.3 to 0.75. The half-life of $^1O_2$ in water is in the range of 4 – 10 x 10^{-6} s,[38, 46] while the life-time of $^1O_2$ in deuterated water (D_2O) is relatively higher than in H_2O.[40] In biological systems $^1O_2$ has a life-time of less than 0.04 ms. As a result their reactivity is limited only within a diameter region of 0.04 µm.[58] The rate of reaction and the half-life of $^1O_2$ depend on the nature of the solvents in which they are generated.[59] Solvents of lower viscous such as acetone, which is used as a spectroscopic standard, has higher triplet-triplet quenching constant relative to higher viscous solvents such as dimethylsulfoxide, which is used in clinical studies.[56] Both medium viscosity and quenching rate of activated species are related to the rate of molecular collision, where increase in the rate of collision, increased the rate deactivation. The reactivity of $^1O_2$ is utilised in

photodynamic therapy (PDT), water purification, chemical synthesis, and for decontamination of biological or chemical samples.[59]

Hydrogen peroxide

Biological sources of H_2O_2 include, dismutation of $O_2^{\bullet-}$ into H_2O_2 and H_2O by the defensive enzymes like manganese-superoxide dismutase (Mn-SOD),[36, 43] reduction of $HOO^{\bullet}$ by superoxide dismutase (SOD), amine oxidases (e.g. diamine oxidase), peroxisomal oxidases (e.g. urate oxidase) and others.[1] H_2O_2 produced both extracellularly and intracellularly (within organelles) must traverse lipid bilayer membrane to show their effects in the cytosolic region. The diffusivity of H_2O_2 across the cell membranes are not the same for all cell membranes.[60] It can diffuse across mitochondria, the site of production, to the cell membrane and causes injuries.[2] The main functions of this molecule include mediating cell proliferation, differentiation, migration of cells and acts as a second messenger in normal cellular signal transduction.[60] Further, it can serve as a precursor in the generation of other ROS. Comparing to wide range of ROS, in general, it is relatively stable, however, huge accumulation could result in severe oxidative related damages. H_2O_2 had also been linked to the cleavage of light and heavy chain linkage in human immunoglobulin G1 (IgG1).[61] In biological systems, it has variable and long half-life (~8 hours)[62] relative to $^1O_2$ (~3.5 μs)[63], and it is mainly decomposed by antioxidant enzymes such as catalase and GPx (GSH).[38]

(b) Radical reactive oxygen species

Though oxygen contains two free electrons it is technically a free radical, but under the general definition of free radicals, it mainly considers only molecules or ions with a single unpaired electron. In cells, removal of an electron from the atoms oxygen, nitrogen, sulphur or carbon contained in a molecule, results in the production of that atom centred free radical. High energy radiation induced homolysis of water would result in the production of two free radicals, a $HO^{\bullet}$ radical and a hydrogen atom ($H^{\bullet}$). $H^{\bullet}$ is the simplest free-radical known. Alkyl radicals ($R^{\bullet}$) can react with thiol group (-SH) on proteins, through an electron transfer process to generate non-free

radical on proteins (-S$^{\bullet}$) and the by-products alkyl anion (R^-) and proton (H^+) (**Equation 1.2**).[1]

$$R^{\bullet} + \text{protein-SH} \rightarrow \text{protein-S}^{\bullet} + R^- + H^+ \qquad \textbf{Equation 1.2}$$

Radical molecules have one or more unpaired electrons, hence they show paramagnetic behaviour and can be attracted by a magnetic field. Using the right level of electromagnetic energy unpaired electrons can be made to absorb it, using which an absorption spectrum can be produced. This technique is used in electron spin resonance spectroscopy since 1970 to study radicals in biology. Some of the examples of free radicals include hydrogen atom ($H^{\bullet}$), trichloromethyl ($CCl_3^{\bullet}$), $O_2^{\bullet-}$, $HO^{\bullet}$ radical, thiyl ($RS^{\bullet}$), peroxyl ($ROO^{\bullet}$), alkoxyl ($RO^{\bullet}$) and oxides of nitrogen ($NOO^{\bullet}$, $NO^{\bullet}$).[64] The two most common types of radical ROS had been considered below in details.

Superoxide

In aerobic organisms, $^3O_2$ is vital for aerobic respiration, which is the source of biological energy producer. During mitochondrial respiration about 1 – 5 % of the total O_2 consumed could leak into inter-mitochondrial membrane space and give rise to $O_2^{\bullet-}$.[36] Most free radicals undergo dismutation reactions, during which two of the same molecules react, where one get oxidised and the other get reduced. Two $O_2^{\bullet-}$ radical molecules react through an electron transfer reaction to form O_2 (oxidised form) and H_2O_2 (reduced form). The biological sources of $O_2^{\bullet-}$ include, autoxidation of small molecules (e.g. adrenalin, dopamine, 5-ALA), aqueous Fe^{2+} (e.g. Fe^{2+}-citrate) and oxyhaemoglobin. Metabolic activities like mitochondrial electron transport chain, endoplasmic reticulum (cytochrome P450 system), cyclooxygenases (COX), lipoxygenases (LOX) and many others could act as the source of the radical.[1] The lifetime of ROS vary between different types of species. Within biological systems $O_2^{\bullet-}$ radical has variable half-life in the time scale range of ns, and it is mainly decomposed by SOD enzymes (**Section 1.1.4**).[38]

Hydroxyl radical

$HO^{\bullet}$ radical has the highest reduction potential (+2.31 V) of all the free radicals encountered in biochemistry. Hence it can react with wide range of biomolecules at the rate close to the diffusion controlled limit, with the reaction rate constants in the range of 10^7 to 10^{10} mol dm^{-3} s^{-1}.[65] $HO^{\bullet}$ radical mediate main cell injuries and they cannot diffuse more than few Angstrom in length (one or two molecular diameters) due to its unstable electronic configuration, hence it immediately reacts with the nearest cellular components. It causes oxidative damages to biological molecules like proteins, carbohydrates, RNA, DNA and lipids, thereby it has a function in the etiology of several diseases (**Table 1.1**).[21] The reactivity of H_2O_2 with DNA, proteins and lipids, have been found to be through the generation of $HO^{\bullet}$ radical from the reaction between H_2O_2 and metals like Fe^{2+} or Cu^{+}, the reaction is known as the *Fenton reaction* (**Equation 1.3**).[38] In the latter reaction, the metal catalyst is oxidised (Fe^{3+}), which is converted back to its reduced form (Fe^{2+}) through the oxidation of $O_2^{\bullet-}$ into $^3O_2$, the overall reaction is called *Haber-Weiss reaction* (**Equation 1.4**).

Fenton reaction:

$$H_2O_2 + Fe^{2+}\ (\text{or } Cu^{+}) \longrightarrow Fe^{3+}\ (\text{or } Cu^{2+}) + \bar{O}H + \dot{O}H$$

(Equation 1.3)

Haber-Weiss reaction:

$$H_2O_2 + Fe^{2+} \longrightarrow Fe^{3+} + \bar{O}H + \dot{O}H$$

$$\bar{O_2} + Fe^{3+} \longrightarrow Fe^{2+} + O_2$$

$$H_2O_2 + \bar{O_2} \longrightarrow O_2 + \bar{O}H + \dot{O}H$$

(**Equation 1.4**)

1.1.1.3 Detecting and measuring common ROS

Chemical based probes are designed to undergo photo-induced electron transfer reactions, displacement reactions, oxidation reactions or to fluoresce, when they react with ROS like H_2O_2, $^1O_2$, $O_2^{\bullet-}$ or $HO^{\bullet}$ radicals.

Spin trapping (hydroxyl and superoxide radicals)

Due to instability of radicals, most of them cannot be directly detected, hence cannot be measured. To overcome the problem of detection, techniques like spin trapping are used, which is a common technique for detecting production of $O_2^{\bullet-}$ and $HO^{\bullet}$ radicals within an aqueous environment. The reaction of radicals with nitroso compounds yields nitroxide radicals, which are more stable than the original radical. 5,5-dimethyl-1-pyrroline-N-oxide (DMPO) and α-phenyl-N-tert-butylnitrone (PBN) are the most common forms of nitroso compounds used for spin trap studies. The rate of $O_2^{\bullet-}$ radical trapping by spin traps such as DMPO and 2,5,5-trimethyl-1-pyrroline N-oxide (TMPO), are highly sensitive to pH changes.[66] Alternative to spin trapping studies is to use fluorescent based probes, which are more sensitive for detecting ROS than the methods based only on absorbance.

Singlet oxygen

$^1O_2$ can be directly measured chemically and spectroscopically.[67] In chemical method, probe like anthracene dipropionic acid (APA) reacts with $^1O_2$ to form endoperoxide, which results in photobleaching thereby leads to changes in concentration, the latter gets measured using changes in absorption intensity.[68] 1,3-Diphenylisobenzofuran (DPBF) had also been used as a probe to quantify $^1O_2$.[69] 2,7-Dichlorodihydrofluorescein ($DCFH_2$)-diacetate (**Figure 1.4**) is another probe for $^1O_2$ detection, it has good selectivity and do not respond to ROS like $O_2^{\bullet-}$ and $HO^{\bullet}$ radicals.[36] The selectivity is due to the formation of endoperoxide with the probe, which results in increased fluorescence. The excitation and emission wavelengths of $DCFH_2$-diacetate are 504 nm and 525 nm, respectively, it is used to study photo-oxidative stress, pathogen attack and wounding.[36] $DCFH_2$-diacetate can also be used to measure cell viability,[70] when $DCFH_2$-diacetate is internalised by live cells, they are oxidised by an enzyme called oxidase, thus resulting in fluorescence. For this dye, fluorescence signal and concentration of ROS are linearly related.[70] Spectrophotometrically bleaching of *p*-nitrosodimethylaniline was measured using changes in optical density at 440 nm, where the intermediate product generated from

the reaction between $^1O_2$ and imidazole was responsible for the bleaching process.[68, 71] Time-resolved measurement of infrared-phosphorescence is also widely used for determining quantum yields and kinetics of photoreactions involving $^1O_2$.[72]

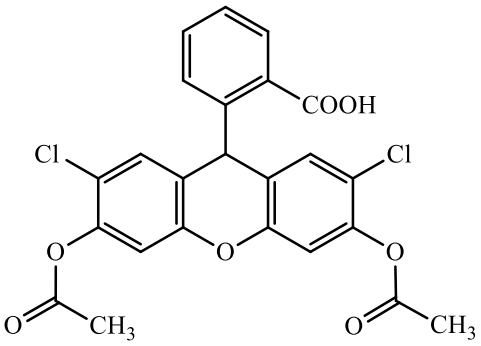

Figure 1.4: *2,7-Dichlorodihydrofluorescein diacetate ($DCFH_2$ -diacetate).*[70]

Superoxide

To indirectly quantify $O_2^{\bullet-}$ spectrophotometrically, molecules such as cytochrome c (measured at 550 nm), acetylated cytochrome c, adrenalin and nitroblue tetrazolium are measured.[1] $O_2^{\bullet-}$ can also be detected using chemiluminescent probes, lucigenin for example, which acts as a source and sink for it.[65]

Hydrogen peroxide

H_2O_2 present at low concentrations (mM) can be directly measured spectrophotometrically at 240 nm.[1] Peroxidase (enzymatic) based assays are conventionally used for detecting H_2O_2. Chemiluminescent (non-enzymatic) assay that is based on reaction of luminol with hypochlorite had also been reported for H_2O_2 detection.[73] 2′,7′−Dichlorofluorescein (DCF) and its diacetyl derivative are widely used as fluorescent probes for H_2O_2 measurements.[36] DCF imaging technique is also used to determine the overall oxidative stress in cell cultures.[1]

1.1.2 Generation of ROS using photosensitisation

1.1.2.1 Photochemistry

In photochemistry, light energy absorption and transferring of the absorbed energy are the two important processes. The modified Jablonski diagram

outlining the energy flow and the processes that occur when light, photosensitiser and oxygen interact during photosensitisation reactions is given in **Figure 1.5**. Fluorescence and phosphorescence are two common forms of photoluminescence. Absorption of a photon ($h\nu_1$) of right energy level by a photosensitiser, results in its excitation from ground singlet state (S_0) to a higher energy (or excited) singlet state (S_n, where n is a positive integer). The relaxation of the excited photosensitiser through electronic transition between spin quantum states, $S_1 \rightarrow S_0$ results in an emission of a photon and the process is known as fluorescence ($h\nu_2$). The life time of S_n photosensitisers ($^1PS^*$) are in the range of nanoseconds (ns), hence the lifespan of fluorescence is in the range of 10^{-8} to 10^{-4} s.[74] The energy of a photon released during fluorescence is usually of lower energy than the photon that caused excitation of the molecule from its S_0.

Under special instances such as in the presence of heavy atoms like heavy metals, one of the paired electrons undergoes a "forbidden" process of inter-system crossing (spin change), to generate excited triplet state (T_n, where n is a positive integer) photosensitiser. The photosensitiser in T_n must change its spin before releasing their excess energy to reach the S_0. Phosphorescence (radiation) and heat energy dissipation (radiationless) are the two common forms through which the excess energy is liberated. Electronic transition between spin quantum states, $T_1 \rightarrow S_0$ results in an emission of a photon and is known as phosphorescence ($h\nu_3$), the energy of the photon released during this process is usually lower than the energy of the photon used for excitation or the photon released during fluorescence. However, the process of spin change has a lower probability, as a result a photosensitiser in T_n state survives longer (µs to s) compared to a photosensitiser in S_n state (ns), hence the lifespan of phosphorescence is in the range of 10^{-4} to 10^{2} s.[74] The longer half-life of T_n state sensitisers, increases the probability of energy transfer to another molecule that could participate in the energy transfer process. When T_n state photosensitiser comes in contact with lower energy triplet state (two unpaired electrons) molecules like $^3O_2$, it readily transfer its energy, thereby the photosensitiser return back to S_0, and $^3O_2$ get excited to $^1O_2$ (**Figure 1.5**).

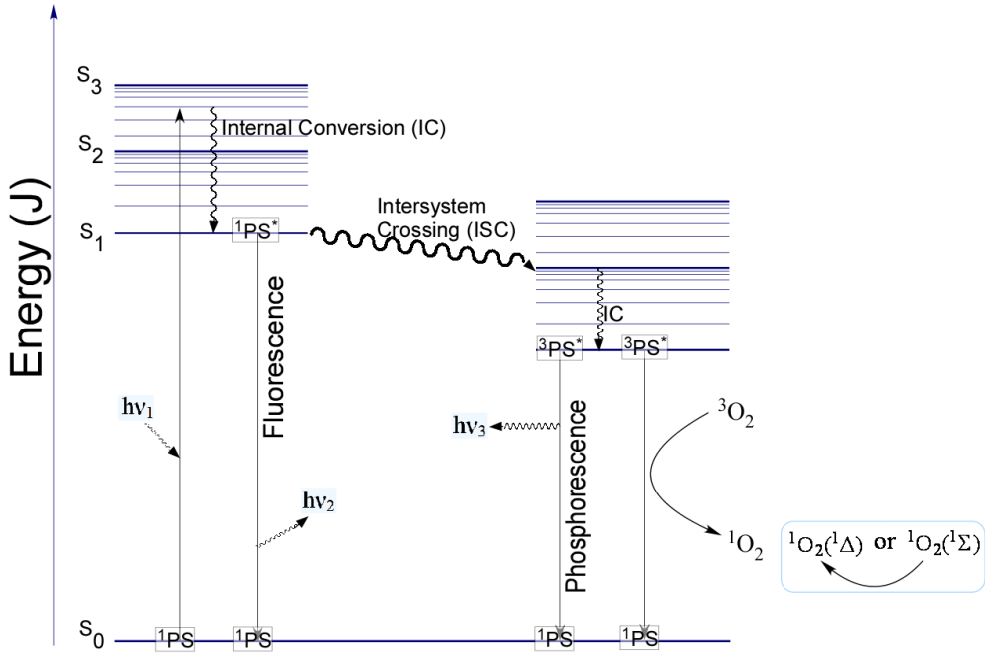

Figure 1.5: *Modified Jablonski diagram illustrating the photophysical and the photochemical interactions during photosensitisation.*

In summary (**Scheme 1.2**), absorption of light energy results in excitation of photosensitiser ($^1PS \rightarrow {}^1PS^*$), and the $^1PS^*$ could stabilise in three ways, emission (fluorescence), internal conversion (heat energy dissipation) or by undergoing inter-system crossing (heat release) to become T_n sensitiser. The latter could further stabilise through three pathways [emission (phosphorescence), **Type I-** or **Type II-**pathways], to reach the ^1PS. Type II-pathway leads to generation of two forms $^1O_2$ (**Section 1.1.1.2**).[49, 75]

Step 1
Absorption of photon $\quad {}^1PS \xrightarrow{h\nu_1} {}^1PS^*$

Step 2
Stabilisation of $^1PS^*$

Singlet-singlet emission (Fluorescence) $\quad {}^1PS^* \rightarrow {}^1PS + h\nu_2$

Internal Conversion $\quad {}^1PS^* \rightarrow {}^1PS + \text{Heat}$

Intersystem Crossing to a triplet state $\quad {}^1PS^* \rightarrow {}^3PS^* + \text{Heat}$

Step 3
Stabilisation of $^3PS^*$

Phosphorescence $\quad {}^3PS^* \rightarrow {}^1PS + h\nu_3$

Energy transfer **Type I** $\quad {}^3PS^* + SH \rightarrow {}^{\cdot}SH \text{ or } S^+ + {}^1PS$

Energy transfer **Type II** $\quad {}^3PS^* + {}^3O_2({}^3\Sigma) \rightarrow {}^1O_2({}^1\Delta) + {}^1O_2({}^1\Sigma) + {}^1PS$

Scheme 1.2: *Summary of photosensitisation reactions involved in generation of $^1O_2$.*

1.1.2.2 Photosensitisers

Strong absorption at longer visible wavelengths, reduced dark toxicity, solubility, selectivity, specificity, high efficiency in ROS production, characterised chemical structure, stability and rapid clearance from the body, are some of the features essential for an ideal photosensitiser.[76, 77]

(a) Classes of photodynamic sensitisers

There are three generations of photosensitisers, grouped as first, second and third generations. For simplicity trivial names were used to identify most of the photosensitisers and not their systematic names.[78] *First generation* photosensitisers are mixtures of several types of molecules of similar relative molecular masses, and they can be excited using visible light. However, the photosensitisers of this generation are not capable of absorbing longer visible wavelengths, and do not get cleared out of the blood circulation rapidly, thus results in prolonged photosensitivity, Photofrin® for example.[79]

Second generation photosensitisers are more pure than the former generation and usually of single type of molecule. These sensitisers can absorb longer wavelengths of visible light,[79] Verteporfin® is an example of commercially available second generation photosensitiser, which has high selectivity towards tumours and gets readily expelled away from the body, thereby the risk of associated side effects are lower. The above chromophore is suited for 690 nm wavelength absorption, which improved tissue penetration by 50% relative to Photofrin®.[77] Other clinically used tetrapyrrolic compounds include Porphyrin®, porphycene (ATMPn), Chlorin (Temoporfin®) and benzoporphyrin (Visudyne®). *Third generation* photosensitisers are the extended version of second generation,[79] with the additional features such as specificity for binding, that is, they are designed to target specific organelles like mitochondria. To gain specificity chromophores are conjugated to biologically essential components like proteins and antibodies.

In addition to the generations used for grouping the photosensitisers, they can also be grouped as one-photon and two photons excitable sensitisers. Photosensitisers like porphyrin derivatives and phthalocyanine derivatives are efficient one-photon excitable sensitisers, while photosensitisers like 2-(9,9-didecyl-7-nitrofluoren-2-yl)benzothiazole could be excited using two-photons.[80]

(b) ROS generation using tetrapyrrole derivatives

PDT makes use of wide range of photosensitisers, which include porphyrin and phthalocyanine derivatives.[81] Porphyrins and phthalocyanines are heterocyclic macromolecules with four modified pyrrole units interconnected.[82] Porphyrin based derivatives are the most common type of photosensitiser studied for PDT reactions, and widely used in clinical based PDT applications.[83] Porphyrin functionalised dendrimers have been synthesised with good level of activity towards photo-induced $^1O_2$ production.[84] A porphyrin derivative capable of reversibly trapping $^1O_2$ (four $^1O_2$ per porphyrin) had also been reported.[59]

In the earlier researches porphyrin derivatives have been isolated from natural sources like cells. Since then several efficient synthetic methods have been developed for the synthesis of variety of porphyrin derivatives, and used as photosensitisers.[85] Synthesis of unsymmetrical porphyrins are more challenging to make and often results in low yield.[86] For successful synthesis of unsymmetrical porphyrin derivatives synthetic techniques like combinatorial chemistry are used.[86]

Phthalocyanines

Phthalocyanines were first synthesised in 1907.[87] Aluminium phthalocyanine tetrasulfonate ($AlPcS_4$) and aluminium chloro sulfonated phthalocyanine (AlSPc) are two examples of metallated phthalocyanines. $AlPcS_4$ is a second generation photosensitiser, it is hydrophilic and can dissolve in aqueous conditions. $AlPcS_4$ has its highest absorption at the wavelength of 673 nm, which is favourable for *in vivo* applications, as the penetration of visible light at this wavelength is also greater than the

wavelengths in the region of around 400 nm. $AlPcS_4$ is used in PDT reactions, and AlSPc had been identified as a potential antitumour photosensitiser.[88]

Photostability

Photosensitisers used for PDT undergo photobleaching during photosensitisation reactions, and the rate of degradation depends on the testing conditions. In a study involving comparison of the spectroscopic properties of different photosensitisers, Photofrin II, dimethoxyhaematoporphyrin, haematoporphyrin, haematoporphyrin derivative, tetraphenylporphine tetrasulphonate (*m*-$TPPS_4$), chlorin e6, $AlPcS_4$ and Photoscan-3, under an aqueous condition of pH 7.2 for their photostability, it was found that $AlPcS_4$ was the most photostable and chlorin e6 was the least photostable.[89] Solvents can also affect properties such as fluorescence, the life-time of photosensitisers in triplet state, photobleaching and $^1O_2$ quantum yields.[90] Methylene blue (MB) is an example of non-porphyrin based photosensitiser. Photosensitisers are also used in environmental science applications like in water disinfection, which again depends on the production of excess of $^1O_2$, which are harmful to microbials.[91]

Photosensitisers in clinical applications

Some of the best known photosensitisers used for clinical PDT are considered here. Photofrin® is a FDA approved photosensitiser, used widely in clinical applications such as oncological treatments.[58, 68] Photofrin®, Levulan®, Visudyne® and Metvix® are all porphyrin based photosensitisers and they contain HpD, ALA, M-ALA and Verteporfin, respectively. ALA-induced endogenous productions of porphyrin (protoporphyrin IX) is also used in PDT and in tumour detection.[58] Photofrin, Purlytin® and Foscan® are commercially available photosensitiser,[92] the latter two are chlorin based photosensitiser, and Foscan® contains the substance called Temoporfin. Photosens®, is an example of phthalocyanine based photosensitiser.[76] Quadra Logic's Photofrin had also been approved for use in clinical trials III and IV.[93]

(c) Metalloporphyrins

With respect to luminescence properties, there are four types of metalloporphyrins classified as fluorescent, phosphorescent, luminescent and non-emitting.[94] Aluminium is a paramagnetic element, metals of this type contain unpaired electrons and do not possess permanent magnetic property, but can show stronger magnetic property than diamagnets in the presence of ferromagnets (usually Fe, Co, Ni). Porphyrin derivatives with diamagnetic metal centres are quenched rapidly from their excited state, and the same is not true with paramagnetic materials such as aluminium.

The poor solubility at physiological pH limits the use of high efficient photosensitisers for *in vivo* applications. Hence a mode of transport to the target site would highly enhance the PDT approach against many different diseases, where the carriers should possess higher specificity and selectivity. Examples of good carriers include oil-in-water emulsions, leptosomes and nanoparticles. The use of carrier systems could alter the quantum yield of $^1O_2$, with reduced number of reactive species diffusing out of the carriers. The above factors depends on the size of the carriers and the permeability across the membrane, further all light energy may not be effectively transferred (or reach) to the photosensitisers due to absorption and scattering by the carrier vehicle. Use of biologically active macromolecules as carriers, antibodies for example, improved the outcome of third generation photosensitisers.[77]

No correlation was observed between metallation of porphyrin derivatives and PDT action.[79] In contrast, some of the metallated porphyrins are more efficient than their non-metallated form, and the type of metal centre can also affect the efficiency. For example, $ZnTPPS_4$ was found to produce higher level of ROS within cells than its corresponding non-metallated form ($TPPS_4$) or Pd metal centred ($PdTPPS_4$) derivatives.[95] Cationic metallated porphyrins are water-soluble.[77] Zinc metal centred phthalocyanines showed preferential accumulation within lysosomes, while *m*-THPC and polyhaematoporphyrin (PHP) showed diffused localisation all over cytoplasm.[96] There are several new photosensitisers constantly developed

for PDT related applications, metallopurpurins derivatives are among them, they have the ability to absorb longer wavelength (red) in the visible light spectrum, hence they are suitable candidate for PDT reactions.[97]

Immobilised photosensitisers

Options of surface chemistry modifications and ability to control optical properties are two main advantages of using quantum dots. Conjugates of photosensitiser loaded quantum dots, and quantum dots on its own had been utilised in PDT.[98] Photosensitisers that are covalently immobilised onto quantum dot had been excited in parallel using two distinct energy wavelengths, thus generating $^1O_2$ for reaction using one wavelength, and the other wavelength was used to capture and study fluorescent images. Photosensitisers immobilised onto quantum dot had also been excited using fluorescence resonance energy transfer (FRET) technique as well as direct excitation. FRET technique was also used to excite photosensitisers covalently bonded onto the nanocrystals.[68]

(d) Water-soluble photosensitisers

Pharmacokinetics and biodistribution of drugs are important factors for their active function, both of which can be improved through conjugation to water-soluble biological polymers like peptides and proteins.[99] Likewise, photosensitisers that are water-insoluble have limited clinical applications. Certain photosensitisers with higher efficiency might be limited in their capacity to be examined as a possible candidate for *in vivo* studies. Aluminium phthalocyanine chloride (AlClPc) for example, has higher efficiency than its water-soluble sulfonated derivatives, however due to its hydrophobic properties it is not used for *in vivo* applications. Water-insoluble AlClPc was modified with the use of water-soluble axial ligands, to produce water-soluble complex without reduction in its efficiency, and had been successfully tested in animal model studies.[100]

Hence, the water-solubility of photosensitisers is important for conducting biological (cells) based photosensitisation reactions. The presence of polar groups on photosensitisers could enhance water solubility in general.

Solubility of solid substances generally increases with temperature, and at molecular level it primarily depends on the functional groups that are mostly exposed to the solvent. Depending on the concentration, porphyrin derivatives could form dimmers or other higher level aggregates in aqueous solution. Introduction of ionic charged groups such as $–COO^-$ and $-SO_3^-$, at peripheral sites alters both chemical and spectroscopic properties.[101] Hydrophilic, amphiphilic and hydrophobic properties of photosensitisers play a key role in internalisation of photosensitisers *in vivo*. Hydrophilic photosensitisers are internalised in the ratio of 2:1, with high ratio in tumour cells relative to normal cells. $TPPS_4$, $AlPcS_4$ and RB are some of the examples of water-soluble photosensitisers used for $^1O_2$ generation.[102]

For water-soluble photosensitisers it had been demonstrated that, using changes in volume it was possible to identify triplet formation.[103] The number of photosensitisers like porphyrin in triplet state, is directly proportional to the amount of ROS generated. For porphyrins, formation of triplet state resulted in contraction of volume, and it was a temperature dependent process. Volume changes were also observed for photosensitisers like methylene blue (MB) and RB, where MB showed -1.5 ml mol^{-1} (or contraction of 1.5 ml mol^{-1}), while RB showed expansion of 1 ml mol^{-1}. Volume changes for methylene blue and RB are low compared to $TPPS_4$, which had a contraction of 10 ± 3 ml mol^{-1}.[103]

Aggregation and solid state porphyrins

Macromolecules like porphyrin derivatives can form aggregation, and it depends on several factors, among which pH, concentration, solubility and the type of porphyrin, plays an important role.[104] Aggregation of porphyrin in aqueous conditions were observed with protoporphyrin IX, deutroporphyrin IX, haematoporphyrin IX and coproporphyrin III.[105] Water-insoluble porphyrin derivatives such as *m*-tetraphenylporphyrin (*m*-TPP) can form self-assembled aggregates.[106] Porphyrin derivatives such as 5,10,15,20-tetrakis(4-pyridyl)-21H,23H-porphyrin (TPyP) can also form aggregates of ordered precipitates, which strongly influences the photophysical properties of the molecules.[107]

For a water-soluble porphyrin derivative tetra-sodium 5,10,15,20-tetrakis(4-sulfonatophenyl)porphyrin (H_2TPPS_4- $4Na^+$) in acidic medium, below pH 2.5, both edge-to-edge (*J*-aggregates) and face-to-face (*H*-aggregates) were observed.[108] The type of aggregation affects the spectra, that is, all aggregation does not have the same effect on the spectrum. UV-visible absorption spectrum was used for elucidation of the type of aggregate, which provided information on the type of association between molecules, but the information on the size of aggregation was limited.[108] For example, octahydroxy porphyrin derivatives could form H-bonding in long range order to form nanoporous crystalline structures.[109] Octahydroxy porphyrins have also been used in fabrication of microporous solids of different sizes.[110]

1.1.3 Cellular oxidative stress

Homeostasis is maintained only when the amounts of ROS are under controlled levels, and when their levels were to be low or high, physiology is impaired. *In vitro*, cellular oxidative stress could be generated using chemicals like menadione (MD) or H_2O_2, and *in vivo*, there are wide varieties of actions through which ROS may be naturally generated, which include enzyme action, auto-oxidation or action of active oxygen on other molecules.[40] The aerobic respiration site where the electron transport chain occurs within mitochondria forms the major intracellular ROS producer. Activated phagocytes could also act as physiological source of unstable oxygen species, where $^1O_2$ is produced from oxidants such as hypochlorite and chloroamine. The net result of cellular oxidative stress is the oxidation of cellular components, mainly DNA, proteins and lipids. It has direct effects on the overall viability status and survival of the cells. **Autophagy**, **apoptosis** and **necrosis** are three distinct modes of cellular disintegration, and are related to the strength and regions of the cells exposed to ROS.

Autophagy

It is considered as one of the first step of defence against oxidative stress conditions.[111] It is an automatic self-degradation process, identified by the formation of autophagosomes, which can be detected using electron

microscopy.[112] In the presence of intra- or extra-cellular ROS, this process may be up-regulated.[111]

Apoptosis

It is a form of programmed cell death, which is used by cells as a method of clearing old cells or cells that no longer function as a healthy cell.[77] Hence this process is vital for tissue homeostasis and health.[113] However, cancer cells are capable of evading it, which too contribute to the lethal effects of cancers.[114] Apoptosis was first described in 1971 and the presence of apoptotic response in relation to PDT was noticed only in 1991. The discovery of PDT-induced apoptosis led to the better understanding of the widespread efficacy associated with its use in treatments. Apoptosis is characterised by both morphological and metabolic changes that occur to a cell, maintenance of ATP levels, nuclear DNA fragmentation,[115] caspase activation, chromatin condensation, disintegration (formation of small fragments) of cells into bubbles like membrane bound particles (blebbing of membrane), cell shrinkage, low levels of inflammation associated with cell denaturation and engulfment of membrane bound particles by cells like macrophages, are regarded as common parameters observed during this process.[58] Metabolic events like phosphorylation of *Bcl-2* and lipid peroxidation favours apoptosis.[116] There are two pathways in which apoptosis could occur, through an intrinsic or an extrinsic mechanism.

Intrinsic pathway is triggered by cellular events like genotoxic insult. Such response is sensed by damage recognising sensors (e.g. p53) that control pro- and anti-apoptotic signals. When the strength of the pro-apoptotic signal increases, it induces events such as mitochondrial release of cytochrome c, which is an intrinsic signalling pathway molecule. A death ligand that binds to death receptor on the surface of cell membrane induces extrinsic signalling pathway molecules (e.g. caspase 8). The release of cytochrome c intrinsically, and caspase 8 activation extrinsically, leads to apoptosis through a common pathway which involve activation of caspase 3 (**Figure 1.6**).[117]

Necrosis

It is a form of cell burst, hence it is an uncontrolled mode of cell death. It could occur for various reasons such as a result of physical injury, infection or due to uncontrolled levels of ROS accumulation. The key difference between apoptosis and necrosis, is the absence or minimised level of inflammatory response (or products) that is observed in apoptosis.[77]

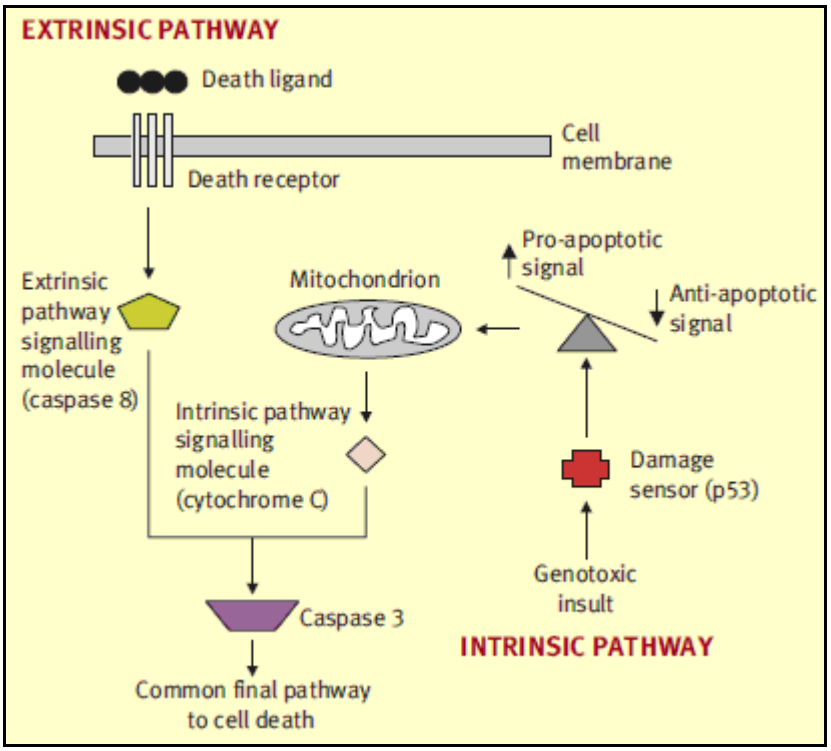

Figure 1.6: *Apoptotic signalling pathways in normal cells.*[117]

1.1.3.1 Effects of ROS on the cellular components

Inflammatory processes, impaired metal storage, dietary imbalance or the combination of all results in persistent oxidative stress, excess lipid peroxidation and protein peroxidation, which all in turn leads to massive DNA damage and deregulation of cell homeostasis, ultimately resulting in malignant diseases.[4]

(a) Lipid Peroxidation

Oxidation of lipids can occur through enzymatic or non-enzymatic pathways, the latter can be free-radical mediated or non-radical mediated.[118] $O_2^{\bullet-}$ radical generated by NADPH-oxidase (NADPH-ox), gets reduced to

H_2O_2 by the action of SOD. Alternatively, $O_2^{\bullet -}$ radical could also react with $NO^{\bullet}$ to form $ONOO^-$. H_2O_2 produced become the substrate for the other two enzymatic antioxidant enzymes, catalase which catalyses the conversion of H_2O_2 into H_2O and O_2, and glutathione (GSH) peroxidase (GPx) which reduces H_2O_2 into H_2O. H_2O_2 can also be split to form $HO^{\bullet}$ radical through the *Fenton reaction*, or myeloperoxidase (MPO) could convert it into hypochlorous acid (HOCl). Reactive species involved in lipid peroxidation of lipoproteins in biological membranes, and the action of enzymatic antioxidants are summarised in **Scheme 1.3**.[15]

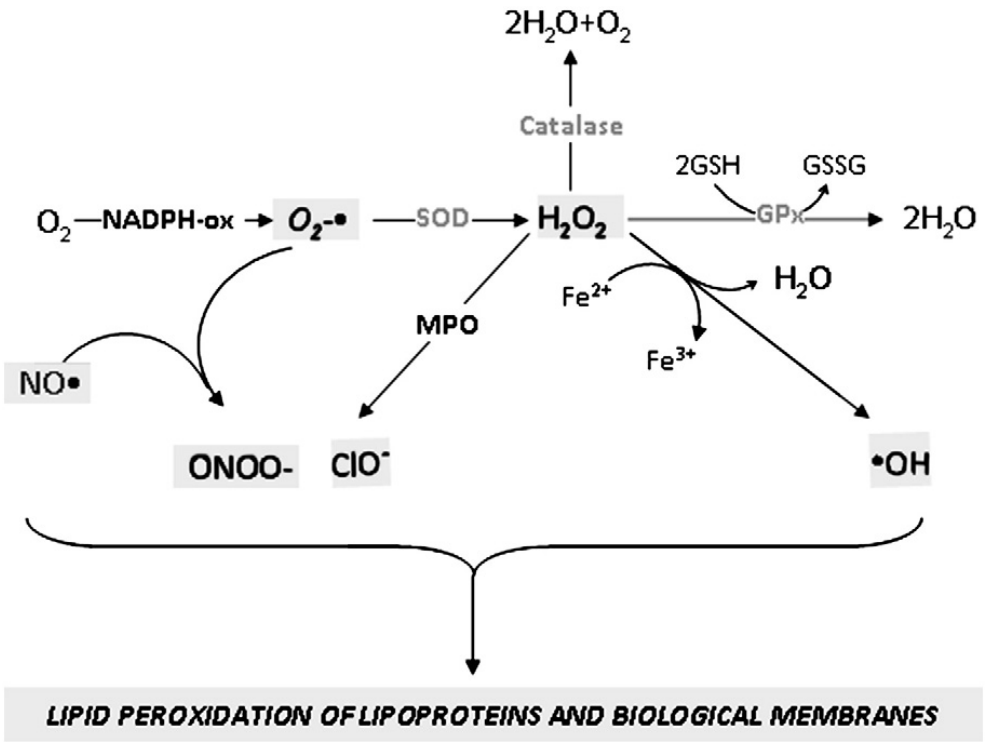

Scheme 1.3: *ROS and RNS involved in lipid peroxidation of lipoproteins in biological membranes and the action of enzymatic antioxidants.*[15]

As seen above, lipid peroxidation is the result of free-radical chain reaction between oxygen and lipids, and it could occur through various pathways. Formation of $O_2^{\bullet -}$ radicals can lead to the formation of $HO^{\bullet}$ radicals, which could cause peroxidation of lipids.[119] Transition metal ions such as iron and copper may also peroxidise polyunsaturated acids.[15] Lipid peroxidation had been linked to the pathogenesis of many diseases.[120]

Reaction of ROS with lipids occurs through three stages, free radical initiation, propagation and termination. Radicals may be generated in the presence of trace metals, light (photo-ionisation or photosensitisation) or heat. Lipid free radicals ($L^{\bullet}$) react with oxygen to generate peroxyl radicals ($LOO^{\bullet}$), they could further react with other lipids to produce more lipid hydroperoxides (LOOH), which are the primary products of auto-oxidation. LOOH can react with more oxygen to release secondary products such as bicyclic endoperoxides, cyclic peroxides, ketohydroperoxides, epoxyhydroperoxides and dihydroperoxides.[121]

A lipid peroxidation reaction pathway that could be involved in degradation of fatty acids on cell membrane is shown in **Scheme 1.4**.[122] Carbon-centred radicals can form as a result of oxidation (hydrogen removal) of methylene groups present in-between *cis*-double bonds. $^3O_2$ could react with the radicals to form two types of $LOO^{\bullet}$, which depends on the region of the molecule where carbon-centred radicals initially formed. $LOO^{\bullet}$ radicals formed towards the end of double bond system could get reduced through reaction with other fatty acids or vitamin E, embedded within phospholipid bilayer to form LOOH. Vitamin E is also involved in quenching of radical chain reactions, thereby slows the rate of lipid peroxidation. Alternatively, if $LOO^{\bullet}$ were to be formed away from the end of double bond system, it would form cyclic endoperoxide radical, which could undergo further reactions to produce isoprostanes and malondialdehyde (MDA) as shown in the scheme.[122]

There are more than 70 forms of oxysterols reported.[123] MDA, 4-hydroxynonenal (HNE), acrolein, crotonaldehyde and 8-isoprostaglandin are some of the key products of lipid peroxidation pathway.[1, 4] MDA was popularly used as a biomarker to detect and quantify lipid peroxidation reactions.[119] However, due to its non-specific nature of binding with thiobarbituric acid, isoprostanes are used.[122] MDA causes damages to DNA through the formation of exocyclic derivatives, hence it is both mutagenic and carcinogenic.[4, 122]

Effects of lipid peroxidation reactions

Following lipid peroxidation reactions, changes to bilipid layer membrane from "fluid-mosaic model" to "lipid-whisker model" was observed.[124] Reorganisation of the membrane components leads to changes in physical properties of the membrane.[125] Decreased fluidity in tumour plasma membrane and its composition had also been correlated.[126] Ultra-sensitive detection methods such as high performance liquid chromatography (HPLC)-electrochemical detection, gas chromatography-mass spectrometry (GC-MS), liquid chromatography (LC)-tandem MS, immunoslotblot assay, immunohistochemistry and immunoaffinity-^{32}P-postlabelling, enabled detection of background concentration of lipid peroxidation products *in vivo*, thereby enabled to study and link them with the development of carcinogenesis.[4] Lipid peroxidation of cell membrane was also linked to immune-mediated bowel disease.[127]

Low density lipid (LDL) and high density lipid (HDL) are involved in transport of lipids, regulation of lipid composition and signal transduction pathways. Lipid peroxidation resulting from reaction with ROS and RNS (produced by brain cells and peripheral cells) of LDL and HDL are involved in multiple sclerosis, that is, multiple sclerosis is associated with oxidative modifications of lipoproteins, which are made of lipids and apoproteins. Presence of lipoproteins similar to HDL have been detected in human cerebrospinal fluid, and it was hypothesised that, in central nervous system (CNS) it might be involved in transport of lipids such as triglycerides and phospholipids, and lipophilic molecules such as tocopherols and carotenoids, from their source of synthesis in cells to locations where they are essential for metabolic activities. Cholesteryl esters are present within lipoproteins, oxidised form of ester called cholesterol ester hydroperoxide, which is the most abundant form of lipid hydroperoxide formed *in vivo*, it is useful as a marker molecule of lipid peroxidation within lipoproteins.[15]

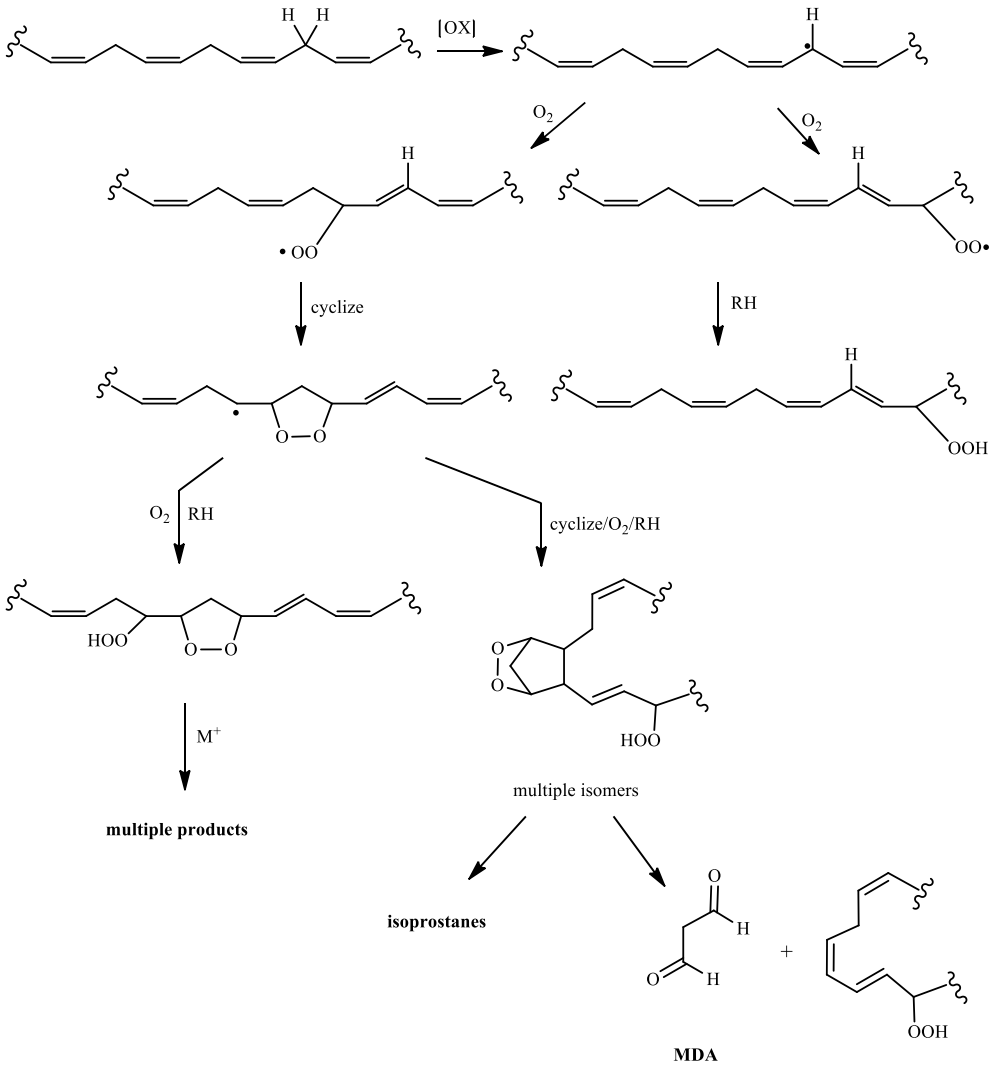

Scheme 1.4: *General pathways of lipid peroxidation.*[122]

(b) Cholesterol oxidation

Oxidation of cholesterol (**Figure 1.7**) is an undesirable reaction in food industry.[128-130] During storage it is a common problem observed in various foods, including mayonnaise and meat products. Using HPLC, the levels of four selected oxidised products, 7-ketocholesterol, 7α-hydroxycholesterol, 7β-hydroxycholesterol and 25-hydroxycholesterol, in mayonnaise were evaluated. It was found that the rate of formation of cholesterol oxides, increased with time and temperature; after a fixed storage period of 165 days at 4 and 25 ºC, the total levels of oxidised cholesterol were 20.3 and 30.2 μg g^{-1}, respectively.[130] Cholesterol can be oxidised through type I and type II processes,[75] and it had also been used as a $^1O_2$ trap.[131] During

photodynamical treatment, 5α-OOH cholesterol peroxide was found to be the most damaging form that is formed within cells.[132]

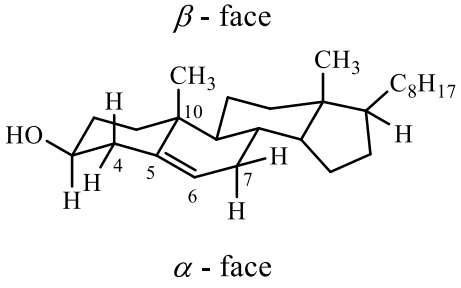

Figure 1.7: *Conformational structure of cholesterol.*[132]

Carotenoids are natural pigments found in plants and diverse microorganisms, and certain forms of them possess antioxidant properties. The relation between the rates of lipid peroxidation on membrane bilayer was studied using homochiral carotenoids, lycopene, β-carotene, zeaxanthin, lutein and astaxanthin, out of which apolar lycopene and β-carotene showed pro-oxidant properties, and astaxanthin showed anti-oxidant properties.[133]

(c) Protein peroxidation

About 68 % dry mass of cells and tissues are proteins. The abundance of proteins show their importance for effective functioning of cells. Due to their abundance they can also be affected by reactive species such as ROS leading to oxidative damages.[134-137] Protein oxidation pathway depends on the biological environment.[138] Oxidation of protein are the chemical modification of amino acids which they were made of, where in addition to the modification of the amino acids, bonds holding the 3D structure of the proteins could also be altered.[139] Both back-bone and side-chain amino acids of proteins could be oxidised under oxidative stress, where $HO^{\bullet}$ radical could cause non-specific protein damage.[140] The number of amino acid derivatives formed as a result of protein oxidation *in vitro* is diverse, and *in vivo* it is even much higher due to the secondary modifications of the oxidised derivatives. The net result of oxidative modifications to the proteins is the malfunction of them. The latter could be due to either active domain region of the protein had been directly modified or unfolded to an incorrect geometry for them to function.[139]

Photo-oxidation can cause generation of intracellular peroxides of proteins.[137] Peroxides of amino acids like tryptophan (Trp), tyrosine (Tyr) and histidine (His) induce oxidation of thiol residues, which results in structural changes and inactivation of enzymes.[40] Cytochrome c oxidation through photosensitiser dye embedded within bilayer of mitochondrial membranes was also observed. Oxidation of cytochrome c, at His 26 of the peptide, H26*KTGPNLHGLFGK, by $^1O_2$ was suggested as a biomarker for detecting mitochondrial oxidative stress *in vivo*. It was also hypothesised that such oxidised proteins and lipids would be responsible for the induction of apoptosis.[141]

The inactivation of enzymes, following exposure to light in the presence of photosensitiser and air was observed in 1903, it was the first systematic report made on photosensitisation reactions. Protein oxidation reactions were also observed when irradiated with white light, where oxidation occurred through the formation of $^1O_2$ generated through the excitation of protein-bound or other chromophores.[136] *In vitro*, oxidation of amino acids on the side-chains of proteins by $^1O_2$ resulted in their inactivation. Under physiological pH $^1O_2$ mostly oxidises the amino acids His, Tyr, Met, Cys and Trp.[138] Natural biological chromophores like riboflavin, flavins and vitamin B2 can also act as photosensitisers.[142] Endogenous cellular sensitisers such as flavins are concentrated enough to cause severe photo-oxidation reactions of proteins.[137] In addition, chemical agents and external factors like UV-radiation could also cause oxidation of protein.[143]

Exposure of proteins to UV-rays caused photo-oxidation of proteins, either through direct photo-ionisation or through excitation of protein-bound chromophores, thereby causing photosensitisation reactions.[136] The range for UV-rays is divided into three regions, UVA (320-400 nm), UVB (280-320 nm) and UVC (100-280 nm). The type of amino acids oxidised depend on the strength of the UV-rays used. On direct exposure, excited species or radicals cause damage to amino acids such as Trp, Tyr, His and Cys. The radicals of amino acids such as Trp, Tyr and Cys, or ROS can further induce secondary damages to other proteins, eventually leading to accumulation of

protein fragmentation, which can modulate cellular events such as induction of cell death through apoptosis or necrosis.[144] Radicals can also react with IgG1 resulting in the breakage of light and heavy chains, disulfide bridges that connects the two chains are broken at the amino acid linkages Cys^{215}LC and Cys^{225}HC, where $HO^{\bullet}$ radical primarily attacks the latter.[61]

The important negative effects of oxidative reactions are the inactivation of key enzymes in cells. It was identified that the protein peroxides formed within cells are not always efficiently removed by enzymatic actions. Compounds such as thiols and ascorbic acid are capable of removing some of the peroxides. Reduced rate of reactive species removal was linked to dysfunction of cells.[145] It was also observed that, in D_2O the effect of $^1O_2$ was enhanced, thereby indicated that heavier medium does not readily quench their activity. In contrast, in the presence of azide, the activity of $^1O_2$ was found to be reduced.[137]

As seen above, oxidative stress leads to the formation of oxidised proteins, for cells to maintain good viable state, such proteins have to be constantly quenched or degraded. Unfolded proteins activates degradation signal, which is an important activity to sustain cell viability.[139] Oxidised proteins are mainly degraded by proteasomal and lysosomal pathways, and incomplete degradation results in accumulation of protein residues within cells, thereby eventually leading to the development of wide range of human pathologies.[140] The proteolytic enzyme proteasome is present throughout the cells, majority of them in nucleus relative to cytosolic regions, it helps in continuous removal of oxidatively modified proteins. Detoxification of oxidants could be either through enzymatic actions like SOD, catalases and the glutathione system, or by chemicals species of low molecular weight called antioxidants (**Section 1.1.4**).[139]

Oxidised proteins can lead to aggregation and cross-linking effects, known as a secondary damage or a bystander effect.[146] Direct covalent cross-linking bond formation could occur between the reactive ends of the oxidised terminals and the side chains of reactive amino acids, alternatively,

indirect bond formation could occur having bifunctional molecules like aldehydes in between. Aggregations formed are insoluble in nature and non-degradable by enzymes, and when sufficient levels get accumulated they becomes lethal to cells. Hence, degradation is an important process to prevent the formation of aggregation.[139]

1.1.3.2 Measuring cellular oxidative stress

Various types of probes for detecting ROS of different kinds had been considered under **Section 1.1.1.3**, and this section focuses on detection of ROS in biological environment. In selecting a probe for detection, multiple parameters had to be considered. Some of which include, the specificity, the rate of reaction, the photo-stability of luminescent based probes and the extent of availability (distribution) in the regions of cells considered.[65] Routinely used methods of detection for oxidised proteins include SDS-gel electrophoresis, electron spin resonance spectroscopy, fluorescence, HPLC, GC-MS, immunoassays, ELISA, immunohistochemistry, RP-HPLC, MS, sodium dedecylsulfate-polyacrylamide gel electrophoresis (SDS-PAGE), chemical methods like proteolysis, hydrolysis, cyanogen bromide (CNBr) cleavage of amino acid analysis, electrochemical detection, ^{1}H-NMR and combinations of other methods.[143]

Oxidative stress in biological systems could be determined by measuring redox potentials, radicals, markers from oxidative damage or by quantifying the antioxidant defence system. For direct quantification, spin trapping methods together with electron spin (pair) resonance (ESR or EPR) could be used. For indirect quantification, markers of oxidative stress can be measured. Oxidised products of DNA damage (e.g. 8-OHdG), lipid peroxidation process (e.g. MDA or isoprostane), protein damage (e.g. carbonyl peroxidation) and immunohistochemical markers could be used for their determination. Evaluation of specific low molecular-weight antioxidants, antioxidant enzymes and total levels of antioxidants are used for quantifying the antioxidant defence system.[39]

ROS in biological systems

Probes used in the biological oxidising environment include, fluoresceins, phenoxazines, ethidines and rhodamines based dyes (**Figure 1.8**).[65] Fluoresceins, $DCFH_2$ for example, it is the most commonly used probe for measuring reactive species in cells. Phenoxazines, Amplex Red is an example of this type and its reactivity is similar to that of $DCFH_2$. Ethidines, hydroethidine for example, it is highly reactive towards $O_2^{\bullet-}$ radical, thus enable both extra- and intra-cellular $O_2^{\bullet-}$ radicals to be detected. Rhodamines, dihydrorhodamine (RhH_2) for example, on reaction with radicals like $HO^{\bullet}$, carbonate ($CO_3^{\bullet-}$) and $NO_2^{\bullet-}$, the dye become fluorescent. It can also react with $O_2^{\bullet-}$ and H_2O_2, in the presence of a catalyst, hence can be used for fluorescence based detection. Fluoresceins and rhodamines are also used as probes for $^{\bullet}NO$ detection.[65]

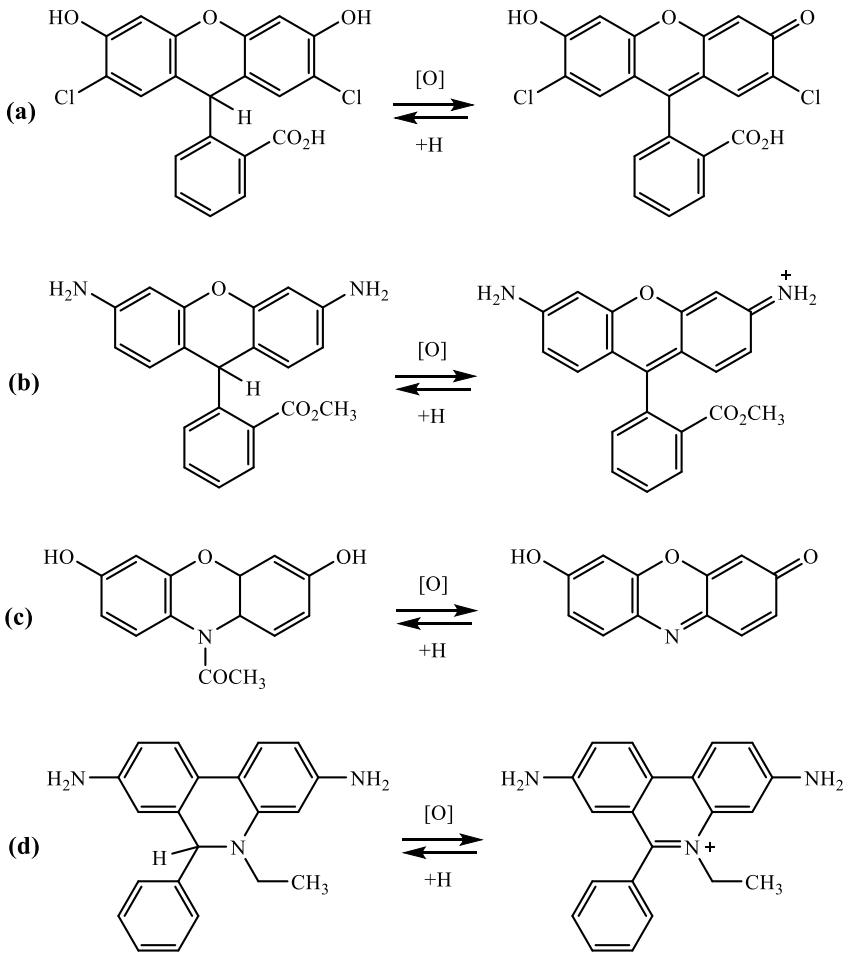

Figure 1.8: *Common probes used for ROS detection in biological systems, reduced (left) and oxidised (right) forms of* **(a)** *dichlorodihydrofluorescein,* **(b)** *dihydrorhodamine,* **(c)** *Amplex red, and* **(d)** *hydroethidine.*[65]

Luminescence is used *in vivo* as the main method of identifying $^1O_2$ on skin constituents (body surface).[67] Generation of $^1O_2$ was observed on sunlight illumination of air-saturated *p*-aminobenzoic acid (PABA), which is used as one of the active ingredients in sunscreen preparations. Furfuryl alcohol (FFA) is a water-soluble $^1O_2$ trapping agent,[147] it is incorporated in sunscreen, where it serves as a trap for $^1O_2$, thereby reduces harmful effects on skin surface.[148]

1.1.4 Chemical and biological antioxidants

All aerobic organisms have antioxidant defence system. It has also been proposed that the evolution of species was as a result of low antioxidants present in the ancient Earth.[1] ROS is constantly generated by cells from various metabolic activities. Cells possess antioxidants to defence themselves against their own cytotoxic waste.[37] When the balance between generation of ROS and their quenching rate is altered, that is, reduction in removal of ROS results in oxidative stress. From the chemical point of view, any substance that is capable of preventing oxidation by oxidants is called an antioxidant. From a biological point of view, the "action of antioxidant" should protect biological organisms from ROS at its fundamental levels, which include cells, tissues and organs.[38] Defence against oxidative stress is primarily grouped into three types of action, prevention of developing an oxidative stress condition, defence using antioxidants and repairing using enzymes.[39, 149] The direct consequence of decrease in antioxidant enzymes or molecules is the increase in oxidative stress, as a result of reactive species accumulation.

Eye is one of sensitive organ with high levels of antioxidants, where unsaturated fatty acids are protected by them.[3] Biological antioxidant defence system consists of mainly three groups, non-enzymic, enzymic (direct) and enzymatic (ancillary enzymes). Examples of non-enzymic systems include vitamin C (ascorbic acid), vitamin E (α-tocopherol), glutathione (GSH), melatonin, α-lipoic acid, ellagic acid, uric acid, β-carotene, quercetin, ubiquinone-10, lycopene and caffeic acid.[1, 3] Enzymic (direct) are of three types, namely SOD, GSH peroxidase and catalase.

Conjugation enzymes, GSSG reductase and repair systems are grouped as enzymatic.[149]

The overall function of antioxidant like glutathione peroxidases (GPxs) is to prevent cancer initiation, through the removal of hydroperoxides formed in cells. Hydroperoxides can act as pro-(at lower levels) and anti-carcinogenic (at high levels), hence its regulator GPxs. In cancer cells GPx-1, -3 and -4 are down-regulated, while GPx2 is up-regulated. The down- and up-regulations are directly or indirectly related to favour tumour growth and metastases.[150]

The antioxidant behaviour of a molecule depends on its surrounding. Vitamin C (ascorbic acid) destroys nitrosamines and free radicals, and it is an important antioxidant in human plasma.[38] Vitamin E (α-tocopherol) destroys lipid peroxides, and according to *in vitro* studies it is known that it prevents cytotoxic action of polyunsaturated fatty acids (PUFAs). Functions of some of the other antioxidants are, β-carotene destroys $^1O_2$, catalase destroys H_2O_2, and GSH reductase destroys H_2O_2 and lipid peroxides.[3]

SOD was the first type of antioxidant enzyme known, and there are three types found in human cells; copper-zinc SOD (Cu, Zn-SOD), manganese-SOD (Mn-SOD) and Extracellular-SOD (EC-SOD). The most important type of intracellular antioxidant is Cu,Zn-SOD.[38] All SODs have the same function of reducing (addition of protons) $O_2^{\bullet -}$ into O_2 and H_2O_2, the latter is further reduced to H_2O (**Equation 1.5**).[2, 151] SOD deficiency can cause increased sensibility to hyperoxia in children with monosomy, and increased SOD expression can results in increased H_2O_2 production, which could lead to inactivation of glycolytic enzymes such as phosphate dehydrogenase and fructose bisphosphatase.[38]

$$2O_2^{\bullet -} + 2H^+ \longrightarrow H_2O_2 + O_2$$

$$H_2O_2 + 2H^+ \longrightarrow 2H_2O$$

Equation 1.5

1.2 Cancer, PDT, Oxidative stress and Immunology

This section covers the overview of what is cancer, the stages in the development of cancer, the relation to oxidative stress, some of the types of treatments used for treating the disease, and the role of immune system in enhancing the PDT treatment *in vivo* into a prolong antitumour immunity. Further, the biological components that would be used for studying the oxidative stress reactions have also been discussed.

1.2.1 Cancer

At high concentrations (oxidative stress) reactive species are harmful, and at moderate concentrations they are vital for metabolic activities, for example, ROS like H_2O_2 is involved in cell signalling processes.[152, 153] Physiological functions of signalling molecules include signal transduction, production of erythropoietin, monitoring and regulations of vascular tone and oxygen tension for ventilation control.[152] As ROS are essential for signalling or attack against pathogens, they are continually produced by living organisms, and the damages associated with their production are always present in cells. However, if the degree of damage is not controlled, it would lead to oxidative stress. Oxidative stress can result from both endogenous and exogenous sources. Damages to DNA through oxidative reactions had been the common reason for mutagenesis in a normal human cell.[27] Oxidative attack on signalling proteins, could lead to their functions being lost, gained or altered.[152] As a result of altered activities of cell function, it eventually results in the development of diseases like cancer. Various types of cancers that are related to oxidative stress are provided in **Table 1.2**,[2] which was adapted from reference **2** and expanded.

Some of the common intra- and extra-cellular sources of ROS, and intracellular antioxidants are shown in **Figure 1.9**. External stimuli such as radiation, UV, chemotherapy and conditions such as hypoxia, cytokines and growth factors secretion can induce production of ROS. Internal defence enzymes such as catalase, SOD, peroxidase and thioredoxin reductase; and secretion of peroxiredoxin and glutathione, reduces or inhibits generation of oxidative stress environments, through the elimination of ROS formed.[2]

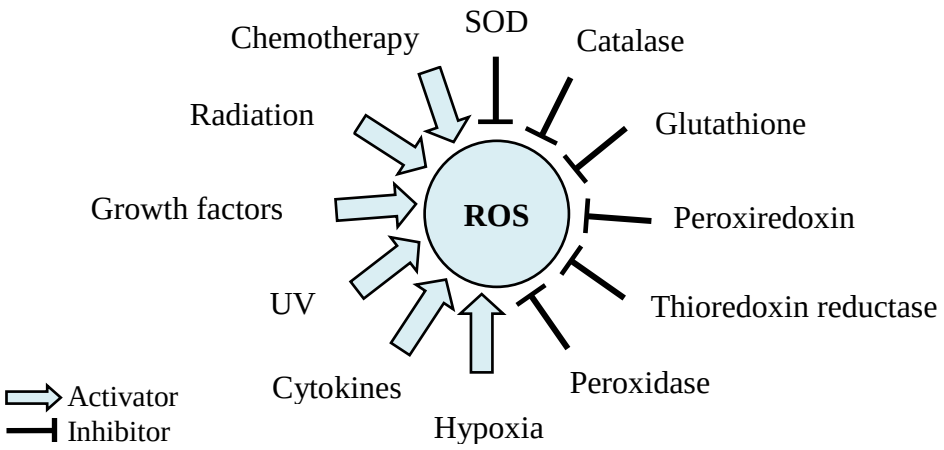

Figure 1.9: *Activators and inhibitors of ROS.*[2]

In recent years, it had been identified that oxidative stress not only causes genomic instability, but also activates signalling pathways which supports tumour development through the processes such as cellular proliferation, angiogenesis and metastasis. In animal models, increased levels of oxidatively modified DNA bases are used as a fingerprint to verify radical attack on DNA. For example, conversion of base 8-hydroxygunosine (8-OHG) into 8-hydroxydeoxyguanosine (8-OHdG) is due to radical attack.[2]

Table 1.2: *Cancers that are related to oxidative stress*

Cancer types	**References**
Bladder	154
Brain tumour	155, 156
Breast	157-161
Cervical	162
Gastric (stomach)	163, 164
Liver	165
Lung	166, 167
Melanoma	168-170
Multiple myeloma	171
Leukemia	172
Lymphoma	173, 174
Oral	175
Ovarian	176
Pancreatic	177, 178
Prostrate	179, 180
Sarcoma	181

1.2.1.1 Stages in the development of cancer

Carcinogenesis is a multistage process, and is grouped into three main stages.[24, 182] They are initiation, promotion and progression, with ROS having a role in each stage (**Figure 1.10**).[2] Exposure of normal (healthy) cells to conditions such as oxidative stress and high energy radiation could induce DNA mutations and DNA-related damages. If the damaged genetic materials were to be not completely repaired, it could lead to *initiation* of abnormal cell development. Such initiated cells could be reluctant to undergo one of the regular important homeostatic events of programmed cells death (apoptosis). Abnormal gene expression, blockage of cell-to-cell communication, modification of second messenger system and anti-apoptotic nature of the transformed cells could lead to formation of many more similar cells, known as the *promotion* stage. If the group of cells continues to be resistance against apoptosis and if their proliferation continues with increasing alterations induced by oxidative stress, it is known as the *progression* stage, which results in the formation of neoplasia (neoplastic cell state). Neoplasia cells would lead to the formation of tumours.[24, 183, 184]

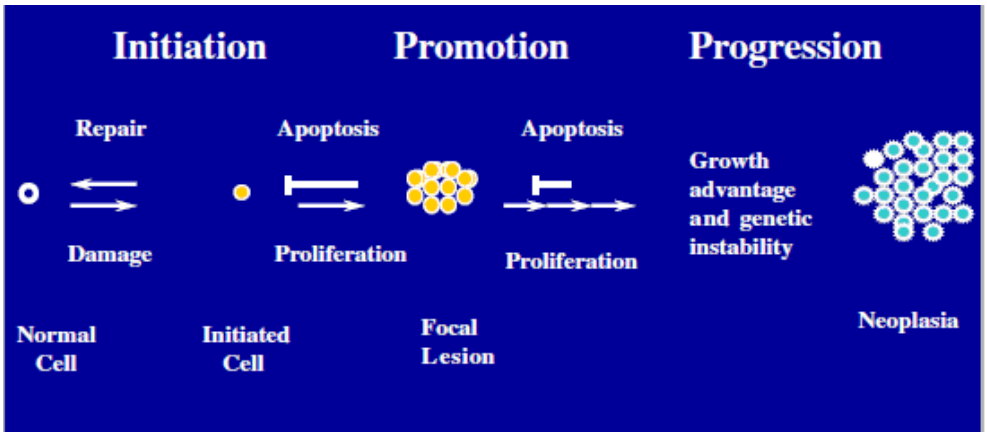

Figure 1.10: *Formation of primary tumour from a normal cell.*[183]

In addition, if the cells attain growth signal independence at any of the stages in the development of cancer, their proliferation would continue for ever until physical parameters do not counter balance with their growth rate. At this point tumour growth can be divided into two phases, avascular and vascular. In the former, low levels of oxygen and nutrition supply could be a

major limiting parameter, and it occurs when the tumour size reaches 1- 2 mm in diameter. When it occurs tumour remains dormant, and is referred to as benign state.[185] To overcome their limitations, tumour cells secrete diffusible tumour angiogenesis factors known as vascular endothelial growth factor (VEGF), which induces the growth of blood capillaries, from main blood vessels supplying the organ with essential nutrition towards the tumour. Angiogenesis is a physiological process through which new blood vessels branches out of the existing ones, this is a default procedure during growth and development of animals. In 1971, it was identified that tumours can also secrete excess of angiogenic factors, which favours the growth of new blood capillaries for providing transport of nutrition and exchange of gases.[186] Newly formed blood capillaries not only supply the tumours with all the essential nutrition required for their rapid growth, but they also provide pathway for primary tumour cells to reach the main blood stream, and thereby to be carried away to anatomically distance organs sites, through a process known as metastases, which increases the survival chances of tumours relative to normal cells. The latter is the most severe condition of this disease, and it causes the most common form of cancer related death.

Metastases of primary tumour are the later stages in the process of progression. It start with local invasion of surrounding healthy cells, followed by intravasation into blood vessels, after managing to survive several obstacles (immune response and physical forces like shear stress) in the circulation, cells stops at a distance site, and through extravasation it reaches the close by organ, where it adapt to thrive in the unfamiliar microenvironment and form colonies of cells to a size that are clinically detectable (**Figure 1.11**).[187] The transforming growth factor-β (TGF-β) modulates cell invasion, microenvironment adaptation and immune regulation. TGF-β is also involved in tumour-suppression effect; hence, its non-regulation could result in development of tumour.[188]

Compositions of cell membranes are vital for cell-cell interactions.[126] Major part of membrane phospholipids are made of PUFA and are highly

susceptible to undergo radical mediated damages, which in turn influence the dynamic state of the cell membrane.[189] A correlation was found between lower phospholipid : protein ratio, higher cholesterol : phospholipid ratio, and decrease in both rate of lipid peroxidation and fluidity of tumour plasma membranes.[126] In the process of invasion by tumour cells, physical properties of epithelial cells are altered and the motility of cells is increased. Cancer cells generate high levels of ROS and they are capable of evading apoptosis.[150] ROS (oxidative stress) also controls the expression of intracellular adhesion molecule-1, (ICAM-1) present in endothelial and epithelial cells.[2]

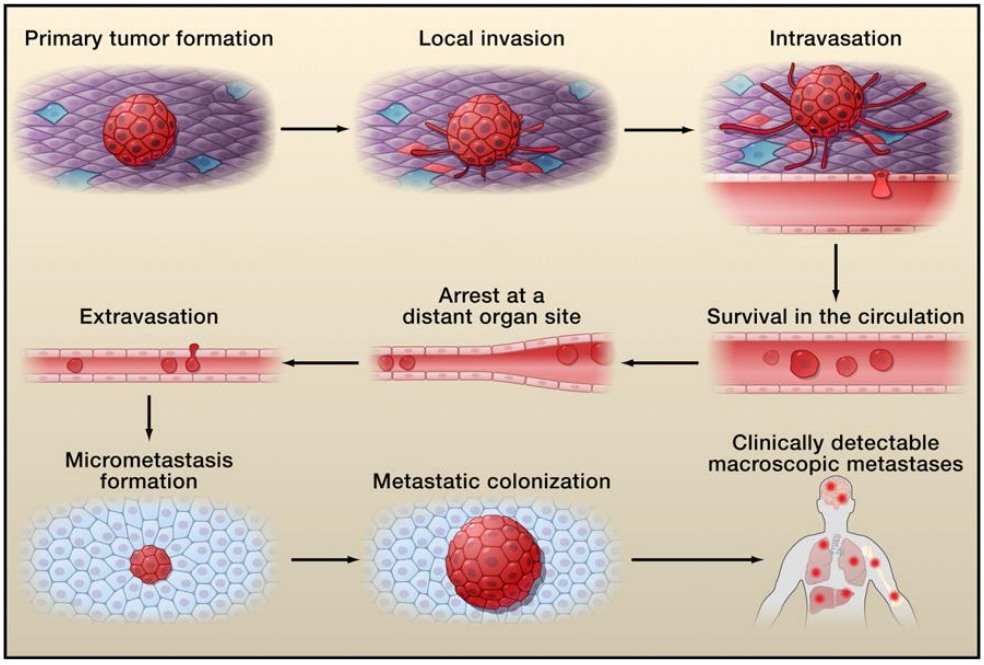

Figure 1.11: *The process involved in metastases of primary tumour.*[187]

1.2.1.2 Characteristics of cancer

Ninety five percent of all cancers had been related to inflammation induced, by life style and environmental stimuli.[190, 191] It had been estimated that, about 15-20 % of human tumours are initiated by infection driven inflammation,[192] and about 15 % of all cancer are initiated by virus.[193] There are certain features that are not found in normal cells but are present in cancer cells, which are used to selectively distinguish the cancer cells. Some of the key characteristics (or hallmarks) of cancers include, the potential to

replicate infinitely, non-responsiveness to anti-growth signals, producing their own growth signals, bypassing apoptosis, uninterrupted angiogenesis and metastasis.[194] After a decade of research from the identification of the above six hallmarks of cancer, evading immune destruction and reprogramming energy metabolism have been proposed as two other additional hallmarks of cancer.[195]

Growth factor independence is one of the hallmarks of cancer, and it results in sustained cell signalling. For example, when endothelial growth factor (EGF) binds to the receptor on the extracellular domain of cell surface membrane, it induces phosphorylation at the intracellular domain of the receptor. The phosphorylated receptor activates several signal transduction pathways, some of which include DNA repair, gene transcription, anti-apoptosis, proliferation, angiogenesis and invasion (**Figure 1.12**).[117]

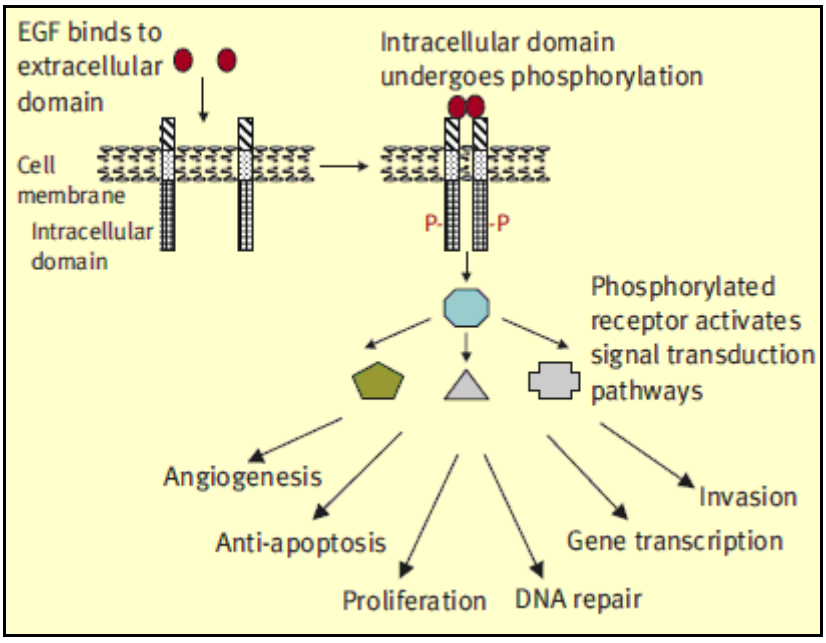

Figure 1.12: *Growth factor independence leads to sustained signalling.*[117]

The biological sites such as cancer tissues, infected tissues, rheumatic joints and wound have some similar properties. They are the additional blood supply, the lower levels of oxygen (a condition known as hypoxic) relative to healthy tissues, and the presence of major type of innate immune cells, leukocytes (major subset of neutrophils and macrophages).[196, 197]

Hypoxic condition results from low blood flow rate (or supply) to the regions containing higher number of cells. Under hypoxic condition, about 30 different genes are regulated by hypoxia inducible factor (HIF)-1α. Hypoxia causes the major subsets of leukocytes to activate several of their genes including the one responsible for VEGF secretion, which is responsible for leaky blood vessels. VEGF secretion depends on the activation of genes by HIF-1α binding to HIF-1β, the binding interactions itself dependent on the levels of oxygen. Hypoxia caused through HIF-1α, activates $^{\bullet}$NO production by $^{\bullet}$NO synthase. $^{\bullet}$NO induces inflammation effects, including swelling, and is used by macrophages to destroy microbes. During respiration, inhibition of electron transfer to $^{3}O_2$ by $^{\bullet}$NO, results in leaking of electrons to form $O_2^{\bullet-}$.[152, 196, 197]

Mutated or modified genes express aberrant patterns, in terms of cancer related theories these patterns could be divided into two groups, tumour suppressor genes and oncogenes. Under certain conditions like oxidative stress, tumour suppressor genes are inactivated (phenotypically recessive) and the oncogenes are activated (phenotypically dominant).[117] Tumour suppressor genes are involved in multiple roles of cell growth facilitation like regulation of cell proliferation, differentiation, tumour angiogenesis and many others.[198] NAD(P)H oxidases (NOX) generate $O_2^{\bullet-}$,[152] and are also involved in the activation of oncogenes, regulation of redox-sensitive signalling pathways leading to cancer development and progression, and in the inactivation of tumour suppressor proteins.[199] Specific point mutation could also lead to activation of oncogenes, and amplification of such genes combined with the synthesis of proteins, alter the biological nature of the cell, hence their fundamental activities.[117] The retinoblastoma protein and the p53 transcription factor are the two important regulators disrupted in cancer cells.[200] The oncogenes *ras* and *myc* were linked to tumour angiogenesis.[201] On the other hand, destruction of tumour suppressor genes during mutation could also inactivate their activity, for example, germline mutations could lead to cancer syndromes. Hence, the net result of tumour suppressor gene inactivation or the activation of oncogenes is the development of cancer.[117]

In addition to the number of adverse effects caused by primary and metastases tumour cells, they do affect the functional neighbouring cells. For example, a higher chance of diabetes developing probability was observed in the patients possessing pancreatic adenocarcinoma, in which the function of insulin secretion and regulation of sugar levels had been affected.[202]

1.2.1.3 Cancer treatments

There are several forms of severe diseases without complete cure. Generally the side effects associated with the use of drugs limit the extent of treatments. Practically most drugs have either short or long term side effects. From several decades of research it is known that there are several forms of cancers, and the cancer cells do not have much variation from that of normal healthy cells. Hence the use of single mode of treatment for cancer had been indefinable, due to the complexity of the biological environment in which they are located. Anticancer treatments using drugs are divided into four groups; chemotherapy, hormonal therapy, targeted therapy and immunotherapy. *Chemotherapy* involves the use of cytotoxic agents specifically designed to interfere with DNA synthesis and cell division. *Hormonal* therapy uses drugs that interfere with hormone receptors on cancer cells to hamper their proliferation signals. *Targeted* therapy makes use of kinase inhibitors and antibodies, to target and inhibit the cancer growth signalling pathways. *Immunotherapy* induces and amplifies anticancer immune response.[193]

Chemotherapy drugs are synthesised to target and interrupt with cancer cells through three different mechanisms of action; (1) through the destruction of mitotic spindle formation with the use of drugs such as pacitaxel (Taxol®). Formations of spindle are important for successful mitotic cell division process, by preventing it, cell proliferation is stopped; (2) through targeting and causing damages to nuclear DNA using drugs such as *cis*-platin (Platinol®), which chemically damages the structure of DNA and RNA, by binding to the minor groove region of the DNA double helix; (3) by blocking synthesis of components (nucleotides) essential for DNA

synthesis, using drugs such as fluorouracil (Adrucil®). There are also other forms of anticancer agents like mitocans, which acts by causing destabilisation to mitochondrial function.[203]

Success of chemotherapy is also partly dependent on the activation of immune system. Hence it was proposed that, combining immune stimuli with cytotoxic chemotherapy agents would enhance (enforce) immune response following chemotherapeutic treatments. Immune stimuli would be responsible for inducing antibodies for cancer vaccines and toll-like receptor (TLR) agonists, these factors target the immune checkpoints; cytotoxic T-lymphocyte associated protein 4 (CTLA4), programmed death 1 (PD1), programmed death ligand (PDL)1 or PDL2. As an example, full therapeutic efficacy of chemotherapeutic drug, imatinib (Gleevec, Novartis), against *myc*-oncogene addicted tumour cells were realised, only in the presence of immune cells CD^{4+} T-cells.[193]

Other forms of cancer treatments

G-protein coupled receptor (GPCR) is the largest family that is involved in cell transduction with more than 800 members, which is approximately coded by 4 % of the human genome. They have 7-transmembrane domain structure with the N-terminal outside the cell and the C-terminal facing the cytosol. GPCRs are also involved in several physiological processes such as cardiac functions and immune functions. Hence malfunctioning of these proteins had also been linked to some of the most common disease like cancer. Greater than 25 % of the drugs on the market targets GPCRs either directly or indirectly, hence it had been proposed that using the information on those drugs, novel strategies could be developed to target aberrant GPCRs for cancer prevention and treatment.[204]

The levels of copper (Cu) in serum and tissue were compared between normal patients and cancer patients. It was found that the cancer patients had higher levels of copper relative to the normal patients. This was true for all the chosen forms of cancers, and it was significantly different in most forms of cancers.[23] Hence, it had been proposed that, the elevated levels of

Cu in malignancies could be used as a potential target for treatment against cancers. D-pen is an example of an anticancer agent targeted at Cu levels.

Essential fatty acids (EFAs) like γ-linolenic acid, arachidonic acid, eicosapentaenoic acid and docosahexaenoic acids, show antitumour activity through the induction of tumour cells to undergo apoptosis. Fatty acids (FAs) are active in inducing apoptosis only in tumours cells over-expressing cytochrome P450. B-cell lymphoma-2 (*Bcl*-2, an integral membrane protein) was capable of inhibiting long chain FA induced apoptosis, while the phosphorylated form of *Bcl*-2 enhanced oxidative reactions on lipids thus forming apoptotic cell death. Cells treated with long chain FAs led to increased lipid peroxidation and phosphorylation, with the reduction in the overall amount of antioxidants. The above observations led to the conclusion that, long chain FAs induce apoptosis by suppressing *Bcl*-2 expression through phosphorylation, and by amplifying lipid peroxidation and P450 activity.[116]

Higher than 50 % of the fifteen published trials suggested that, stress management through psychotherapy and support, alters cancer progression rate. Further, the study suggests that no adverse effects on cancer survival were observed with the use of psychotherapy. It was also predicted that, under stressed conditions shorter cancer survival could be linked to factors like reduced activities of natural killer cells, sympathetic nervous system activation of VEGF, and increased level of pro-inflammatory cytokines.[205]

1.2.2 Photodynamic therapy (PDT)

The photophysical and photochemical properties of photosensitisation had been considered under **Section 1.1.2**. This section covers the nature of photosensitisation reactions *in vivo* and *in vitro* for the generation of localised oxidative stress environments, and its importance for treating diseases like cancer through the induction of immediate and long-term (antitumour immunity) effects.

In vivo, ROS generation could be induced as a result of endogenous metabolic activities such as aerobic respiration or can be triggered by external factors such as high energy electromagnetic irradiation, UV rays for example. For systematic generation of ROS, photosensitisation reactions could be used, this technique is utilised in photodynamic therapy (PDT) reactions. The concept of PDT reaction is similar to radiotherapy, the key difference being that PDT primarily generates $^1O_2$, while radiotherapy generates $HO^{\bullet}$ radical.[206] PDT is a successful and a promising treatment method used for treating a variety of neoplastic diseases[207] like cancers and skin disorder conditions. Its uses have been reviewed many times in the recent years.[208]

PDT is minimal invasive, more selective relative to chemotherapy, can be repeated several times, and toxicity of photosensitisers are lower in the absence of light. It causes cellular destruction through a free radical oxidative process, and it does not affect the connective tissues. The extent of scarring is lower relative to thermal reactions, and it does not affect nerves and blood vessels, but as a desirable feature, it would affect blood capillaries entangled with cells or tissues at the site of treatment.[208]

PDT makes use of visible light for the activation of photosensitisers (**Section 1.2.2.3**). Chromophores are naturally present within cells. However, for PDT reactions, visible light excitable photosensitisers with known properties are administered, and allowed sufficient time for internalisation and localisation within cells of the tissues, before irradiating with light.[209] All sensitisation reactions have a common mechanism of action; type II ($^1O_2$ or ROS generation) or type I (radical products) mechanism **Section 1.1.2.1**).[93] The rate of $^1O_2$ production depends on the amount of photosensitiser internalised,[96] oxygen concentration and light dose, hence the efficacy of the PDT reactions.[210, 211] The second generation photosensitisers like phthalocyanines, show increased PDT effects with reduced side effects.[93] It was also shown that intracellular viscosity within a cell increases during photoinduced cell death.[212]

PDT can be used against drug-resistant malignant cells or tissues. Various studies have suggested that PDT mainly induce apoptosis[138] and not necrosis. However, depending on the site of sensitiser location, apoptosis might or might not be observed. Apoptosis is induced by mitochondria localised sensitisers such as Photofrin, and protoporphyrin IX secreted through 5-aminolevulinic acid (ALA)-induction.[58] It was proposed that, following PDT using Pc 4 as the sensitiser, induction of apoptosis could be the result of the formation of lipid hydroperoxides and protein oxidation products.[40, 141] Necrosis is primarily caused by plasma membrane bound sensitisers.[58] Fragmentation of DNA through secondary ROS, generated by the photosensitisation of cellular membrane bound photosensitiser (deuteroporphyrin) had also been demonstrated in human lymphoblast WTK-1 cells. It had been predicted that, products of lipid peroxidation could be the secondary form of ROS that were responsible for the above observation. It was also shown that α-tocopherol acetate localised in membrane and cytoplasmic (trolox) antioxidants inhibited DNA damage.[47]

1.2.2.1 Treating cancer using PDT

Photosensitisation process involved in the generation of $^1O_2$, the direct and indirect effects of oxidative stress on cells and tissues around the region of its generation are shown in **Figure 1.13**. *In vivo*, the key processes involved during or following the photosensitisation reactions are, the destruction of malignant cells and tissues through induction of apoptosis and necrosis,[83] inflammation, immune cells (dendritic cells (DCs) and neutrophils) are recruited to the site of damage, and causes shutdown of microvessels supplying essential nutrition to the solid tumour. *In vivo*, non-internalised (delocalised) photosensitisers in the tissue environment could have non-specific PDT effects on healthy cells surrounding cancer (sarcoma) cells. The induction of local acute inflammatory response are developed as a result of activation of alternative pathways, damages to tumour and stromal cells, induction of signalling cascades, and early vascular modifications.[206]

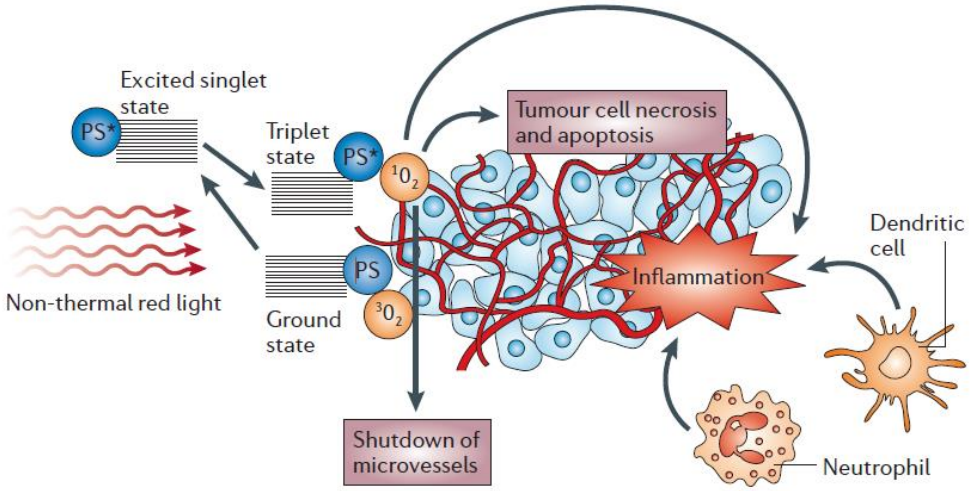

Figure 1.13: *The PDT mechanism of action on tumours.*[83]

There are three forms of cell death (**Section 1.1.3**) that could occur following PDT. 1) Apoptosis, main form of damage if the photosensitisers were to be predominantly localised within the cellular organelles like mitochondria or endoplasmic reticulum (ER), 2) necrosis, when photosensitisers mainly localised in plasma membrane or lysosomes, and 3) autophagy associated cell death, which is a process to eliminate photo-oxidatively damaged cellular components like proteins, when the process becomes ineffective it leads to cell death.[206]

PDT experiments *in vitro* and *in vivo* do not exactly produce the same results.[83] It was also reported that the optimal PDT regimen for producing local tumour cures, were not the same as for producing inflammation and stimulating immune responses.[83] *In vitro*, the main outcomes of tumour PDT treatment are the induction of apoptosis and necrosis. The rate and the ratios of these processes (apoptosis and necrosis) depends on features like the total PDT dose, intracellular localisation of photosensitisers, the fluence rate, oxygen concentration and the type of cells being treated.

In vivo, PDT reactions are also conducted in combination with immune stimulatory agents to activate the immune system, PDT with microbial adjuvants for example. PDT with microbial adjuvants involve injection of innate immune response inducing factors derived from micro-organisms

into tumours or its surrounding regions before, during or after PDT treatment. In a study of this class, the activation of TLRs or similar pattern recognition molecules on the surface of macrophages and DCs were observed.[83]

1.2.2.2 Localisation of photosensitisers and targets of photodamage

Auto-fluorescence of cells

Cells can fluoresce even in the absence of an external fluorescent chemical agent, it is known as auto-fluorescence. Within cells, organelles such as mitochondria and lysosomes could act as sources of fluorescence. Fluorescence from mitochondria could be altered, but not the one from lysosomes. Auto-fluorescence could be observed with the use of high energy light such as UV rays.[213] Some of the chemical chromophores responsible for auto-fluorescence of a cell include, reduced nicotinamide adenine dinucleotide (NADH, Ex 365 nm, Em 450 nm), riboflavin and flavin coenzymes (e.g. flavin adenine dinucleotide, FAD, Ex 360 and 450 nm, Em 520 nm).

Photosensitiser internalisation by cells

Surface of a cell is a complex environment, where numerous proteins (receptors, channels), carbohydrates and other components like vitamins are embedded. Such complex environments also tightly regulate molecules that is internalised and released. The structural properties of photosensitiser have a huge impact on their availability around cells, hence on the rate of internalisation into cytosolic regions and organelles.

In conventional *in vitro* PDT reactions, the cells are incubated with a chemically well characterised photosensitiser of known concentration, and allowed to internalise for several minutes to hours. Following which the cells are washed and transferred to a photosensitiser-free medium, and irradiated with a known level of light dose. The PDT treated cells are incubated for a fixed length of time before being analysed using one of the standard methods of analysis like 3-(4,5-dimethylthiazol-2-yl)-2,5-diphenyltetrazolium bromide (MTT) assay. Hence the established methods

of PDT reactions commonly make use of internalised photosensitisers (intracellular oxidative stress), and do not involve having photosensitiser in solution (extracellular oxidative stress) during light treatment, that is, conventional *in vitro* PDT reactions mainly rely on the generation of intracellular oxidative stress. Similarly *in vivo*, photosensitisers are administered several hours before light treatment to allow internalisation by cells in the target regions. *In vivo* all photosensitisers would not be internalised, or the tissue fluid around the cells in the region of irradiation would not be free of photosensitisers. Hence, *in vivo* the photosensitisation reactions would generate both intra- and extra-cellular oxidative stress induced effects.

Targets of photodamage

Intracellular localisations of photosensitisers are crucial for efficient PDT action.[207] The luminescence properties of sensitisers are used to detect their region of localisation within cells. Regions of binding site can affect the intensity of fluorescence. Hence there is no correlation between the strength of photodynamic action and the strength of fluorescence. Further, due to small radius through which $^1O_2$ can travel before being quenched, the severities of photodynamic action at subcellular components are used for predicting the selectivity of the photosensitisers.[58]

To enhance selectivity and efficacy, photosensitisers are bioconjugated using functional group like isothiocyanate,[214] to biological macromolecules such as peptides and proteins[215] that have selective binding with the target malignant cells. Tumour cells usually express certain receptors more than the others.[216] On tumour cell's surface, low-density lipoproteins (LDL) and folate receptors are over-expressed, hence the photosensitisers conjugated to LDL or folate molecules would improve selectivity.[79] For example, rat bladder transitional cell carcinoma over-expressing transferrin receptor show selectivity towards liposomal binding. It was utilised in selectively accumulating $AlPcS_4$ conjugated to liposomal onto the carcinoma, where liposomal showed specificity towards the receptor.[216] In another test for selectivity, PEG coupled *m*-THPC showed improved tumour localisation *in*

vivo, where the conjugation did not alter the phototoxicity of the photosensitiser.[217] $AlPcS_4$ encapsulated in transferrin-conjugated PEG liposome was also used to selectively localise the photosensitisers onto HeLa cells overexpressing transferrin receptor.[88] Poor solubility of photosensitisers *in vivo*, under physiological conditions affects their efficacy. The portion of localisation of photosensitiser in tumour:normal tissues was about 15:2 for hydrophobic photosensitisers, and it was about 2:1 for hydrophilic photosensitisers.[79]

Tumour-selective accumulation of photosensitisers is crucial for better PDT outcome.[216] Photosensitisers conjugated to monoclonal antibodies (MAbs) are also used to improve selectivity of a photosensitiser towards a tumour site. In a study testing the latter, the potential of using a hydrophobic (*m*-THPC) and a hydrophilic ($AlPcS_4$) photosensitisers coupled to MAb were compared, in which $AlPcS_4$-MAb showed higher selectivity potential.[218] Increasing the specificity of photosensitiser localisation, towards a biological target site has also shown considerable growth in the recent times. Antibodies and their fragments have been utilised along with wide range of methods for achieving specificity.[219]

Organelle specificity

It was observed that, anionic groups bearing photosensitisers preferentially localised in cytoplasm and relocated to nucleus when illuminated, whereas cationic group bearing photosensitisers preferentially localised in mitochondria.[79] Targeting mitochondria is an essential feature of a photosensitiser to produce effective PDT outcome. Photofrin induced photodamage primarily occurs at mitochondria.[58] Chemicals like mitocans, selectively localises in mitochondria and destabilises its activity, thereby induces apoptosis.[203] The photosensitisers, porphycene monomer, monocationic porphyrin and lysyl chlorin p6 selectively localises in the organelles mitochondria, membranes and lysosomes, respectively.[58] Fluorescent probes such as rhodamine 123, DioC6(3) and rhodamine phalloidin are used for monitoring changes in organelles of cells following

PDT.[209] Internalised sensitisers are mostly found in organelles in the cytoplasm and not in the nuclei. Hence during PDT, the chances for DNA damage or mutations leading to carcinogenesis are lower.[58]

1.2.2.3 Delivering light energy

Conventional photosensitisation reactions make use of tissue localised photosensitisers for inducing tissue damage, through the generation of cytotoxic species, primarily $^1O_2$.[220] The amount of light dose on its own can be used to control the level of PDT action,[221] provided that all other conditions are maintained at optimum levels. *In vivo*, all conditions cannot be maintained at optimum levels at all times. For example, depletion of oxygen levels and photobleaching of photosensitisers hence reduction in their concentration, cannot be avoided with the progress of the reaction. Hence controlling all three independent dynamic variables of PDT would always be challenging, and in addition the biological complexity adds more variations over the control.[222]

The amount of light dose required for photosensitisation reactions during PDT depends mainly on the rate of restoring oxygen concentration, the rate of photobleaching and the quantum yield of the photosensitiser used. Commonly, longer wavelength (lower energy) electromagnetic radiations can penetrate tissues better than shorter wavelengths (higher energy). Most photosensitisers developed for PDT processes are such that they are suitable for absorbing energy in the visible spectrum for excitation, that is, in the wavelength region 380 to 720 nm.[97] Other than visible light, UVA and UVB are also used for treatment, UVA rays can penetrate deep into skin tissues relative to UVB rays, which results in excitation of cellular chromophores thereby $^1O_2$ generation.[67]

The relationship between the partial pressure of O_2 (pO_2) available at the site of tumour treatment, and the light dose are critical parameters for effective photodynamic therapeutic outcome, and this has clinical importance in determining the success of the treatment.[221, 223] The higher levels of irradiance, together with higher concentration of photosensitisers

would also result in inefficient PDT treatment,[224] while the use of lower fluence rates result in enhanced efficiency of the treatment, and also favoured normal cells survival.[220] It had been shown in clinical and preclinical settings, the use of high fluence rate results in rapid depletion of oxygen.[221] Alternatively, to improve efficiency without lowering the fluence rate, photosensitiser concentration has to be lowered.[225]

It is essential that sufficient amount of light energy reaches the photosensitiser for effective photodynamic action. The penetration of light depends on the permittivity (ε) of the medium it is travelling through. The ε of light in vacuum (ε_0) is 8.854 x 10^{-12} F m^{-1} (or C^2 N^{-1} m^{-2}), and the ε of light in air at Standard Temperature and Pressure (STP) is $1.0005\varepsilon_0$.[226] The ε of light in solid and condensed matter (e.g. tissues) are higher than in gas medium. As a consequence, the strength of penetration of light intensity (electromagnetic field) reduces with the increasing dense and length of the medium.

For photochemical reactions, light energy is delivered in the range of hundreds of Watts, whereas for photobiological reactions like PDT, light energy in the range of mW cm^{-2} is used.[88] PDT reactions make use of light sources like halogen lamp with filters,[88] laser sources and LED arrays,[227] the latter is used in applications like photodynamic treatment of skin lesions. Apart from the type of light source, it is also important to consider inhomogeneities in the uniformity of the light sources, when calculating the light doses to use in PDT.[227]

$^1O_2$ generation is directly proportional to $^3O_2$ consumption. The rate of $^1O_2$ would increase with the amount of photosensitisers and fluence rates. Mathematical models and experimental data agreed on the fact that, during photosensitisation reactions tissue oxygenation is a dynamic process and light dose dependent. The rate of oxygen consumption within tissues could be influenced by photobleaching and quantum efficiency of photosensitisers, and slow rate of gas exchange with the environment of the tumour site. To maintain adequate levels of oxygen during PDT, the use of

low fluence rate or the fractionation of light delivery (light and dark intervals in the range of 20 to 50 s) are two common approaches. Treatments involving the use of these two approaches showed higher effectiveness in delaying re-growth of tumours.[58] Hence, the rate at which the light energy is delivered influences the success of the photosensitisation reactions.

PDT associated vascular damage results in long term tumour control. The vascular effects depend on the type of photosensitiser. The use of high fluence rate protects microvascular patency, while low fluence rate causes shutdown of normal microvascular perfusion. For example, patients treated for basal cell carcinoma lesion using Photofrin (1 mg kg^{-1}), and high light dose of 150 mW cm^{-2} was found to be ineffective (no effect) due to rapid depletion of $^3O_2$.[58]

1.2.2.4 The effects of PDT on cancer

PDT is a FDA-approved modality, and is capable of inducing immune response.[228] It is an effective treatment against diseases like head and neck tumour lesions.[208] $^1O_2$ generated by the internalised or cell membrane localised photosensitiser, affect varieties of lipids and proteins (**Section 1.1.3.1**) present around its region of generation. Lipids of cell surface membrane get oxidised by ROS to yield lipid hydroperoxides, which transfer the effect within the cells by altering the surrounding molecules.[206] In addition to the destruction of tumours, the treatment also destroys factors like urokinase plasminogen activators (uPA), vascular endothelial growth factors (VEGF) and matrix metalloproteinases (MMPs), which could otherwise induce invasion and metastasise of tumour.[208] PDT also leads to vascular damage, activation of immune response and induction of inflammation at the site of photosensitisation reaction, which would activate immune response that could lead to anticancer immunity (**Section 1.2.3.1**).[206] Swelling and formation of necrotic tissue had been observed as two common properties of PDT causing direct cytotoxicity and microvascular damage.[208]

Following 24 hours from PDT, 235 genes were significantly up-regulated on top of the early PDT response genes such as FOS, JUN, heat-shock protein (HSP) and histone genes. Some of the other key genes up-regulated following PDT include aldo-keto reductases, chemokine fibroblast growth factors, HSP40-genes, and interleukin genes. Their important functions are the attraction and activation of immune cells (granulocyte), and in angiogenesis. It was deduced that combining PDT and chemotherapy would enhance antitumour responses.[229]

All PDT treatment does not become a complete form of treatment. It has certain drawbacks like incomplete removal of tumour on the margins of treated lesion. Depending on the rate of photosensitiser clearance from the circulation, light sensitivity could also last up to six weeks from the time of treatment. Chemotherapy, operations and radiotherapy are the conventional and the alternative forms of treatments to PDT.[208] In addition to the use of photosensitisation reactions for treating malignant cells or tissues, it is also used to eliminate microbial species, hence suitable for decontamination processes.[230] Varieties of biological assays are used to determine range of influence on cells exposed to oxidative stress environments (photodynamically treated),[47] and some of them are considered in **Section 1.2.4**.

1.2.3 Oxidative stress (PDT) induced activation of immune system

Though it is not always the case *in vitro*, *in vivo* (in rodent) for the tumour systems treated using several photosensitisers, the direct PDT tumour cell kill was found to be less than 2 logs, while 6-8 logs reduction were required for tumour cure.[58] It was also identified from multiple researches that, in addition to the direct destruction of tumour cells by photosensitisation treatments, other different forms of mechanisms should exist to make the treatment much more effective, than what would be expected from the duration of PDT alone. The activation of the immune responses at the site of vascular damages were identified as the cause for the added effectiveness.[206]

1.2.3.1 Antitumour immunity

The direct consequence of selective localised oxidative stress (PDT action) is that it can oxidise key cellular components like receptors, signal transduction channels and molecules, along with the induction of up- or down-regulations of gene expressions. PDT can also leave behind number of photo-oxidatively damaged cellular components from numerous apoptotic, necrotic or autophagy cells. These oxidised materials can induce immune response through several indirect methods. Antitumour immune response was first demonstrated in 1994, when PDT treated tumour-draining lymph node (TDLN) cells were transferred to naive host, development of resistance against subsequent tumour challenge was observed. In 1999, the above demonstration of antitumour immune response was re-tested by a different research group, and concluded that immune memory gets generated following PDT treatment.[228, 231] From multiple studies like above it is clear that, photosensitisation reactions *in vivo* activate antitumour immune response.[83]

PDT has the ability to stimulate and suppress different parts of the immune system, various induction and inhibition target pathways are involved in it.[83] It was also observed that cancer therapy which principally induces necrosis activate the immune system more effectively than the methods that predominantly kill cells through apoptotic pathway. *In vivo*, within minutes from the PDT reactions, neutrophils are attracted to the site of inflammation. It was hypothesised that these immune cells acts as a coordinator of antitumour response.[228]

There are two stages of inflammation, initial stage known as acute inflammation and the secondary stage called chronic inflammation. PDT initiated inflammatory signalling pathways initiates and supports large accumulation of leukocytes, monocytes (macrophages), mast cells and neutrophils. Neutrophils rapidly accumulate at the site of PDT treatment, and remains within tumour blood vessels, where it contributes to various forms of destruction to the tumour blood vessels and tumour tissues. Neutrophils also release chemotactic substances, which induces attraction of

more immune cells to the site.[58] Leukocytes are also readily recruited to the site of damage, where more oxygen is consumed resulting in the release of additional ROS, thereby leading to further enhancement in the levels of oxidative stress.[2]

The production of soluble mediators such as arachidonic acids, cytokines and chemokines recruit more inflammatory cells to the site, and these mediators activate signal transduction cascade pathways. The transcription factors (**Figure 1.14**), nuclear factor-κB (NF-κB), HIF-1α, activator protein-1 (AP-1), p53 (a tumour suppressor gene), specificity protein 1 (Sp1), peroxisome proliferator-activated receptor γ (PPARγ), nuclear factor of activated T-cells and NF-E2 related factor-2 (Nr-f2) are the mediators of cellular oxidative stress responses.[2] The transcription factor NF-κB is also directly or indirectly involved in transformation of cells, cancers, inflammation, the survival of cancer stem cells, the survival of tumours, proliferation of tumours, and in invasion, angiogenesis and metastasis of cancer.[191] The gene products of the transcription factors; signal transducer and activator of transcription 3 (STAT3), activator protein-1 (AP-1) and NF-κB, are tumour necrosis factor (TNF), interleukin (IL)-1, IL-6, chemokines, COX-2, 5-LOX, matrix metalloproteases (MMP), VEGF and adhesion molecules.[2]

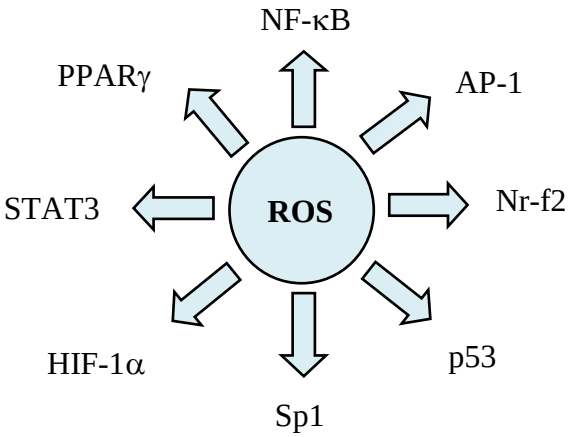

Figure 1.14: *Transcription factors that are modulated by ROS.*[2]

Hence the efficacy of a PDT treatment depends on the successful induction of antitumour immunity.[228, 232] One of the convincing evidence was that, immune-compromised (or immune-suppressed) mice showed decreased long-term tumour control.[228] Hence immunotherapy coupled to PDT improve therapeutic outcome.[233]

1.2.3.2 Immune response

The importance of antitumour response following PDT reactions had been well established in several studies (**Section 1.2.3.1**). As part of the immune responses the natural killer cells and the DCs get activated. DCs are antigen-presenting cells, and their maturation controls the function of B- and T-lymphocytes, which are the mediators of immunity.[193, 234] DCs mediate immune responses leading to the development of resistance against tumours and infecting microbes, dendritic cell-targeted vaccines would also enhance the effect of resistance. However, the DCs could also be used by tumour cells and infecting microbes to evade immune response.[235] Immunogenic cell deaths are mediated by damage-associated molecular patterns (DAMPs).[236]

One of the antitumour immune response involves activation of antigen presenting cells (APCs), which in turn activates cytokine secreting effector cells like T-cells. Hence it was proposed that inflammatory mediators released by tumour cells during photosensitisation, stimulate T-cell proliferation and cytokine secretion by T-cells, interferon-γ (INF- γ) for example.[237] In a clinical study, the changes to the immune response was measured in patients treated with PDT for basal cell carcinoma, where an increase (50-130 %) in the number of peripheral-blood T cells was observed.[83]

Though several advancements had been made in immunotherapy-induced responses, selecting the correct design for the clinical studies (trials) to test and measure all the maximum effects remain one of the greatest challenges. Other forms of immune-inducing therapies are radiation and radiofrequency ablation.[193]

From the above discussions, it is clear that the detrimental effects of photosensitisation arise through the formation of highly reactive species like ROS, RNS or their unstable intermediates. The direct consequence of excess production of reactive species is the generation of local oxidative stress environments. For complete cure from cancer, following the induction of PDT action, it is vital for the immune system to be activated, which would facilitate elimination of tumours that have metastasised from the treated primary site,[238] and to act against similar tumour challenges in the future.

In summary, there are two classes of effects following PDT reactions, direct and indirect. Direct effects involve denaturation of tumour cells through apoptosis, necrosis (necrotic cells release cell death-associated molecular patterns (CDAMs), DAMPs and tumour associated antigens) or autophagy associated cell death, and would subsequently induce acute inflammatory response. Indirect effects involve damages to the vasculature, resulting in release of complement components, antibodies and serum proteins. In which platelet aggregation, increased permeability and leukocyte extravasation occurs, and again subsequently acute inflammatory response is induced. Acute inflammatory response induced by both direct and indirect effects leads to the induction of systemic antitumour immunity. The two types of PDT effects that arise following PDT treatment, and the effects that lead to antitumour immunity are summarised in **Figure 1.15**, where colon cancer was used as an example.[206]

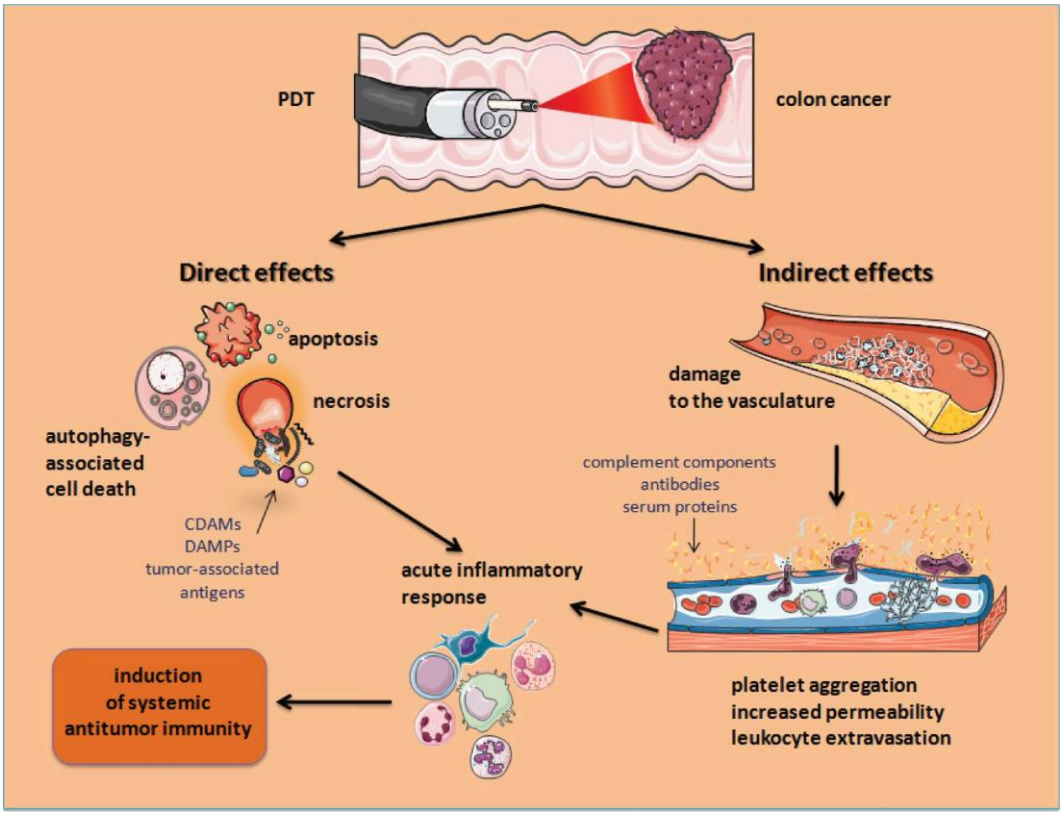

Figure 1.15: *PDT-induced antitumour immunity*.[206]

1.2.4 The components used to study the effects of oxidative stress *in vitro*

1.2.4.1 COLO320 cell line

Colorectal cancer is the third most common form of cancer.[239] In 1979, two human cell lines of colon carcinoma were reported, COLO320 and COLO321.[240] The primary colon carcinoma biopsy from which the above two cells lines were obtained is shown in **Figure 1.16**. It was described that both cell lines had properties of amine precursor uptake and decarboxylation. COLO320 and COLO321 cells showed rapid growth rate with non-sticking properties to the culture flask. These cells contained few microvilli (or desmosomes) relative to other colon carcinoma cell lines.[240] COLO320 cell line is considered to be similar to that of neuroendocrine cell type, a cell type found in human colonic mucosa. COLO320 cells were noted to secrete adrenocorticotropic hormone (ACTH), parathyroid hormone (PTH) and serotonin, and they express profusion of c-*myc* mRNA. The c-*myc* gene could have a role in cell proliferation and differentiation.[241]

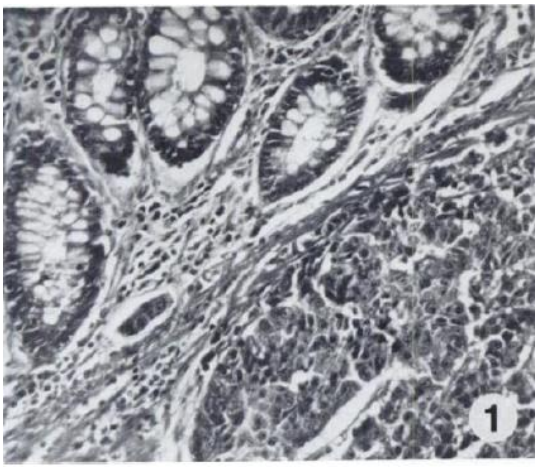

Figure 1.16: *Biopsy from the primary colon carcinoma, magnification* x*130.*[240]

COLO320 cells grow in colonies, which is favoured by the c-*myc* mRNA expression. The above claim had been tested by exposing COLO320 cells to sodium butyrate (NaBT, 5 mM) over 7 days, which resulted in greater than 60 % decrease in colony forming capacity, and 3 times decrease in c-*myc* expression was also observed.[241]

1.2.4.2 Measuring the effects of oxidative stress *in vitro*

With increased understanding of cellular events that occur during apoptosis, more advanced methods were developed to detect various stages of apoptosis, which include measuring changes in cell permeability together with phospholipid composition of the membrane, and DNA fragmentation analysis. In this section, only the measurement of phospholipid composition of the plasma membrane would be discussed.

(a) Annexin V

Apoptosis (**Section 1.1.3**) is important both in physiology and pathology. During apoptosis, phosphatidylserine is expressed on the cell's surface, while healthy cells predominantly contain phosphatidylserine within inner leaflet of the cell membrane. Annexin V binds to negatively charged phospholipid phosphatidylserine with high affinity and selectivity. The binding occurs through calcium dependent pathway, and is helpful in the identification of early stages of apoptosis.[242]

Annexin V was initially isolated from human placenta during late 1970s, and it belongs to annexin family of proteins.[242] Annexin V is made of 319 amino acids and has a planar cyclic structure with 4 domains. An X-ray structure of annexin V and the chemical structure of propidium iodide are shown in **Figure 1.17**, where the green spheres indicate calcium ions.

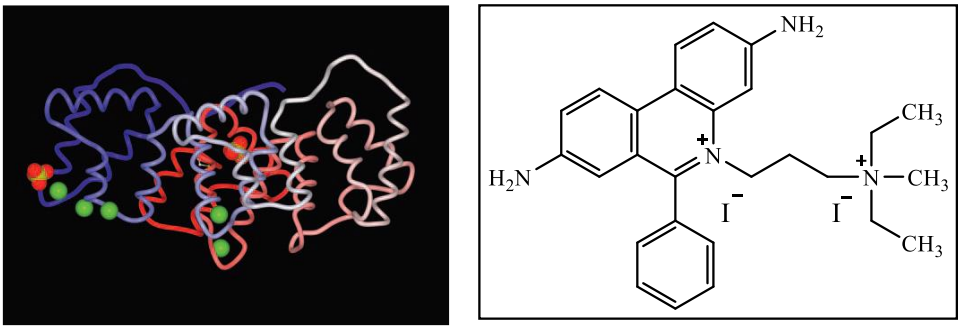

Figure 1.17: *X-ray structure of annexin A5 protein (left)[242] and the chemical structure of propidium iodide (right).*

Using the above principles fluorescence based detection system (fluorescence microscopy or flow cytometry) was developed, to distinguish viable, apoptotic and necrotic cells. To achieve this, annexin V labelled fluorescein isothiocyanate is used as a reporter molecule of fluorescence signals from apoptotic cells. The plasma membrane integrity would not be maintained in non-viable cells, hence fluorescent dye propidium iodide (3,8-diamino-5-[3-(diethylmethylammonio)propyl]-6-phenylphenanthridinium diiodide, **Figure 1.17**) could reach DNA and intercalate with it, which is used to detect late apoptotic or necrotic cells. The cells that show negative signals for both fluorophores are used to identify the healthy cells.[242]

(b) Phosphatidylserine

Sources of phosphatidylserine

Phosphatidylserine has a role in the activation of several proteins. It is involved in signalling processes such as in blood coagulation, bone formation, act as precursor for synthesis of other phospholipids, and in regulation of apoptosis. Phosphatidylserine are primarily synthesised by the endoplasmic reticulum (ER). In ER, in the presence of an enzyme phosphatidylserine synthase-I, phosphatidylcholine reacts with L-serine to

form phosphatidylserine and choline. Similarly in the presence of an enzyme phosphatidylserine synthase-II, phosphatidylethanolamine reacts with serine to form phosphatidylserine, and ethanolamine as the by-product. Phosphatidylserine decarboxylase enzyme within mitochondria converts phosphatidylserine back into carbon dioxide (CO_2) and phosphatidylethanolamine; the latter could get converted back to phosphatidylserine in the ER (**Scheme 1.5**).[243, 244]

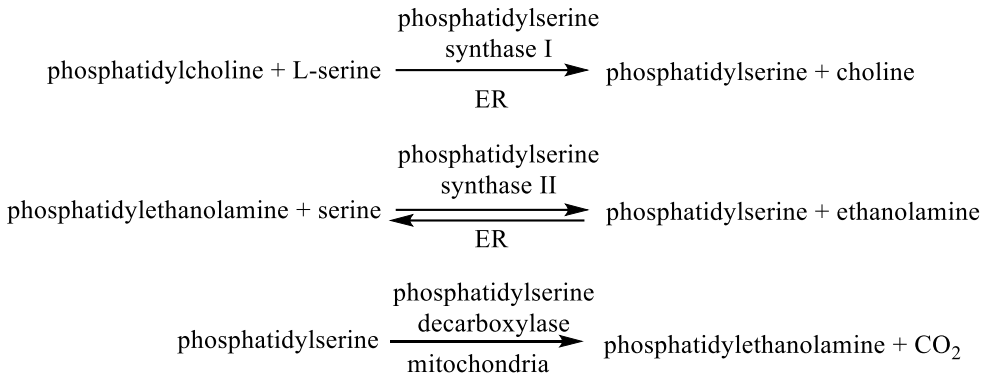

Scheme 1.5: *Synthesis of phosphatidylserine in the endoplasmic reticulum.*

Apoptotic cells trigger phagocytosis through the generation of signals on their surface. Two such signals are expression of victronectin receptor specific ligand and expression of phosphatidylserine on their outer leaflet of cell membrane. From the flow cytometric analysis of T-lymphocytes undergoing apoptosis, it was identified that two mechanisms are simultaneously involved in exposing phosphatidylserine on the extracellular membrane. They were the down-regulation of ATP-dependent aminophospholipid translocase and the activation of a non-specific lipid scramblase. Further it was identified that, to the phosphatidylserine exposed on external cell membrane of apoptotic T-lymphocytes, coagulation factors (Va and Xa) formed prothrombinase complex, which was determined using merocyanine 540 (MC540), a fluorescent membrane binding probe.[245]

Oxidative stress induced release of cytochrome c from mitochondria, lead to oxidation of phosphatidylserine bound to the inner plasma membrane. Selective oxidation of plasma membrane bound phosphatidylserine also lead

to its translocation from inner to outer cell membrane during apoptosis.[246] Cells exposed to ROS, especially when they were generated within cytosolic region, would lead to oxidation of phosphatidylserine present on the inner cellular membrane, before being externalised to the outer cellular membrane. It had been identified that only oxidatively modified phosphatidylserine with truncated *sn-2* acyl group, and γ–hydroxy-α,β-unsaturated or γ–oxo-α,β-unsaturated acyl moieties possessing cells gets identified by the receptors on macrophage as signal for engulfment, thereby apoptotic cells are selectively eliminated.

Detecting phosphatidylserine

Phosphatidylserine (**Figure 1.18**) can be detected by various methods, such as using antibodies with high selectivity or biochemical fractionation coupled with MS for detecting various forms of phosphatidylserine. It can also be detected using annexin V and discosidin-C2 (GFP-LactC2), both of which provides dynamic information. In addition, annexin V detection method is highly specific and can be tagged to multiple chromophores for easy detection, and discosidin-C2 (GFP-LactC2) can be used for intracellular imaging.[247]

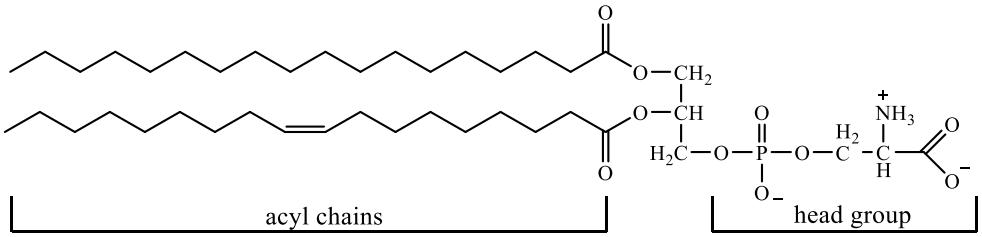

Figure 1.18: *Chemical structure of phosphatidylserine.*[247]

(c) Lactate dehydrogenase (LDH) enzyme release

Lactate dehydrogenase (LDH) enzyme catalyses the conversion of pyruvic acid to lactic acid, and it is present in both plants and animals. In blood, the level of LDH is usually expected to be less than 250 units litre^{-1}, increased level of LDH concentration had been used for identifying conditions of major diseases, like Alzheimer's disease,[248] hematologic disease,[249] heart failure,[250] liver disease,[251] malignant tumours[250] and myocardial infarction.[252, 253] There are five different types of LDH isozymes, LDH-1 to

LDH-5, all have tetrameric structure.[254] LDH-1 is present predominately in heart, and is made of four identical monomer subunits called 'heart' or '**H**' type, similarly LDH-5 is present mostly in muscles with four identical monomer subunits called 'muscle' or '**M**' type. Other three isoenzymes LDH-2 to -4 have been suggested to contain the subunits $\mathbf{H_3M}$, $\mathbf{H_2M_2}$ and $\mathbf{HM_3}$, respectively.[253] These isoenzymes are selectively distributed in different ratios in different organs as shown in the **Table 1.3**.[254]

Since the discovery of LDH isoenzymes in 1957, and the discovery of their tissue specificity in 1959, both of which increased their diagnostic value.[253] Analysis of LDH in erythrocyte from normal men and women showed that, there are five isoenzymes present in similar proportions. Younger cells contained mainly LDH-5, while matured cells were dominated by LDH-1. Presence of higher levels of LDH in matured cells represented loss of the activity of isoenzymes. Further, relative rise in the levels of LDH-1 indicated the presence of an aged cell population. Hence it was recommended that, the measurement of erythrocyte LDH isoenzymes could be of clinical importance, in the rapid assessment to the changes in the dynamic state of erythropoietic activity.[249]

Table 1.3: *Lactate dehydrogenase isoenzymes and their relative abundance in different organs, heart* (**H**) *and muscles* (**M**).

LDH Isoenzyme	Organs	Monomer subunits
LDH-1	Heart	$\mathbf{H_4}$
LDH-2	Spleen and lymph nodes	$\mathbf{H_3M}$
LDH-3	Lungs	$\mathbf{H_2M_2}$
LDH-4	Kidneys and pancreas	$\mathbf{HM_3}$
LDH-5	Liver and skeletal muscles	$\mathbf{M_4}$

Congestive heart failure, trauma, cirrhosis, pulmonary embolism, hypoalbuminemia, infections, kidney failure and malignancy are common causes of pleural effusions. Analysis of LDH isoenzyme patterns present in pleural fluid collected was helpful for determining differential diagnosis,

and it allowed up to 74 % success for definitive diagnosis. With this approach, cognitive heart failure, infection and malignancy were positively predicted at the success rate of 96 %, 88 % and 63 % respectively.[250]

Serum LDH levels were used as prognostics tools for correlating disease progression. In oncology, it was established that LDH levels in serum increases as a result of tumours releasing LDH. The level of LDH in serum was used as a marker to correlate the progression (growth or regression) of the disease. One of the consequence of such evaluation showed that, the serum LDH levels of metastatic diseased patients were significantly higher relative to patients with the localised form of the disease. The correlation was positive for the diseases such as leukaemia, lymphoma and malignant neoplasms.[255]

The release of cytoplasmic enzyme LDH by cells had also been used for assessing damages to cell membrane[256], and cell death was also linked to the levels of LDH released.[257] Hence LDH release had been used for measuring viability changes[258], and supernatant was used for determining LDH levels.[259] To determine total amount of LDH, detergent (Triton X-100, 1 %) had been used for lysing cells, thereby to release their contents into supernatant.[257] LDH released by cells were also used to evaluate cell membrane integrity. Significant increase in lipid peroxidation and leakage of LDH out of cells were observed following 90 minutes of exposing liver cell line HepG2 to 500 µmol dm^{-3} of *tert*-butylhydroperoxide (TBHP) at 37 ^{o}C. Further, metabolic activities such as protein synthesis and mitochondrial respiration were unaffected, which suggested that only plasma membrane was affected by TBHP.[260]

Normal tissues from man contain all five isoenzymes of LDH in similar proportions, and the ratios vary prominently under several pathological conditions. Isoenzymes of LDH from normal tissues can be extracted from tissues using electrophoretic techniques (**Figure 1.19**).[249] Sulphite (SO_3^{2-}) and oxalate ($C_2O_4^{2-}$) was found to inhibit electrophoretically fast isoenzymes (LDH-1 and -2), it was also identified that the slow isoenzymes

(LDH-4 and -5) would be inhibited in the presence of urea ($CO(NH_2)_2$). Oxalate was used to inhibit LDH activity in patients with myocardial infarction, and in patients with liver disease.[253]

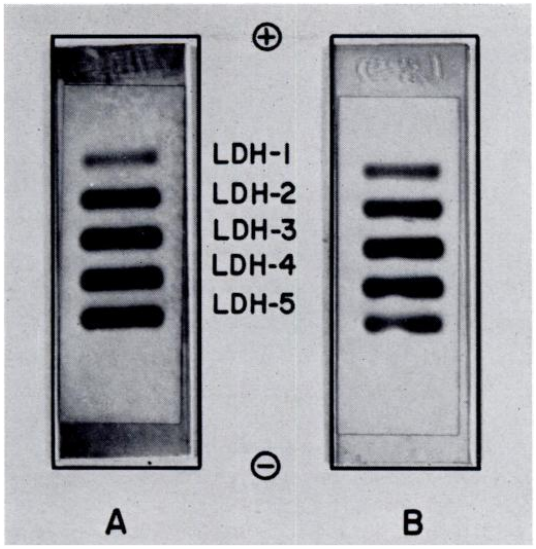

Figure 1.19: *Lactate dehydrogenase isoenzymes patterns viewed on electrophoresis, haemolysis achieved using* **(A)** *0.25 M sucrose-0.156 M NaCl and* **(B)** *0.25 M sucrose.*[249]

1.3 Microfluidics, applications and surface treatments

This section covers the general idea of what is microfluidics, why was it utilised in this project and some of its principles. It also discusses the types of applications in which they are commonly used in the fields of chemistry and biology. The later part of this section covers the methods used for fabrication of microfluidic chips, and some of surface treatment reactions used for the modification of glass channel surfaces to immobilise chemically characterised molecules.

1.3.1 Microfluidics

The term microfluidic is generally used to identify devices that make use of channels or chambers in the dimension range of 0.1 to 1000 μm. The sizes of biological cells from all three domains, archaea, bacteria and eukaryote are in the scale of micrometres, hence the use of micro dimensional channels are of sensible method to handle and study them. The size match between biological elements and micro-scale devices, along with the ability

to incorporate multiple functions to these devices are the fundamental reasons for using this approach.

In addition, microreactors provide high surface area to volume ratio (5 -50 x 10^3 m^2 m^{-3}) relative to conventional reactors (1 - 10 x 10^2 m^2 m^{-3}).[261] This property is useful for higher levels of interaction between the surface of the microreactors and substances used within it. The latter enables rapid transfer of heat in and out of the microenvironment within chips, which is used for conducting reactions such as polymerase chain reactions (PCR). The narrow and shallower channels enable uniform distribution of thermal, magnetic and electromagnetic energy, including light energy to be relatively equally distributed all along the depth of the channels.

Microfluidic devices offer improved performances with reduced time scale, hence rapid process, and it is possible to run multi-systems in parallel,[262] thereby throughput could be improved with reduced levels of byproducts. Furthermore, small sizes of these devices enable it to be integrated in other applications and are cheaper to produce. Microfluidic systems designed for a specific task is considered to be ideal, when they show high-speed performance, portability, reliability, reproducibility, accuracy, easy handling and of low-cost. Moreover, nanofluidic technology could also be incorporated into microfluidic devices to enable digital switching of fluid between different microfluidic channels.

1.3.1.1 Applications of microfluidics for photochemical reactions

There are several types of light dependent reactions performed within microfluidic devices using light energy in different regions of electromagnetic spectrum. Microfluidic devices have been used in photocatalysis reactions as they provide large surface area-to-volume ratio, hence the reaction efficiency relative to traditional reactors.[263] For the same reason they are also used in photoredox reactions.[264] Using microflow photochemical systems, homogeneous and heterogeneous photochemical reactions like photo-addition, -rearrangement, -reduction, -carboxylation and -oxygenation, have been conducted.[265] Space-time (4D) productivity

and photonic efficiency are the two main parameters compared between batch reactors and microreactors.[266]

Many heterogeneous catalysts and phase transfer-reactions within micro-structured environments have been reported. Heterogeneous reactions involve use of immobilised catalytic reagents, which considerably reduce the time length of processing in separation of the product, as well as the cost, enabled by reusability. Titanium dioxide (TiO_2) was used as an inorganic photosensitiser for photo-catalysed photosensitisation of chemical reactions (photochemistry). TiO_2 had been immobilised within microreactors and tested for its presence using degradation of 4-chlorophenol reaction.[267] Photonic efficiency (the initial rate of reaction per incident monochromatic light intensity) for the degradation reaction was calculated, where the photonic efficiency decreased with the concentration of 4-chlorophenol.[267] Oxidation of carbon monoxide (CO) and methanol (CH_3OH) using photocatalysis reaction with TiO_2 as the sensitiser within a micro-reactor have also been demonstrated.[268] Photocatalysis reactions were also used in the degradation of organic waste to release CO_2 and H_2O as the main products. Furthermore it have been used as solar energy harvesters, where energy gets stored within chemical bonds through the formation of higher energy products.[268]

Both micro- and scaled up macro-flow reactors for organic photochemical synthesis are emerging methods for the synthesis of easy and pure products.[265, 269] Four selected examples involving generation of $^1O_2$ are considered here. The production of $^1O_2$ using photosensitiser inside a nanoscale reactor had been demonstrated, where α-terpinene was converted into ascaridole, using RB, oxygen and light (**Scheme 1.6**), in which the photosensitiser and the substrate were in solution. They were introduced into microfluidic channels using two different inlets, and allowed to mix inside the channel region where photosensitisation reaction occurred.[270]

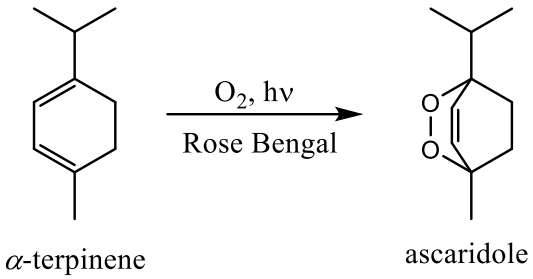

Scheme 1.6: *Ascaridole synthesis using photosensitisation reaction.*[270]

For conventional photochemical reactors, light energies are used in the scale of hundreds of W m^{-2} to overcome filter effects of outer bulk reactants. However, for microfluidic reactors recently LEDs were also used as the light source, in the oxidation of citronellol through the generation of $^1O_2$ using a photosensitisation reaction.[266] In another study, cyclopentadiene had been oxidised to its endoperoxide form using a Falling-Film microreactor, and reduced to its alcohol form off-chip (**Scheme 1.7**).[261] $^1O_2$ was also generated *in situ* in a continuous flow photochemical reactor, where the use of high flow rate and high interfacial surface area resulted in high throughput and efficient chemical oxidation reactions.[271]

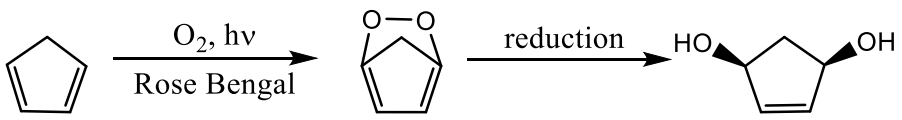

Scheme 1.7: *Photooxygenation of cyclopentadiene.*[261]

1.3.1.2 Biological applications of microfluidic approach

Microfluidic technology had also been widely applied in biological sciences. Some of the applications in this area include, analysis of cells for cell-cell interactions,[272] cell-matrix interactions, cell-surface interactions, stem cell research,[213] cell sorting,[273] enzyme assays, immunoassays, proteomics,[274-277] neuroscience,[278, 279] oncology[213, 280, 281] and in genomic studies (DNA studies)[274, 282-284]. Microfluidic technology is also widely used in point-of-care biomedical systems,[285-287] and in bioanalytical applications involving nucleic acid, protein, cellular and DNA sequence analyses[288].

It was shown under a microfluidic protocol, the cancer cells circulating in the blood circulation are more resistant to haemodynamic shear stress (fluid shear stress), than the non-transformed cells.[289] Using this technology, the microenvironments and cytomics of cancer cells, and pharmacological screening in real-time (4D) have also been studied.[262] Microfluidic bioreactors have been used for monitoring oxygen levels in continuous cell culture systems.[290] Integrated microfluidic devices had been used to isolate white blood cells from whole blood, and polymerase chain reaction was carried out.[291]

Microfluidic devices have facilitated advancement in understanding the fundamental aspects of microbial ecology like growth, cell-cell interactions, sensing and population dynamics,[292] and also used in monitoring water borne pathogens[293]. The complexity of microfluidic applications had increased, and it is moving from 3D cell culture to organs within chips, with a potential forecast of replacing animal models for *in vivo* testing.[294]

Photodynamic reactions using microreactors

Microfluidic based PDT-mimicking reactions is an emerging field, with relatively low number (less than ten) of reports in the scientific community, two studies are considered below as examples. A microsystem was used to evaluate PDT procedures, where it was used for treating separated and mixed cultures of normal (Balb-3T3) and carcinoma (human lung) on the level of cell kill. It was concluded that the PDT procedure was more selective to cancer cells than to normal cells.[295] In another study, a microfluidic chip was used to screen surface-modified nanoparticles on multiple cell lines, to determine their specificity for targeting cancer cells.[296] In the two studies described above, they involved attachment of cells to the surface of the microfluidic system, that is, not a flow system.

1.3.2 Fluid dynamics

Flow behaviour at micro-scale considerably varies from macroscopic forms. For example, Newtonian fluids could show non-Newtonian behaviour at higher rates of shear and extension. Within micro-channels the flow rates

can be too low, compared to the benefits of heat transfer and high surface area to volume ratio offered by these devices.

Flow patterns

Flow of liquids (e.g. water) and fine powdery solids (e.g. flour) are controlled by the balance between pressure and viscous forces acting on them. Flowing (moving) fluids could have primarily two types of distinct motions, laminar and turbulent. *Laminar* motion is characterised by smooth and steady flow patterns, in which fluids flow parallel to each other and mixing occurs only through diffusion. *Turbulent* flow is characterised by fluctuation and agitation in motion of a moving fluid, in which fluids do not move in a defined direction and mixing could occur at a higher and a variable rate. Commonly a dimensionless quantity called *Reynolds number* (Re, **Equation 1.6**), is used to predict if the motion is laminar, turbulent or a mixture of both. Re is dependent on the characteristic flow velocity (V), the characteristic dimensions (D) of the ducts through which the liquid flows and the kinematic viscosity (ν). The kinematic viscosity itself depends on the dynamic viscosity (μ) and the density (ρ) of the liquid. Re correlates the viscous behaviour of all Newtonian fluids, and it is a thermodynamic property dependent on temperature and pressure.[297]

$$\mathrm{Re} = \frac{VD}{\nu} = \frac{\rho VD}{\mu} \qquad \textbf{Equation 1.6}$$

For circular ducts, the Re values can be used to predict the type of flow. Generally, the Re values between 0 to 2300 indicate laminar flow, the Re values higher than 4000 indicate turbulent flow and the Re values in-between 2300 to 4000 suggest that it is a 'transitional flow', that is, changing from laminar to turbulent or *vice versa*.[297] As far as the combination of parameters (**Equation 1.6**) are regulated to obtain the Re values within the ranges specified above, the average velocity, the nature of the fluid or the dimension of the circular duct, do not affect the flow patterns. However, the above values are only a guide and can be varied considerably depending on the conditions used for flow. For example, with

the use of a duct with highly smooth surface, the Re values can be increased much higher than 4000 (up to 1 x 10^5) while maintaining the flow laminar. Growing boundary layers, inviscid core flow and merging of boundary layers in the hydrodynamic entrance length (*Le*) region of a circular pipe, are shown in **Figure 1.20**, where velocity of fluid varies as a function of both radius (*r)* and the forward distance (*x*).[297] When the flow is fully developed, fluid velocity (*u(r)*) varies symmetrically and parabolically decreasing along the radius from the centre. The maximum and minimum flow velocities are at the centre and near the walls of the duct, respectively, with parabolic variation in flow velocities in-between the two extremes as shown in the figure.

The density, hence the viscosity of water varies with temperature.[298] Viscosities of fluids are only weakly affected by pressure changes, and greatly affected by temperature changes. When the temperature rises, dynamic viscosity decreases for liquids and it increases for gases.

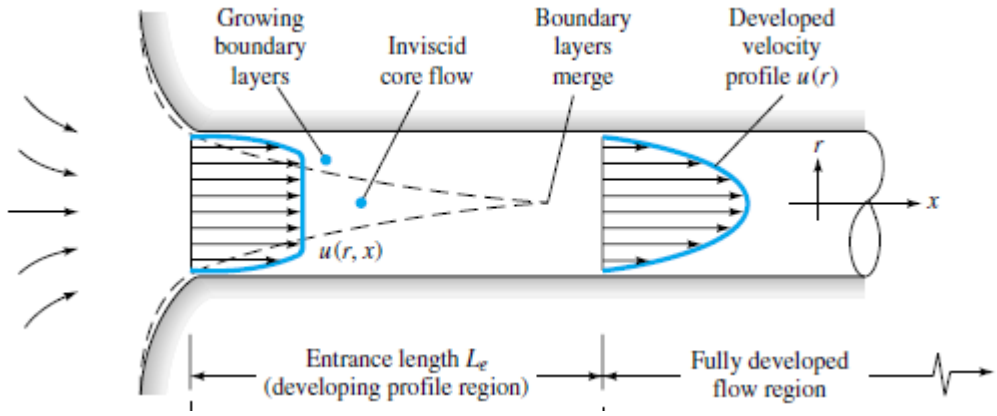

Figure 1.20: *A typical laminar flow profile in a circular pipe*.[297]

Newtonian and non-Newtonian fluids

Shear stress force applied on common fluids such as water, oil and air are directly proportional to the strain rate and the velocity gradient (**Equation 1.7**).

$$\tau \alpha \frac{d\theta}{dt} \alpha \frac{du}{dy} \qquad \textbf{Equation 1.7}$$

Where, τ is the shear stress, $\frac{d\theta}{dt}$ is the strain rate and $\frac{du}{dy}$ is the velocity gradient. The constant of proportionality between shear stress and shear strain rate, or shear stress and velocity gradient, is known as the coefficient of viscosity, μ. Fluids that obey the **Equation 1.8** are said to be Newtonian fluids, water for example.[297]

$$\tau = \mu \frac{d\theta}{dt} = \mu \frac{du}{dy} \qquad \textbf{Equation 1.8}$$

The correlations between shear stress and strain rate for Newtonian and four other non-Newtonian fluids are compared in **Figure 1.21**. Fluids such as toothpaste, that resist flow until the yield stress is applied, it is known as *Bingham plastic*. Shear-thinning or *pseudoplastic*, where fluid resistance decreases with the increase in shear strain rate. A strong form of shear-thinning effect is called *plastic*. Shear-thickening or *dilatant* is the opposite form of shear-thinning effect, where with increase in applied stress, fluid increases resistance.[297]

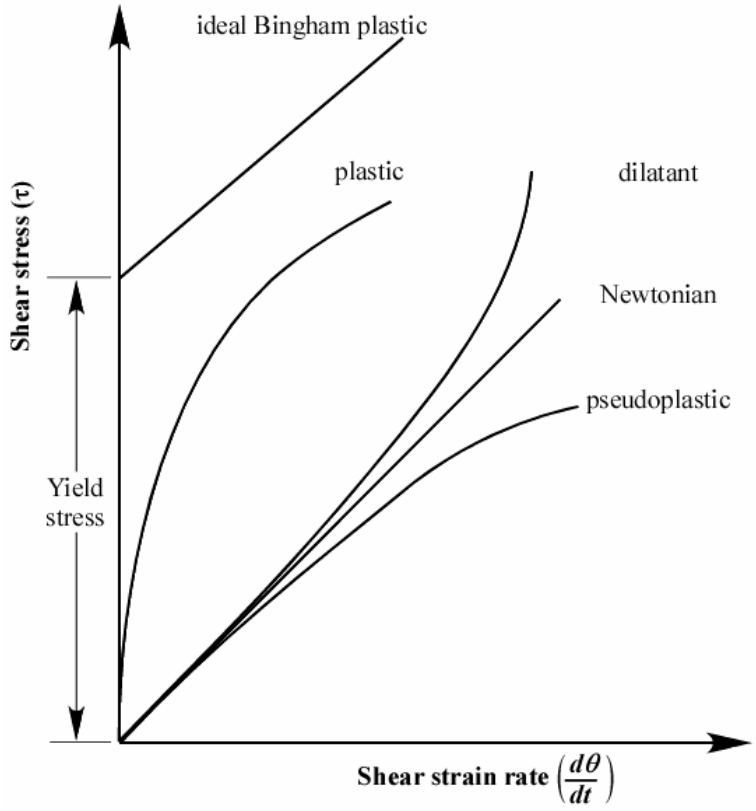

Figure 1.21: *Correlations between shear stress and shear strain rate for various types of viscous materials.*[297]

Sedimentation of particles

A computational model system for the rate of particle transport for *in vitro* systems containing liquid medium indicated that, the particles smaller than 10 nm are transported at a higher rate and mainly by diffusion, the particles bigger than 200 nm are transported by sedimentation, and the particles between 10 and 100 nm are transported by both diffusion and sedimentation, but relatively at a reduced rate.[299] Hence, *in vitro,* under no external forces such as pumping, photosensitiser molecules like porphyrin in solution, which are smaller than 10 nm, would be mainly transported by diffusion, while the cells in the size range of several micrometres, would be transported by sedimentation.

1.3.3 Microfluidic chip fabrication

Silicon, fused silica, glass, metals and polymers are the routinely used materials for the fabrication of microfluidic devices.[300] The properties of silicon substrates are well characterised as they are widely used in semiconductor industry, and the first microfluidic analytical system was made out of it. However, opaqueness to visible light and the associated fabrication cost, made it less useful for most of the common types of microfluidic applications. Hence, glasses such as fused silica, soda-lime, borosilicate and quartz are common materials for microfluidic chip fabrication.[301] Silicon and glass has similar surface properties, where silane based surface modifications (covalent attachments) are possible.[301, 302] For large scale use of cheap and non-reusable (disposable) microfluidic devices, they are made of materials like PDMS and plastics such as polymethyl methacrylate (PMMA), polystyrene, and cyclic olefin copolymer (COC).[288, 301] Certain applications also make use of paper based microfluidic devices,[303] as a form of low cost device.

Methods used for microchip fabrication are through direct write technique or replication technique. Some of the other microfabrication techniques include wire imprinting, laser ablation, mechanical machining and hot embossing. Glass microfluidic devices are fabricated using acid (wet) etching together with machine drilling, the latter is optional.[301]

Mechanically drilled metal based microfluidic devices could be used for high pressure applications, but they are less common. Various bonding techniques are employed in microchip fabrication.[304] The plastic microfluidic devices are made using the techniques like injection moulding or hot embossing.[301]

Polydimethylsiloxane (PDMS) is a polymer (elastomer) material, which is gas permeable, transparent and hydrophobic in nature.[305] Casting based soft-lithography is used for the fabrication of PDMS based devices.[306] PDMS polymers are transparent to visible light and their flexibility enables incorporation of valves and pumps for control. The surface had to be oxygen plasma treated to enable surface treatment and the polymer is incompatible with organic solvents.[301] The permeability of polymer to gases might or might not be a beneficial property depending on the applications of interests.

1.3.4 Surface treatments

This section covers some of the methods used for covalently immobilising molecules of interest, thereby to enable heterogeneous reactions. Heterogeneous assays commonly make use of phyisorption, bio-affinity interactions and covalent bond attachments to a solid surface. Some of them make use of spacer molecules for improved performances.[301] There are two types of surface treatment methods, dynamic and permanent coatings. Dynamic coating is a non-covalent interaction, it could occur through interactions such as H-bonding or electrostatic interactions. This method usually requires continuous supply of coating molecules to be present in the running buffer. Alternatively, permanent coatings are formed through covalent bonds, which are stronger and can be held in place for much longer period than dynamic coating.[307] Such treated surfaces are used in applications like electrophoresis[308] and for glucose level determination[309].

Glass (silica) surfaces

The natural abundance and chemical nature of silica places it as one of the most essential element, in both man made and environmental systems. It is

used in wide varieties of technical applications such as for making glass-wares, microfluidic devices and as a matrix board for integrated electronic circuit boards. Presence of water can affect the physical properties of silica. Experimental techniques could be used to obtain information on macroscopic aspects of glass surface, and simulated computer based calculations using software such as molecular dynamics or ab inito, could be used to determine microscopic details of interactions.[310]

1.3.4.1 Silanisation of glass surface

Silylation is used as a method for modifying surfaces like common glass to alter their physical and chemical properties, such as wettability and covalent reactivity of the surface. $R_nSiX_{(4-n)}$ is the general formula for organosilanes, where X is a hydrolysable group such as alkoxy, halogen, acyloxy, or amine. The reaction properties for wide range of silyl compounds are known, among which trimethylsilyl group (Me_3Si-) is a common silylation agent used. The specificity of the reaction, the strength of the donor groups, the by-products formed and the associated cost are few main factors to consider in selecting an appropriate silylating agent.[311]

Silylating agent like Me_2HSi- is more susceptible to hydrolysis. The hydrolytic stability of such reagents could be increased by replacing H atom with a bulkier group such as phenyl, t-butyl or triisopropyl groups. During silylation of silica surface, weakly interacting hydrogen atoms on the surface of the material get replaced with a silyloxy bond, that is, silanising agents are immobilised through the formation of siloxane (Si-O-Si) bonds. Uniform orientation of molecules is essential for the formation of monolayers.[311]

Immobilisation of monolayer and multilayers

Glass, quartz, silicon-oxide and tin-oxide have been used as solid supports to immobilise molecules of interest. Silanising agents such as bromine terminated and iodide terminated R group possessing trialkoxy silanising agents were reported to have formed monolayer, where the attachment was through nucleophilic substitution reaction.[312] Monolayer formation of

organo-silanes using chemical vapour deposition (CVD) technique is also possible, the method relies on heating, increasing pressure or applying vacuum within a closed system with organosilane inside.[313] Self-assembled monolayer formation of dialkyldisulfides and alkyltrichlorosilanes onto gold and silicon surface had also been observed.[314] Bifunctional silanes could result in the formation of multiple layers through adsorption process.[315]

(3-Aminopropyl)triethoxysilane

Silanising agent, (3-aminopropyl)triethoxysilane (APTES) had been used in several immobilisation reactions as a primary starting silanisation agent to carry out other secondary reactions on top of it.[316] APTES is widely used when a hydrophilic surface or an amino terminated surface is essential for further conjugation reactions. To obtain high primary amine contents onto a treated surface area, the use of right conditions are essential.[317] Atomic force microscopy (AFM) images of APTES treated silicon surface is shown in **Figure 1.22**.[318]

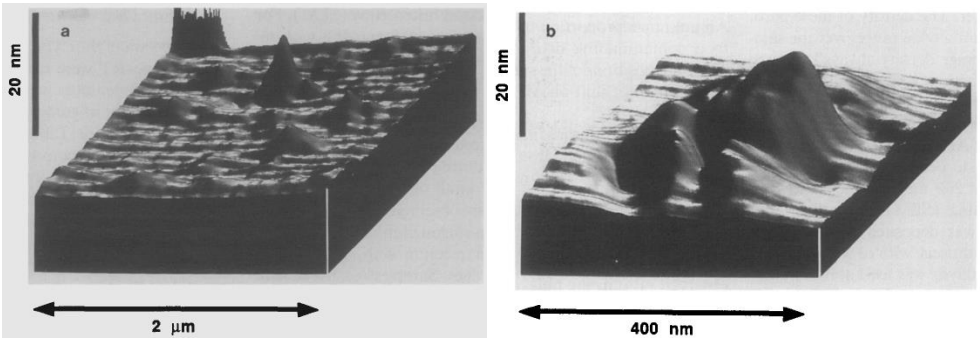

Figure 1.22: *AFM images of APTES treated silicon at two levels of magnifications.*[318]

To a monolayer of amine group terminated silanising agent, protein had been immobilised through three consecutive step reactions.[312] Aminosilanised surfaces are used for immobilisation of biological macromolecules like proteins, oligonucleotides,[319] enzymes, DNA and antibodies. Hence chemistry of APTES immobilisation had been extensively studied. APTES was also used as a primary surface modifier for two forms of clays, laponite and K10-montmorillonite, to immobilise copper (II) acetylacetonate in the following reaction step.[320]

Surface modification of polar polymer surfaces using APTES was tested on surfaces made of polymers of esters, amides, carbonates, imides and acrylics. Surface modification using APTES in protic solvents was unsuccessful, hence it was proposed that APTES molecules are initially adsorbed through H-bonding between amino group on APTES and oxygen atoms on the surface. The proposed mechanism was in parallel with the formation of multilayers on silica surfaces.[321]

Following surface treatment with APTES onto silica surfaces, they can exist in several orientations (**Figure 1.23(a)**),[322] and immobilisation could also occur through different kinds of attachments, H-bonding for example[323]. Non-controlled silanisation process could lead to surface roughness and formation of multilayers or precipitates (**Figure 1.23(b)**). APTES treated surface had been studied using silicon (^{29}Si) and carbon (^{13}C) NMR,[322] and using Fourier transform infrared spectroscopy (FTIR) and ellipsometry it was shown that, the structure and the thickness of APTES treated surface, depends on the type of solvent in which APTES was dissolved, and on the length of the reaction allowed[324]. It was also shown that APTES treatment carried using dry organic (anhydrous toluene) and polar (water) solvents would have different types of attachment to the glass surface. When using anhydrous toluene, depending on the length of the reaction multiple layers of silanising agents deposited, and the thickness of the layers varied between 10 to 144 Å. In contrast, when PBS solution was used, the thickness of the layers varied only between 8 to 13 Å. Further, it was identified using water contact angle measurement, the surface treatment carried out using the organic solvent resulted in more hydrophobic surface than when PBS was used, and using fluorescent measurement it was also identified that the number of amino groups were about 3 to 10 times higher than with PBS.[324]

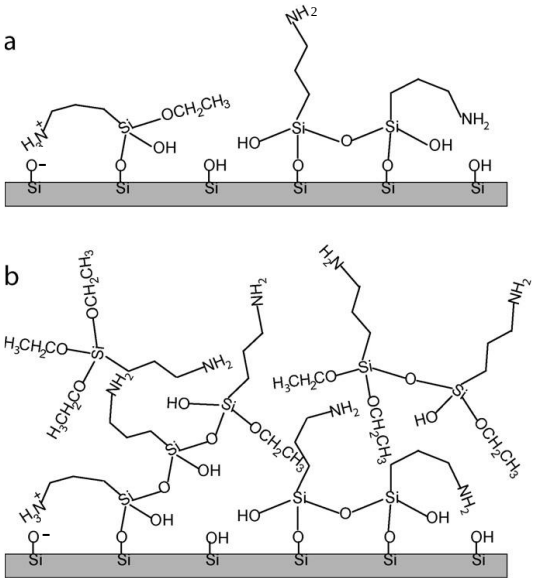

Figure 1.23: *Formation of* **(a)** *monolayer and* **(b)** *multilayers of APTES onto a silicon surface.*[324]

Silica surface immobilisation mechanism

Wider versatility of modifying the surface have led to wider applications, with increased demand for understanding their basic principles and mechanisms leading to such modifications.[325] (3-Aminopropyl) dimethylethoxysilane (APDMES) was immobilised onto silica surface using triethylamine as the catalyst, where the silanising agent was used in its gas-phase. In the reaction, the initial attachment of APDMES occurred through the formation of H-bonding between the hydroxyl groups on the surface, and the ethoxy (alkoxy) and amino groups of the reagent molecules. The number of Si-O-Si covalent bonding increased as the reaction proceeded, and towards the end of the reaction about 50 % of molecules remained adsorbed through H-bonding. The use of triethylamine together with APDMES (1:10) accelerated the formation of Si-O-Si bond, but did not improve the number of Si-O-Si covalent bonds formed.[323]

Silanising groups with 3-, 2-, 1-alkoxy groups containing agents were tested for their varying stability. Where dry toluene was used as the solvent for the immobilisation of silane on to the surface, the use of alternative solvents such as hexane had negligible effect on the immobilisation mechanism. It was found that, when no curing was conducted the stability was in the order of

(1) tri- > (2) di- > (3) mono-ethoxy or -methoxy, and when heated for 3 hours the tendency for the formation of more covalent bonds to the surface from H-bonding increased, hence curing time of 3 hours at 80 ºC yielded maximum stability of the surface.[325]

1.3.4.2 Photosensitisers onto solid support

Porphyrin sensitisers

Uses of immobilised sensitisers allow rapid and easier separation of products from sensitisers.[326] Fifty years ago, the use of insoluble styrene-divinylbenzene (Merrifield polymer) as a solid support for the synthesis of polypeptide had been introduced.[50] Porphyrin derivatives have been covalently attached to modified (aminomethylated[326]) Merrifield polymers, porphyrins immobilised in this manner were capable of generating $^1O_2$, which was utilised for conducting oxidation reactions.[327] Similarly, silica gel beads (~10 µm) supported monopyridyltriphenylporphyrin (PyTPP) had also been used for photodecomposition of phenol.[328]

Microfluidic technique increases the surface area to volume ratio, thereby the amount of photosensitiser that can be immobilised, hence the ROS production per unit surface area and possibilities of bringing oxidisable substrates closer to the site of ROS production. Porphyrin was covalently attached to aminoalkylated silica surface using which [4+2] photooxidation and "ene" reactions were carried out, where the yield increased with longer reaction times. Longer reaction time was a drawback of the method, it was suggested that the latter observation could be due to quenching of $^1O_2$ by silica surface.[329] Porphyrin derivatives had been covalently attached and used for photosensitisation reactions, where efficiency of $^1O_2$ generation was dependent on spacer groups and the polymer backbone.[326] Water soluble porphyrins had been deposited through adsorption onto glass surface,[330] and in a different study, another porphyrin derivative was immobilised onto PDMS and used for $^1O_2$ generation[305].

Photosensitiser, *meso*-tetra(*N*-methyl-4-pyridyl)porphyrin had been covalently immobilised onto porous Vycor glass (PVG) through

adsorption.[331, 332] It was proposed that the attachment was through cationic exchange of silanols (Si-OH) on the surface of the solid support, and was confirmed using decrease in pH of the solution in the immediate vicinity. Through this method maximum loading of up to 1.1 x 10^{-6} mol g^{-1} was achieved, which corresponded to less than 1 % coverage of the PVG surface. Using this model quenching of photoexcited sensitiser by $^3O_2$ was studied, and it was found that the quenching behaviour was strongly depended on the dynamics of the quencher.[331]

Immobilisation of metallated (Co^{2+} or Zn^{2+}) porphyrins (tetraphenyl porphyrin) onto a surface that was previously treated with a silanising agent to contain pyridine ligand was also reported. The immobilisation was achieved through coordination bond between their metal centres and the ligand. Further, the reaction was a self-assembly process and resulted in the formation of monolayers.[333]

Immobilisation using ionic interactions was also possible[334], however their stability in the presence of highly polar solvents such as water would be much lower or unstable. Electrostatically immobilised photosensitisers (porphyrins and phthalocyanines) showed increase in absorbance with the increase in the number of deposited layers, which was used for identifying the regularity and the uniformity of the layers deposited.[334]

Non-porphyrin sensitisers

Sol-gel technique was used for immobilisation of the photosensitisers, RB, chlorin e6 and methylene blue (MB). Such immobilised sensitisers were evaluated for use in waste water treatment using solar light energy as the light source.[335] RB had been widely used in many studies for the generation of $^1O_2$, both in solution and in its immobilised form.[335-337] Polymer based RB did not show appreciable leaching in organic solvents such as methylene chloride, chloroform, carbon tetrachloride (CCl_4), chlorotrifluoromethane (CF_3Cl), benzene, toluene, pentane, carbon disulfide, acetone and methanol. Sensitisers, eosin Y, fluorescein, chlorophyllin and haematoporphyrin had also been immobilised, and used for photochemical reactions. The time

required for 50 % conversion of a specified reaction was considered between all five different sensitisers. It was found that with the use of RB, the conversion reached 50 % in short time scale relative to the remaining four sensitisers considered.[336] To chloromethylated styrene-divinylbenzene RB was immobilised, and used for conducting all three types of photochemistry reactions, 1,2-cycloaddition, an "ene" type reaction and 1,4-cycloaddition, through the generation of $^1O_2$.[50]

The spectroscopic properties of dyes can vary when in solution and when dry (not solvated or not dissolved). For example, thionine-Y zeolite, when dry showed higher absorption wavelength of 605 nm, and when in solution formed aggregates and showed lower absorption wavelength (557 nm).[305]

Contact angle measurements

Surface energies of self-assembled monolayers (SAM)-modified surfaces can be calculated using contact angle measurement values. Wettability of a surface by a solvent is an important property for performing solid surface based chemistry. The measurement of contact angle formed by a stationary solvent, mostly water, is used for wettability studies.[338]

There are several ways of measuring wettability, three important ways of measuring wettability of a surface include, tilting-plate goniometry (TPG), captive drop goniometry (CDG) and Wilhelmy-balance tensiometry (WBT), among which the latter is considered to be the gold standard. A single measurement of contact angle does not provide sufficient details about the wettability of a silane treated surface. Further for any of the chosen method of measurement a maximal advancing angle (θ_a) and minimal receding angles (θ_r) are measured.[339] Various polymers were covalently immobilised onto silica surface of microchannels suitable for capillary electrophoresis systems, silane-based "click-chemistry" reactions were used for the attachments. Such modified surfaces were characterised by measuring contact angles and the changes in electroosmotic flow.[302] Hence contact angle measurement is a useful method for verifying the success of surface treatment, another example is considered below.

Chlorosomes structures derived from bacterium *Chloroflexus aurantiacus* was covalently immobilised onto glass surfaces, in the development of a biophotonic device. Successful immobilisation was verified using AFM techniques, absorbance and fluorescence spectroscopic methods, electrochemical impedance spectroscopy and chronoamperometric studies. It was claimed that such biophotonic devices could find their applications in the development of charge coupled devices (CCDs) and in space fuel cell applications. For the above surface treatment, APTES was used as the first step in immobilisation. Following which contact angle measurements were used to verify APTES treatment, where a cleaned non-surface treated glass had a contact angle of 30.1 ± 0.2º, and an APTES treated glass surface had a contact angle of 83.8 ± 0.1º.[340] As the contact angle was less than 90º before and after surface APTES treatment, hence could be considered as hydrophilic in both cases, but the extent of hydrophilicity is reduced.

1.3.4.3 Magnetic nanoparticles as a solid support

The uses of magnetic nanoparticles allow separation of products from mixtures using external magnetic forces, which make the post-processing steps easier, for example to selectively control proteins within a reaction mixture.[341] Superparamagnetic iron-oxide nanoparticles are used for *in vitro* and *in vivo* applications. They are synthesised using hydrophobic crystal growth at high temperature to obtain monodisperse materials, and the surface is modified using biocompatible polymers, which are mostly used for *in vitro* studies. Alternatively they are synthesised by precipitating iron salts (Fe^{2+}, Fe^{3+}) out of an alkaline solution, and followed by modifying their surface using dextran, which are mainly used for *in vivo* applications.[342]

Carbon layer coated cobalt (Co) nanoparticles had been synthesised, through the addition of acetylene to pure Co nanoparticles-forming process. Higher thermal stability (up to 1908 ºC) was observed for these carbon-coated core-shell nanoparticles, where thermal stability was assessed based on changes in mass. Saturation magnetisation for bulk and for per unit metal were the same, which supported high purity grade.[341] Co nanoparticles

coated with carbon layer had also been used for immobilisation of inorganic catalyst.[343]

1.4 Research gap

The review above clearly illustrates that the reactive species are fundamental for many biological activities. It was also seen that their uncontrolled levels leads to oxidative stress, which causes several forms of unpredictable effects that eventually results in several severe diseases including cancer, Alzheimer's and Parkinson's diseases (neurological), obesity and diabetes (metabolic), etc. Understanding and linking the type of diseases to the quantitative levels of oxidative stress and the types of reactive species, would lead to improved understanding of the life cycle of various diseases, thereby would help in the treatment approaches like the development of targeted drugs against the diseases.

As a given cell can only tolerate a limited amount of ROS (the most common form of reactive species), the levels of oxidative stress can be used as a measure for monitoring damages. To be able to understand the link between the level of damage and the viability status of cells, it is vital to carry out systematic, reasonably straightforward, adaptable and reproducible studies. The complexity of biological environments, short half-life (instability) of reactive molecules or radicals, varying levels of antioxidants in and out of cells, and no immediate symptoms expressed for this condition, makes it challenging to correlate the strength of oxidative stress and the levels of harmful effects directly.

Photodynamic therapy is an oxidative stress ($^1O_2$) dependent approach used for treating malignant diseases. As seen in **Section 1.2.2.2**, the established methods for *in vitro* PDT reactions commonly make use of internalised photosensitisers for the generation of intracellular oxidative stress, and *in vivo* all the administered photosensitisers would not be internalised and some would be present around the cells in tissue fluid in the region of irradiation. Hence, *in vivo* the photosensitisation reactions would generate

both intra- and extra-cellular oxidative stress induced effects. To be able to narrow down the broad view of uncontrolled high levels of ROS that results in destruction of oxidation of biological substrates like cells of malignant diseases, to statistically analysable and predictable information, extracellular oxidative stress reactions would be used as a model to develop an instrument and methods that would enable such studies.

1.5 Aims

The aim of this study was to develop an instrument and a method to carry out oxidative stress reactions (OSR). Three different types of OSR would be carried out; microfluidic flow OSR (MFOSR) with immobilised photosensitiser, microbatch OSR (MBOSR) and MFOSR with photosensitiser in solution. To carry out the reactions using microfluidic approach, various microfluidic chips would be designed, fabricated, in some cases photosensitisers covalently immobilised and used for the reactions together with an optimised flow system for improved cell recovery. MBOSR would be used to determine the optimum conditions to use in the MFOSR with photosensitiser in solution.

Outline

The background information of the research, the project interests and the aims are provided in this chapter. The materials, methods, the properties of the developed instrument and the type of pumping systems tested are listed and described under **Chapter 2**. The types of microfluidic chip designs, surface treatments and the verifications for the presence of immobilised photosensitisers are given in **Chapter 3**. The results corresponding to OSR have been discussed under **Chapters 4, 5** and **6**. The results for MFOSR with immobilised photosensitiser are discussed in **Chapter 4**, **Chapter 5** discusses the MBOSR and the trends associated with the increase or decrease in the light dose and the concentrations of the photosensitiser, and **Chapter 6** discusses the MFOSR with photosensitiser in solution. The overall conclusions for the thesis and the possible future directions have been summarised in **Chapter 7**.

CHAPTER 2 - Experimental materials and methods

2.1 General information and materials used in the experiments

This chapter provides the experimental methods that were used for obtaining the results discussed in **Chapters 3** to **6**. The solvents, acids, bases, photosensitisers and other reagents used, and their distributors are provided in **Table 2.1**. The table also provides the materials used for cell culture and the kits used for assays. Aqueous chemical solutions for microfluidic applications were prepared using water with the inorganic-resistivity of 18.2 MΩ cm at 25 ºC, which was obtained by purifying using ELGA option 4 coupled with ELGA UHG PS system (ELGA process water, UK). The solutions made were filtered using 0.22 micron sterile syringe filters (EMD Millipore) to remove any debris, which could otherwise possibly be introduced into the microfluidic channels.

Table 2.1: *The materials used in the experiments.*

Solvents	
Acetone, Laboratory Reagent Grade	Fisher Scientific
Acetonitrile, HPLC Grade	Fisher Scientific
Chloroform D, H_2O < 0.01%	Euriso-top®, Derbyshire, UK
Dichloromethane	Fisher Scientific
Hexane, HPLC Grade	Fisher Scientific
Hexane from petroleum fraction, Laboratory Reagent Grade	Fisher Scientific
Methanol, HPLC Grade	Fisher Scientific
Ethanol, Analytical Reagent Grade	Fisher Scientific
Propan-2-ol	Fisher Scientific
Tetrahydrofuran, Laboratory Reagent Grade	Fisher Scientific
Toluene, extra dry with molecular sieves, water < 50 ppm, Acroseal®	Acros Organics, New Jersey, USA
Diethyl ether	Fisher Scientific
Propionic acid	Alfa Aesar, Lancashire, UK
Acids and Bases	
Sodium hydroxide pellets	Fisher Scientific
Concentrated sulphuric acid	Fisher Scientific
Hydrochloric acid	Fisher Scientific
Magnesium sulphate	Fisher Scientific
Potassium carbonate	Fisher Scientific
Triethylamine	Sigma-Aldrich, Dorset, UK

continued…

continued…

Table 2.1: *The materials used in the experiments.*

Reagents	
Pyrrole	Sigma-Aldrich
4-Acetamidobenzaldehyde	Sigma-Aldrich and Acros Organics
Hydrogen peroxide 100, Laboratory Reagent Grade	Fisher Scientific
Cholesterol	Sigma-Aldrich
(3-Aminopropyl)triethoxysilane	Sigma-Aldrich and Acros Organics
Triethoxy(ethyl)silane	Sigma-Aldrich
Sodium borohydride	Alfa Aesar
Photosensitisers	
Porphyrin derivatives	In-house
meso-Tetrakis(4-sulfonatophenyl) porphyrin	Frontier Scientific, Inc., Utah, USA Inochem, Ltd. (Distributor), Lancashire, UK
Aluminium (III) phthalocyanine tetrasulfonate	Frontier Scientific, Inc.
Rhodamine B Isothiocyanate	Sigma-Aldrich
Rose Bengal	Sigma Aldrich and Alfa Aesar
Cell culture	
Phosphate buffered saline (PBS) tablets	Gibco (Invitrogen), UK
RPMI-1640 with L-Glutamine	Lonza
RPMI-1640 without Phenol Red and without L-Glutamine	GE health care, UK
Fetal Bovine Serum (FBS)	Gibco® Life Technologies, UK
Penicillin Streptomycin	Gibco® Life Technologies
Assay Kits	
Annexin V FITC	AbD SeroTec, Kidlington, UK
LDH assay kit	Roche Applied Science, Sussex, UK
Trypan blue (0.4 %)	Gibco® Life Technologies

2.2. The instrument developed for oxidative stress reactions

Photosensitisation reactions in PDT use monochromatic and narrow range visible light emitting sources for the excitation of photosensitisers to their higher energy states, usually from their ground state (S_0) to excited states (S_1 or S_2). *In vivo*, visible lights of higher wavelengths (approximately greater than 600 nm) are usually employed due to their ability to penetrate much deeper into tissue than higher energy wavelengths (~ 380 to 600 nm). In this research, two white light emitting diode (LED) arrays, capable of emitting multiple wavelengths were used as the visible light source for conducting photosensitisation reactions.

2.2.1 Instrument setup

To conduct the microbatch oxidative stress reactions (MBOSR) and the microfluidic flow oxidative stress reactions (MFOSR), it was crucial and a prerequisite for the use of a higher energy visible light (380 - 720 nm) source with low levels of heat emission. Neutral white LED arrays were selected, as they were capable of emitting a broad range of wavelengths in the visible light region with low heat output.

2.2.1.1 One LED array setup

An instrument (**Figure 2.1**) was built according to the author's design for conducting oxidative stress reactions (OSR). A single neutral white light emitting diode (LED) array (420-750 nm, 24 V, 1.25 A, Bridglux) was fitted onto a polished metal surface of a heat sink using two screws, with thermal conducting paste underneath the LED array. The LED array contained 24 LEDs arranged in a grid pattern of 4 rows by 6 columns within a circular region of 17 mm in diameter, and were covered by a thin layer of resin (yellow colour) to protect against damages to individual LEDs and their circuits (**Figure 2.2**). To the grated side (opposite side) of the heat sink, a cooler fan (12 V, 100 mA) with a cross-sectional diameter of 5 cm was attached. Both heat sink and the cooler fan were obtained from an unused desktop computer.

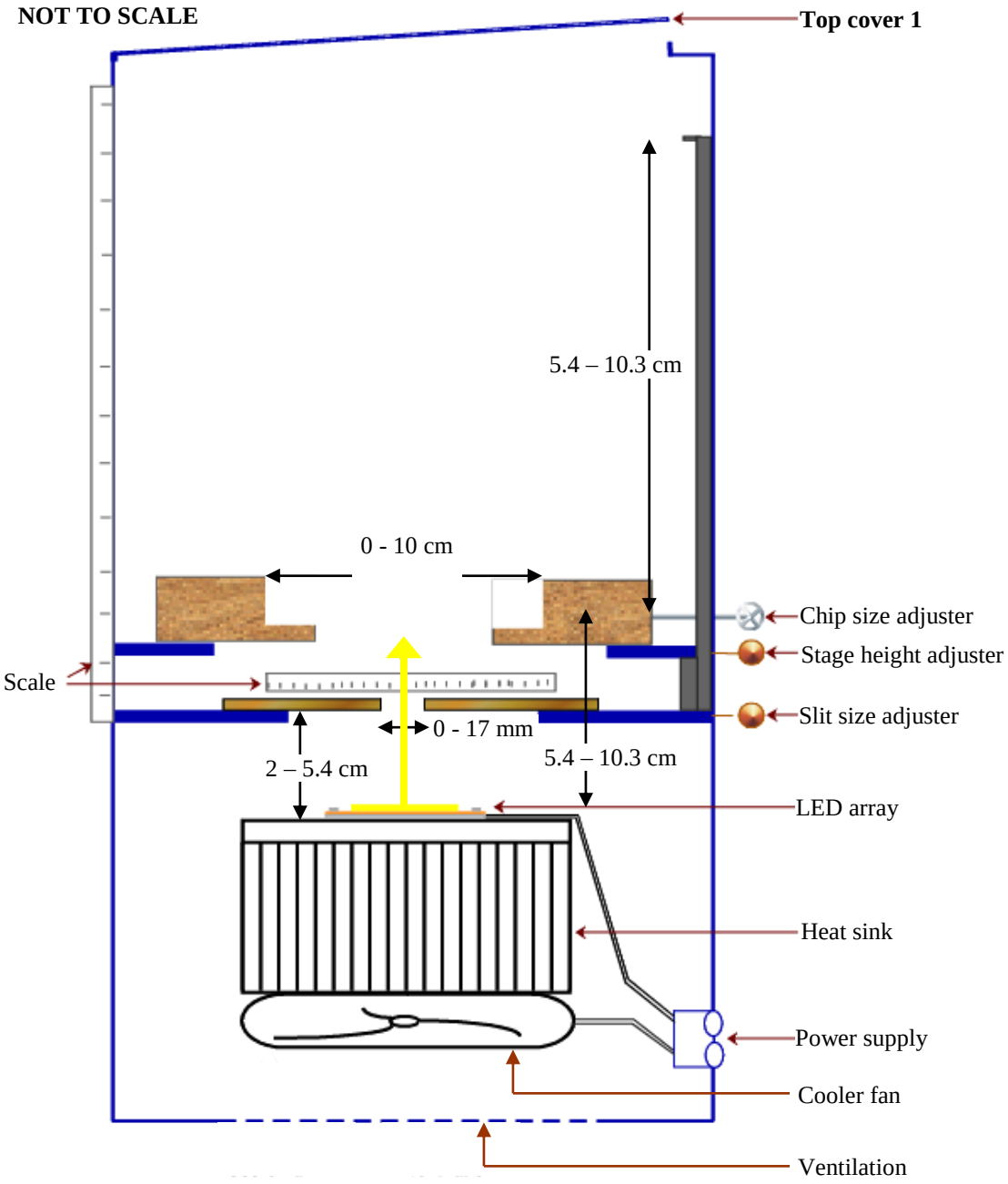

Figure 2.1: *Instrument setup with one LED array*.

In order to control the region of illumination, a light-letting slit was installed vertically above the LED array, for which the slit widths (0-17 mm) and its vertical height (2–5.4 cm) were adjustable. Perpendicularly above the light-letting slit a stage was fitted with a pair of chip holders, and their horizontal distance was variable between 0-10 cm to enable accommodation of chips of different lengths. Top-down view of the instrument is given in **Figure 2.3**. The thread-screw chip holders on the stage could be used for inlet and outlet connections to a microfluidic chip. Alternatively, externally

assembled microfluidic chip setup (**Section 2.4.3**) can be placed on the stage, for running photosensitisation reactions. The vertical height of the stage from the LED array was also adjustable (5.4–10.3 cm) to enable variation in fluence rate. All the above components were fitted onto a metal block base (0.5 x 20.5 x 28 cm) and the entire setup was covered using a metal casing (20.5 x 27.0 x 28.5 cm), with a lid on top for easy access. To reduce internal reflections within the box, the inner surface of the metal box was completely painted in black to absorb excess light radiation.

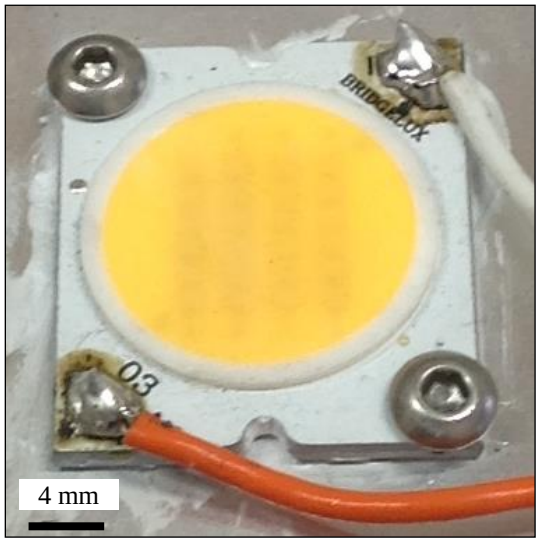

Figure 2.2: *The LED array used as the white light source.*

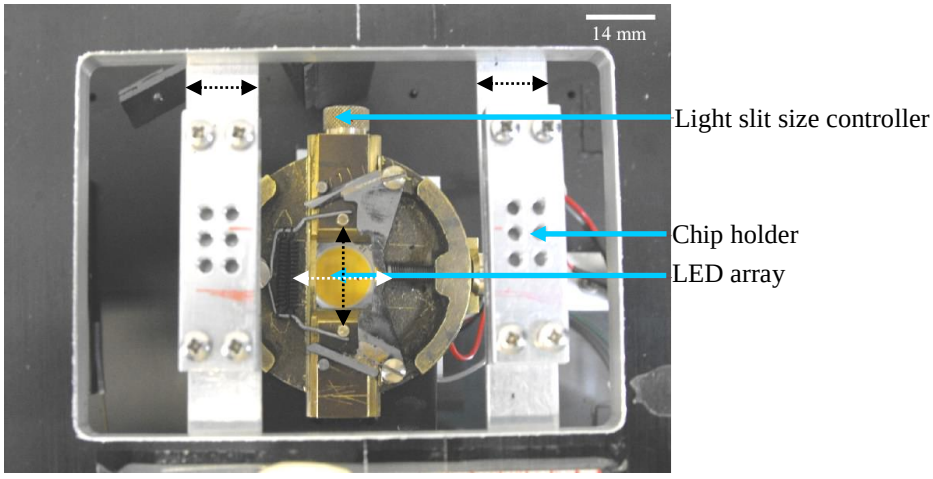

Figure 2.3: *Top-down view of the bottom LED array, light-letting slit and the chip holders, within the instrument box.*

To control the LED array setup, a fused (two fuses, 230 V, 315 mA) power-pack unit was also built, with ON-OFF switch, LED-driver and a

potentiometer. The potentiometer was produced using three resistors (RV1 50, RV2 100 and R1 110 kΩ), it was used to limit the maximum current supplied to the LED array and for varying the light intensity output. In the electrical connection circuit path of the LED array, a switch was incorporated to turn the LED array ON and OFF with the help of a LED driver. The power-pack was electrically double insulated and two fuses (230 V, 315 mA) were used near the connection to the main power supply, to improve overall safety. The cooler fan was controlled by the main power supply. The arrangement of the electrical circuit is shown in **Figure 2.4**. The components required for the LED array setup was purchased from Farnell element 14 electrical components (UK) and from RS components (UK).

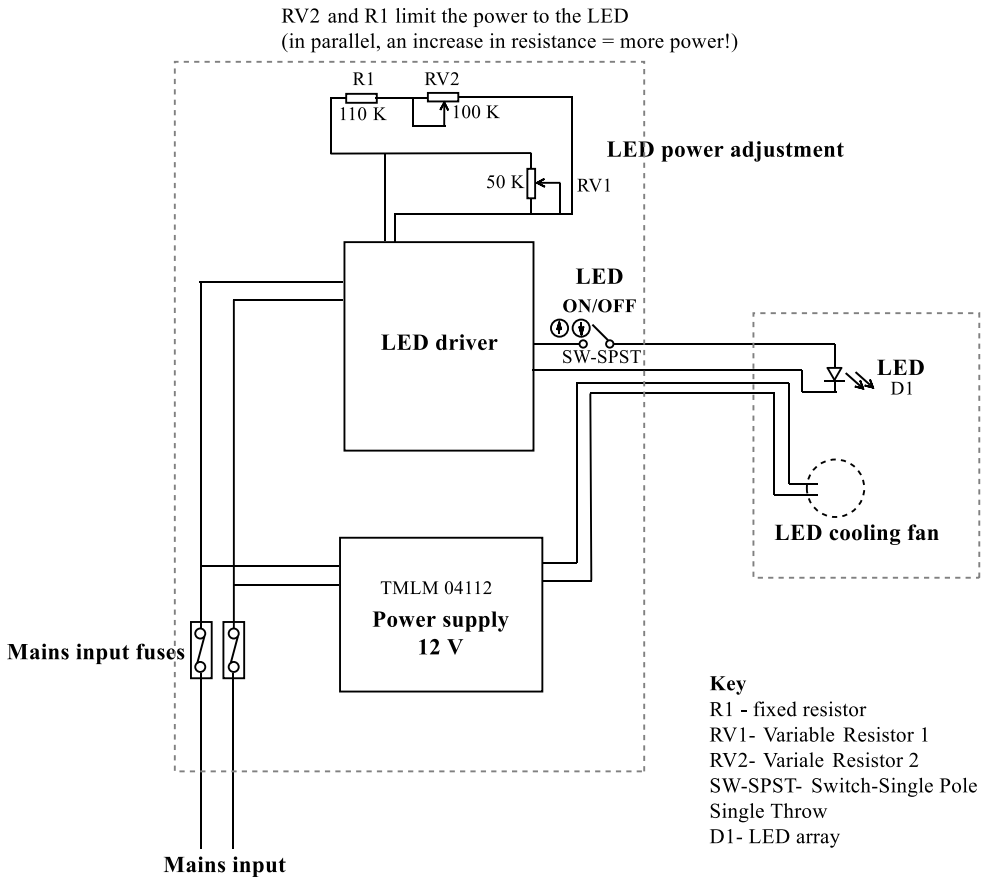

Figure 2.4: *The circuit diagram of electrical connections and the arrangement of components within the power-pack unit.*

The instrument was built according to the design laid out in **Figure 2.1**, which was made to stand vertical with the dimensions 20.5 x 27.0 x 28.5 cm^3 (**Figure 2.5**). The upright arrangement of the design allowed the

microfluidic chips to be orientated horizontally and stably within the chip holder without additional means of securing the chip in place. Overall, the developed instrument contained a light source with low heat output, and the excess heat generated was continuously removed out of the box by the integrated cooler fans. The strength of the light energy was controllable with the use of the light intensity-output controller incorporated into the power-pack unit. The distance between the light source and the microfluidic chip was made adjustable. Next to the LED array, slits were positioned to control the regions of the microfluidic chip to be irradiated, and the entire instrument was completely covered using a metal casing thus preventing entry of any stray light from the surrounding and reaching the microfluidic chip placed on its platform.

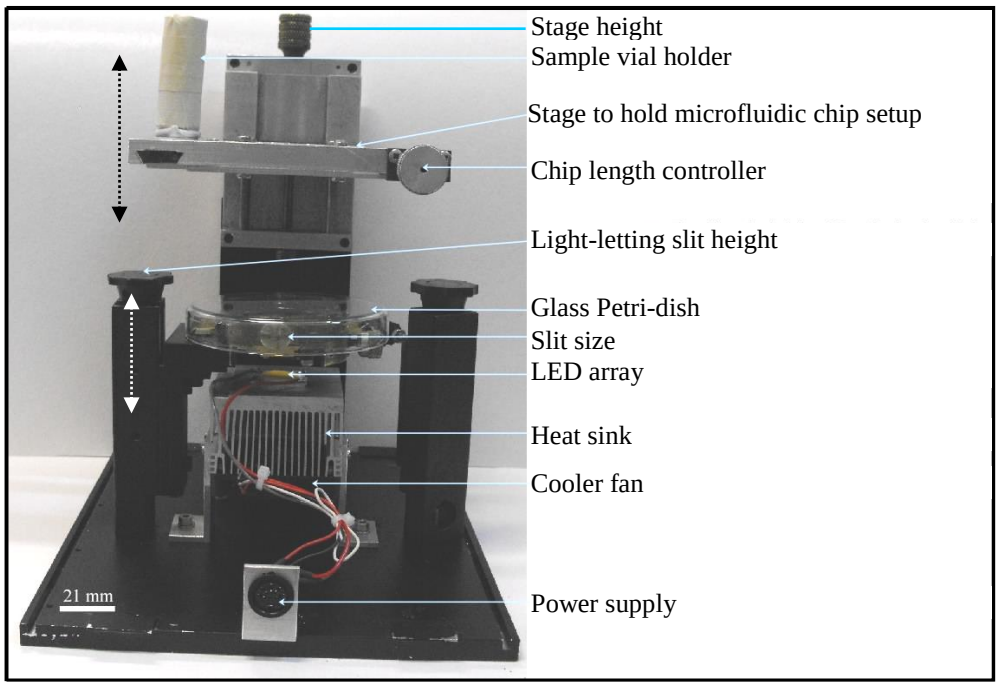

Figure 2.5: *The instrument setup that was built with single LED array.*

The alignment of the bottom LED array, light-letting slits and the chip holder stage were on the same plane of vertical axis **(Figures 2.1, 2.3** and **2.5)**. This alignment was important as it gave the shortest distance between the LED arrays and the microfluidic chip, thereby unnecessary reduction in the light energy and the wastage of unwanted spaces within the instrument box was minimized.

2.2.1.2 Two LED array setup

From the initial MFOSR with immobilised photosensitiser, it was determined that with the use of single LED array, the total length of time that was essential to irradiate the flowing cells with a given strength of light dose was too long (several minutes). It was established from early experiments, with the use of lower flow rates (0.1 - 5 µl min^{-1}) to achieve higher light dose, higher number of cells were retained within microfluidic channels, thereby resulting in insufficient numbers (less than 1x 10^4) of cells being collected for analysis. Hence, the use of lower flow rates to achieve higher light dose was not a reasonable approach for the cell work considered. To attain higher light dose while maintaining higher flow rates (20 - 50 µl min^{-1}), it was essential to increase the fluence rate or the length of the channels. Hence to increase the fluence rate, integration of a similar second LED array was considered as the most sensible solution, thereby to mitigate the situation of changing multiple parameters like chip designs and the type of light source.

The second LED array (420-750 nm, 24 V, 1.25 A, Bridglux) was fitted onto a metal heat sink with a cooler fan (12 V, 100 mA) and the unit was suspended (from top) onto a second lid made for the instrument (**Figures 2.6** and **2.7**). The extension protruding out of the box was used to vary the vertical height (0 - 9 cm) of the second LED array, relative to the stage used for placing the microfluidic chip, which was also used to vary the fluence rate. The top (second) LED array was positioned in vertical alignment with the bottom LED array, and the stage for placing the microfluidic chip setup (**Section 2.4.3**) was in-between the two LED arrays. This type of arrangement was essential to deliver maximum strength of fluence rate as possible. Further the cooler fans were facing away from the stage for effective removal of heat out of the instrument box from above and below. The second LED array and its cooler fan were controlled using an external stabilised power supply (L30B, Farnell).

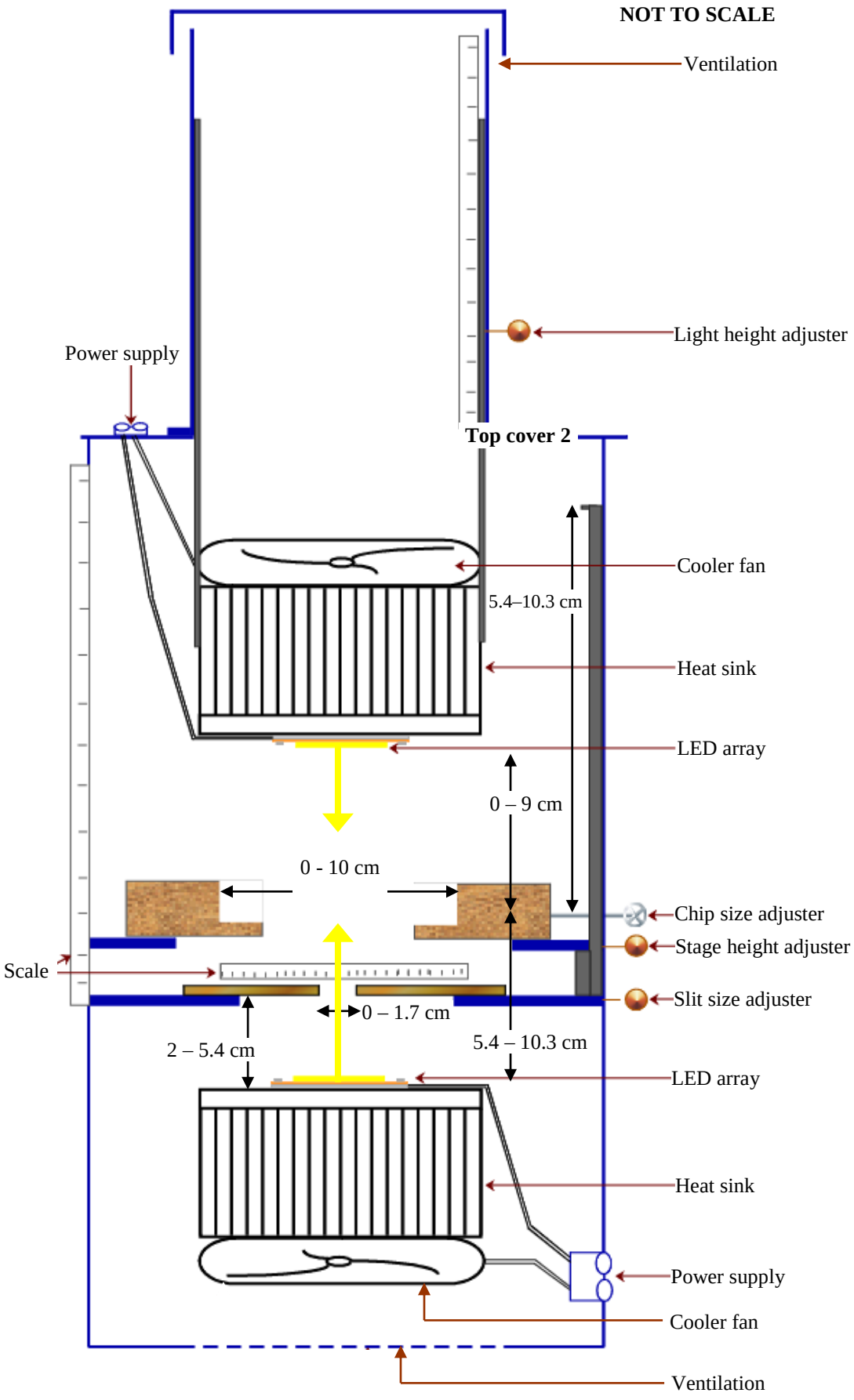

Figure 2.6: *Instrument setup with two LED arrays.*

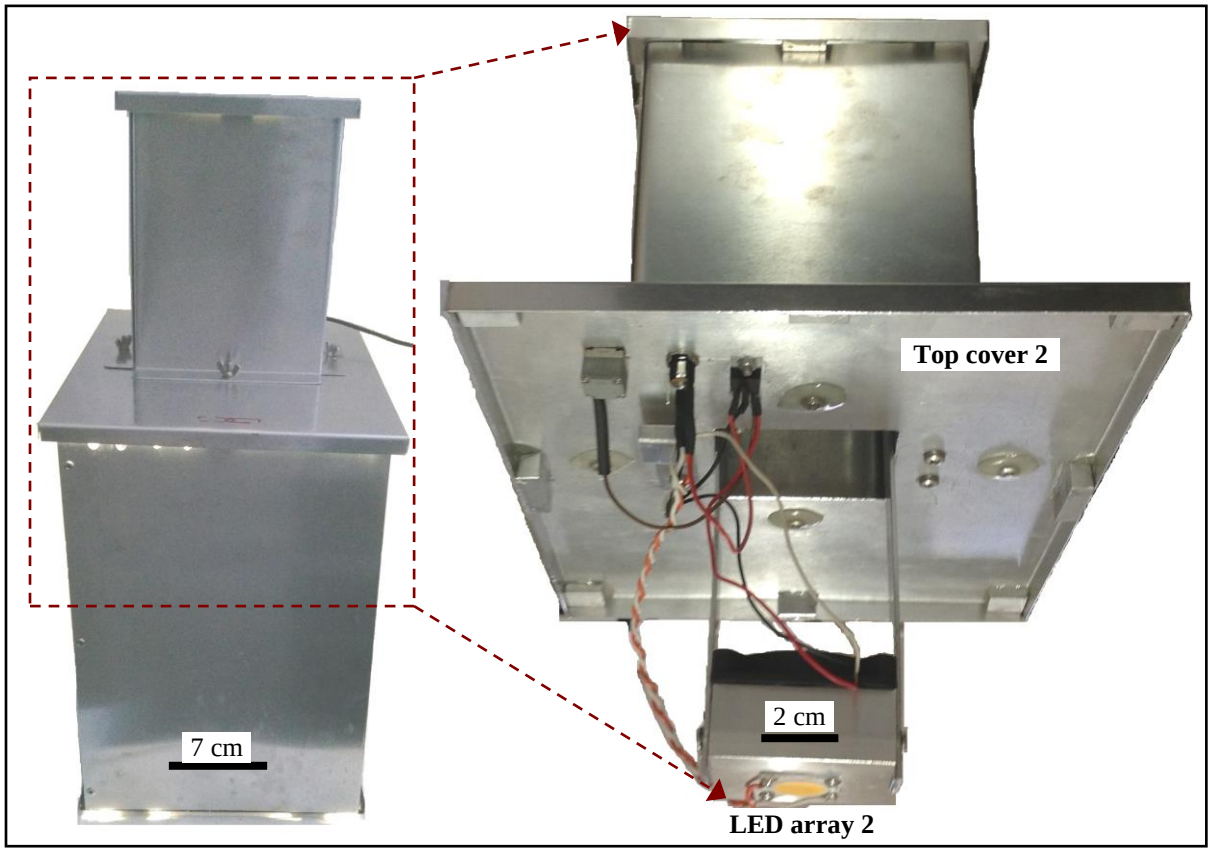

Figure 2.7: *The instrument setup that was built with two LED arrays.*

2.2.1.3 Components of microfluidic oxidative stress reactions

There were three key components vital for running MFOSR, they were;
1) pump - to force cell suspension through microfluidic chip at a fixed flow rate, 2) an instrument with high energy visible light emission, and 3) microfluidic chip setup.

For the initial MFOSR, syringe (1 ml, BD Plastipak, Oxford, UK) and syringe pump (e.g. Pump 11 Plus, Pump 11 Elite or Harvard PHD-2000, Harvard Apparatus, Kent, UK) were used to flow cell suspensions through the microfluidic channels. The complete setup is shown in **Figure 2.8,** where the cells were flowing through a photosensitiser immobilised chip during a typical MFOSR. The flow rates required were controlled using the settings on the pump before starting to pump the cells through the microfluidic channels. The cells suspended in liquid medium were pumped through the capillary tubings connected to the inlet of the chip, through the microfluidic channels and collected in a sample vial at the outlets for

analysis. The power-pack unit on the right hand side of **Figure 2.8** contained a switch to turn the primary LED array system ON and OFF, and a light intensity output controller to adjust the strength of light irradiance.

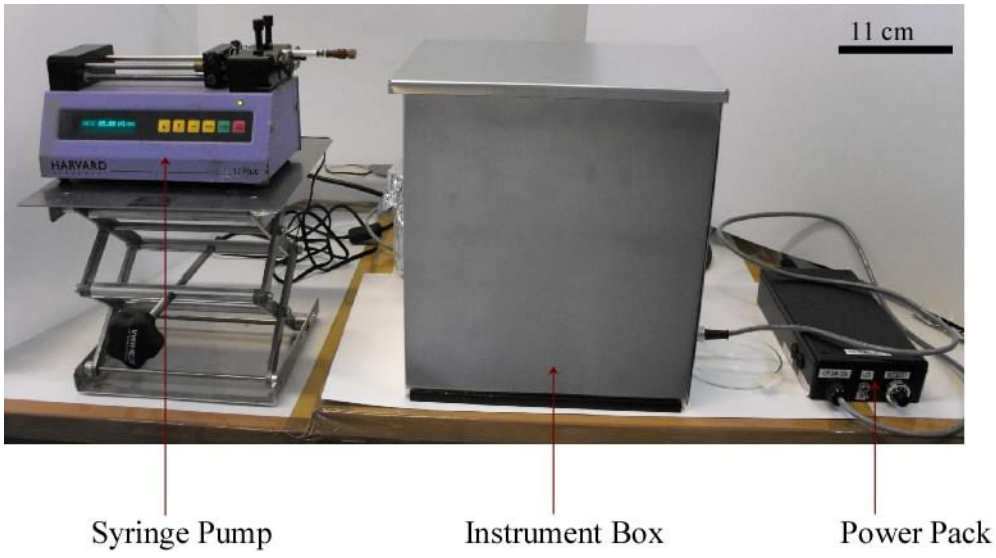

Figure 2.8: *Typical arrangement of syringe pump, the instrument (microfluidic setup inside) and the power pack unit, during microfluidic photolysis reactions.*

As shown in **Figure 2.9**, the LED arrays were the only source of light that irradiated the microfluidic chip within the instrument. The microfluidic chip can be either surface treated or non-surface treated, which was dependent on the type of experiment of interest. In both cases the setup would look similar; with the only difference being the channel surfaces would be chemically non-treated or would contain immobilised photosensitiser. The sample collection vial (1.5 ml polypropylene tube) was placed within the metal casing of the instrument, close to the outlet of the microfluidic chip into a holder that was covered with aluminium foil, to avoid exposure to light. Since the radiant intensity at a given distance was known from the light measurements, it was possible to calculate the total light energy delivered to the samples using the length of exposure to light as the only variable. For the MFOSR, the latter was determined using the residence time of cells within the illuminated regions of microfluidic channels.

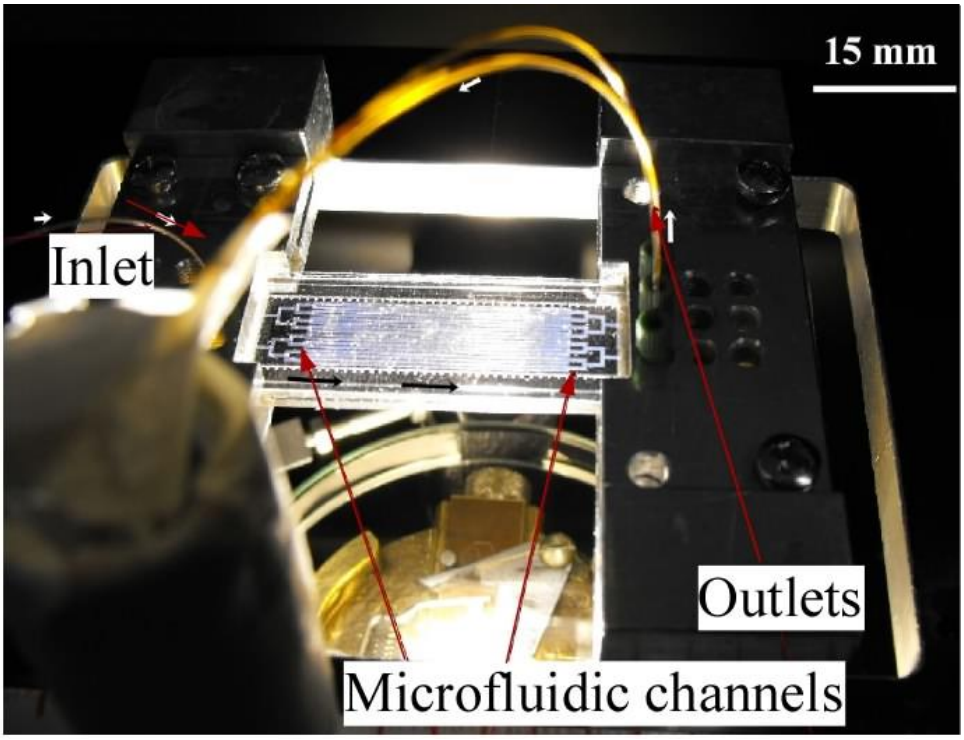

Figure 2.9: *Typical view of the microfluidic flow oxidative stress reaction experimental setup.*

2.2.2 Light energy delivered

A visible light radiometer (Molectron, pyroelectric power meter) with a light sensor (PM150 detector head) of diameter 19 mm and a readout unit (PowerMax® 500A) was used to measure the light energy in terms of irradiance (mW). The radiant intensities (I_R, W) were recorded using 100 mW full scale of deflection settings on the light meter. The light energy falling on the light sensor surface was varied using the light intensity output controller, by varying the distance, or the combination of both. Using similar adjustments, illuminance (photometric) light measurements (lux) were also recorded using a light meter (Amprobe LM-120) fitted with a silicon photodiode in the sensor head.

2.2.2.1 LED arrays as the visible light source

The neutral white LED arrays capable of emitting wide range of wavelengths in the visible light region were employed for the photosensitisation reactions. It was essential to measure and quantify the amount of light fluence that reached the photosensitisers and the cells within the microfluidic channels at a known distance from the light source. There

were two possible forms of measurements for the visible light source; photometric and radiometric, the former being the measure of illuminance and the latter was the measure of irradiance. The conversions between the radiometric and the photometric units were not a linear scale transformation, especially when multiple wavelengths of light are involved. Hence the light energies at known distances were directly measured in terms of the radiometric units (mW), and were used for calculating and designing the reactions. Further, this measurement enabled direct comparison of results with the existing studies in the PDT field.

The amount of light energy reaching within the channels would be reduced, due to being reflected and refracted at different angles, relative to the strength of light energy falling on the outer surface. The microfluidic chips were made of 2 x 1 mm thick borosilicate glasses, in which the etched channels would be approximately half-way between the 2 mm thick chip. Hence, when measuring light energies, a glass slide of 1 mm thick was placed on top of the light sensor. The use of a glass slide similar in chemical composition and thickness, accounted for the fraction of light that was deviated without reaching the channels.

2.2.2.2 LED arrays as the white light source

The LED arrays emitted white light (visible) in the wavelength range of 420-750 nm (**Figure 2.10**). Porphyrin derivatives were used as the photosensitisers for both MBOSR and MFOSR. The sensitisers had absorption at multiple wavelengths within the visible light spectrum. Hence, a single light source with wide range of wavelengths was advantageous for the microfluidic photolysis reactions considered, as it allowed switching between different types and classes of photosensitisers (with different excitation and emission wavelengths), without the need to change the light source.

The spectrum of relative light emission intensity against wavelength (**Figure 2.10**) shows that, the relative intensity of the light output was constant between the wavelengths 550 - 600 nm, and the wavelength of the

maximum light emission (relative intensity of 1.0) was at around 450 nm. The maximum intensity at 450 nm was a useful property of the light source, as porphyrin derivatives usually show an intense absorption at around 430 nm, called the Soret band.

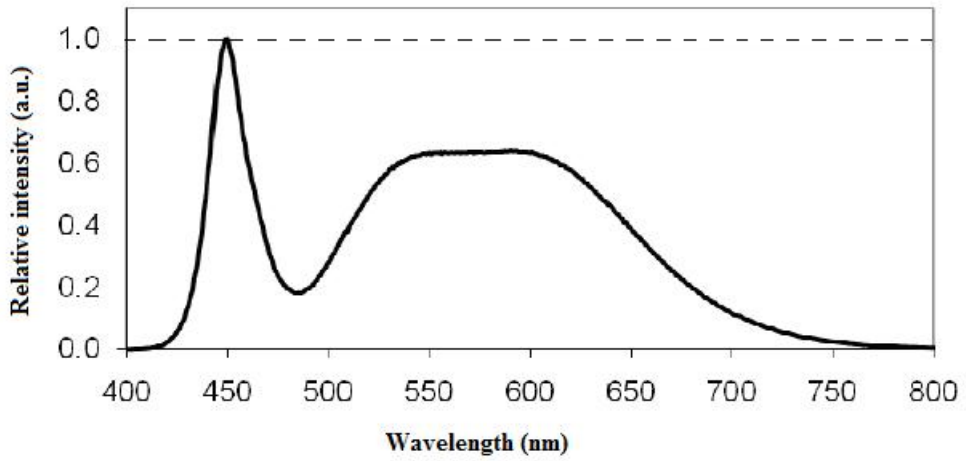

Figure 2.10: *Emission spectrum of the neutral white LED array, showing the relative intensity of light emitted against their characteristics wavelengths, at rated test current, Tj=25 °C (data obtained from the Bridgelux product data sheet).*

2.2.2.3 Light intensity (illuminance) emitted

Illuminance (E_L) is the measure of photometric light per unit area. It has the units of lumens per meter squared (lm m^{-2}) and lumens per foot squared (lm ft^{-2}), also commonly referred as Lux (lux) and footcandle (fc), respectively. Photometry is the measurement of light's brightness or luminous intensity (I_L). Luminous intensity is the wavelength-weighted power per unit solid angle, that is, it is associated with the measurment of light energy relative to the most perceived wavelength (555 nm) sensed by the eyes. The wavelength of 555 nm is the maximum response recorded in the photopic vision measurement, and it is also the intersection point on the scotopic vision response curve, which has its maximum response at the wavelength of 507 nm. Illuminance (E_L) is directly proportional to luminous intensity (I_L) and inversely proportional to the square of its distance (r), **Equation 2.1**. Where, E_L is the illuminance in lm m^{-2} or lux, I_L is the luminous intensity in lm sr^{-1} and r is the distance to the light source in m.

$$E_L = \frac{I_L}{r^2} \qquad \textbf{Equation 2.1}$$

Illuminance (photometric) measurements were made using a light meter (Amprobe LM-120) with the sensor head fitted with a silicon photodiode and filter. The light meter was capable of measuring visible light from multiple sources, and the readings were recorded in lux (1 lux = 1 lm m^{-2}) units. The light intensity output (illuminance) controller switch on the power-pack unit was used to control the level of current supplied to the LED array, thereby the luminance. Illuminance from the bottom LED array was measured at a distance of 10.3 ± 0.1 cm, with the light output controller set at full (10.0 a.u.), for which the maximum luminance of 35250.0 lux was recorded. When the light controller was set at minimum (0.0 a.u.), luminance of 4587.5 lux was recorded. Luminance intensities were recorded at the intervals of 0.5 a.u. between the minimum and the maximum range (0.0 to 10.0 a.u.) of the controller. The light intensity measurements were repeated four times and the averaged values were used to plot (**Figure 2.11**) the calibration curve of illuminance (lux) against controller reading output (a.u.). Illuminance from the LED array increased with the controller readings (**Figure 2.11**), and was not linearly related, but the trend was a curve with two minor turning regions.

As the measurement of I_L do not represent the true strength of the radiant flux from the light source, and were only the measure of wavelength-weighted light energy per unit solid angle, the total light energy irradiated by the light source was remeasured in terms of irradiance. For the same reason, the latter was the most commonly employed scale for measuring the amount of light energy used in photochemical and photosensitisation reactions.

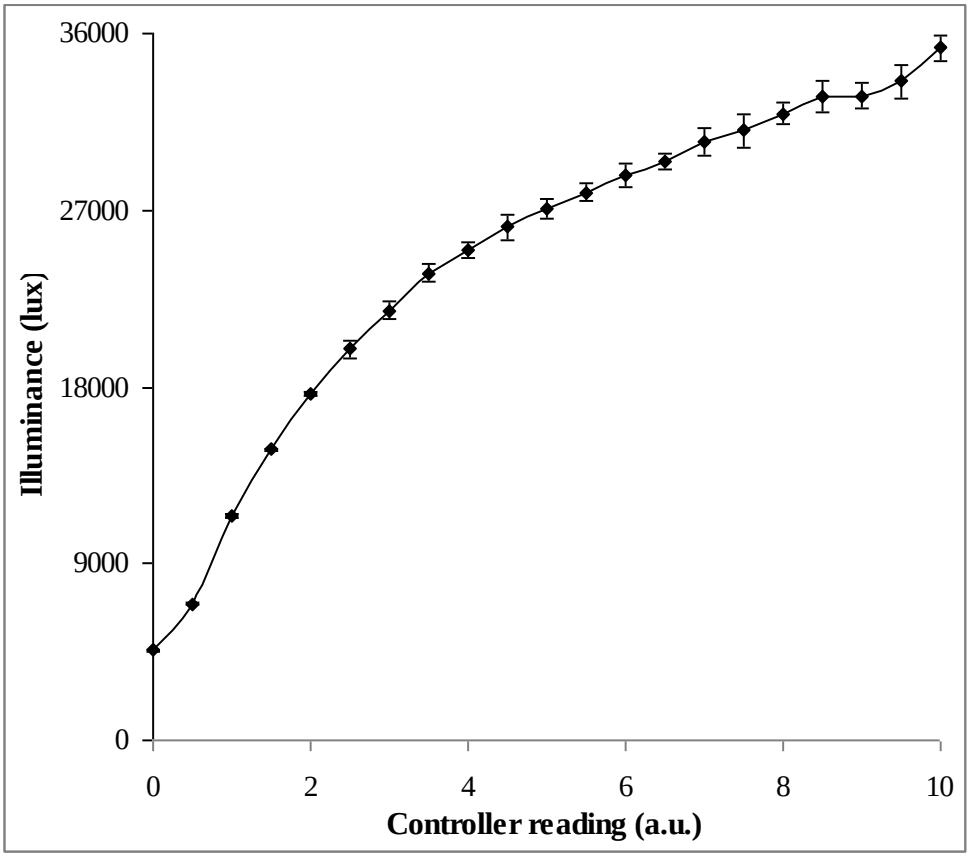

Figure 2.11: *Calibration curve of light intensity output (lux) against controller reading values (a.u.), at a fixed distance of 10.3 ± 0.1 cm from the bottom LED array. Standard deviation errors of n = 4.*

2.2.2.4 Light energy (irradiance) emitted

In radiometry, radiant energy is measured. Irradiance is the measure of radiometric light per unit area, which has the units of watts per meter squared (W m^{-2}). Radiant intensity (I_R) is the radiant flux (ϕ) per unit solid angle, and the I_R measurements account for all the photons falling on a given surface at a known distance from the light emitting source. Hence, irradiance is the measure of the total light energy striking per square unit surface area from a known distance from the light source. Similar to illuminance, irradiance (E_R) is directly proportional to radiant intensity (I_R) and inversely proportional to the square of its distance (r), **Equation 2.2**. Where, E_R is the irradiance in W m^{-2} or J s^{-1}, I_R is the radiant intensity in W sr^{-1} and r is the distance to the light source in m.

$$E_R = \frac{I_R}{r^2}$$ **Equation 2.2**

According to **Equation 2.2**, reducing the distance (*r*) between the LED arrays and the microfluidic chip would increase the amount of light energy striking the microfluidic channels. The outcome of a photosensitisation reaction is linked to the total amount of light energy that was delivered at a predetermined rate. To enable comparison with the results reported for PDT reactions using conventional methods, it was essential to know the quantity of light energy delivered to the samples in terms of the energy units. As illustrated in the spectrum in **Figure 2.10**, the LED arrays were capable of producing wide range of wavelengths. Therefore, the light energies of all frequencies had to be measured simultaneously. A radiometer that was capable of measuring white light energies (multiple wavelengths) was used to make irradiance measurements.

To capture and record the light energy emitted by the LED arrays, radiometer was used together with a circular light sensor of diameter 19 mm. The corresponding surface area of the sensor was calculated to be 2.84 cm^2. The radiant intensities (I_R in W) were recorded using 100 mW full scale of deflection settings on the light meter. Using the values for detector surface area and the radiant intensities, irradiance, (E_R in W m^{-2}) at known distances from the light source was calculated. The light output controller on the power-pack unit of the primary LED array setup was used to manage the levels of radiant intensity output, where the smallest variable level was 0.1 a.u.. The maximum light energy recorded with the light intensity controller set at its maximum (10.0 a.u.) and the light sensor at a distance of 5.4 ± 0.1 cm was 34.91 mW cm^{-2}, and at a distance of 10.3 ± 0.1 cm was 10.76 mW cm^{-2}. Having the light intensity output controller set at its minimum (0.0 a.u.), the amount of light energy recorded at the distances of 10.3 ± 0.1 and 5.4 ± 0.1 cm were 1.76 and 4.76 mW cm^{-2} respectively. These were the maximum and the minimum strengths of the light energy output at the distances specified, along with which at the increment of 0.5 a.u., many other measurements were also recorded and calibration curves

were plotted (**Figure 2.12**). The amount of light energy recorded for the controller readings at 9.0 and 10.0 a.u. were the same, which could be due to insensitivity of the light meter under the settings it was used.

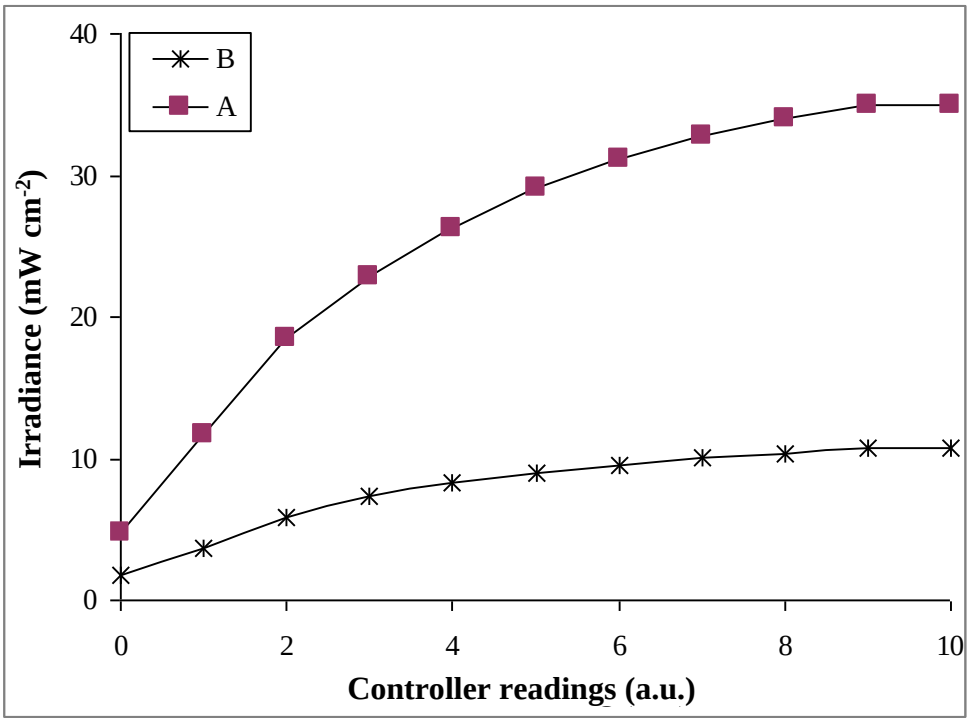

Figure 2.12: *The calibration curves of light irradiance from one of the two LED array against the light output controller reading. Plot* **A** *was at a distance of 5.4 ± 0.1 cm, and plot* **B** *was at a distance of 10.3 ± 0.1 cm, from the bottom LED array.*

There were two ways of altering the rate at which the light energy was delivered to the samples; one was to vary the distance between the LED arrays and the sample, and the other was to vary the light intensity output (radiant flux (ϕ)) using the controller fitted to the power-pack unit of the instrument. The total amount of light energy received by each cells flowing within the microfluidic channels would be the product of exposure time (s) and the radiant intensity (mW cm^{-2}). The length of exposure to irradiance, referred to as the residence time, was directly linked to the flow rate used, hence the amount of light dose delivered.

Due to the design of the setup, the shortest and the longest distance achievable between the bottom LED array and the chip stage were 5.4 ± 0.1 and 10.3 ± 0.1 cm (**Figure 2.12**). However, the second LED array (from

top) was movable much closer to the chip. But it was not preferable to have it within mm scale of vicinity, as at smaller distances transfer of thermal radiation would become significant. Hence the top LED array was used at a distance of 3.4 ± 0.1 cm away from the stage. The calibration curve of maximum irradiance against distance from single LED array (top) is given in **Figure 2.13**. For conducting oxidative stress reactions, the LED arrays were most commonly used at the distances of 3.4 ± 0.1 and 5.4 ± 0.1 cm from the stage.

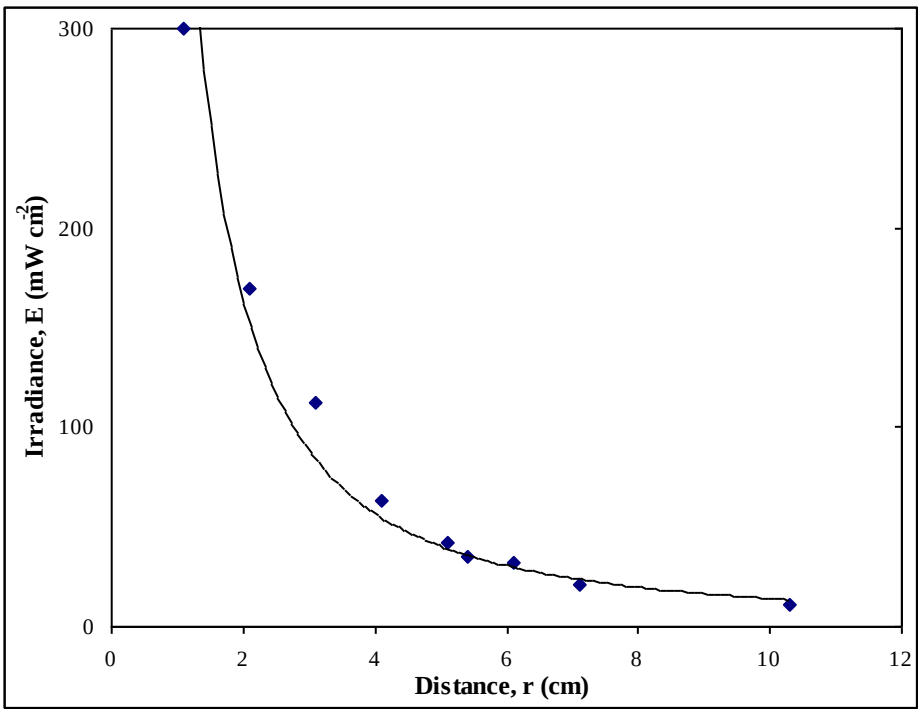

Figure 2.13: *Maximum light irradiance from one of the two LED array (top) against distance.*

When using the light irradiance readings for the MFOSR, the following three major assumptions were made, 1) The amount of light energy reaching the cells within the microfluidic channels were independent of the chip designs used, as the thickness of all the fabricated glass chips were the same, 2) the amount of light energy scattered out of the channels of a given design were negligible and 3) the variation in the strength of light energy along 60 or 120 µm deep channels would be constant and uniform at all regions along the depth.

The key variables, the distance to the LED arrays, the light intensity output controller reading, the total irradiance from both the LED arrays, and the time (residence time) for which the cells were illuminated were known. Using the above parameters, the fluence rate and the total light doses were calculated for the photo-oxidation experiments.

2.2.3 Thermocouple measurements

The temperature variation due to heat radiation from the bottom LED array was measured as a function of time (minutes) using *Pico Technology, USB TC-08* thermocouple data logger. The temperature variations were measured at three different points; a thermal sensor-tip was placed on top of the heat-sink, the other was between two glass slides having it on the stage where the microfluidic chip would normally be placed for irradiation, and the third sensor was left at room temperature. As a control for thermal changes, the measurements were initially carried out having the LED array power OFF, and later the measurements were repeated with the LED array switched ON.

2.2.3.1 Temperature fluctuations due to heat from the light

Heat released from the artificial light emitters is one of the major issues often faced with the use of high intensity light emitting sources. It can lead to rapid increase in the temperature of the surfaces directly exposed to such sources. With sufficient length of illumination, the temperature within the instrument box could increase. This occurrence of increased heat would have negative effects on the experimental results of the photosensitisation reactions, as high temperature itself could induce changes in cell viability. Therefore, it was crucial to evaluate the temperature changes as a function of time, when the LED array was turned ON. The temperature variations due to heat radiation from the light sources were measured and recorded against time, using a thermal sensor at a fixed distance from the bottom LED array. It was essential to maintain the overall temperature fluctuations within the instrument box at an acceptable limit, preferably between 20 °C and 37 °C. Increase in temperatures higher than 37 °C would have detrimental effects on the metabolic activities of the cells, and the results

collected from such conditions would lead to incorrect conclusions about the photosensitisation reactions conducted using the instrument.

As a control, temperature variations were recorded having the entire instrument turned OFF. The results were used to compare that any temperature variations on the tip of the metallic thermocouple sensors were not an artefact. The temperature changes were measured over 1 hour, at one minute time intervals (**Figure 2.14**). The measurements showed that, the room temperature at which the experiments were conducted had an average temperature of 20.35 ± 0.15 °C. The temperature variations recorded using the thermocouple device was much more precise compared to the analogue thermometer measurements.

When the measurements were repeated with the instrument turned ON, it was observed that the temperature of the chip directly facing the LED array increased above the room temperature over time. From the observation, it was concluded that the objects directly facing the LED array get heated up a few degrees as a result of thermal irradiation from the LED array (**Figure 2.15**). When the measurements were repeated, the results exhibited few degrees of rose in temperature on top of the starting temperature. Hence the results were not averaged out or used to determine standard deviations, as it had no true meaning to the actual temperature changes observed. Over the 60 minutes intervals considered the highest temperature recorded as a result of heat emission from the LED array at 5.4 cm was always well below 37 °C (~ 21.0 - 23.5 °C). The cells can tolerate well up to this temperature, as they were cultured or incubated at this temperature.

By maintaining the temperature of the heat sink close to the room temperature, through continuous removal of heat using the cooler fans, enabled to keep up with the recommended life span of the LED arrays, and reduced accumulation of heat within the instrument. Inefficiency in the removal of heat energy would lead to rise in temperature within the instrument box, and as a consequence heat the microfluidic chip placed

within it. Excessive heating would results in thermal denaturation of the cells flowing through the channels, rather than through the cascade effects induced by the photo-oxidation reactions from ROS production. Changes in the number of cells or their healthy state, due to the nature of the experimental setup rather than from the experimental conditions would influence the data collected, hence the corresponding conclusion. Overall it was concluded that the total heat accumulated within the box over an hour was not high enough to influence the biological aspects of the cells used for the OSR.

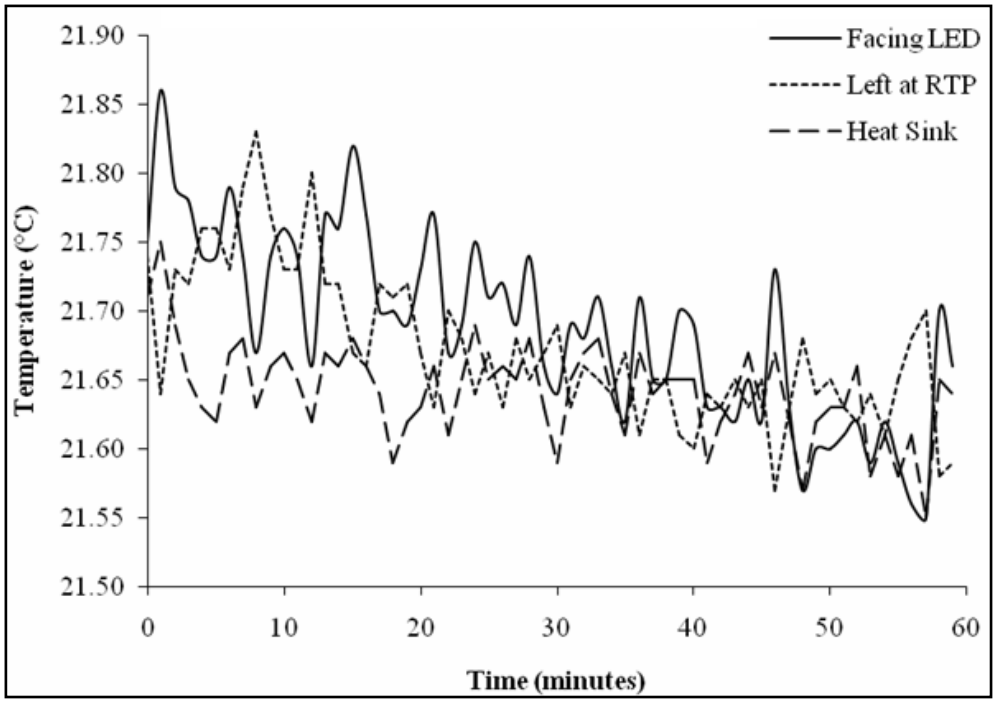

Figure 2.14: *The variations in the temperature with time, when the instrument was OFF and the sensors placed facing the LED array, on the heat sink and left at RTP.*

If the temperature of the heat sinks were to increase, the temperature inside the box would also rise indicating an ineffective removal of heat out of the box. With the instrument turned ON, it was not possible to measure the temperature changes on the heat sink using the thermocouple metal sensor, that is, the readings obtained were anomalous and such data points are not shown on the plot in **Figure 2.15**. The thermocouple sensors were made of metal, when it came in contact with another metal surface like the heat sink which had adjacent live electrical connections, the measurements failed. Therefore, an analogue mercury thermometer was used to measure the

temperature variations on the heat sink and the measurements showed similar temperature variations to its surrounding, that is, similar temperature variations to that observed for the sensor facing the LED array.

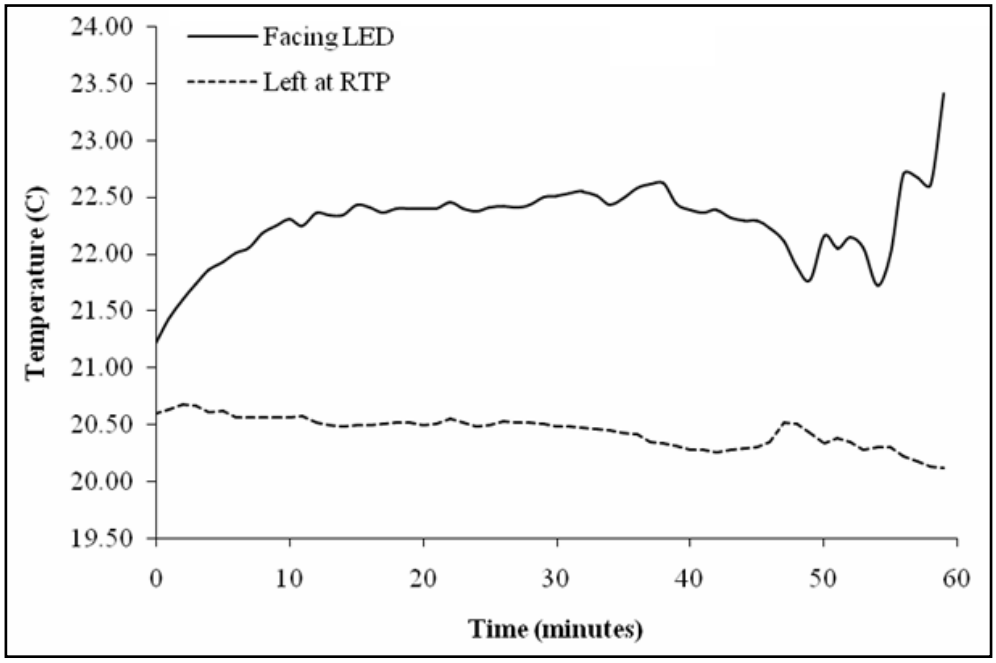

Figure 2.15: *The temperature variations within the instrument box at a distance of 5.4 ± 0.1 cm away from the LED array, which was ON at its full power.*

2.3 Pumping methods

Number of different methods for flowing homogenous liquids of different densities through microfluidic channels were considered and applied. This section covers three different types of pumping systems used; syringe pump, pressure pump and peristaltic pump.

2.3.1 Syringe pump

Syringe pumps are one of the most commonly used fluidic pumping system. They are widely used in medical fields such as for slow and constant administration of drugs. In recent times, in addition to the use of syringe pumps for microfluidics and nanofluidics applications, they are also widely used for application such as electrospinning, microdialysis and mass spectrometry for injection of samples at lower flow rates. Hence, in this research, syringe pump was the first default choice of pumping system for conducting MFOSR.

Low responsiveness, strong hysteresis, limited volume of samples and motor step related oscillations in the flow, are some of the drawbacks associated with the use of syringe pumps. However, these limitations were not the major issues for pumping cells at a fixed flow rate for the photosensitisation experiments. There was an additional problem associated with the use of syringe pump for cell based experiments, which was the sedimentation of cells to the bottom of the syringe. The gravitational force acting on cells caused them to move to the bottom of the container. Cells and particles those were heavier to remain in suspension, sedimented to the bottom of the syringe to reduce their gravitational potential energy. This was the state with the cells suspended in RPMI medium or in PBS solution.

Two distinct flow rates (5 and 50 µl min^{-1}) have been studied using the syringe pump (e.g. Harvard PHD-2000 or Harvard plus), having the microfluidic chip under a phase contrast inverted light microscope. At a lower flow rate (5 µl min^{-1}) only few number of cells passed through the channels to reach the collection vial at the outlet, while with the use of higher flow rate (50 µl min^{-1}), more cells moved through the micro-channels and got collected at the outlet. The differences in the number of cells collected were due to the differences in the length of time spent by the cells within the syringe. At slower flow rate (5 µl min^{-1}) cells spent higher length of time (ten times) within the syringe relative to higher flow rate (50 µl min^{-1}). The higher the length of time spent within the syringe, the higher the chances of cells settling within the syringe without flowing through the channels. The flow rate was inversely related to the residence time, that is, increasing the flow rate would decrease the residence time and *vice versa*. Longer exposure time delivers higher light dose, consequently higher the probability of favouring photochemical and photobiological reactions. Therefore, to irradiate using higher light dose slower flow rate had to be used. The maximum or the higher level of flow rate was limited by the set of conditions essential for the microfluidic reactions. Under most of the chosen microfluidic oxidative stress conditions, the use of slower flow rate was essential to deliver the total intended light dose to the flowing cells.

Syringe pumps were useful for maintaining constant flow rate. However, presence of blockages within the channels led to increased backpressure, and even under such circumstances constant flow rate was maintained at the expense of high backpressure. It was observed overtime (~10 min) the cells sedimented to the bottom of the syringe, and at two minutes intervals it was essential to manually rotate the syringe along the horizontal axis to bring the cells back into suspension. Settling of cells to the bottom surface of syringes could not be prevented, even when the syringe pump and the syringe were placed at an angle greater than zero (0-90°). Cells those settled to the surface of the container did not flow through the capillary connecting to the inlet of the chip, and remained within the syringe even towards the end of the experiment. To overcome sedimentation of cells, a number of different interfaces between syringe pump and inlet of microfluidic chips were developed, as illustrated in the following sections.

Similar to solid microparticles (1.21×10^8 particles ml^{-1}, polystyrene beads) cells settled down due to the action of gravitational force. The rate at which it occurred was dependent on the density of the medium and the physical parameters of the suspended particles. Similar types of sedimentations were observed with magnetic nanoparticles (Turbobeads) and microbeads. With the use of magnetic nanoparticles the magnetic attraction between the particles led to aggregation followed by sedimentation as large units. Settling of microbeads due to gravitational force occurred over a wide range of timings, which was dependent on the viscosity of the medium, and mainly on the concentration and the density of the suspended element. To resuspend the sedimented particles, methods such as agitation or gentle tapping of the container wall were not effective to redistribute the cells or the particles uniformly back in suspension.

Interfaces used to maintain cells in suspension

In order to maintain higher number of cells in suspension, different types of interfaces were developed to use along with the syringe pump setup. The types of interfaces were *spiral cell-container*, *serpentine cell-container* and *cylindrical chamber attached to a rotator*. Each of these interfacing

methods were tested with the target of maintaining larger proportion of cells in suspension, thereby higher number of cells flow through the microfluidic channels and into the collection vial, with minimum or no alterations to their healthy status.

(a) Spiral cell-suspension container

The use of *spiral cell-container* was recognised as one of the first interfacing method to keep the cells equally distributed in solution for longer time and possibly for the full length of the experiment. The typical length of the experiments was about 30 minutes, but it varied depending on the amount of samples that had to be pumped through the chips and the flow rates used. Spiral shaped cell containers were initially made of flexible plastic tubing (ID 0.050″, OD 0.090″), by wrapping around a plastic rod of 1 cm in diameter. Following an initial success of maintaining cells in suspension for longer time in comparison to solely using a syringe pump without an interface, the same design was made of glass (ID2300 OD3000 µm, **Figures 2.16**) and was used for the flow oxidative stress reactions.

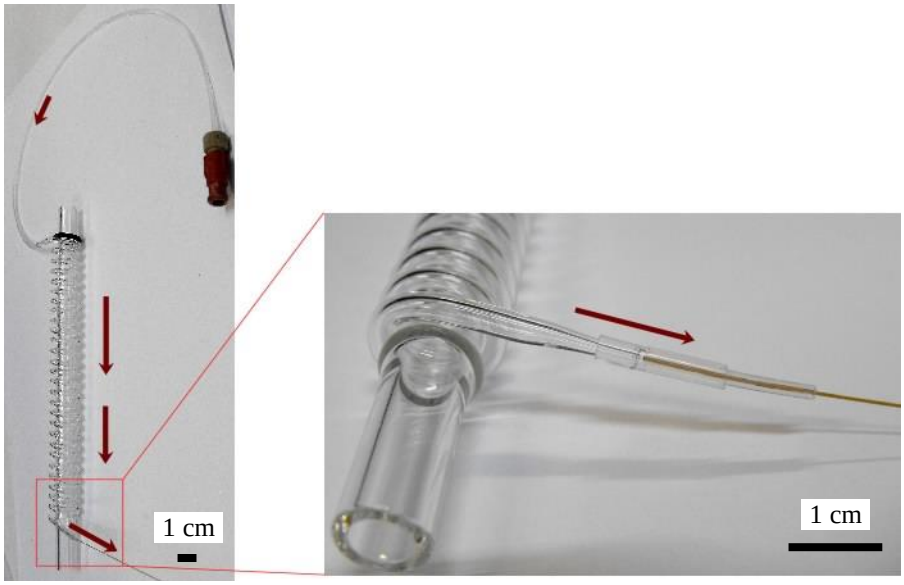

Figure 2.16: *Spiral cell-container made of glass into which cells would be preloaded to maintain cells in suspension without allowing them to sediment.*

Cell suspension was loaded into the *spiral cell-container*, and connected to the capillary tubing from the syringe on the syringe pump at one end, and to the fused capillary at the inlet of the microfluidic chip at the other end. The

incoming liquid from the syringe on the syringe pump displaced the preloaded sample at a similar flow rate at which it entered; the latter was set on the syringe pump. The displaced cell suspension was pushed into the inlet of the chip.

The use of *spiral cell-container* allowed transfer of higher percentage of cells across the microfluidic channels (**Figure 2.17**) to the collection vial (outlet). The results illustrated that this interface design was advantageous compared to using only the syringe on a syringe pump placed either horizontally or at an angle. The successes of flowing cells across the microfluidic channels to the collection vials were measured as the *percentage recovery* of cells relative to the *untreated* controls. The measure of *percentage recovery* of cells allowed quantitative comparison between different experiments. The *spiral cell-container* interface design was effective and worked well at higher flow rates (e.g. 50 µl min^{-1}), and at slower flow rates (e.g. 5 µl min^{-1}) the cells needed to be in suspension for longer time, which led to sedimentation of cells to the nearest glass surface. For slower flow rates, the design was not proficient enough in maintaining higher percentage of cells in suspension.

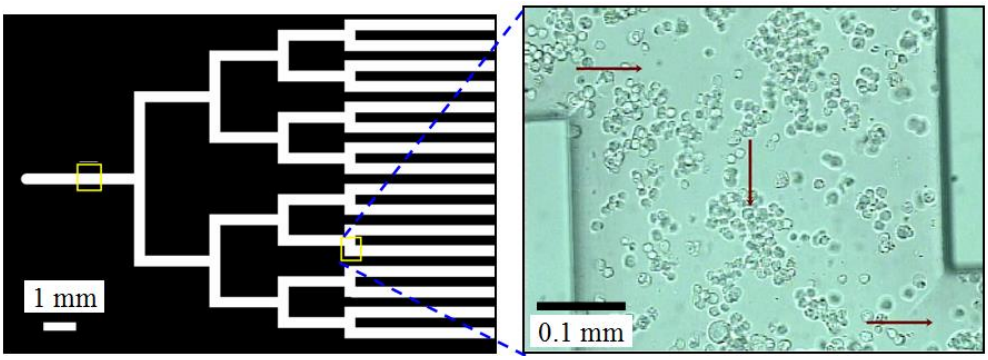

Figure 2.17: *The typical level of cells that flows within the channels homogenously at the beginning, with the use of the spiral cell-container.*

Cell suspensions flowed at higher flow rates prevented the cells from settling to the bottom of the container, but the steep rise in backpressure within the *spiral cell-container* was unavoidable. The high backpressure caused leakages at the capillary connections, and interruptions to the cell

viability was also suspected. The rise in backpressure may not be an issue for experiments that do not involve cells, but with cells the rise in pressure can severely affect their viability, thus inducing various modes of cell death.

With the use of this design it was originally predicted that, even if the cells were to settle to the immediate bottom regions within the containers, they would still be relatively spread apart from each other. But when using slower flow rates (e.g. 5 µl min^{-1}), the cells those settled to the immediate bottom of the container formed local centres, to which more and more cells anchored on top to form several small cell clumps along different regions of the *spiral cell-container* (**Figure 2.18**). Hence the purpose of using the *spiral cell-container* approach to reduce the number of cells gathering and clumping together was not completely achieved.

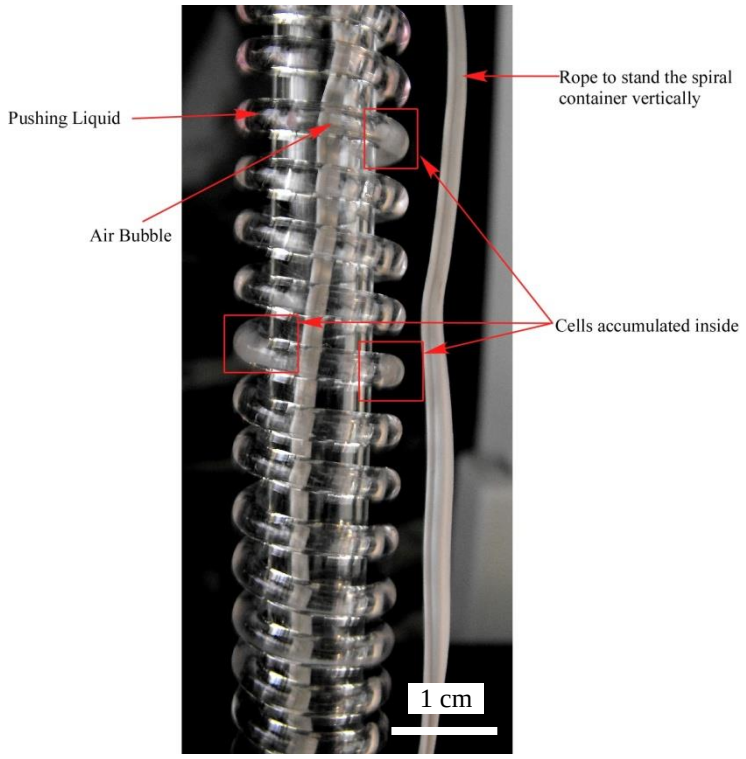

Figure 2.18: *Cells clumped together at different regions within the spiral cell-container.*

For the purpose of the experiments, it was desirable to have cells flowing through chips at a constant rate, that is, being evenly distributed and flowing along the laminar stream of the medium. **Figure 2.17** shows the typical amount of cells that flows through the microfluidic channels at the

beginning of each experiment, however, the number of cells dropped from several hundreds to single digits per 360^2 μm^2. The latter state continued until the final few drops of cell suspension rushed out into the microfluidic chip with several ten-thousands of cells per 360^2 μm^2, containing all or most part of the remaining cells that accumulated overtime within the *spiral-cell container* **(Figure 2.19**). The latter situation was similar to that was observed when simple syringes were used.

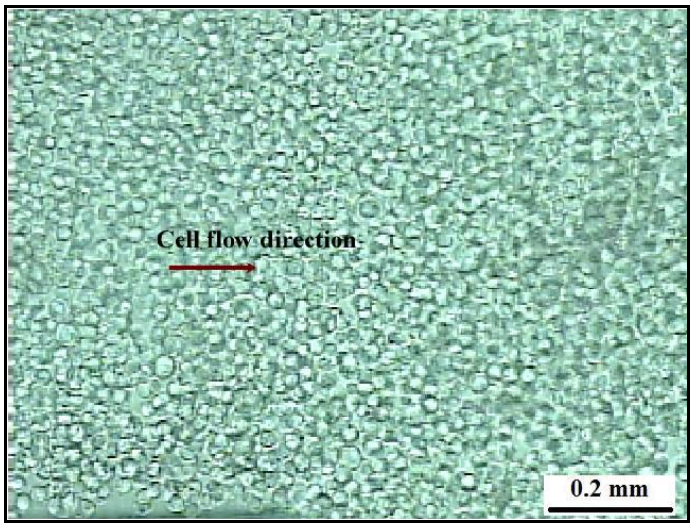

Figure 2.19: *The last few drops of cell suspension carrying several ten-thousands of cells collected within the spiral cell-container flowing through the microfluidic channels.*

(b) Serpentine cell-container

The second type of interface developed was the *serpentine cell-container* (**Figure 2.20**), the principle design of this was similar to that of the *spiral cell-container*. This design relied on continuous fall of cells either vertically or at an angle to maintain them in suspension. There were possibilities for the cells to gather together when moving through tilt regions of lower angles, but it was predicted that when flowing through the vertical regions of the containers they would separate out into individual cells. However, the cells remained attached to one another more strongly, and did not detach into single cells even when moving through the perpendicular regions of the container. At lower flow rate (~5 µl min^{-1}), similar to the *spiral cell-container* accumulation and aggregation of cells at different regions all along the container was unavoidable, and the approach worked better with higher flow rate (~50 µl min^{-1}). The experimental observations revealed that

the design was not good at maintaining cells individually in suspension for longer time.

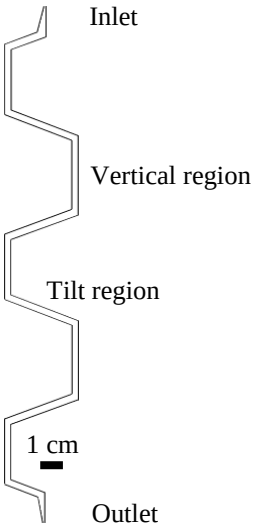

Figure 2.20: *Serpentine cell-container.*

(c) Chamber attached to a rotator

Following limited success with the *spiral* and the *serpentine* interfaces for use with the syringe pump; a third type of interface was developed. It involved the use of *linear chamber* (~ 2.5 ml) *attached to a rotator*, where the rotator rotates between the angles 0° and 180° (**Figure 2.21**). The rotator box, excluding the handle had the dimensions of 7.5 x 15.5 x 5.9 cm^3.

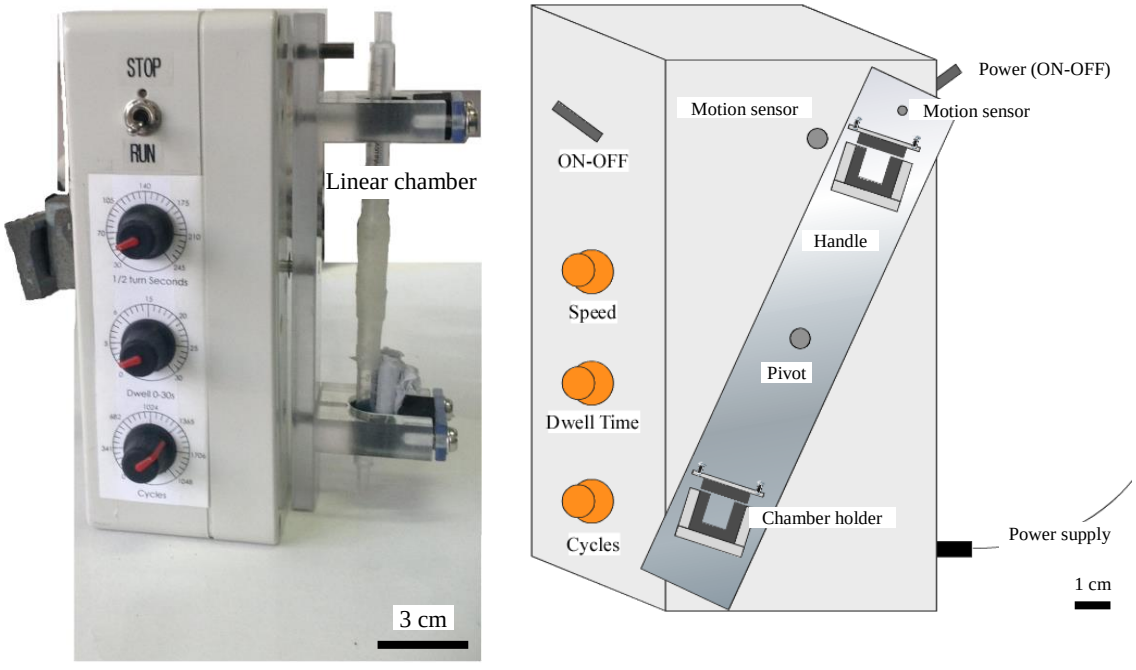

Figure 2.21: *Rotator to hold the linear chamber cell suspension container.*

Once the cells were re-suspended in colourless RPMI-1640 medium, they were preloaded into the linear chamber, similar to the one shown in **Figure 2.22**. The chamber was placed within the holders on the rotating handle and secured using screws. When the rotator was turned ON, the handle rotated between 0° and 180°, and enabled continuous mixing of cell suspension thereby maintaining the cells in suspension for the required length of time. The rotator was able to vary the speed of rotation, the number of cycles it had to rotate and the length of time (dwell-time) it should remain inverted before rotating back to its original state (**Figure 2.21**). A motion sensor was used to enable control over the dwell-time of the rotating handle when in its inverted position. 'Dwell-time' controller button was used to control how long the rotating handle must be delayed in the inverted vertical orientation before rotating back to its starting orientation. 'Speed' controller button was used to vary the speed of rotation, and the 'Cycles' controller button was used to control the number of rotations that occurred before stopping. 'Chamber-holders' on the handle were used to secure the cell-containers loaded with cell suspension.

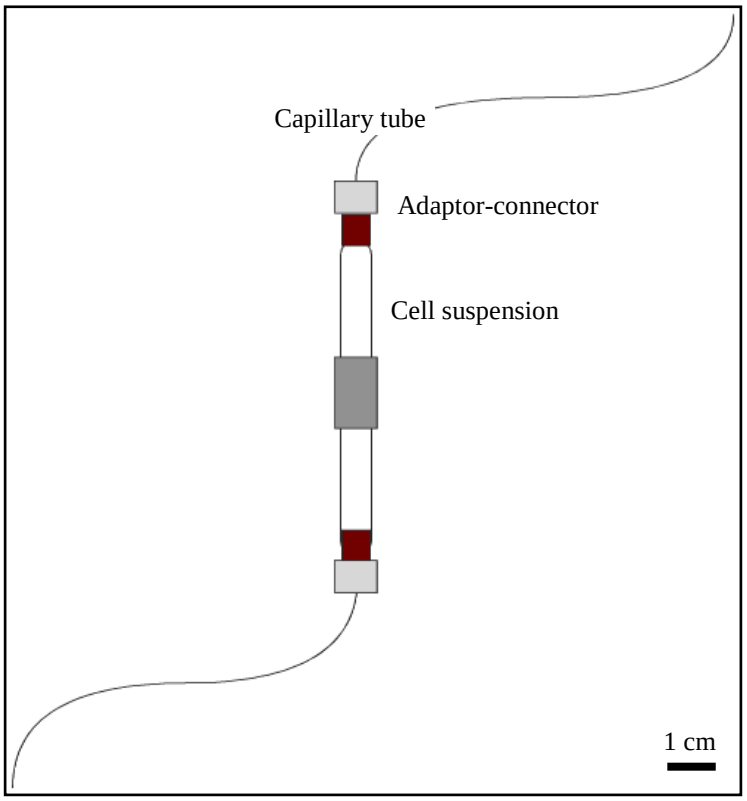

Figure 2.22: *Linear chamber for loading cell suspension, with capillary tubings at the ends.*

Liquid pumped out of the syringe using a syringe pump, flowed into the *cell suspension chamber* and displaced equal volume of cell suspension out through the capillary connected to the inlet of the microfluidic chip. Single air bubble that was deliberately introduced into the *chamber* ensured that, the cell suspension and the incoming liquid from the syringe into the chamber did not get mixed and thereby dilutes the cell concentration in the suspension.

The rotator was capable of maintaining the cell suspension in the linear chamber for several hours, which was more than the time required for the total length of the experiments. Though the method was effective in maintaining the cells in suspension for longer period, the necessity to use longer capillary tubings (ID 0.3 mm, OD 1.58 mm), 2 x 35 cm long, was a drawback. The use of longer tubings were essential to allow rotation of the handle to which the chamber was attached, but this resulted in prolonged journey for the cells before reaching the inlet of the chip.

Summary of the interfacing methods

The amount of cells eluted out with each interfacing methods were slightly higher than that of simply using a syringe and a syringe pump. Each method of interfaces had their own advantages and inadequacies as discussed above. As an additional choice of interfacing method, *spiral-cell container* was attached to the rotator handle to see if settling of cells can be reduced, but use of longer capillary tubings again increased the back pressure and caused leaking in the connections. Due to one or more issues identified with each type of interfacing methods that were developed for use with the syringe pump based flow system, other different types of flow system were tested for better results.

2.3.2 Pressure pump

Using Fluigent® pressure pump and an inert gas such as nitrogen, positive pressure was applied to the surface of the cell suspension which was held within a closed sample reservoir. The applied positive pressure forced the sample out of the cell container through the capillary which was immersed

in the sample (**Figure 2.23**). The relative levels of positive pressure applied within the closed sample vial were directly proportional to the flow rate within the microfluidic channels and hence the volume of cell suspension transferred across.

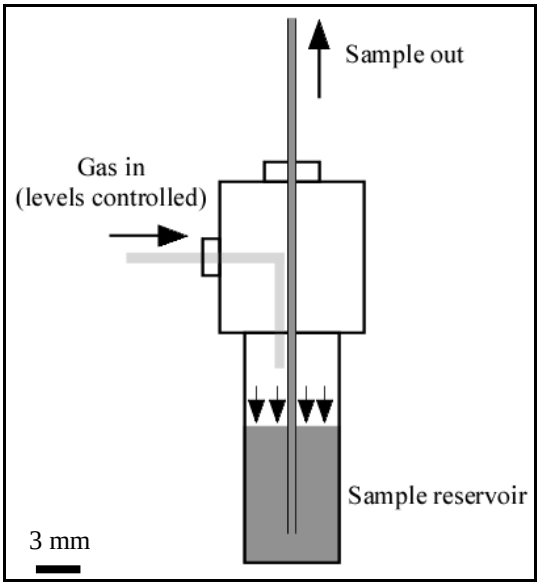

Figure 2.23: *Principle of pumping samples using pressurised controlled levels of inert gas.*

The control over the flow rate using pressure difference ensured that the samples flowed at a fixed flow rate with the known levels of pressure, provided that it was a closed flow system and the microfluidic channels were free of blockages. Presence of partly or completely blocked channels altered the flow behaviour to a greater extent than the blockages-free channels and the pressure levels in the channels became unpredictable. Under extreme levels of obstructions within the microfluidic channels, the relative backpressure increased high enough to completely stop the flow resulting from the maximum input positive pressure of 377 mbar.

The use of pressure pump guaranteed a constant level of pressure on the samples, but a constant flow rate could not be assured. With increased levels of blockages, the level of pressure required to continue the flow also increased rapidly. The pressure range for the pump was limited between -30 to +377 mbar, and in the presence of blocked channels the upper limits of pressure were reached much faster. Furthermore, the flow through the

microfluidic channels came to a halt quicker under increased backpressure. Due to the design of the container to store sample (**Figure 2.23**) before being pumped into the chip, the cells rapidly settled to the bottom of the container and no cells were seen to flow through the chip after 5 - 10 minutes from the start of the experiment. Hence, the use of pressure pump setup for flowing cells was not a good choice compared to syringe pump.

Hence the use of flow system based on either syringe pump or pressure pump, and even with modified interfaces for the syringe pump, did not transfer sufficient number of cells through the microfluidic channels to reach the collection vial at the other end of the chip.

2.3.3 Peristaltic pump

Peristaltic pump is a type of positive displacement pump. The term peristalsis refers to the process of generating wave-like movement, through repeated contraction and expansion of flexible tubing, thereby pushes the contents forward. Like syringe pumps, peristaltic systems are also widely used for many different applications, for example in medicine, dialysis and also the heart-lung machines utilise this technology, as the level of haemolysis is kept to minimum. It is also used for other purposes like chemical handling, in food industries and in scientific research.

Generally with increased flow rate, shear-stress is also increased. Positive displacement pumps like peristaltic pump are suitable for handling shear-stress sensitive fluids. There are certain drawbacks associated with peristaltic pumps, such as, tubing can lose their flexibility with time and have to be frequently replaced. Fluids moving through peristaltic pumps, especially at lower flow rates, show pulsated movement, which makes it not suitable for applications that require smooth flow. However, for the purpose of the MFOSR, the pulsated movement was not an issue, and only the total residence times of cells were measured.

Two or more rollers rotating along the tubing on the peristaltic pump causes alternating compression and expansion of it, by pressing it against the walls

of the pump and by releasing it, respectively. During compression, fluid previously held within the tubing was discharged and created a good seal, which resulted in generation of vacuum within the tubing. If this side of the tubing were to be immersed in liquid sample, the sample would be drawn up into the tubing to fill the void space, thereby maintaining the total volume within the tubing constant. Hence, the inlet side of the peristaltic tubing (40 cm) was immersed into the sample-vial containing the cell suspension and a magnetic stirrer, while the other side of the tubing was connected to the fused capillary at the inlet side of the microfluidic chip (**Figure 2.24**). Incorporation of a magnetic stirrer enabled stirring facility to maintain cells in suspension, where this was not possible with the other two types of pumping systems considered previously.

The flow rate for the peristaltic pump used was dependent on multiple parameters; which includes, the thickness and the ID of the peristaltic tubing, the extent to which the tubings were compressed by the rollers, the speed of pumping (rotating rollers), and the viscosity of the liquid or the liquid-solid mixture that was pumped. Two different ID sizes of standard Tygon® LMT-55 2-stop peristaltic tubings having the same wall thickness (0.86 mm) and length (400 mm) were tested for flowing cell suspension. The peristaltic tubing with the ID 0.76 mm was chosen as the most favourable size to interface to the inlet of the microfluidic chip, as it was capable of transferring higher number of cells without significant alterations to their viability. But the lower limit of flow rate was limited by the ID size of the tubing, for the setup with the ID 0.76 mm it was restricted around 21 µl min^{-1}. With the use of lower ID 0.19 mm, it was possible to achieve flow rates lower than 5 µl min^{-1}, but the lower ID tubing resulted in reduced throughput, increased blockages and considerably increased backpressure. Furthermore, the level of cell accumulation increased with time when using the smaller sized tubing, hence was not suitable. The overall arrangement of the peristaltic pump setup for the flow photosensitisation reaction is shown in **Figure 2.24**.

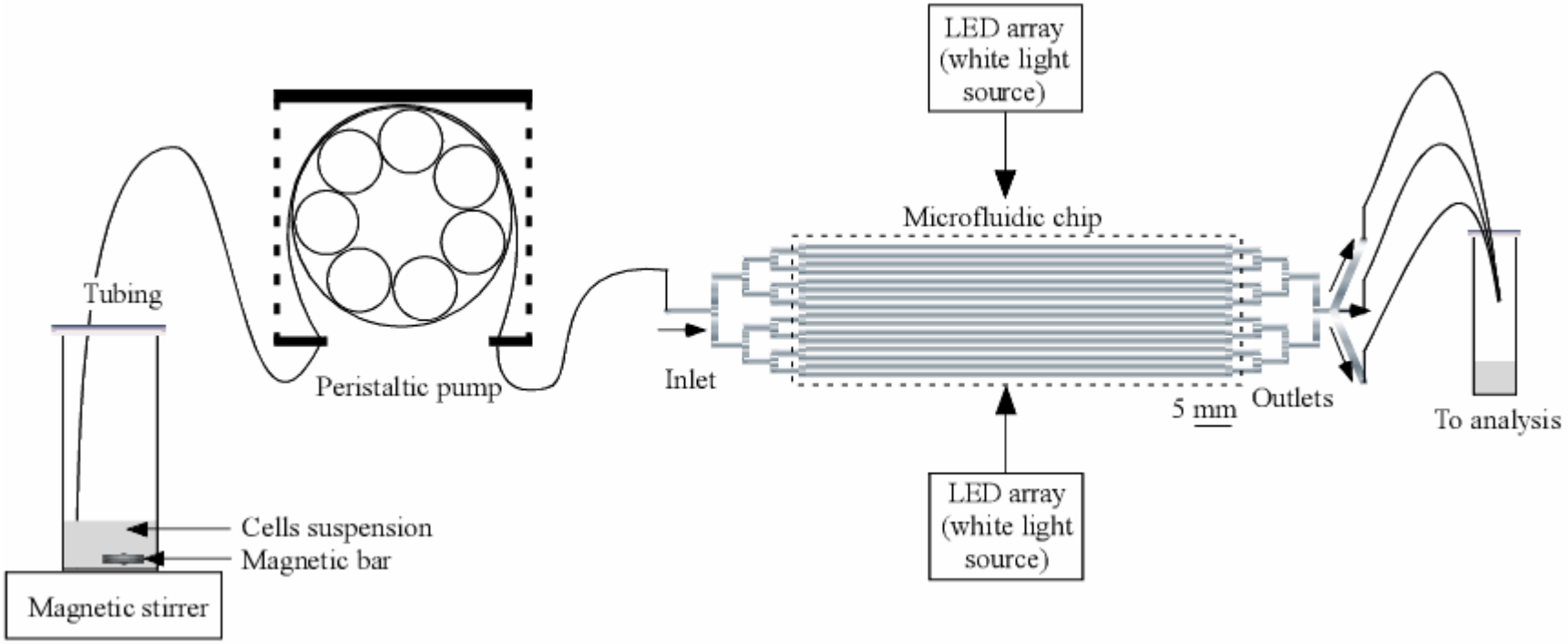

Figure 2.24: *The overall arrangement of the setup for conducting microfluidic extracellular oxidative stress reactions.*

Summary of Sections 2.2 and 2.3

The optimised instrument for conducting microfluidic flow oxidative stress (PDT-type) reaction was built, and their physical properties like illuminance, irradiance and heat build-up were measured. The instrument was initially built with single LED array and later a similar second LED array was incorporated to increase the fluence rate of light, thereby the total light dose. Various types of pumping systems were considered, studied and evaluated, and finally the peristaltic pump with magnetic stirrer was chosen as the most suitable method of pumping cell suspension (**Table 2.2**). The speed at which the cells flowed through the channels was not the same as the flow rates set on the pumps. The true speeds of flowing cells were measured under modelled experimental conditions, as it was helpful to account for the presence of any blockages and any possible leakages, at different junctions and connections from the point of cell entry to the elution collection vial.

Table 2.2: *Summary of the pumping systems used.*

Type of pump	**Applicability and suitability**
Syringe pump (Harvard PHD-2000 or Harvard plus)	Wide range of flow rates possible. Controls over the flow rates were much more precise than other two types of pumping systems. Not suitable for slow flow rate pumping of cells, microparticles or magnetic nanoparticles suspended in liquid samples.
Pressure pump (Fluigent®)	Pressure could be precisely maintained. The range of flow rate was rather limited due to limited pressure range (-37 to +377 mbar) and the precision of the flow rates were low. Not suitable for pumping cells, microparticles or magnetic nanoparticles (Turbobeads) suspended in liquid samples.
Peristaltic pump (Gilson Minipuls 2)	Suitable for both slow and fast flow rates of pumping liquid samples. Suitable for pumping cells, microparticles or diamagnetic nanoparticles suspended in liquids. Larger objects may get squeezed but not a problem with micron sized substances like cells. Peristaltic tubings have to be replaced regularly.

2.4 Synthesis, microfluidics and surface treatments

2.4.1 Synthesis of porphyrin derivatives

The porphyrin derivatives **1** to **4** were synthesised according to the methods described in the literature.[344] The reagents, solvents and their distributors are provided in **Table 2.1**.

5-(4-Acetamidophenyl)-10,15,20-tri-(3,5-dimethoxyphenyl)porphyrin [**1**]

3,5-Dimethoxybenzaldehyde (14.30 g, 0.086 mol) and 4-acetamidobenzaldehyde (4.56 g, 0.028 mol) were added to propionic acid (500 ml). Freshly distilled pyrrole (8 ml, 0.116 mol) was added drop-wise to the mixture and heated under reflux for 70 minutes. Propionic acid was removed under reduced pressure and the resulting mixture was redissolved in toluene (2 x 100 ml) and the solvent was removed under reduced pressure. The product was purified from the crude reaction mixture by chromatography, eluting with dichloromethane:ethylacetate (4:1) and the product was obtained as purple crystals (1.9 g, 3.9 %). R_f = 0.36 (dichloromethane:ethylacetate 4:1), ^{1}H NMR (400 MHz, $CDCl_3$, δ) -2.82 (br s, 2H, *NH*), 2.37 (s, 3H, *CH_3*), 3.97 (s, 18H, *10+15+20-m-CH_3*), 6.91 (t, 3H, *10+15+20-p-Ar*), 7.40 (d, 6H, *10+15+20-o-Ar*), 7.91 (d, 2H, J = 8 Hz, *5-m-Ar*), 8.17 (m, 2H, J = 8 Hz, *5-o-Ar*), 8.84-8.95 (m, 8H, *β-H*).

5-(4-Aminophenyl)-10,15,20-tri-(3,5-dimethoxyphenyl)porphyrin [**2**]

Porphyrin [**1**] (1 eq., 3.87 g, 4.54 x 10^{-3} mol) was dissolved in aqueous HCl (5 M, 500 ml) and heated under reflux for 3 hours. The solvent was removed under reduced pressure and the obtained solid product was re-dissolved in dichloromethane:triethylamine (9:1, 200 ml) and stirred at room temperature (~20 ºC) for 10 min. The solution was washed with water (3 x 200 ml) and saturated brine (200 ml). The extracted organic layer was dried using magnesium sulphate and the solvent was removed under reduced pressure. The product was purified by column chromatography, eluting with dichloromethane:ethylacetate (4:1) solvent mixture and the product was obtained as purple crystals (1.35 g, 36.7 %). R_f = 0.68 (dichloromethane:ethylacetate 4:1); ^{1}H NMR (400 MHz, $CDCl_3$, δ) -2.78 (br

s, 2H, *NH*), 3.97 (s, 18H, *10+15+20-m-*CH_3), 6.91 (t, 3H, *10+15+20-p-Ar*), 7.08 (d, 2H, J = 8 Hz, *5-m-Ar*), 7.41 (m, 6H, *10+15+20-o-Ar*), 8.00 (m, 2H, J = 8 Hz, *5-o-Ar*), 8.94 (m, 8H, *β-H*).

5-(4-Aminophenyl)-10,15,20-tri-(3,5-dihydroxyphenyl)porphyrin [**3**]

Porphyrin [**2**] (1 eq., 0.56 g, 6.98 x 10^{-4} mol) was dissolved in freshly distilled dichloromethane (50 ml), to which boron tribromide (15 eq., 10.50 ml, 1 mol dm^{-3}) was added under an argon atmosphere and stirred at room temperature (~20 ºC) for 19 hours. The reaction mixture was cooled to 0 ºC and purified water (2 ml) was added and the mixture was allowed to warm up to room temperature. The solvents were removed under reduced pressure and the solid product was redissolved in dichloromethane:triethylamine (9:1, 100 ml) solvent mixture, washed with water (3 x 100 ml) and saturated brine (100 ml). The extracted organic layer was dried using magnesium sulphate and the solvent was evaporated under reduced pressure to obtain the product. Porphyrin [**3**] was purified by column chromatography**,** where dichloromethane:methanol (4:1) solvent mixture was used as the eluting solvent and the product was obtained as purple crystals (0.27 g, 53.63 %). R_f = 0.80 (dichloromethane:ethyl acetate 4:1).

5-(4-Isothiocyanatophenyl)-10,15,20-tri-(3,5-dihydroxyphenyl)porphyrin [**4**]

Porphyrin [**3**] (1 eq., 50 mg, 6.89 x 10^{-5} mol) was dissolved in freshly distilled dichloromethane (20 ml), to which 1,1'-thiocarbonyldi-2(*1H*)-pyridone (1.1 equiv, 17.6 mg, 7.58 x 10^{-5} mol) was added. The reaction mixture was stirred at room temperature (~20 ºC) under argon atmosphere for 1 hour and concentrated under reduced pressure. Dichloromethane was added, ultrasonicated and the contents were filtered to obtain the product as purple crystals (50 mg, 96.15 %). ^{1}H NMR (400 MHz, $CDCl_3$, *δ*) 6.38-6.41, (m, 2H, *β-H*), 6.52-6.54 (m, 2H, *β-H*), 6.72 (t, 3H, *10+15+20-p-Ar*), 7.14-7.16 (m, 6H, *10+15+20-o-Ar*), 7.40-7.42 (m, 2H, *β-H*), 7.56-7.61 (m, 2H, *5-m-Ar*), 7.71-7.73 (m, 2H, *5-o-Ar*), 8.23-8.25 (m, 2H, *β-H*), 9.00 (br s, 6H, *10+15+20-m-OH*); UV-Vis (methanol, λ_{max}, nm) 418, 514, 549, 589 and 647.

2.4.2 Fabrication of glass microfluidic chip

Microfluidic chips were fabricated using photolithography together with wet etching technique.[345] The chip designs on the photomask (acetate sheet) which was printed from a *AutoCAD* software drawings were transferred onto a 1 mm thick white crown B-270 glass slide (Telic Company, Valencia, California, USA) containing a chromium layer (1200 Å thick) and a photoresist layer (positive thin AZ 1518). The designs were transferred by placing the photomask (JD Photo-Tools, Lancashire, UK) on top of the glass slide and irradiating with UV-light (4-5 mW cm^{-2}, LV204, UV Exposure Unit, Mega Electronics, Cambridge, UK) for a minute.

The patterns were developed by removing the photoresist layer (1 minute in 50 % Microposit Developer Concentrate in water, Chestech Ltd., Warwickshire, UK) and the chromium layer (1 minute in Microposit Chrome Etch 18 solution). The glass surface free of photoresist and chromium layers was isotropically etched using a glass etching solution [2 ml hydrofluoric acid-1.3%, 20 ml phosphoric acid-13.3 % and 128 ml water-85.3 %; RTP etching rate 0.13 μm min^{-1}], and rinsed with sodium bicarbonate (1.2 mol dm^{-3}) and water. The inlet and outlet holes (diameter of 360 μm) were machine drilled, prior to the removal of the remaining photoresist (using acetone) and chromium (using Chrome Etch 18 solution) layers on the non-patterned regions of the B-270 glass slide. The etched channels were cleaned thoroughly using acetone, propan-2-ol and by ultra-sonicating for 10 minutes, to remove any grease and dirt. The etched channels on the glass slide were covered with a similar size unetched clean and optically clear glass slide, and then placed in between two smooth stainless steel blocks and thermally bonded in a furnace (EF3, Vecstar Furnaces, Chesterfield, UK) at 590 °C for 5 hours.

2.4.3 Microfluidic chip setup

Microfluidic chips were held within a pair of chip holders (**Figure 2.25**) using screws for locking them in place. The chip holders of inlet and outlet ends were made of two separate parts (not connected to each other) to

permit flexibility in the chip designs. The chip holders were made of metal blocks, which contained nine screw holes (3 rows by 3 columns) at 5 mm distance from each other. Hence, when the microfluidic chips were designed using *AutoCAD*, the same equal spacing of 5 mm was maintained between adjacent inlets and outlets. Fused capillaries were interfaced at the inlet(s) and outlet(s) of the microfluidic chip, using the chip holders and the adaptors (ferrule and PEEK nut) as illustrated below in **Figure 2.25**.

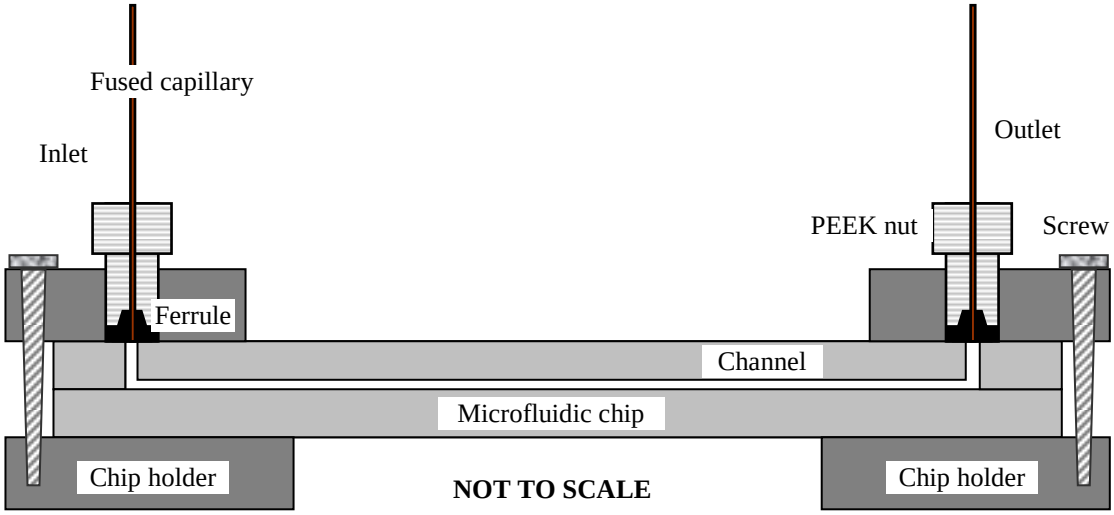

Figure 2.25: *Cross-sectional view of the assembled microfluidic chip setup.*

Microfluidic chip holders were made of metal blocks with nine screw-type holes on each block, with the distance to the adjacent holes being 5 mm from each other (**Figure 2.26**). The same equal spacing of 5 mm was maintained between the adjacent inlets and adjacent outlets of microfluidic chips when they were designed in *AutoCAD*. Fused capillaries for inlet and outlets were connected onto the microfluidic chip using the chip holders and the capillary connectors with adaptors. Chip holders for inlet side and outlet side were made of two parts to enable flexibility when varying the lengths of the chip designs. The capillaries on the inlet(s) and outlet(s) sides were connected to the pumping side and a collection vial, respectively. For microfluidic photolysis reactions, microfluidic chip connected to the external chip holders and fused capillaries were positioned vertically above the LED array on top of the stage.

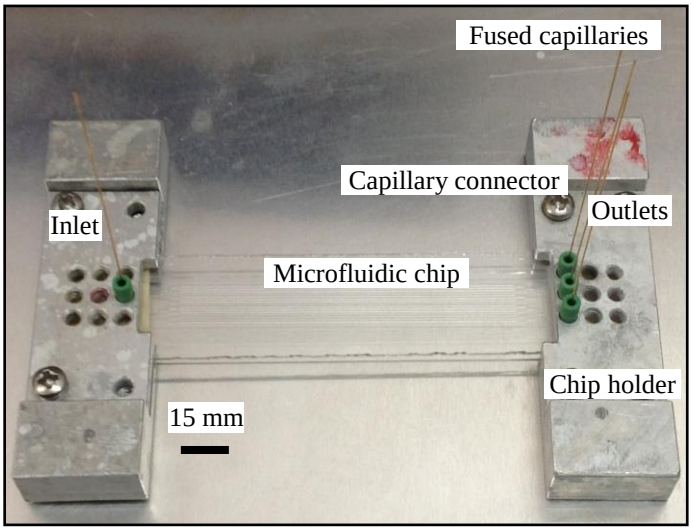

Figure 2.26: *Microfluidic chip placed within the chip holder with fused capillaries for inlet and outlets.*

2.4.4 Surface treatment of glass chips

2.4.4.1 Cleaning microfluidic chips

Organic debris and other materials present within microfluidic channels were burnt off in a furnace at 480 °C for 4 hours. Once cooled down to room temperature, the chips were further cleaned using piranha solution (100 ml, concentrated sulfuric acid: hydrogen peroxide 3:1), at 100 °C for 1 hour. For treatment using piranha solution, concentrated sulfuric acid (75 ml, 36.9 %) was heated to 70 °C to which hydrogen peroxide (25 ml, 100 vol.) was added over 30 minutes. The latter method destroyed any organic materials contained within chips by providing a highly oxidising environment. The contents were gradually cooled down to room temperature and the piranha solution was neutralised by adding sodium hydroxide pellets slowly. Following neutralisation, the solution was poured down the sink while diluting it with excess tap water. The chips and the channels were washed with deionised water to remove any acid. Further, the chips were immersed in deionised water and ultra-sonicated for 10 minutes at room temperature.

2.4.4.2 Converting cationic glass surface into anionic

Cationic surface of the microfluidic channels, after cleaning using piranha solution, were treated with aqueous NaOH (1 mol dm^{-3}). The channels were

filled with aqueous NaOH and stood for 10 minutes to remove protons off the surface. Alternatively, aqueous NaOH (1 mol dm^{-3}, 1 ml) was flowed through the channels at a flow rate of 16 µl min^{-1}. The channels were flushed with excess deionised water (3 x 1 ml), followed by methanol (3 x 1 ml) and extra dry toluene (3 x 1 ml) to remove all aqueous NaOH and water out of the channels. The resulting anionic hydrophilic surface was used in the silanisation treatment.

2.4.4.3 Silanisation and photosensitiser immobilisation

Silanisation and photosensitiser immobilisation at 120 ºC

Cleaned chips with anionic channel surface were flushed with methanol (1 ml) and extra dry toluene (1 ml), to ensure that the channels were mostly free of water molecules. Presence of excess water leads to rapid polymerisation of silanes, which results in formation of precipitates within the channels. The channels were filled with APTES [10 % v/v in extra dry toluene (water content less than 50 ppm)] and incubated at 120 ºC for 30 minutes. Once again the channels were flushed with extra dry toluene (3 ml) and methanol (3 ml), to remove any unbound APTES, and the channels were dried using a stream of nitrogen gas. The chips were left in an oven at 120 ºC for 30 minutes before immobilising photosensitisers. Dry channels were filled with photosensitiser [**4**] solution (1 mg in 3 ml methanol) and the chips were placed in an oven at 120 ºC for 10 minutes and the channels were flushed with methanol to remove any unbound photosensitisers. The process was repeated two more times, so that the total time the channels were filled with photosensitiser solution at 120 ºC was 30 minutes.

Silanisation and photosensitiser immobilisation at 18 ºC

Cleaned chips with anionic surface were flushed with methanol (1 ml) and extra dry toluene (1 ml). The channels were filled with APTES (10 % by volume) diluted in extra dry toluene (water content less than 50 ppm) and incubated for 1 hour at room temperature (~18 °C) having inlets and outlets sealed. Alternatively, the APTES mixture was flowed through the channels at a flow rate of 3 µl min^{-1} for 3 hours using a syringe pump, having fused capillaries [7 cm long, inner diameter (ID) 150 µm, outer diameter (OD)

375 µm] at inlet(s) and outlet(s) as described under **Section 2.4.3**. The channels were flushed with extra dry toluene (3 x 1 ml) and methanol (3 x 1 ml) to remove any unbound APTES, and the channels were dried using a stream of nitrogen gas before leaving in an oven at 120 °C for 1 hour. In place of APTES, triethoxy(ethyl)silane was used as a control to verify if amino group in APTES was essential before photosensitiser immobilisation.

Photosensitiser [**4**] (1 mg) was dissolved in MeOH (3 ml) and dry diisopropylethylamine (0.1 ml) was added to ensure that the amino groups on the surface were maintained neutral for nucleophilic attack of the sensitisers to form covalent bonds. APTES treated microfluidic channels were filled with photosensitiser solution and incubated for 1 hour at room temperature (~18 ℃) having inlets and outlets sealed. Alternatively, photosensitiser solution (1 ml) was flowed through APTES treated microfluidic channels for 3 hours. The channels were flushed with methanol (3 ml) and sonicated for 10 minutes having the chips immersed in methanol, to remove the photosensitisers non-covalently attached to the surfaces. The channels were dried by passing a stream of nitrogen gas, and the microfluidic chips were wrapped in an aluminium foil to avoid photobleaching and stored in the dark for later use. Using the same procedure described above, the photosensitisers [**3**, **5**, or **6**] (**Figure 2.27**) were also immobilised. The channels surfaces silanised at 120 ℃ had also been tested for photosensitiser immobilisation at 18 ℃ and *vice versa*.

In order to immobilise photosensitisers bearing only nucleophilic groups, bromoacetyl bromide (1 ml, 10 % by volume) diluted in extra dry toluene was flowed (16 µl min^{-1}) through the channels that was previously surface treated to immobilise APTES. Extra dry toluene (3 x 1 ml) was used to remove excess reagents. A photosensitiser [**3-6** or **8**] (1 mg) bearing nucleophilic groups (carboxylic, hydroxy or both) was dissolved in MeOH (3 ml). The channels were filled with the solution and sealed, or flowed through the channels as described above. The scheme of nucleophilic and electrophilic photosensitiser immobilisation is summarised in **Scheme 2.1** below.

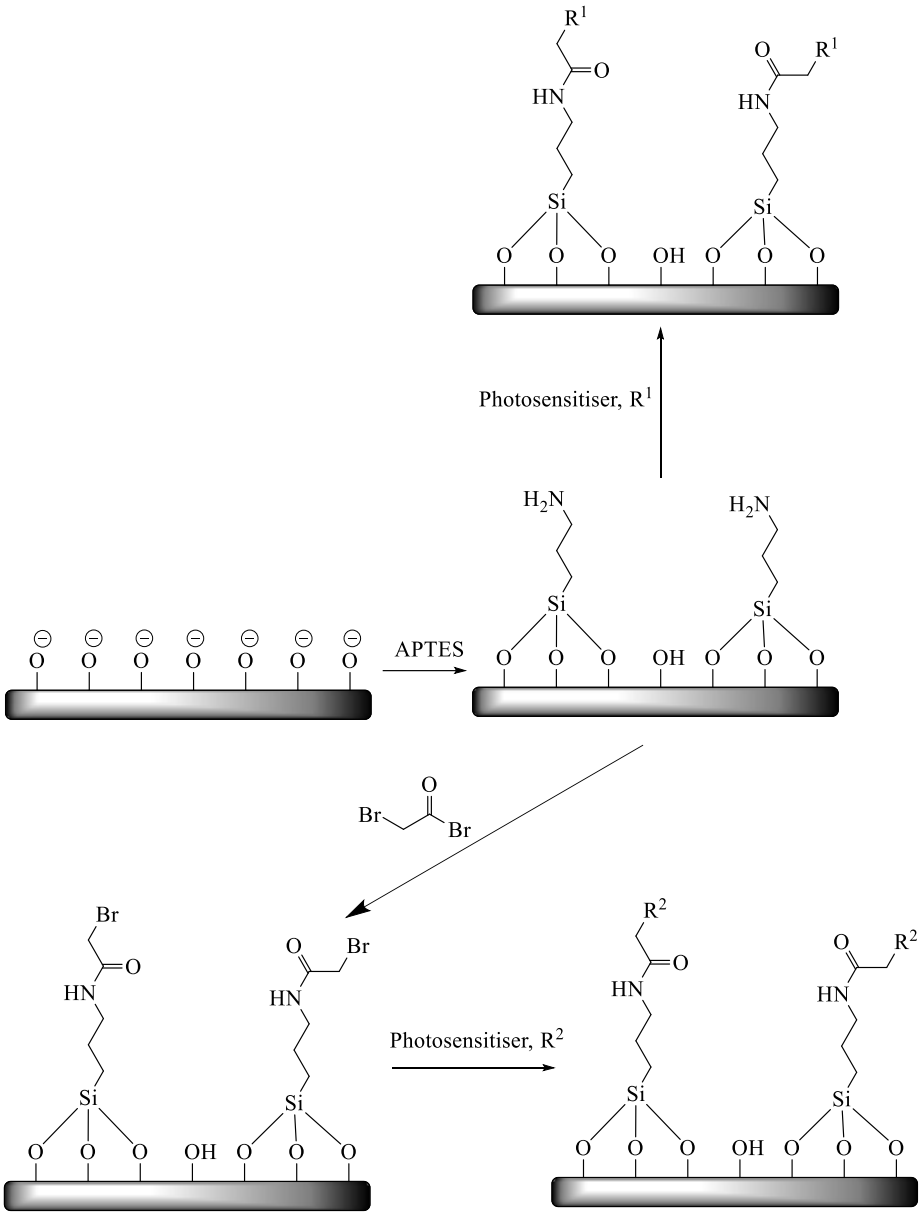

Scheme 2.1: *Summarises the silanisation and photosensitiser immobilisation, where R^1 and R^2 are electrophilic (isothiocyanate) and nucleophilic (carboxylic or hydroxy) reactive groups containing photosensitisers respectively.*

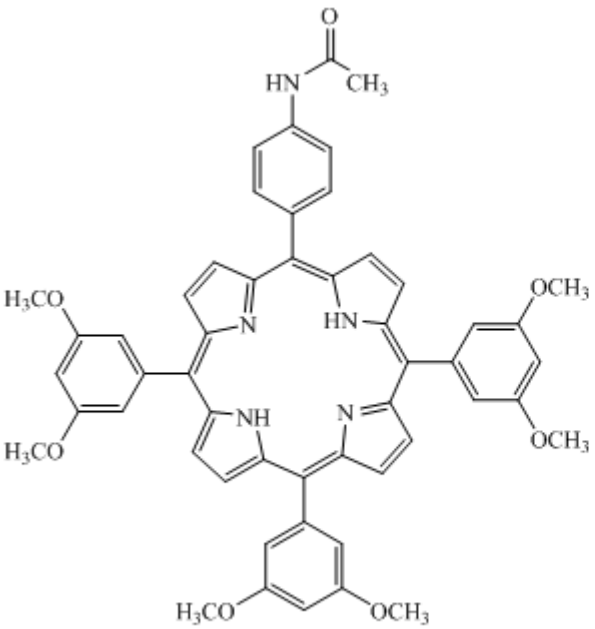

[1]

5-(4-Acetamidophenyl)-10,15,20-tri-(3,5-dimethoxyphenyl)porphyrin

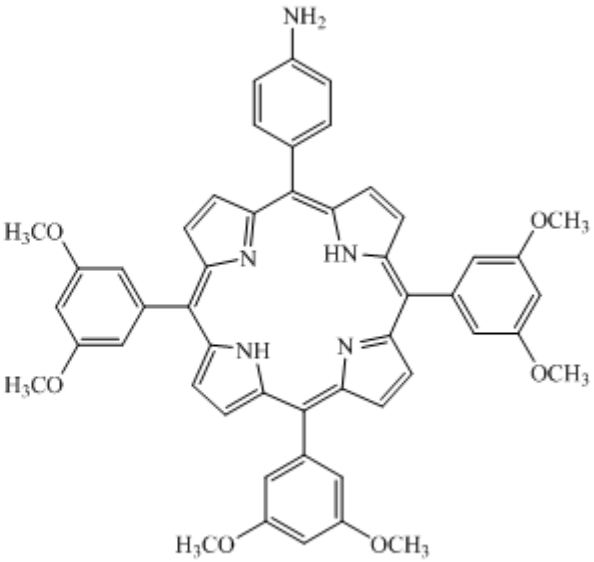

[2]

5-(4-Aminophenyl)-10,15,20-tri-(3,5-dimethoxyphenyl)porphyrin

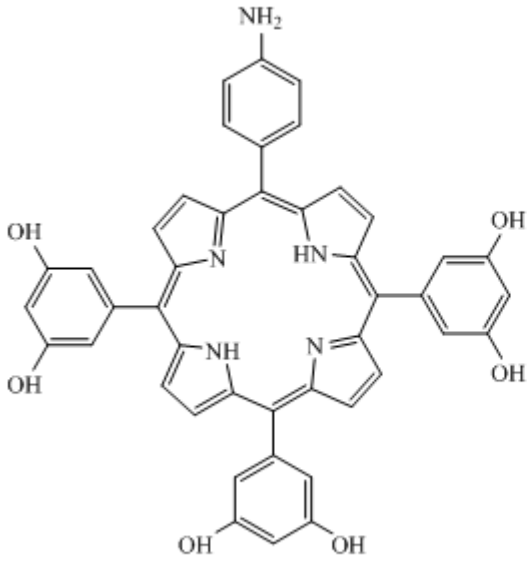

[3]

5-(4-Aminophenyl)-10,15,20-tri-(3,5-dihydroxyphenyl)porphyrin

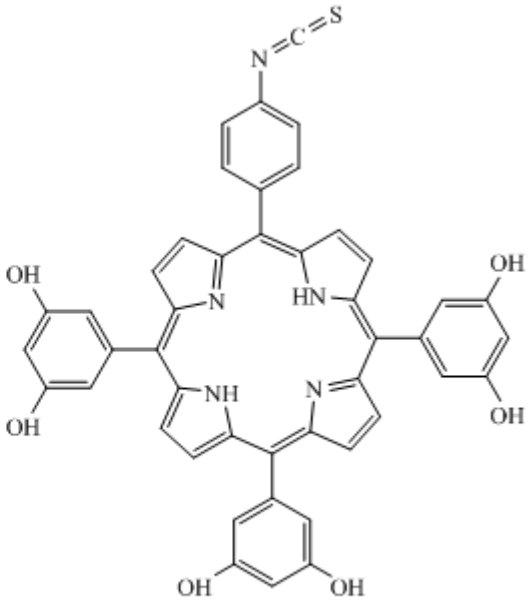

[4]

5-(4-Isothiocyanatophenyl)-10,15,20-tri-(3,5-dihydroxyphenyl)porphyrin

Figure 2.27: *Chemical structures of the photosensitisers **1** - **8**.*

continued…

continued…

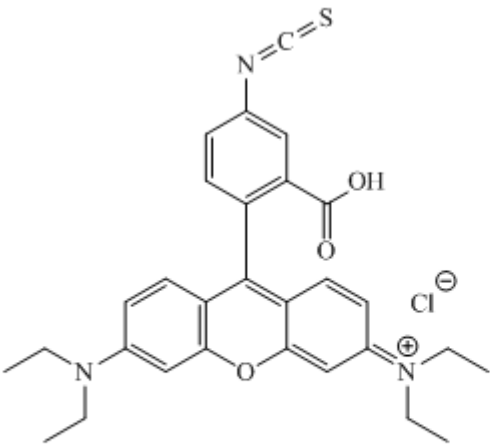

[5]

Rhodamine B Isothiocyanate (RBI)

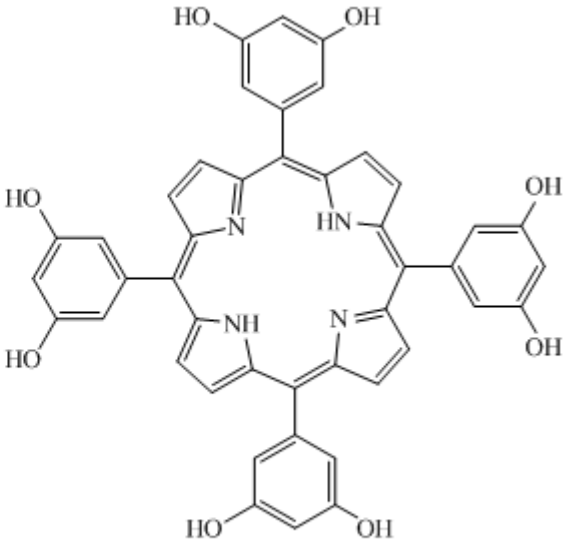

[6]

5,10,15,20-tetra-(3,5-dihydroxyphenyl)porphyrin

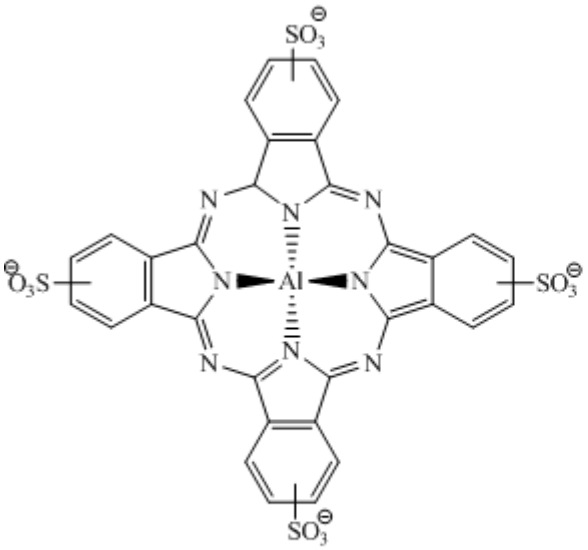

[7]

Aluminium (III) phthalocyanine tetrasulfonate

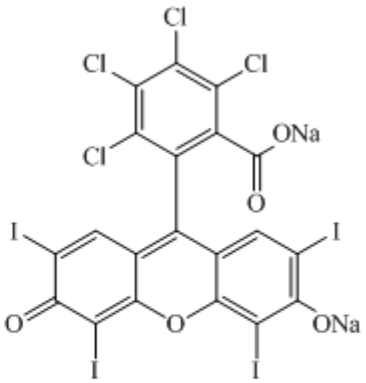

[8]

Rose Bengal (RB)

Figure 2.27: *Chemical structures of the photosensitisers **1** - **8**.*

2.4.5 Measurements to verify immobilisation of photosensitisers

UV-Visible absorption measurements

UV-Vis absorption spectrum of photosensitiser [**4**] dissolved in methanol was measured using a UV-Vis absorption spectrometer (Varian Cary® 50 UV-Vis spectrophotometer), where cuvette with 1 cm path length was used. Immobilised photosensitiser [**4**] was hydrolysed off the chip surface by filling the channels with aqueous sodium hydroxide (1 mol dm^{-3}) and stood at room temperature and pressure (RTP) for 10 minutes before the contents were flushed and collected at the outlets, and UV-Vis absorption spectrum was recorded. UV-Vis absorption spectrum for the photosensitiser [**4**], immobilised on the channel surfaces were also measured directly. The experimental arrangement used for the measurements is shown in **Figure 2.28**. Using a similar setup, UV-Vis absorption spectrum for the controls, non-treated glass slide, non-treated microfluidic channels of **Design 5** (page 180) and APTES only treated microfluidic channels of **Design 5**, were also determined.

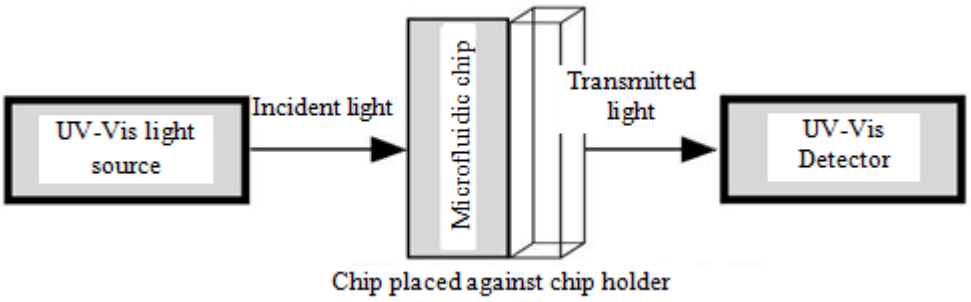

Figure 2.28: *Setup used to measure UV-Vis absorption.*

Fluorescence measurements

Fluorescence from photosensitiser [**4**] immobilised channels were observed using various levels of magnifications (2x, 4x, 10x , 20x and 40x), under an inverted fluorescence microscopy (Nikon Eclipse Ti or Nikon TE2000, Nikon UK Limited, Surrey, UK) together with the CCD camera (Retiga-EXL, QImaging or Mintron™ MTV-63V1N) for capturing images using the software (Image-Pro® plus software or WinDVD Creator 2 software). Nikon filter cubes B-2A (Ex 450 - 490 nm, DM 500, Em > 515 nm) and G-2A (Ex= 510 – 560 nm, DM 565 nm, Em > 590 nm) were used for observing fluorescence. Acquisition time was increased up to 3 s to enable weak

fluorescence to be captured. Similarly fluorescence from other photosensitisers [**3**, **5**, **6** or **8**] immobilised channels were also observed under similar settings.

Fluorescence spectrum was measured using a fluorescence spectrometer (Varian Cary Eclipse fluorescence spectrophotometer) and a standard 1 cm path length all four sides clear quartz cuvette. An emission spectrum for photosensitiser [**4**] dissolved in methanol was acquired, using an excitation wavelength of 400 nm and emission wavelengths greater than 550 nm were recorded. Immobilised photosensitiser [**4**] was hydrolysed off the chip surface using aqueous sodium hydroxide (1 mol dm^{-3}), and the liquid collected was measured for fluorescence using the spectrometer with the same settings as above. In order to measure the fluorescence signals while having photosensitisers in their immobilised form, cuvette holder was removed and the microfluidic chip containing immobilised photosensitiser [**4**] was positioned facing the excitation monochromator and the detector at an angle 45º to each other (**Figure 2.29**). The immobilised sensitiser was excited at wavelengths (λ_{Ex}) 281, 400, and 418 nm, and the emission wavelengths (λ_{Em}) greater than 300, 430 and 550 nm were recorded respectively.

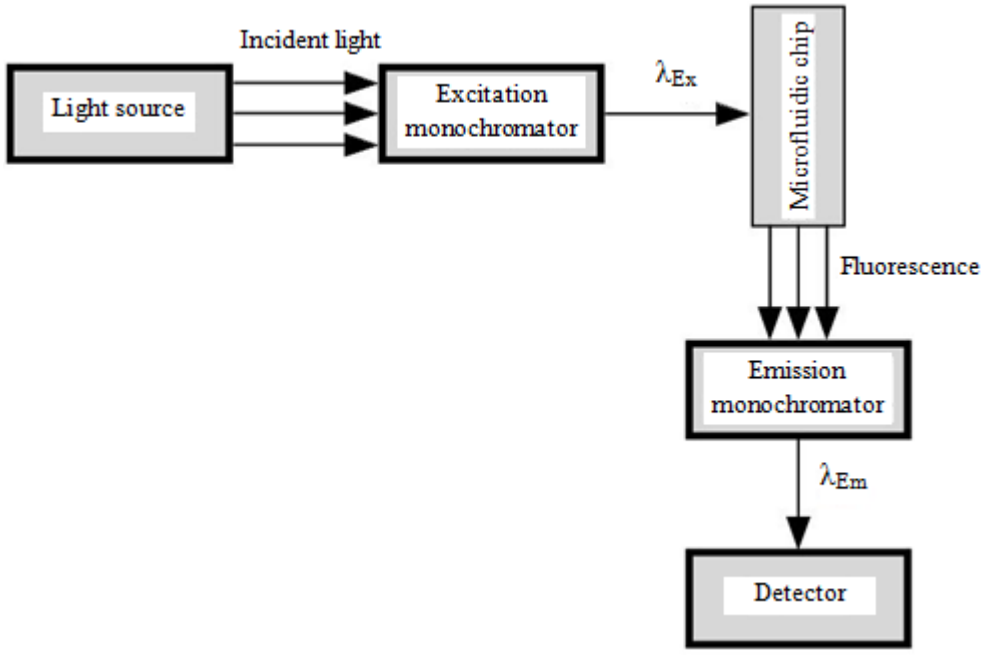

Figure 2.29: *Setup used to measure fluorescence.*

Colorimetric analysis

Photosensitiser [**4**] immobilised microfluidic channels were filled with concentrated H_2SO_4 (5 % by volume) in ethanol and the colour change was observed.

2.4.6 Cholesterol oxidation reactions

Cholesterol oxidation reactions were carried out as reported in the literature with certain modifications.[75] Photosensitiser [**4**] stock solution (1 μmol dm^{-3}, 100 ml) was made in methanol. Cholesterol, 3β-hydroxy-5-cholestene or 5-cholesten-3β-ol (Sigma Aldrich) was recrystallised in hot methanol and dissolved in a mixture of dichloromethane: methanol (9:1, 10 ml) to make a concentration of 10 mmol dm^{-3} stock solution.

Off-chip cholesterol oxidation reaction

Stock solutions of photosensitiser [**4**] (1 μmol dm^{-3}, 5 ml) and cholesterol (10 mmol dm^{-3}, 5 ml) were mixed together in an Erlenmeyer flask (50 ml). The contents were exposed to white light from a single LED array at a fluence rate of 34.91 mW cm^{-2} for 70 minutes to deliver a total light dose of 146.62 J cm^{-2}. Sodium borohydride ($NaBH_4$) was added to the reaction mixture to reduce peroxides (primarily 5α-OOH) into alcohols (5α-OH). Most of the solvent was vaporised by passing a stream of inert (nitrogen) gas and the reduced volume was replaced with methanol to maintain the volume of the sample constant, hence the concentration. The samples were analysed using normal-phase TLC and reversed-phase HPLC. As a control, the above steps were repeated without photosensitiser.

Normal-phase TLC analysis

The reaction mixture was pre-concentrated onto a normal-phase TLC plate and the TLC was developed two times in the solvent mixture of hexane: ethyl acetate (1:1). The developed TLCs were dipped in concentrated H_2SO_4 (5 % by volume) in ethanol, before heating on a hot plate to visualise the deep blue (oxidised cholesterol) and magenta (non-oxidised cholesterol) coloured spots.[75]

Reversed-phase HPLC analysis

The cholesterol oxidation reaction mixture was also analysed using reversed-phase HPLC.[346] Polar mobile phase of acetonitrile: methanol (2:3, 500 ml) along with 5 µ sized C18 coated particles filled 15 cm long HPLC column (phenomenex) was used. The mobile phase was pumped at a flow rate of 1 ml min^{-1} and UV absorption wavelength of 205 nm was used for detection.

On-chip cholesterol oxidation reactions

As in the off-chip cholesterol oxidation reaction, the stock cholesterol solution was made. The cholesterol solution was pumped through the photosensitiser [**4**] immobilised microfluidic channels (**Design 5**) using a syringe pump (Pump 11 Plus or Pump 11 Elite, Harvard Apparatus, Kent, UK) and a glass syringe (1 ml, Hamilton), at the fixed flow rates of 0.5, 1, 2.5 or 5 µl min^{-1} for varying length of times, until 200 µl of the sample was flowed through. To the samples collected (200 µl), $NaBH_4$ was added. Following the reduction reaction most of the solvent was vaporised by passing a stream of nitrogen gas, which was then re-diluted by adding methanol (180 µl, HPLC grade) to maintain the volume constant (200 µl), hence the concentration. The samples were analysed using normal-phase TLC and reversed-phase HPLC as described earlier.

2.5 Photosensitiser immobilised microfluidic flow oxidative stress reactions

The first part of this section (**2.5.1 - 2.5.6**) focuses on the methods used for conducting microfluidic flow oxidative stress reactions (MFOSR) in micro-channel surfaces coated with the photosensitiser [**4**]. The second part of this section (**2.5.7**) describes the method used in the immobilisation of photosensitisers onto magnetic nanoparticles possessing amino group.

2.5.1 Cell culture

Colon carcinoma cell line COLO320 was the only cell line that was used to study the effects of extracellular oxidative stress induced PDT-type

reactions.[240] The COLO320 cells were cultured in complete medium of Roswell Park Memorial Institute-1640 (RPMI-1640, GE health care, UK), at 37 ^{o}C, 5 % CO_2 and 95 % humidity. To the RPMI-1640 medium (500 ml) with L-glutamine, fetal bovine serum (FBS, 10 %) and penicillin-streptomycin (final concentration 100 U ml^{-1}) were added to produce the complete medium. The cells were non-adherent to the surface of the culture flasks and had a doubling time of 24 hours.

2.5.2 Cell sample preparation

When cells have reached 100 % confluence in a T75 or 2 x T25 flasks (Sarstedt), the cell suspension was collected in a 50 ml universal tube (Sarstedt or Falcon®) along with the growth medium and centrifuged (Heraeus® Biofuge Primo) at 162 x g for 10 minutes. The supernatant was discarded and the cell pellet was resuspended in phenol red-free RPMI-1640 medium. The cell concentration was adjusted within the range of 0.5 – 1.5 x 10^6 cells ml^{-1} and the required volumes of cell suspension were used in the experiments. The viability of cells was determined using a haemocytometer coupled with trypan blue stain as described below.

2.5.3 Trypan blue exclusion assay

Trypan blue stain (0.4 % w/v) was used to determine the dead cells.[347] The cell membrane of the dead cells become permeable, through which trypan blue enters and binds with the intracellular proteins. The dead cells, those stained blue, were distinguished from the unstained live cells under a light microscope (LEICA DM IRB). Trypan blue assay was used for determining the initial cell viability, and also the absolute percentages of viabilities and recoveries after the reactions.

From an evenly distributed cell suspension, an aliquot (20 µl) was transferred to a 0.5 ml polypropylene tube containing trypan blue (0.4 %, 20 µl). The contents were mixed well, placed on a Neubauer haemocytometer and analysed under a light microscope. The numbers of stained and unstained cells were counted four times and their average was used to

calculate the *percentage viability* (**Equation 2.3**) and the *percentage recovery* (**Equation 2.4**).

$$Percentage\ viability = \left(1 - \frac{L_{live\ cells}}{T_{total\ cells}}\right) \times 100\% \qquad \textbf{Equation 2.3}$$

Where, $L_{live\ cells}$ is the number of live cells present in a sample and $T_{total\ cells}$ is the total number of cells in the sample.

$$Percentage\ recovery = \frac{S_{cells\ collected}}{T_{Untreated\ total\ cells}} \times 100\% \qquad \textbf{Equation 2.4}$$

Where, $S_{cells\ collected}$ is the total number of cells in a tested sample and the $T_{untreatd\ total\ cells}$ is the total number of cells in the *untreated* control sample.

2.5.4 The conditions and the controls used in the reactions

A total of three samples were used in each experiment; two controls and a testing sample. The samples were labelled as *untreated*, *photosensitiser dark-toxicity* and *photodynamically sensitised*. The *untreated* control samples were kept in complete RPMI-1640 medium in the dark at RTP without photosensitiser and light. The *photodynamically sensitised* control samples were flowed through photosensitiser immobilised microfluidic channels at a fixed flow rate (set based on the residence times) to deliver a light dose of 3.7 J cm^{-2}. The *photosensitiser dark-toxicity* control samples were also flowed through the photosensitiser immobilised microfluidic channels at a fixed flow rate for the same length of time as for the *photodynamically sensitised* sample, but without light. Following the treatments, the samples were incubated for a fixed length of time (2.5 or 24 hours) at 37 ^{o}C, 5 % CO_2 and 95 % humidity, before being analysed using flow cytometry to assess annexin-V:FITC and propidium iodide levels, to determine the ratios of apoptotic and necrotic cells respectively, relative to the number of cells in the healthy-mode.[242]

The microfluidic chip **Design 5**, containing 3 cm long 16-parallel channels of 300 µm width on the photomask were isotropically etched to a depth of

60 µm (**Figures 3.6** and **3.7)**. The channels were surface treated to immobilise photosensitiser [**4**], which was used to conduct the photosensitiser immobilised MFOSR. The microfluidic chip was setup as described below (**Section 2.5.5**) and the cells were flowed through the microfluidic chip using a peristaltic pump (GILSON, Minipuls 2, Anachem, LU1 3JJ, UK) at a flow rate of ~21 µl min^{-1}. Light dose of 3.7 J cm^{-2} was delivered by irradiating the chip using two white light emitting LED arrays, at the total fluence rate of 110 mW cm^{-2}. Each set of experiments were repeated minimum of three times and the average number of healthy, apoptosis and necrosis were measured and presented along with their SD error bars.

2.5.5 Microfluidic flow oxidative stress reaction setup

Photosensitiser immobilised microfluidic chip (**Design 5**) was setup using fused capillaries (7 cm long) interfacing at the inlet and outlet holes of the chip (**Figure 2.25**). The capillaries were held in place using chip holders and adapters as described under **Section 2.4.3**. The ID and OD of the capillaries were 150 and 375 µm, respectively. The chip setup was positioned on the stage within the instrument (**Figure 2.6**) and irradiated while the cells were flowed through the channels. The cell samples were flowed using a peristaltic pump (GILSON, Minipuls 2) and a 2-stop peristaltic tubing (Tygon® LMT-55) with the ID of 0.76 mm and length of 40 cm. The cells were maintained in suspension with the use of a magnetic stirrer bar (1 cm long) and a magnetic stirrer. The cells were collected at the outlets and incubated for a fixed interval (2.5 or 24 hours) and analysed using flow cytometry (**Section 2.5.6**).

2.5.6 Sample preparation and data acquisition using flow cytometry

Binding buffer (1 ml) provided along with the Annexin V assay kit (AbD SeroTec, Kidlington, UK) was diluted, 1:4 in double distilled water. The cells were washed with PBS and resuspended in diluted binding buffer, adjusting the cell density within the range, 2-5 x 10^5 cells ml^{-1}. Annexin V:FITC (5 µl) was add to cell suspension (195 µl) and incubated for 10 minutes in the dark, at room temperature (~20 °C). Annexin-V:FITC was

used to determine the apoptotic cells, by measuring the translocated phosphatidylserine[242] present on the plasma membrane of the cells. The cells were washed with pre-diluted binding buffer (190 µl) to remove excess unbound annexin V: FITC and resuspended in the diluted binding buffer (190 µl), to which propidium iodide (10 µl) solution was added and the samples were analysed using flow cytometry. Propidium iodide was used to determine both dead and damaged cells.[242]

The flow cytometry instrument, BD FACSCalibur™ and the software, BD CellQuest™ Pro were used for acquiring data. The same software was used for analysis, where the quadrant and the statistical tools were used to determine the ratio of cells in healthy-, apoptotic- and necrotic-modes in terms of percentages. The flow cytometer was set to count 1 x 10^4 events before it stopped sending the acquisition data to storage gate. The threshold limits were set using positive and negative controls to recognise true events from that of the background noise. The same settings were used for obtaining all the flow cytometry results reported.

2.5.7 Immobilisation of photosensitisers onto nanoparticles

TurboBeads™-Amine (1 mg, Sigma Aldrich) of particle size less than 50 nm, possessing the functional group -Ph-CH_2-NH_2 with the loading capacity greater than 0.1 mmol g^{-1} were used. Photosensitiser **5** (3 mg) was dissolved in methanol (1 ml) and mixed together with the nanoparticles (1 mg). The suspension was allowed to mix on a 360° rotator for 16, 24, 48, 72 or 168 hours. Excess non-immobilised photosensitisers in solution were removed, while having the nanoparticles held together within the sample vial using a 1.0 cm x 0.5 cm disc shaped neodymium-iron-boron (NdFeB) magnet (Magnet Sales and Services Ltd., Swindon, UK). The nanoparticles were washed with methanol (3 x 1 ml) to remove sensitisers non-covalently bound (sticking) onto the surface of the nanoparticles. Photosensitiser immobilised nanoparticles were viewed under a fluorescence microscope (Nikon Eclipse Ti-ϵ, Ex= 510 – 560 nm, DM 565 nm, Em > 590 nm) to

verify their presence. Using the same method described above, rose bengal (RB) was also immobilised onto the surface of the magnetic nanoparticles.

Photosensitiser immobilised TurboBeads™-Amine were resuspended in an indicator-free RPMI-1640 (1 ml) to give a concentration of 1 mg ml^{-1}. After mixing the contents thoroughly, the suspension was loaded into a syringe (1 ml, BD Plastipak, Oxford, UK) and flowed through the microfluidic chip (**Design 5**) with 60 µm depth channels using a syringe pump. The connections and the chip setup used were similar to what was described under **Section 2.4.3**. Fused capillaries of 7 cm long with the ID 150 and OD 375 µm were used for interfacing at the inlet and outlet holes.

2.6 Microbatch oxidative stress reactions

2.6.1 General procedures (used in Chapters 5 and 6)

In order to determine the parameters essential for inducing photosensitisation effects under the microfluidic flow conditions, the microbatch oxidative stress reactions (MBOSR) were conducted having photosensitisers in solution. For the reactions considered in **Chapters 5** and **6**, $AlPcS_4.Cl$ (10 or 100 µM) dissolved in an indicator-free RPMI-1640 medium was used. The mixture was filtered through a 0.22 micron sterile syringe filter (EMD Millipore), to sterilise and to remove any debris particles.

COLO320 cells grown in complete RPMI-1640 medium (**Section 2.5.1**), was collected, centrifuged (162 x g, 10 minutes, Heraeus® Biofuge Primo) and resuspended in an indicator-free RPMI-1640 medium to make the stock sample. The cell concentration was used within the range of 0.5 - 1.5 x 10^6 cells ml^{-1} and cell suspension of volume 0.5 or 1.0 ml was used for each samples. The samples were irradiated using two white light emitting LED arrays at the distances 5.4 and 3.4 cm to deliver the intended light dose using a combined fluence rate of 110 mW cm^{-2}. The treated samples were incubated for 2.5 or 24 hours, at 37 ^oC, 5 % CO_2 and 95 % humidity, before being analysed using haemocytometer to determine the percentage

recoveries and their cell viabilities (**Section 2.5.3**). The fraction of cells damaged were estimated by measuring the levels of LDH present in the supernatants, using a LDH assay kit (Roche Applied Science, Sussex, UK), **Section 2.6.5** covers the method used in detail. The ratio of cells in healthy- apoptotic- and necrotic-modes were measured flow cytometrically with the indicators annexin-V:FITC and propidium iodide respectively (**Section 2.5.6**).

2.6.2 MBOSR using 6-well plates

The initial MBOSR were conducted using multi-well plates (6-well plates). The *photodynamically sensitised* and the *photosensitiser dark-toxicity* samples were suspended in an indicator-free RPMI-1640 containing dissolved $AlPcS_4$ (10, 100 or 500 µM). The *untreated* and the *light-only toxicity* samples were also suspended in an indicator-free RPMI-1640 but without $AlPcS_4$. The *untreated* and the *photosensitiser dark-toxicity* samples were stored in the dark at room temperature (~20 ºC) for the same length of time as for the other two samples. The cell suspensions (1.0 ml) of the samples *photodynamically sensitised* and *light-only toxicity* were added to the wells in triplicates and irradiated using white light at a fluence rate of 110 mW cm^{-2} for 34 or 83 s. Following the treatment the samples were incubated and analysed after 2.5 or 24 hours using the trypan blue assay (**Section 2.5.3**) and flow cytometry (**Section 2.5.6**).

2.6.3 MBOSR using polypropylene tubes

When using multi-well plates, due to the impracticability of collecting all of the remaining cells following the OSR, the reactions were conducted using 1.5 ml polypropylene tubes (eppendorf tubes). Four samples were used for each of these reactions; three controls and a treatment sample. The four samples were labelled as *untreated*, *photosensitiser dark-toxicity*, *photodynamically sensitised* and *light-only toxicity*. The *untreated* control sample was maintained in the dark at RTP without photosensitiser and light treatment. The *photosensitiser dark-toxicity* control sample was mixed with $AlPcS_4$ (10 or 100 µM) containing medium and left at RTP in the dark for the same length of time as for the *photodynamically sensitised* sample. The

photodynamically sensitised sample was mixed with $AlPcS_4$ (10 or 100 µM) containing medium and exposed to a known level of light dose (3.7, 9.1 or 11.6 J cm^{-2}), which was the sample under test. The *light-only toxicity* control sample was exposed to the same level of light dose as that for the *photodynamically sensitised* sample, but without $AlPcS_4$ in the medium. In order to isolate the cells from photosensitiser in solution, immediately following the treatments, all four samples were washed (Qualitron DW41 Micro-centrifuge, 2000 x g, 1 minute) three times using fresh indicator-free RPMI-1640. The cells were resuspended in complete medium (same volume as that was used initially) and the samples were incubated for a fixed interval (2.5 or 24 hours) before analysing using various methods as described under the **Section 2.6.1**. In all the reactions, cells were in contact with the photosensitiser for a maximum of 5 minutes, which included the time for mixing the cells with photosensitiser containing medium before irradiation, the length of irradiation and the time consumed for washings to isolate the cells from the photosensitiser containing solution. A total of twelve combinations of microbatch oxidative stress reaction conditions were tested, using three different light doses, two different photosensitiser concentrations and at two different time intervals of analysis.

2.6.4 LDH assay calibration

It was essential to calibrate the maximum levels of LDH released against the number of cells lysed. For a given cell concentration, two levels of LDH were measurable; spontaneous or naturally releasable level referred to as the *low control* (*LC*) and the total level of LDH that could be released as a result of lysing all the cells to release their cytosolic contents, referred to as the *high control* (*HC*). The following LDH assay method was adapted and modified from the Roche Applied Science protocol.[348]

The assay medium was prepared by adding FBS (1 % v/v) to RPMI-1640 medium with phenol red and L-glutamine. The cells were washed (Heraeus® Megafuge® 3.0 R, 488 x g 1500 rpm, 3 minutes) and resuspended in the assay medium. An entire 96-well flat-bottom plate was filled with the assay medium (50 µl $well^{-1}$). The cell suspension (50 µl, 2 x 10^6 cells ml^{-1}) was

added in triplicates to the wells containing the assay medium and the cells were titrated by two-fold serial dilutions across the plate. As a background control, three of the wells were filled only with the assay medium (50 µl well^{-1}). To the *HC* test wells, lysis solution of Triton X-100 (50 µl well^{-1}) was added and to the *LC* test wells only assay medium (50 µl well^{-1}) was added, and the microplate was incubated for 2.5 or 24 hours at 37 ^{o}C, 5 % CO_2 and 95 % humidity. The 96-well microplate was centrifuged (Heraeus® Megafuge® 3.0 R) at 488 x g for 3 minutes. Without disturbing the cell pellets, the supernatants (50 µl well^{-1}) were removed and transferred into the wells of another optically clear 96-well flat bottom microplate. In order to determine the LDH activity in the supernatants, freshly prepared reaction mixture (50 µl) was added to each well and incubated for 10, 20, 30 and 40 minutes at 37 ^{o}C, 5 % CO_2 and 95 % humidity. The reaction mixture was prepared by mixing the catalyst and the dye solution (provided along with the LDH assay kit) together in the ratio of 1:45 respectively. The absorbance was measured using the ELISA reader (BIO-TEK®, Synergy HT) at a monochromatic wavelength of 490 nm. Higher absorbance readings indicated higher number of fragmented cells.

2.6.5 LDH assay for the samples

Immediately after the MBOSR (**Section 2.6.3**), supernatants (0 hour) were collected for all four samples and the cells were washed (2000 x g, 1 minute) further 3 times using fresh indicator-free RPMI-1640 medium without photosensitiser, before resuspending the cells in the same volume of complete medium and incubated for 2.5 or 24 hours at 37 ^{o}C, 5 % CO_2 and 95 % humidity. Repeated washing (**Section 2.6.3**) was essential to remove any photosensitisers present in the *photosensitiser-dark toxicity* control and the *photodynamically sensitised* sample. The supernatants from the incubated samples were collected for analysis, and the cells were resuspended and re-incubated in the same volume of complete medium.

To determine the LDH activity in the supernatants, supernatants (50 µl well^{-1}) were added in triplicates to 96-well plate followed by the addition of the freshly prepared (**Section 2.6.4**) reaction mixture (50 µl) to each well and

incubated for 30 minutes at 37 ºC, 5 % CO_2 and 95 % humidity. From the calibration curves (**Section 2.6.4**) it was determined that 30 minutes of assay development time was sufficient. Hence the samples were incubated only for this length of time, before adding HCl (1 mol dm^{-3}) to stop the reaction prior to analysis using the ELISA reader as mentioned in the previous **Section 2.6.4**. Each LDH assay was performed in triplicate and the error bars are the SD of three repeats (3 x 3 wells).

2.6.6 Control to verify photosensitiser internalisation

To verify if the photosensitiser ($AlPcS_4$) had been internalised during the length of the MBOSR, the cells were incubated with a known concentration of $AlPcS_4$ (10 or 100 µM) for a fixed length of time (5, 10, 20 or 30 minutes) and the cells were analysed under a fluorescence microscope (LEICA DM IRB) with a monochromatic light source (CAIRN ARC LAMP, CAIRN OPTOSCAN and Newport®) for excitation. The cells that were pre-incubated with $AlPcS_4$ were excited using monochromatic wavelengths of 385 or 430 nm and the emission wavelengths (fluorescence) above 610 nm were observed. The acquisition settings of bandwidth 30 nm, maximum gain of 5 and the acquisition time of 5 s were used for recording the fluorescence images.

2.7 MFOSR having photosensitiser in solution

This section describes the MFOSR carried out using photosensitiser ($AlPcS_4$) in solution. Similar to the MBOSR, in the MFOSR with photosensitiser in solution, a total of four samples were used in each experiment; three controls and a treated sample. The samples were labelled as *untreated*, *photosensitiser dark-toxicity*, *photodynamically sensitised* and *light-only toxicity*. All the samples were flowed through the channels (**Design 6**, page 180) and collected at the outlets except the *untreated* control.

The stock cell suspension was prepared as described under **Section 2.6.1**, from which 0.5 ml cell suspension was used for each samples. The

untreated control sample was stood in an indicator-free RPMI-1640 medium in the dark at RTP, without photosensitiser and treatment. The *photodynamically sensitised* sample was mixed with the photosensitiser containing medium and flowed through microfluidic channels at a fixed flow rate (~21 µl min^{-1}), to deliver a light dose of 9.1 J cm^{-2}, at the fluence rate of 110 mW cm^{-2}, which was the sample under test. The *photosensitiser dark-toxicity* control sample was resuspended in $AlPcS_4$ dissolved in medium and flowed through microfluidic channels at a fixed flow rate (set based on the residence times), for the same length of time as for the *photodynamically sensitised* sample, but without irradiation. The *light-only toxicity* control sample was suspended in phenol red-free RPMI medium and flowed through microfluidic channels at a fixed known flow rate, to deliver the same amount of light dose as that for the *photodynamically sensitised* sample. The samples were washed (2000 x g, 1 minute) three times using sterile indicator-free RPMI-1640 medium and resuspended in complete medium (same volume as that was used initially). The samples were incubated and analysed using various methods as described under **Section 2.6.1**.

2.8 Statistical analysis using *analysis of variance* and *post-hoc* testing

Two types of statistical tests were performed on the results obtained for the OSR. The *analysis of variance* was used to test if the means were significantly different at $p < 0.05$, following which Tukey's *post-hoc* testing was conducted to identify the sample(s) that were significantly different from each other. The average height of the bars and their SD error bars were also used to identify the possibilities for significant differences, thereby the agreement with the statistical analysis was verified.

Single factor *analysis of variance* was used to determine if there were significant differences between the mean of the samples at $p < 0.05$. The *post-hoc* testing of Tukey's *Honestly Significant Difference (HSD)* was used to distinguish the significantly different samples. The *HSD* values were

determined using the **Equation 2.5** and the calculated values were compared against the differences between the means of all the samples in all the possible forms of combinations.

$$HSD = q\sqrt{\frac{MS_{within}}{n}} \qquad \textbf{Equation 2.5}$$

Where, *HSD* is the honestly significant difference, q is the critical-value obtained using the boundary conditions; level of significance (α), degrees of freedom (df) and number of means (K), MS_{within} is the mean square within groups and n is the number of samples. For the results with K = 3 or 4 means, df of 6 or 8 and q-values of 4.34 or 4.53 were used respectively, at α 0.05. As the *post-hoc* testing considers all the means of the samples simultaneously, the interpretations were considered to be more reliable.

CHAPTER 3 - Microfluidics and surface treatments

This chapter focuses on the microfluidic chip designs made, including the parameters considered when designing them and the dimensions of the etched (fabricated) channels. The methods developed for immobilising photosensitisers onto the surface of the microfluidic devices fabricated out of borosilicate glass, and the methods used to verify their presence were also considered here. Moreover, using cholesterol as the substrate it was demonstrated that the photosensitiser immobilised channels could be used for carrying out photosensitisation reactions.

In this project surface treatment reactions were carried out for five main reasons; to enhance the reusability of photosensitisers, to avoid photosensitisers from mixing with the substrate, to prevent photosensitisers from being internalised by cells, to prevent photosensitisers from being carried away in solution, and more than all to generate defined levels of extracellular oxidative stress environments thereby to study their effects.

3.1 Chemistry

3.1.1 Conjugation chemistry

In general, surface treatment reactions onto solid materials would involve altering their mechanical properties and overall thickness. The covalent immobilisation of target molecules such as photosensitisers onto a solid support can be achieved with the use of conjugation chemistry. Some of the possible approaches that can be used for linking molecules through covalent attachment include; 1) direct coupling between the photosensitisers and the solid support, provided that both coupling centres have well-matched functional groups, 2) surface modification of the solid support to match the functional group on photosensitisers followed by coupling reaction between the functional groups, 3) using intermediate bifunctional linkers (homo- or hetro-) that contain compatible functional groups between the solid support and the photosensitiser of interest. The above four possibilities of immobilising molecules onto a solid surface or solid support through the formation of covalent bonds are summarised in **Scheme 3.1** below.

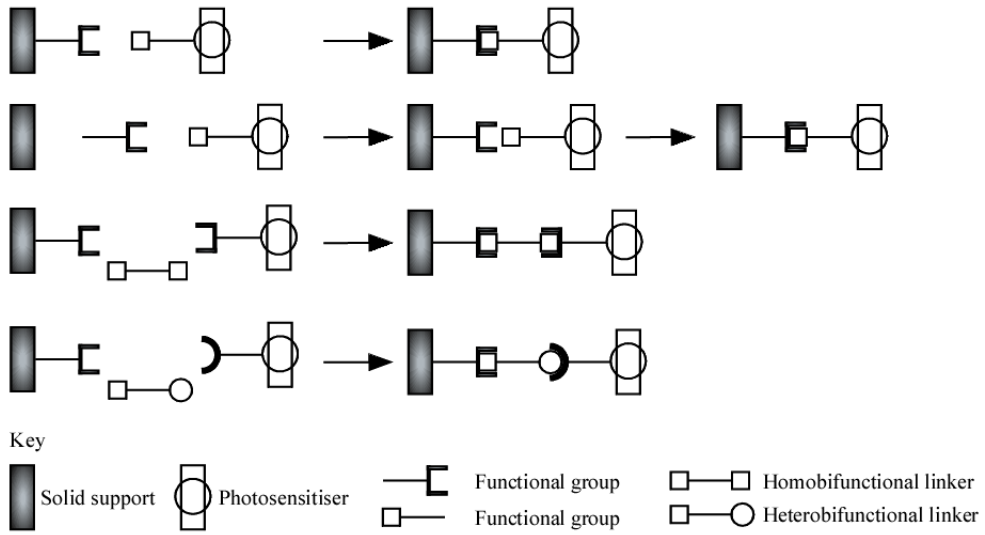

Scheme 3.1: *Conjugation chemistry methods for immobilising photosensitisers onto a solid support. From top to bottom; direct coupling, surface modified coupling, homobifunctional coupling and heterobifunctional coupling between solid supports and photosensitisers.*

There are several other immobilisation methods available for chosen molecules like photosensitisers, some of which are through weak interactions such as adsorption, hydrogen bonding and polarity differences or static charge interactions.[330, 333, 334] However, charge based interactions are not suitable for applications where highly polar solvents such as water are used. As use of aqueous media for cell based reactions are unavoidable, immobilisation of photosensitisers using electronegativity differences or ionic interactions were not considered as a choice within the scope of this project.

In general, the amino functional group on APTES is the most commonly used nucleophilic partner for conjugating to a wide range of electrophilic centres through the formation of strong covalent bonds such as amide and thiourea bonds. To minimise variations within the project, only two types of surface modified conjugation chemistry were employed, one was the formation of thiourea bonds through the reaction between an isothiocyanate (-NCS) group on the photosensitiser and an amino group on the surface, and the other was the reaction of these amines with a carboxylic group on the photosensitiser, forming amide bonds. However, other types of reaction

could also be equally applied with few modifications to the methods described in the experimental chapter. In addition, there are also other efficient means of attaching molecules onto solid surfaces, such as using 'click-chemistry', some of the key reactions in this domain include, azide-alkyne, thiol-click, Diels-Alder and photo-click.[302, 349]

3.1.2 Photosensitisers used for conjugation

Photoactive molecules referred within this chapter are provided in **Figure 3.1**. These photosensitisers were immobilised on to the channels of microfluidic chips and their presence on the channel surfaces were verified using multiple methods including; UV-visible measurements, fluorescence measurements, colorimetric confirmation and cholesterol oxidation.

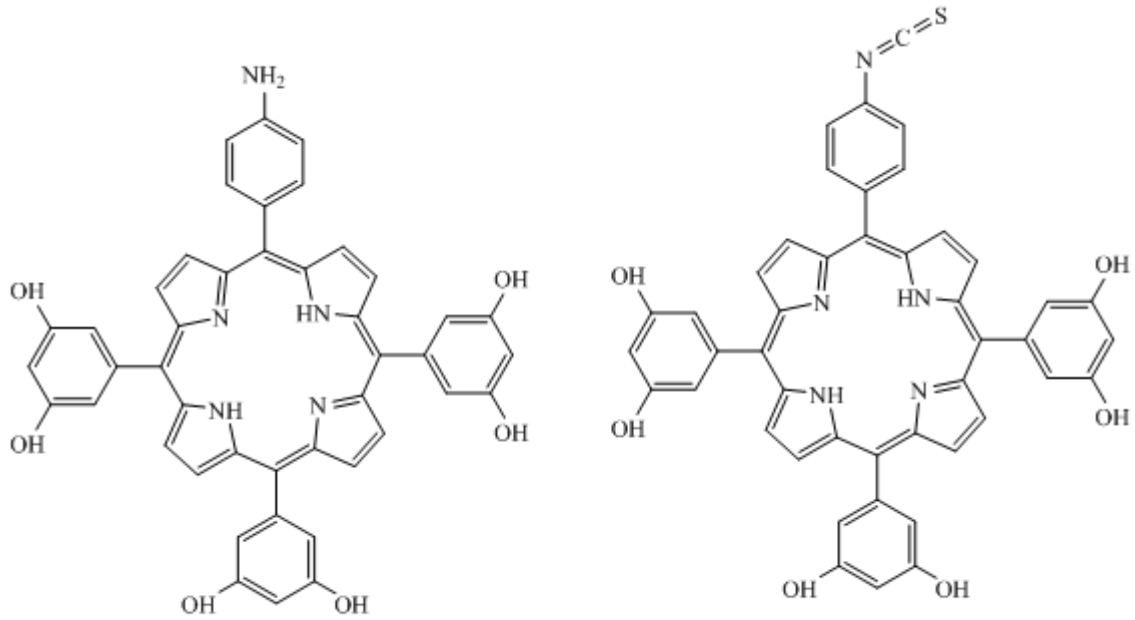

[3]

5-(4-Aminophenyl)-10,15,20-tri-(3,5-dihydroxyphenyl)porphyrin

[4]

5-(4-Isothiocyanatophenyl)-10,15,20-tri-(3,5-dihydroxyphenyl)porphyrin

Figure 3.1: *Photosensitisers used for immobilisation.*

continued…

continued…

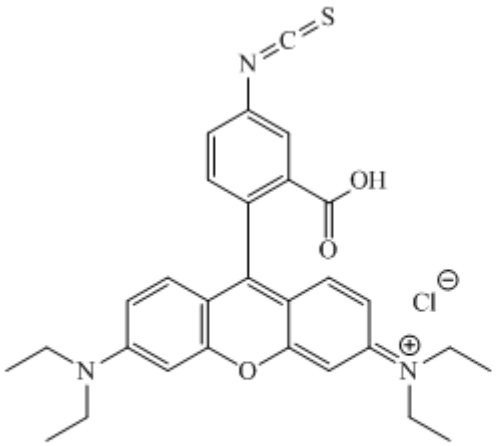

[5]

Rhodamine B Isothiocyanate (RBI)

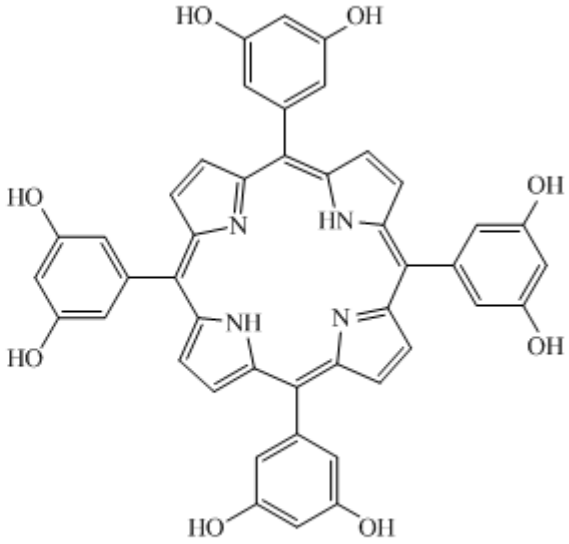

[6]

5,10,15,20-Tetra-(3,5-dihydroxyphenyl)porphyrin

Figure 3.1: *Photosensitisers used for immobilisation.*

3.1.3 General quantum features

The higher the quantum yield (Φ) of a sensitiser the more efficient is the photosensitiser in producing reactive oxygen species. According to the International Union of Pure Applied Chemistry (IUPAC), the integral quantum yield is the number of events triggered per photon absorbed and for a photochemical reaction the quantum yield is the amount of reactant consumed or the amount of product formed per photons absorbed from a monochromatic radiation. The quantum yields of photosensitisers depend on several factors; including the nature of the solvent in which they are dissolved, the temperature, the structural rigidity, the concentration, the pH, the levels of oxygen dissolved in solution and the type of light source used for excitation.

Solvent: There are three important characteristics of solvents to be considered; their polarity, viscosity and the heavy atom effects. With the use of polar solvents, the energy for the process of π-π* transition is lowered and with the use of higher viscous solvents the collisional related

deactivation is reduced. The existence of heavy atoms in a solvent increases inter-system crossing (ISC) thereby decreases fluorescence and phosphorescence.

Temperature: Increases in temperature increase the kinetic energy of molecules, thus increasing the collisional frequency, deactivating the excited molecules much more rapidly through non-radiative processes.

Structural rigidity: In general, the rigid molecules have higher fluorescence because the molecules with higher rigidity are more resonance stabilised, hence better chromophores, while the fluorescence of flexible molecules can be rapidly quenched due to increased collisional deactivation.

Concentration: The increase in fluorescence with increase in concentration of the fluorophore is linear only at concentrations corresponding to absorbance values lower than 0.05 a.u. At very higher concentrations various effects such as aggregation, internal reflections and reduced incident ray penetration can reduce the output of luminescent properties.

pH: Changes in pH can result in protonation or deprotonation of fluorescent molecules which affects the luminescent properties. Commonly the fluorescent wavelengths are higher at higher pH.

Oxygen concentration: Presence of dissolved oxygen promotes ISC due to its paramagnetic nature and matches in energy level of ground state oxygen, which is in the triplet state, with the energy level of phosphorescence resulting in transfer of energy from triplet state photosensitiser and causing excitation of the oxygen molecule. This process quenches phosphorescence and enhances singlet oxygen production.

Light source: Stronger light intensity increases the chances of exciting higher number of molecules for fluorescence and phosphorescence. Therefore, intense radiant sources normally produce intense fluorescent or phosphorescent signals.

In addition to the quantum yield of a photosensitiser, their half-life and photobleaching rates also play an important role in the reusability of the sensitisers, hence in their reliability for the reactions.

3.2 Microfluidics

3.2.1 Microfluidics for cells

Various microfluidic chip designs were considered and drawn using the *AutoCAD* software. The channel designs and their dimensions were the two key areas deeply considered when generating the microfluidic chip designs. The choices for appropriate channel dimensions were essential to reduce build-up of backpressure and to obtain the desired path lengths for the reactions. In order to reduce build-up of backpressures and blockages of the channels, the channels were designed wider to ensure enough space for the flowing cells. Further the dimensions such as width of the channels were decided based on the properties of cells to be used, importantly cell size and their stickiness to the glass surfaces. Magnitudes and shapes of the channel branching regions were also considered with care to avoid or reduce blockages. To reduce time consumption and expense, only few of the selected designs from the photomask were fabricated into microfluidic devices.

The devices were evaluated for the minimum reduction in the number of cells at the collection end, by flowing cells through the channels. In comparison to the use of a lower flow rate (5 µl min^{-1}), at a higher flow rate (50 µl min^{-1}) the number of cells dropping out of flowing fluid to the surface of the channels were reduced. However, the higher limits of the flow rates were a compromise between the essential residence time, the length of the channels and importantly the level of shear-stress that would affect the healthy status of the cells. There are three types of stress forces, tensional-stress, compressional-stress and shear-stress. Shear-stress is the result of forces acting parallel to a given surface to induce stress. Generally, the higher the flow rate the higher the shear-stress induced on cells. The variables like the surface area to volume ratio, the back pressure, the residence time and the designs that would have minimum chances of causing blockages were studied, before deciding on the optimum chip design(s) for the cell based microfluidic photosensitisation reactions.

When designing the microfluidic patterns, certain designs were avoided at the early stages for several reasons. The designs considered as inappropriate were; 1) the use of microfluidic chambers with or without pillars in them, where the surface area to volume ratios were greatly reduced relative to using several parallel channels, 2) the designs with more than 16-parallel channels, that is, 32 or higher, due to handling difficulties and 3) the designs with inlets and outlets on the same side of the chip, where the backpressure increased steeply.

The 16-parallel channels and the serpentine channel designs were found to be more suitable for the purpose of the experiments described here. Both of these designs were critically assessed by carrying out preliminary experiments with microbeads (5 µm) and coloured solution (printer ink or food dye diluted in water), from which their appropriateness were evaluated. The flow patterns of cells suspended in RPMI medium, microbeads suspended in water and the flow of coloured liquids were observed under an inverted light microscope. It was noticed that with the use of sharp perpendicular splitting patterned (T-shaped) branching channels, most of the particles suspended in solution flowed through short curved paths as shown in **Figure 3.2**.

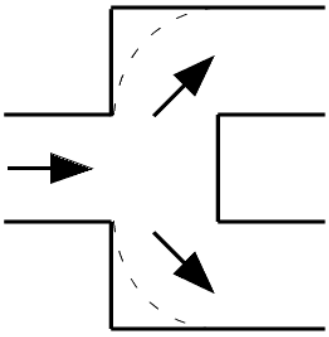

Figure 3.2: *At the channel branching points, most of the flow was through short curved path as indicated by the dotted lines.*

The microfluidic chip designs having inlets and outlets on the same side had a common problem of rise in backpressure. Hence such designs were not of great interest to use in cell based work. Based on the results it was

established that, the use of 16-parallel channel designs with the inlet(s) and outlet(s) on opposite sides were more appropriate than the serpentine channel designs, or the other designs considered for cell based reactions. Although the serpentine channel designs were not suitable with cells based experiments, they could be used for conducting photochemical reactions, where there are no issues about shear-stress forces as with cells.

3.2.2 Microfluidic chip designs

A total of 25 microfluidic chip designs were drawn using the *AutoCAD* software, and the corresponding designs were printed on to an acetate sheet to produce the photomask. From the photomask, only few of the selected designs (**Figures 3.3** and **3.4**) were fabricated (**Section 2.4.2** of **Chapter 2**) into microfluidic devices made of borosilicate glass.

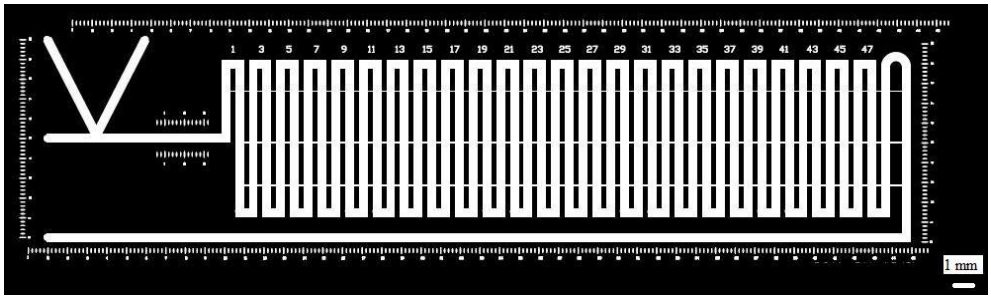

Design 1

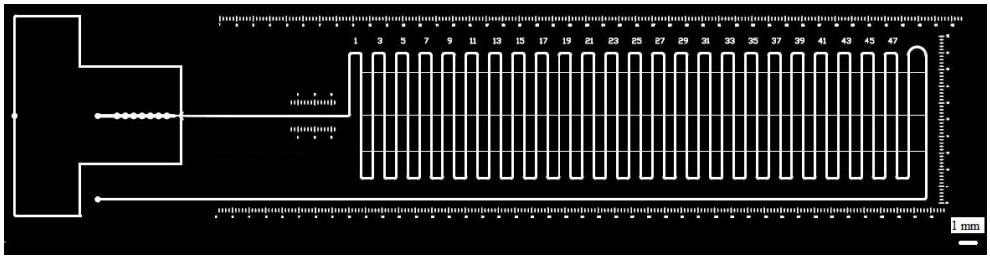

Design 2

Figure 3.3: *Designs of the microfluidic chip with serpentine channels.*

The microfluidic multi-parallel channel designs that were designed, fabricated and tested for the experiments are provided in **Figures 3.3** and **3.4**. The **Designs 3** and **4** those had 16-parallel channels as their main stretching with flow-focusing pattern on their inlet side were used for the

generation of oxygen gas bubbles within the channels. The **Design 3** had the inlets and the outlet on opposite sides of the chip, whereas in **Design 4** they were on the same side of the chip. The **Designs 5** and **6** had 16-parallel channels, with 3 and 7 cm long channel regions respectively. The latter two were regularly used for conducting the reactions reported in this chapter and in **Chapters 4** and **6**. Initially the **Design 5** was chosen as the best design and had been extensively used in surface treatment studies, for photochemical reactions and for conducting cells based reactions (**Chapter 4**). Due to inadequate length of exposure to light with the use of 3 cm long parallel channels, the **Design 6** was made with 7 cm long parallel channels and used in the later experiments (**Chapter 6**). The **Designs 7 - 11** were also fabricated and tested for their applicability to use in the photosensitisation reactions.

The closed atmosphere inside the microfluidic environment (channels) could easily become oxygen depleted. Hence, it was vital to enrich the microfluidic channels with sufficient amount of oxygen gas using an external oxygen gas supply, so that sufficient amount of oxygen would be present for an effective and an acceptable level of singlet oxygen production. One way of achieving higher oxygen concentrations within the channels was to pump oxygen gas, which would form bubbles when mixed with a flowing liquid inside. Though bubbles can be generated simply using designs with two or more inlets leading to the same channel (**Designs 1** and **5 - 10**), flow-focusing or T-junction **Designs 2, 3** and **4** were useful for the production of gas bubbles within the microfluidic channels. The introduction of oxygen gas as bubbles within microfluidic channels was helpful in maintaining constant supply of oxygen for ROS production (**Section 3.3**).

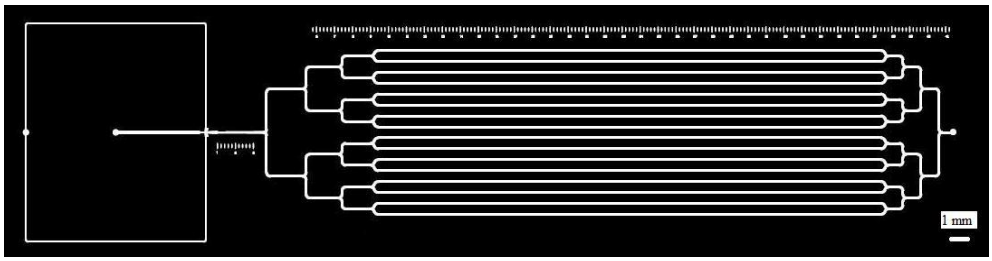

Design 3

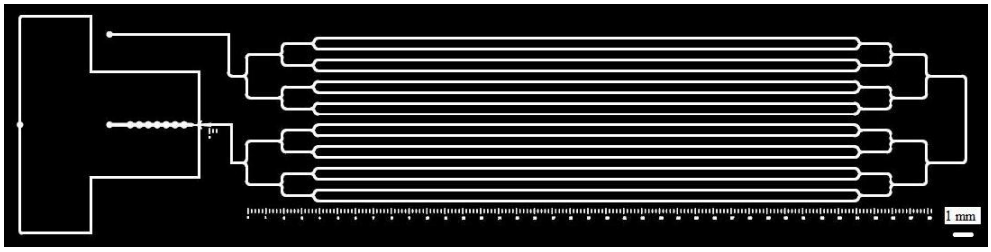

Design 4

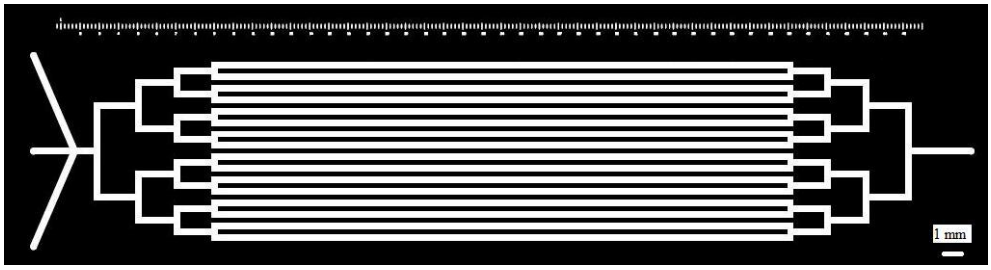

Design 5

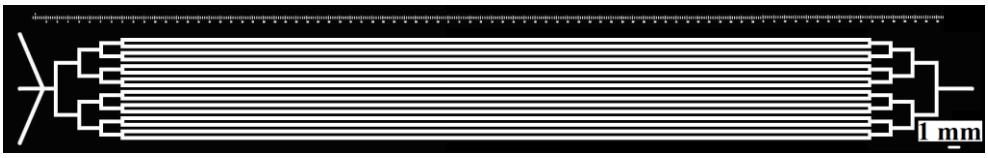

Design 6

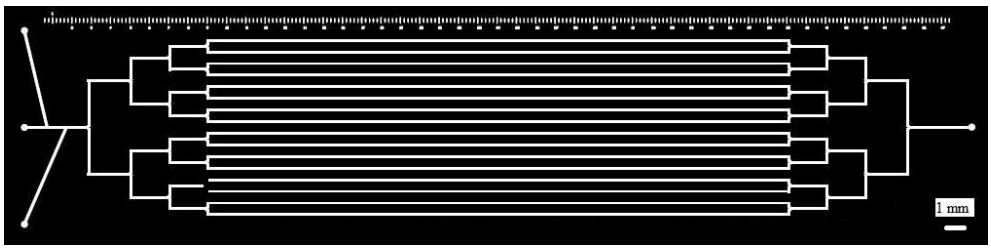

Design 7

Figure 3.4: *Designs of the microfluidic chip with 16-parallel channels.*

continued…

continued…

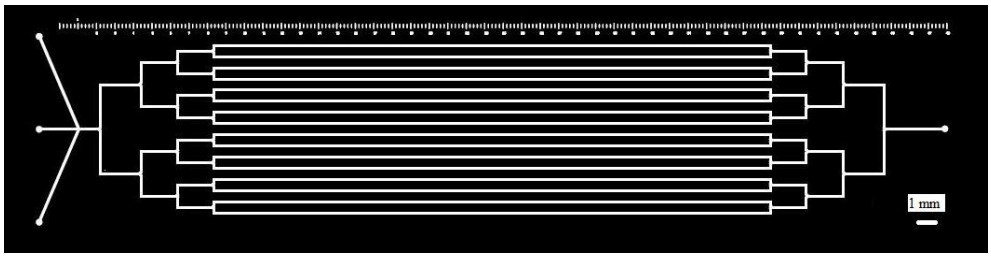

Design 8

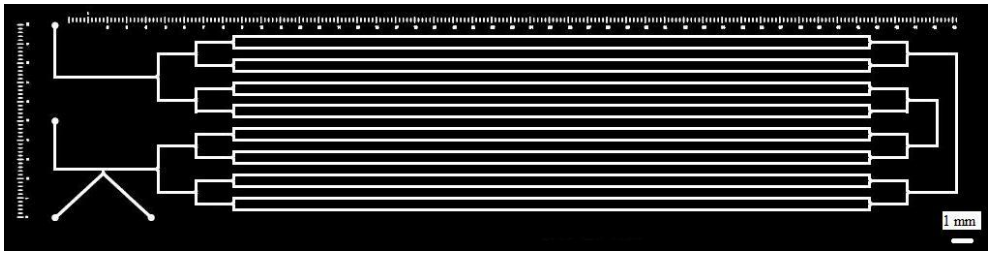

Design 9

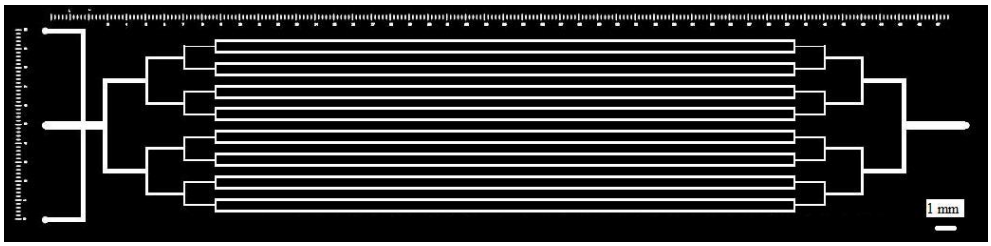

Design 10

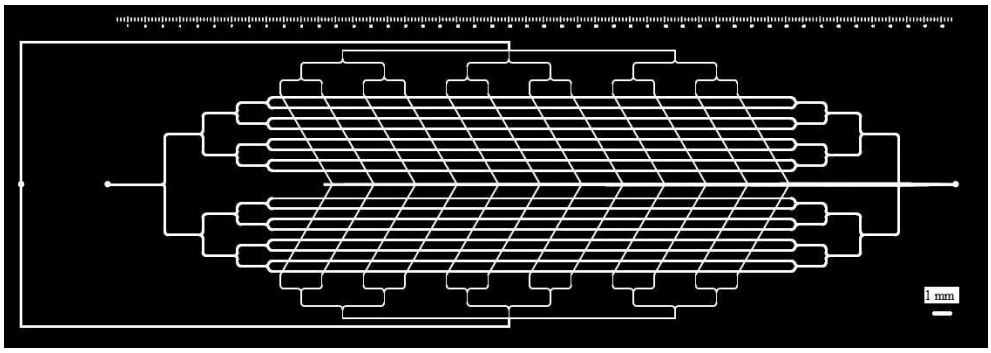

Design 11

Figure 3.4: *Designs of the microfluidic chip with 16-parallel channels.*

3.2.3 Parallel channel designs

Among various types of microfluidic chip designs considered in the above section **3.2.2**, the **Designs 5** and **6** were found to be the most appropriate type for the kinds of cell based experiments considered in **Chapters 4** and **6**. The surface area to volume ratio was calculated for various depths of the microfluidic channels, and a graph was plotted. The correlation between the surface area to volume ratio (mm^2 μl^{-1}) versus the depth of the channels (µm) is shown in **Figure 3.5**.

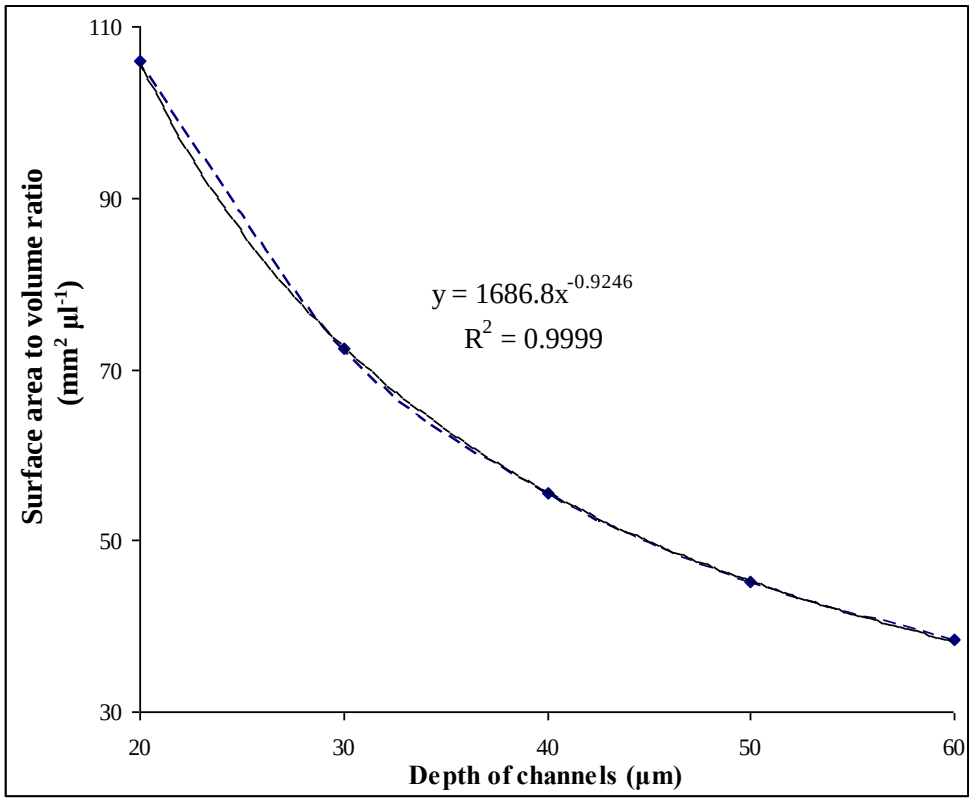

Figure 3.5: *The relationship between the surface area to volume ratio of microfluidic channels against their depths; (---) is the line connecting the data points, and (—) shows the predicted trend curve.*

The trend curve fitted to the data points in **Figure 3.5** revealed an inverse power-based (non-linear) relationship (**Equation 3.1**) between the surface area to volume ratio and the depth of the channels. The obtained coefficient of determination (R^2) for the trend curve was 0.9999, which is 1.00 to 3 s.f., indicated a strong correlation for the relationship predicted. The analysis of y-residual plot for the above set of data produced a non-random (U-shaped)

pattern, representing the fact that a linear regression model was not the right choice for the above sets of constraints considered.

The plot in **Figure 3.5** and the corresponding **Equation 3.1** were useful in predicting the surface area to volume ratio of any depths of the channels, those were singly isotropically etched from a photomask width of 300 µm. From the trend of the curve and the equation it was clear that, with increase in the channel depth, the surface area to volume ratio decreases in a predictable pattern. The trend was a common scenario for all isotropically etched channels from 2D photomask drawings.

$$S_V = 1686.8\ C_d^{-0.9246} \qquad \textbf{Equation 3.1}$$

Where, S_V is the surface area to volume ratio in $mm^2\ \mu l^{-1}$ and C_d is the depth of the microfluidic channels in µm. In the S_V calculations, it was assumed that the surfaces of the isotropically etched microfluidic channels were perfectly smooth and presences of any defects were negligible to be incorporated in the calculations. However, viewing under an inverted light microscope showed that the channels etched for lower depths such as 20 and 30 µm, had much smoother surface than the ones etched to the depths of 50 and 60 µm. The channels of lower depths were etched at room temperature, whereas higher temperature was essential for etching higher channel depths. The length of exposure to the etching solution was used as the controllable parameter for varying the channel depths (**Section 2.4.2 of 2.4**).

3.2.4 Microfluidic chip fabrication

The microchips are usually constructed using silica glass materials, polydimethylsiloxane (PDMS) or combination of both.[301, 305] Most of the cell based microfluidic researches make use of PDMS as it enables easy fabrication, provided that pre-made moulds were available. Mould is the intended chip design, usually mechanically drilled onto a metal block of few centimetres in dimensions. Several PDMS chips can be made in a short time scale, and in addition it does not require much expertise relative to what

would be essential for producing the glass based microfluidic devices. The PDMS based microfluidic devices can be made permeable to diffusion of gases between adjacent channels.[305] However, PDMS is non-compatible with organic solvents such as toluene.[301] For the experiments considered in the following chapter, the photosensitisers had to be immobilised on to the surface of the microfluidic channels which involved the use of organic solvents such as toluene, hence PDMS was not employed for making the microfluidic chips.

Microfluidic devices of various designs were fabricated through the transfer of designs from the photomask onto a chrome coated borosilicate glass of 1 mm thickness. The transferred patterns were developed using a developing solvent, and using the wet etching method the microfluidic channels were produced. The detailed methods of fabrication can be found in **Chapter 2**. The etched glass slides were thermally bonded to a cover glass slide of 1 mm thickness, to produce closed channels. The fabricated microfluidic chips were tested for their nature of flow schemes, laminar and turbulent, under various flow rates. In order to visualise the flow patterns within the microfluidic environments, different coloured food dyes or printer inks diluted in water (18 MΩ at 25 °C, miliQ, 0.22 μm filtered) were pumped through and observed under an inverted light microscope.

Microbeads (5 μm in diameter) were also pumped through the microfluidic chip, to test the possibilities of pumping micron sized particles and to study their behaviour within the multi-parallel (16-parallel) channels (**Figure 3.4**). The serpentine channel designs had a drawback of relatively high backpressure, hence were not used for cell based work.

Backpressure is the added force that is caused as a result of accumulated drag force of liquid moving through the channels. Within this thesis, the term ‘relative-backpressure’ must be regarded as the additional pressure on top of the pressures that may exists in the absence of fluid flow at any given flow rate, flowing at a known distance from a defined origin. One type of unavoidable pre-existing pressure was the atmospheric pressure.

3.2.5 Isotropic etching

Isotropic etching is where the etching occurs to the same level of extent in both *x*- and *y*-axes directions (**Figure 3.6**). The microfluidic channels were fabricated from the photomask using wet isotropic etching procedure, as described under **Section 2.4.2** of **Chapter 2**. The parallel channel microfluidic chips, **Designs 5** and **6** were chosen for the cell based flow experiments, as it enabled high throughput with less build-up of backpressure relative to other channel designs considered in **Figures 3.3** and **3.4**. A typical cross-sectional view of an isotropically etched channel, where the channel was etched to a depth of 60 µm using the pattern transferred from a photomask having width of 300 µm, is shown in **Figure 3.6**.

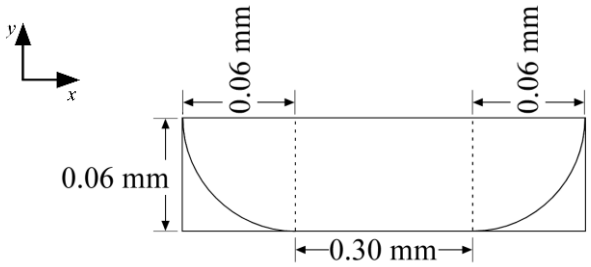

Figure 3.6: *Cross-sectional view of an isotropically etched 60 µm depth microfluidic channel, from a photomask width of 300 µm.*

Followed by the use of microfluidic devices of 60 µm depth, 3 cm long parallel channels (**Figure 3.7**) for cell based reactions, 7 cm long parallel channels of the same depth were utilised to increase the residence time. Increase in length of the parallel channels also increased the backpressure. To reduce the backpressure within the 7 cm long parallel channels, double etched 120 µm depth (2 x 60 µm) channels of 7 cm in length were fabricated and used for the experiments (**Figure 3.8**).

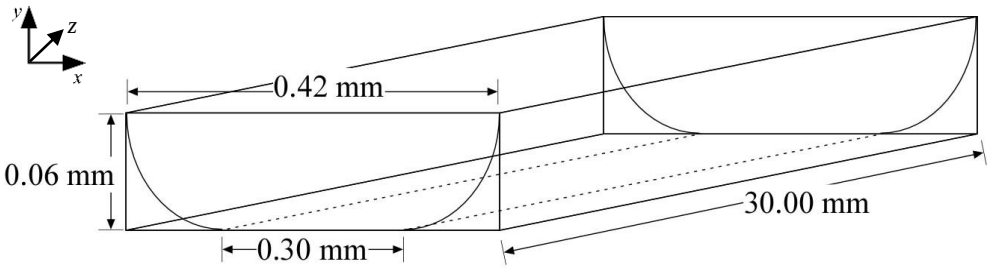

Figure 3.7: *A cross-sectional and a side view of an isotropically etched 60 µm depth and 3 cm long microfluidic channel.*

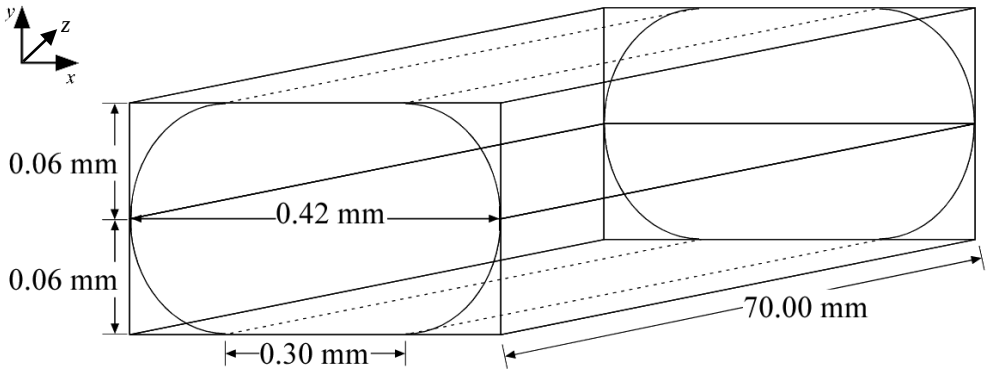

Figure 3.8: *A cross-sectional and a side view of an isotropically double etched 120 μm (60 μm + 60 μm) depth and 7 cm long microfluidic channel.*

For the fabricated microfluidic devices, the inlet and the outlet holes were machine drilled and were of constant size of 360 μm. The width of the channels varied between 300 μm (at the bottom) and 420 μm (at the top) as illustrated in **Figures 3.6-3.8**. Fused capillaries with varying sizes of inner diameters (ID), but with constant outer diameter (OD 375 μm) were tested interfacing to the inlet and the outlet holes on the microfluidic chips. The fused capillary with ID of 20 μm was the smallest size tested, and it had the highest backpressure relative to other dimensions discussed below. For example, in order to pump water which has a dynamic viscosity of 0.9 cP at 25 °C, at a flow rate of 1 μl min^{-1} along a 10 cm long fused capillary tube, the relative-backpressure raised to 3819 mbar (3.769 atm), thus making both the introduction and the collection of samples into and out of the chip extremely difficult. Under the same conditions, for the fused capillaries of ID 100 μm, the obtained maximum relative-backpressure was 6.1 mbar. The fused capillaries with the ID of 200 and 250 μm were also tested, however they were relatively more fragile than the one with ID of 150 μm or less, hence they were not utilised in the experiments. The fused capillaries with the dimensions, ID 150 μm and OD 375 μm was selected as the best possible size and were used for all the experiments. With this dimension the relative-backpressure increased only to 1.2 mbar under the same set of conditions that were considered for IDs 20 and 100 μm.

3.3 Production of oxygen gas bubbles

As pointed out in the earlier sections of this chapter, it was essential to enrich the microfluidic environments with sufficient amount of oxygen for an effective production of ROS. Several methods were used for the production of constant size oxygen gas (or air) bubbles consistently within the microfluidic channels. The methods of using pressure pump, syringe pump, peristaltic pump and direct supply (connection) of oxygen gas from the gas cylinder to microfluidic devices were tried one after the other. Unlike pumping liquid, pumping of gas into the microfluidic channels required additional materials for interfacing gas reservoirs to the controllers at the inlets of the microfluidic chips.

3.3.1 Pressure pump

The generation of gas bubbles using pressure pump (Fluigent®) was straightforward. In order to produce oxygen gas bubbles the flow rates were controlled using the pressure differences. With the increased pressure difference the speed of flow increased and *vice versa*. The pressure within the microfluidic channels in the absence of flowing fluids was assumed to be the same as the atmospheric pressure (1 atm), and the pressures externally applied using the pump were regarded as the positive pressure. Hence pressure differences were created by applying positive pressures to the closed sample vials. There were issues getting the correct balances of positive pressures within the sample vials that contained liquids and the vials that were filled with oxygen gas to produce liquid-gas bubble mixtures. Reproducibly getting similar sized bubbles between each experiment, and the speed at which the system equilibrated, took enormous amount of time and efforts. This method was helpful for easier introduction of gas bubbles, but the control over the size of gas bubbles were demanding as the level of pressure alone could not be used as a direct measure of number of gas bubble generated or for the production of constant size gas bubbles. Efficient mixing of liquids and gases within the microfluidic chips (**Design 4**) were linked to several factors such as the densities, the temperature at which the mixing occurred and the type of flow designs used for mixing. Due to the limited pressure range achievable using the pressure

pump, pumping of high viscous fluids such as RPMI medium containing cells or PBS solution containing cells were rather complex than solely pumping liquids such as methanol (0.79 g cm^{-3}, 20 °C) and water (1.00 g cm^{-3}, 20 °C). Further, the pump was very sensitive to slight variations in the pressure within the microfluidic environment, and the controls over the adjustable pressure range was restricted within few hundreds of mbar scale (-30 to 377 mbar).

With the use of pressure pump the reproducibility of similar size bubbles were both time consuming and were not always successful. Further due to the nature of the pressure pump setup (**Section 2.3.2** of **Chapter 2**), the cells settled-down to the bottom of the container swiftly and stopped flowing though capillaries connections to reach the microfluidic channels. The use of magnetic stirrer for re-suspension was not possible due to small sizes (space restriction) of the sample containers, and moreover timing was critical for the cell based reactions. Therefore the use of pressure pump was avoided for the cell based reactions. However, the pressure pump would be a useful choice for the photochemical reactions, where the reactants can be allowed to stand in the sample vials for longer times before beginning the reactions. Furthermore, the chemical reactants would be completely dissolved (solvated) and usually would be of similar densities, hence magnetic stirrers are not essential for re-suspension or mixing, but with cells this was not the case.

3.3.2 Syringe pump

The use of syringe pump for pumping oxygen gas required the use of a second syringe pump, for dispensing gas at a higher flow rate than that was used for flowing liquid or cell suspension. The volume of oxygen gas that could be filled within syringes were rather limited, hence the production of bubbles did not last for a long time (~1 to 3 minutes). The production of bubbles using syringe pumps was also challenging mainly because of the high density differences between that of liquids (e.g. water, 1.00 g cm^{-3}) and gases (e.g. oxygen, 1.33 x 10^{-3} g cm^{-3}), which varied by a factor of 752 times at 20 °C and 1 atm. As a result, balancing the pressure of the gas

introduced and the speed of liquid flow were not straightforward. With few modifications and adjustments to the inlet side of the interfacing, the peristaltic pump was also tested for generating gas bubbles. The control over the accuracy and the precision of producing gas bubbles using the above methods were low.

3.3.3 Direct gas supply

Alternative to using the pumping systems discussed above, oxygen gas was introduced into the channels through direct connection from an oxygen gas cylinder (controlled using regulators fitted to it) or by manually pumping using a syringe filled with oxygen gas. When supplying gas directly, a digital pressure-gauge was fitted along the line connecting the gas cylinder and the capillary tubes at the inlet of microfluidic chip to enable control over the levels of incoming gas. However, this type of setup took a long time to reach a steady state. When pumping methanol (0.79 g cm^{-3}, 20 °C) through the chip **Design 4** in the flow rate range of 2.5 to 3.5 µl min^{-1}, the pressure of incoming gas had to be in the range of 3 to 4 psi. Similarly, when flowing the same liquid at the speed of 7 µl min^{-1}, the level of gas pressure had to be around 7 psi for balancing backward flow and for the production of gas bubbles. For methanol, which has a density lower than that of water, the levels of pressure (psi) and the speed of liquid flow (µl min^{-1}) were almost in the ratio of 1:1. However for higher dense liquids like water (1.00 g cm^{-3}, 20 °C) when flowed at the rate of 3.5 µl min^{-1}, the gas pressure had to be in the range of 16 to 19 psi, which was about 5 times higher than what was essential with methanol. Similar to the methods discussed above, the production of similar sized bubbles at regular intervals were challenging. Irrespective to the choice of the methods used for gas bubble production, there were several technical difficulties and inconsistencies with the uniformity, the stability and the reproducibility of similar sized gas bubbles. Nonetheless, the latter method was used to introduce gas into microfluidic chip during some of the photochemical oxidation reactions conducted using cholesterol as the substrate. Using the chip **Design 4**, direct gas supply from gas cylinder and syringe pump for

flowing colour ink (for visualisation), gas bubbles were produced within the channels (**Figures 3.9** and **3.10**).

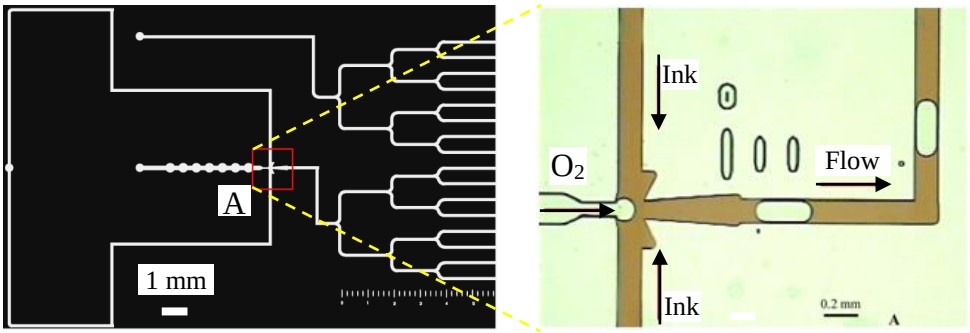

(a) **(b)**

Figure 3.9: (a) *Flow-focusing* **Design 4** *used in generation of gas bubbles and* **(b)** *when generating gas bubbles, to use in photochemical reactions.*

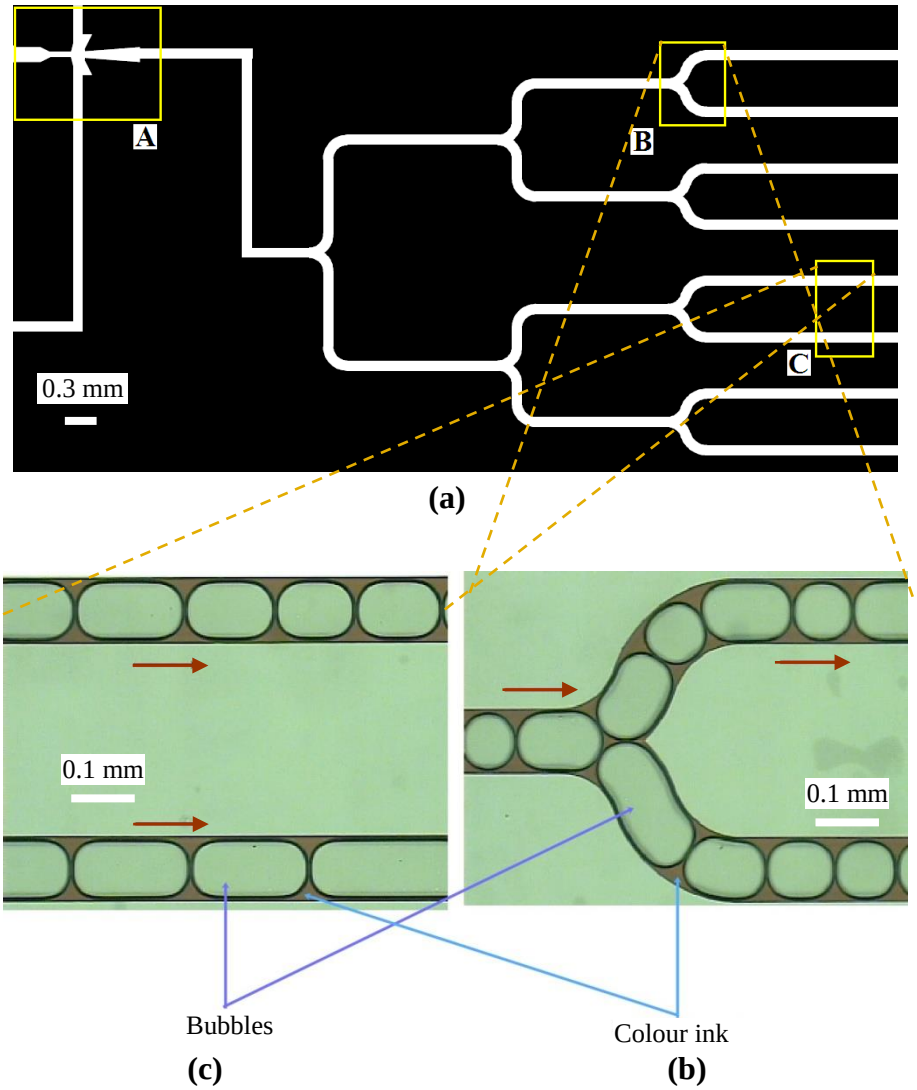

Figure 3.10: (a) *Shows a part of the channel* **Design 4** *and highlights the regions of gas-liquid composition viewed in* **(b)** *and* **(c)**.

Figure 3.10 shows the variations in the size of the gas bubbles produced, and the ratios in which the gas bubbles and the coloured liquid occupied the space within the microfluidic channels. The colour liquid was magenta printer ink diluted in water. Both liquid and gas bubbles were flowing from left to right as indicated by the arrows. **Figure 3.10 (b)** and **(c)** shows gas bubbles separating out into two branching parallel channels and when gas-liquid mixture was flowing in two of the 16-parallel channels, respectively.

Though for enriching the microfluidic environment with oxygen, oxygen gas bubbles can be produced within the channels, but the method was only suitable for photochemical reactions and not for the reactions involving cells. The introduction of oxygen gas bubbles into the microfluidic environment results in creation of heterogeneous atmospheres, an unfavourable condition for the cells. The presence of excess oxygen close to the cells would greatly affect their viability. Therefore this method of enriching oxygen gas would be useful for chemical reactions, where the number of possible reactions are usually limited and can be predicted using the knowledge of chemical synthesis and the reactivity of the molecules. In addition, using advanced spectroscopic methods such as Mass Spectrometry (MS) and Nuclear Magnetic Resonance (NMR), the chemical compositions can be precisely studied. However, with cells, under a single new set of condition, numerous factors could change simultaneously, making it difficult to trace all of it. Though the introduction of oxygen gas bubbles was considered as a reputable method for enhancing the concentration of oxygen within the microfluidic environment, the method was limited for use with chemical or photochemical reactions like cholesterol oxidation reactions.

There were two alternative methods for increasing the levels of oxygen concentration within the microfluidic environment. One of them was to pre-oxygenate the medium and to introduce it through a second inlet. Within the channels when the pre-oxygenated medium meets with cells carrying medium, oxygen gas would diffuse into solutions carrying cells. The other method was to pre-oxygenate the medium before suspending the cells in it.

There were restrictions associated with the latter two methods, the amount of gas that can be dissolved in an aqueous medium is sensitive to temperature and has a maximum limit at a given temperature. For water, which makes up most of an aqueous medium, the maximum amount of oxygen gas that can be dissolved at room temperature (20 ºC) is 8.9 mg dm^{-3}. No additional oxygen gas can be introduced at this temperature without modifications to the contents of the aqueous medium. However, the oxidative stress reactions (OSR) were conducted relying only on the amount of oxygen gas that was present in the dissolved form within the medium in which the cells were suspended.

3.4 Surface treatment of microfluidic chip

The chemical composition of common glass is silicon and oxygen atoms linked through covalent bonds in a tetrahedral arrangement to form a silicon oxide solid state structure (**Figure 3.11**). The surface of glass has hydroxyl groups (-OH) which can be utilised to immobilise multifunctional silanising agents like APTES, which provide nucleophilic amine sites for the covalent attachment of photosensitisers bearing electrophilic functional groups like isothiocyanate. Procedures for cleaning glass surfaces of microfluidic chips, followed by APTES treatment and photosensitiser immobilisation are described under **Section 2.4.4** of **Chapter 2**.

3.4.1 Chemical composition of a treated glass surface

APTES is one of the most commonly used silanising agent for glass surface treatments.[322, 323, 350, 351] APTES was immobilised onto the microfluidic glass surface through the formation of silicon oxide (siloxane) covalent bonds. Isothiocyanate (NCS) group functionalised photosensitisers ([**4**] and [**5**]) were covalently immobilised through the formation of thiourea bonds between the amino groups of APTES and the NCS groups of the photosensitisers. The chemical structure in **Figure 3.11** proposes one of the possible forms in which a glass surface treated with APTES and photosensitiser [**4**] would exist. It should be noted that the thiourea bonds are chemically labile in the presence of strong acids and bases, this fact was

utilised to hydrolyse the immobilised photosensitisers off the chip surface and measured using spectroscopic methods to show that, they were the right photosensitisers and were successfully immobilised within the channels.

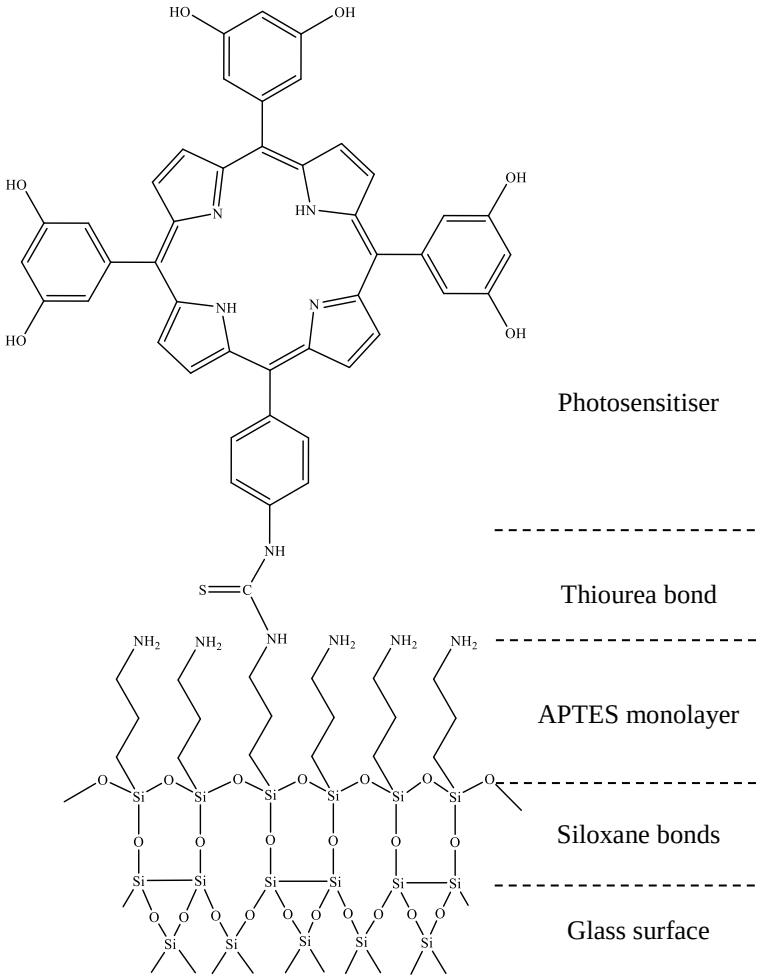

Figure 3.11: *The chemical structure of APTES and photosensitiser* [**4**] *immobilised glass surface.*

3.4.2 Hydrophobic and hydrophilic surfaces

Glass surfaces that have not been chemically treated are hydrophilic in nature due to the presence of hydroxyl terminal groups, and during chemical surface treatment they are susceptible to be modified by the reagents like silanising agents. Hydrophilic surfaces would have a contact angle much less than 90º and in general, as the hydrophilicity reduces, contact angle increases.

3.4.2.1 Silanisation using 3-aminopropyl(triethoxy)silane

It was repeatedly observed that the glass surface treatment using APTES reduced the hydrophilicity of the glass surface, but was not capable of rendering the glass surface completely hydrophobic. The extent of hydrophobicity was dependent on the type of functional groups present on the silanising agent. The changes to the glass surface properties were identified using the contact angle measurements between an aqueous medium and an air interface of the treated surface. In one of its theoretical immobilised forms, every three hydrophilic hydroxyl groups (–OH or $–O^-$) on the glass surface are replaced by three silicon oxide bonds from a single APTES molecules, providing a hydrophilic amino group. Provided that the amino groups remains perpendicular to the plane of attachment, in such situation the hydrophilic nature of the glass surface would be expected to be reduced by three times. As the effect of changes in hydrophilicity due to APTES surface treatment was smaller, hence the contact angles also did not vary considerably (**Figures 3.12** and **3.13(a)**). It was also observed that relative to non-surface treated channels, the APTES treated surfaces showed higher resistance when pumping aqueous liquids. The above facts were useful in predicting if the silanisation treatment was successful. In addition, when a mixture of water and air bubbles were introduced into APTES treated channels, air bubbles became completely covered in water (aqueous), indicating that the surface was hydrophilic (**Figures 3.12** and **3.13(a)**). Apart from the contact angle measurements, the latter description of air bubble being covered by an aqueous medium was also used to evaluate the hydrophilic nature of channel surfaces.

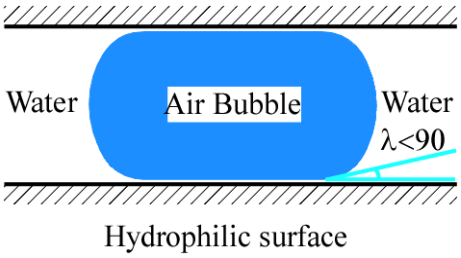

Figure 3.12*: Typical wettability and contact angle view of an APTES treated surface.*

3.4.2.2 Silanisation using triethoxy(ethyl)silane

Microfluidic glass channels were surface treated with triethoxy(ethyl)silane and the contact angle measurement was repeated. Following surface treatment with triethoxy(ethyl)silane, the microfluidic glass channel surfaces became hydrophobic (**Figures 3.13(b)** and **3.14**). The types of interactions between water, air and glass surfaces at two different levels of hydrophobicity are illustrated in **Figure 3.14**, where contact angles of 90º or greater indicated hydrophobicity (**Figure 3.13(b)**). Hence triethoxy(ethyl)silane could be used for surface treatments when a hydrophobic environment was crucial and the contact angle measurement could be used to determine the degree of hydrophobicity (**Figure 3.14**). It was constantly observed that the level of pressure required for pumping water through microfluidic channels with hydrophobic surface was higher than that was required for identical non-surface treated channels. The changes in the levels of pressure required for pumping aqueous liquid was also an indirect indication for an altered channel surface property.

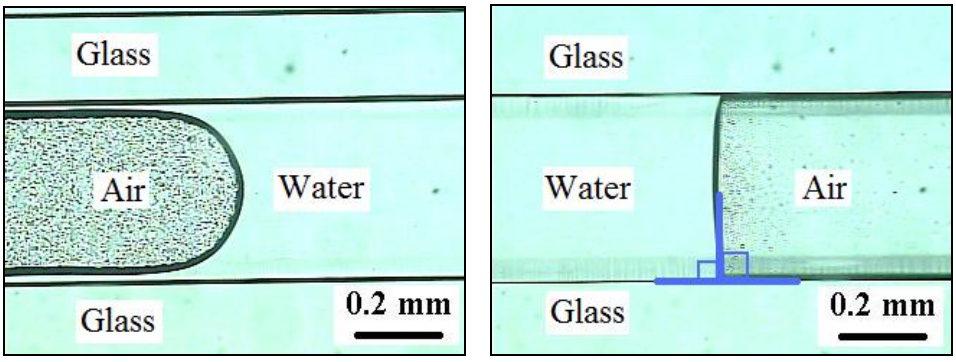

(a) **(b)**

Figure 3.13: (a) *Glass channel surfaces either non-treated or APTES treated were hydrophilic and* **(b)** *channel surface treated with triethoxy(ethyl)silane were hydrophobic.*

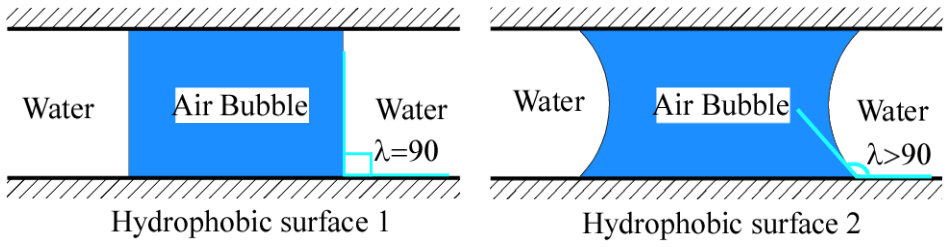

(a) **(b)**

Figure 3.14: (a) *Surface 1, typical hydrophobic behaviour following silanisation using triethoxy(ethyl)silane.* **(b)** *Surface 2 much more hydrophobic than the surface 1, in each it shows the interaction between water, air, and glass surface.*

3.4.3 Silanisation and photosensitiser immobilisation

The initial microfluidic flow oxidative stress reactions (MFOSR) were conducted using immobilised photosensitisers, hence attempts were made to immobilise maximum levels of photosensitiser onto the channel surfaces. The efforts to immobilise various types of photosensitisers onto the glass surfaces non-treated with APTES were unsuccessful, clearly indicating that the photosensitisers (**Figure 3.1)** did not simply stain the glass surfaces and silanisation was must. To understand the mechanism, it was tested if the presence of amino ($–NH_2$) group was essential to enable immobilisation of photosensitiser possessing –NCS group. From the study of using triethoxy(ethyl)silane as the silanising agent, which contained triethoxy groups and a simple ethyl hydrocarbon chain, it was found that the photosensitisers did not immobilise and the channels remained colourless. It indicated the necessity for amino groups to be present for photosensitiser attachment.

Two different temperatures, 18 °C and 120 °C were tested for surface treatments and the results were identical at both temperatures (**Table 3.1**). The common theme from the studies was that the surface has to be APTES treated for successful immobilisation of photosensitisers. The fluorescent intensity from the photosensitiser [**4**] immobilised channels were not intense enough to be readily observed in real-time, but longer acquisition time of about 3 s or higher enabled fluorescence to be detected by microscopy. The surface treatments carried out at room temperature (18 °C) required a longer time (7 hours) for the processes of treating with silanising agent and for the immobilisation of photosensitisers, which was more than three times the time required for the same processes at 120 °C (2 hours). The time scales of 7 and 2 hours above do not include pre-surface treatments of cleaning with piranha solution, burning of the debris by heating in a furnace at 450 °C for 4 hours and treating with aqueous sodium hydroxide, which were the common steps for the immobilisation at both temperatures (**Section 2.4.4** of **Chapter 2**).

Table 3.1: *Summary of different combinations of surface treatment methods and photosensitisers tested for immobilisation at 18 and 120 °C.*

Photosensitiser	Surface property	Result	Appearance	Conclusion	Fluorescence microscope
[**3**]	APTES treated	Immobilised	Pale yellow coloured channels	APTES treatment was mandatory	Fluorescence was not intense enough to be observed by eyes, but longer acquisition time of about 3 s enabled fluorescence view
	Plain glass surface	Not immobilised	Colourless channels	Surface must be APTES treated	No fluorescence
[**4**]	APTES treated	Immobilised	Yellow coloured channels	APTES treatment was mandatory	Fluorescence was not intense enough to be observed by eyes, but longer acquisition time of about 3 s enabled fluorescence view
	Plain glass surface	Not immobilised	Colourless channels	Surface must be APTES treated	No fluorescence
[**5**]	APTES treated	Immobilised	Clear Pink channels	APTES treatment was mandatory	Bright orange colour fluorescence readily observable bye eyes
	Plain glass surface	Not immobilised	Colourless	Surface must be APTES treated	No fluorescence
[**6**]	APTES treated	Immobilised	Pale yellow coloured channels	APTES treatment was mandatory	Fluorescence was not intense enough to be observed by eyes, but longer acquisition time of about 3 s enabled fluorescence view
	Plain glass surface	Not immobilised	Colourless channels	Surface must be APTES treated	No fluorescence

Each of the reactions given in **Table 3.1** were repeated a minimum of three times. The optimum conditions and the methods used are given under **Section 2.4.4** of **Chapter 2**. The immobilisation of the more easily synthesised and symmetrical octahydroxy porphyrin [**6**] onto an APTES treated glass surface was possible. The possibility of immobilising photosensitisers via hydroxyl groups onto an APTES treated glass surfaces led to a further study on the type of mechanism through which the immobilisation could have occurred. APTES treated surfaces mainly expose $–NH_2$ group for reacting with the molecules possessing electrophilic groups.

Under the conditions used for the surface treatment reaction, it was unlikely to have direct bonding between $–NH_2$ and –OH groups, as both can act as good nucleophiles. Hence, it was hypothesised that $–NH_2$ groups could have been protonated to give ammonium ions ($–NH_3^+$) to which lone pairs on the hydroxyl groups (-OH) of photosensitisers could have been ionically attracted to form ionic bonds. The $–NH_2$ group can be protonated more readily relative to –OH group, because nitrogen (N, χ =3.04) is less electronegative than oxygen (O, χ =3.44), hence this type of biased protonation could be expected. Further, the addition of triethylamine, as a non-nucleophilic base, to the photosensitiser solution would have enhanced the deprotonation of the relatively acidic phenoxy groups.

However, if the attachments were to be only through the ionic interactions, the photosensitisers should have been readily released from the surfaces in the presence of an aqueous medium like RPMI or PBS solution. If de-immobilisation occurred, the non-bonded photosensitisers would have been washed out of the channels, due to the mechanical forces from the aqueous liquid flowed through. However, the latter descriptions were not observed when water was flowed through the channels, which suggested that the immobilisation was not through ionic interactions. To elucidate the (general) mechanism for the immobilisation of APTES and photosensitisers were studied rigorously using photosensitisers of similar chemical structures but with minor variations. The conditions and the corresponding results are provided in **Table 3.1**. From the results it was concluded that, nucleophilic phenoxy groups on photosensitisers like [**6**] could have reacted with APTES to form siloxane bond, thereby immobilised.

3.5 Photosensitiser immobilisation

3.5.1 Immobilisation of porphyrin derivatives

As seen in the previous section, two different temperatures, 18 °C and 120 °C were tested for surface treatments with APTES followed by the immobilisation of the photosensitisers (**Figure 3.1**). At 120 °C, the total time for APTES treatment and photosensitiser immobilisation was about 2

hours, which was the shortest time consumed for a surface treatment process. Whereas the surface treatment carried out at 18 °C required a minimum of 7 hours. Regardless of the longer time required for APTES and photosensitiser immobilisation at 18 °C, the use of lower temperature was regarded as the most appropriate method for surface treatment, as most of the photosensitisers are stable at this temperature and the photosensitisation reactions would also be conducted at around this temperature. Moreover, the methods developed to use at room temperature do not impose limitations on the process of photosensitiser immobilisation and can be used with wide range of photosensitisers thus offering flexibility. Furthermore, the qualitative observations showed that, with the use of lower temperature (18 °C) photosensitiser coatings were more uniform on the channels relative to what was observed for the surface treatment at 120 °C (**Figure 3.15**).

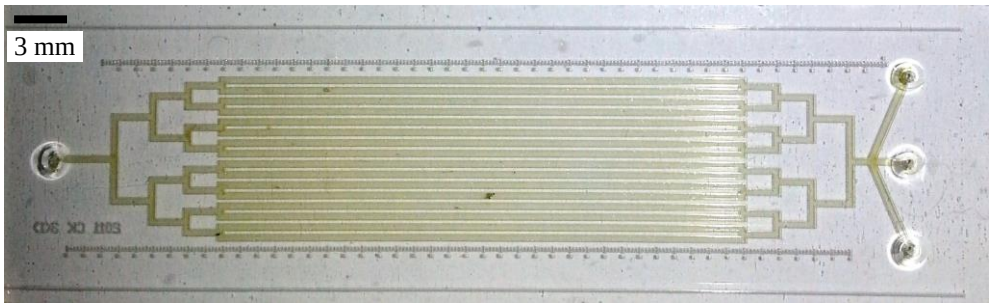

Figure 3.15: *Microfluidic chip* **Design 5** *channels coated with photosensitiser* [**4**] *at 120 °C.*

3.5.2 Immobilisation of rhodamine B isothiocyanate

Rhodamine B isothiocyanate (RBI, [**5**]) was used as a fluorophore, which was capable of producing bright fluorescence with high signal to noise ratio. However, RBI is a poor sensitiser due to its reduced efficiency of undergoing inter-system crossing (ISC) to form T_n photosensitiser, which would lead to the production of singlet oxygen.

Absorbance and emission spectra (**Figure 3.16**) of RBI dissolved in methanol were recorded using a standard UV-visible absorption spectrometer and fluorescence spectrometer, the path length of the cuvette was 1 cm. It was found that the maximum absorbance peak for RBI was in the green region (543 nm) of the visible spectrum and the maximum

emission (fluorescence) peak was in the orange region (573 nm). The microfluidic channels with immobilised photosensitiser [**5**] (**Figure 3.17(a)**) were viewed under a fluorescence microscope. The fluorescence from RBI immobilised chips were readily observable (real-time) with high signal to noise ratio under a fluorescence microscope (**Figure 3.17(b)**). The fluorescent property of RBI was consistent both in solution and when immobilised.

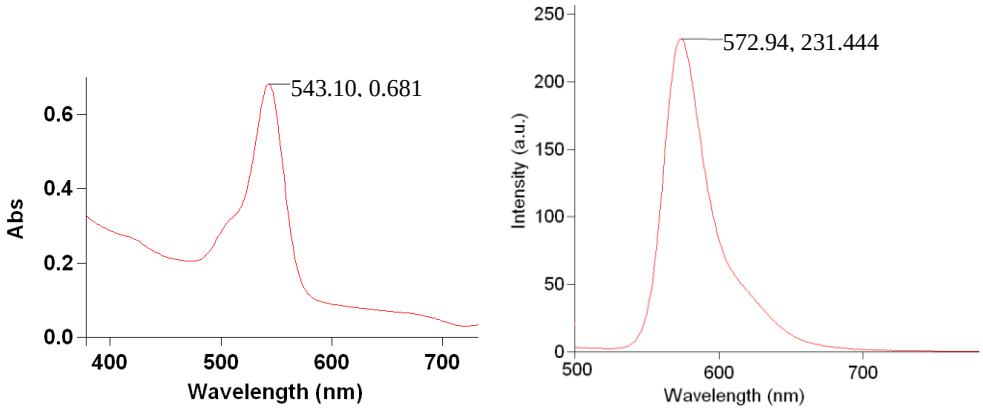

Figure 3.16: *UV-visible absorption spectrum and fluorescence spectrum of Rhodamine B Isothiocyanate dissolved in methanol, excitation wavelength 535 nm.*

The fluorescence from the immobilised photosensitiser [**5**] was brighter and sharper compared to the porphyrin derivatives, [**3**]**,** [**4**] or [**6**]**,** coated chips. The view of fluorescing microfluidic channels containing immobilised photosensitiser [**5**] is shown in **Figure 3.17(b)**. The images were acquired using 700 ms of acquisition time. The channels were filled with methanol, as pointed out below, the presence of solvent was essential for maximum fluorescence response of the immobilised photosensitiser. As the channels were not always sufficiently coloured to detect by eye, observing under microscope for fluorescence was an essential method to determine if the photosensitiser [**5**] had been immobilised.

The microfluidic channels containing immobilised RBI were filled with methanol and replaced with air, which resulted in wetting of the channel surface with methanol, while containing air bubbles in most of the other regions of the channels. When they were viewed under a fluorescence microscope only the regions of the channels covered in methanol showed

fluorescence while the regions filled with air had no fluorescence (**Figure 3.18**), the image does not represent the true colour of fluorescence. From the above observations and other similar ones, it was concluded that the surface of the channels fluoresce or fluorescence is enhanced in the presence of solvents, while dry channels or regions filled with air had little or no fluorescence. **Figure 3.19** further supports the same fact, that is, the regions covered with solvent fluoresce or show increased fluorescence, while the regions without solvent had little or no fluorescence.

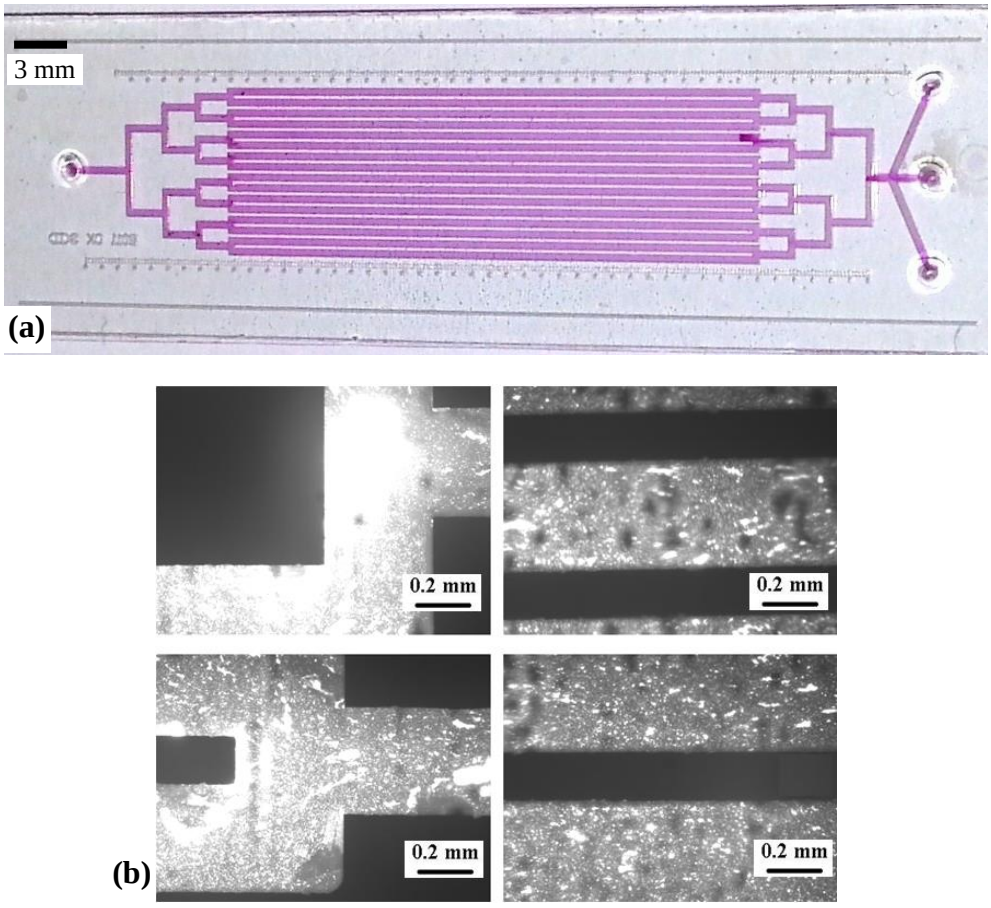

Figure 3.17: (a) *Microfluidic chip* **Design 5** *channels coated with photosensitiser* [**5**] *at 120 °C and* **(b)** *fluorescence of photosensitiser* [**5**] *coated channels, filled with methanol, 700 ms acquisition time.*

The increased fluorescence around the regions of air bubble indicated the presence of solvent near the channel surface (**Figure 3.19**). This would be possible only when the polarity of the surface and the solvents were similar. Methanol being a polar solvent preferentially covered the surface to hold the

air bubble away from the surface, which suggested that the surface was hydrophilic.

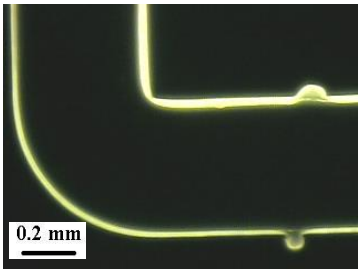

Figure 3.18: *A channel region of* **Design 5** *containing RBI immobilised at 120 °C.*

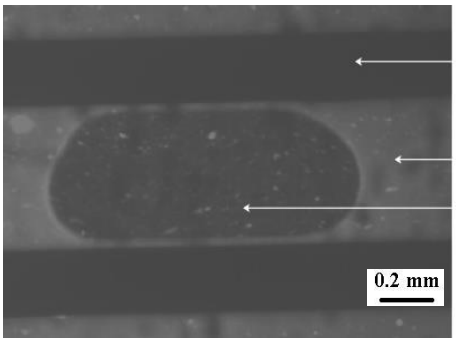

Figure 3.19: *Microfluidic chip* **Design 5** *coated with photosensitiser* [**5**] *at 20 °C. The fluorescence intensity was enhanced in methanol filled regions relative to air bubble regions.*

3.6 Measurements to verify immobilisation of photosensitisers

In order to demonstrate that the photosensitiser [**4**] was immobilised through covalent bond formation and were not just an accumulation or staining of some unknown residues within the microfluidic channels, several verification tests were carried out. The methods of confirmation included UV-visible absorption measurements, fluorescence measurements, colorimetric measurements and photochemical reactions.

The glass surfaces cleaned with piranha solution and aqueous sodium hydroxide would have cationic and anionic surfaces respectively (**Section 2.4.4** of **Chapter 2**). The first step of the surface treatment involved treating the anionic hydrophilic glass surface with APTES. The possibilities in which APTES could bind to an anionic reactive solid surface such as glass

are illustrated in **Figure 3.20**. The immobilised APTES could exist in several orientations, various structural possibilities have been reported.[324] Silanising agents carrying different numbers of alkoxy groups possess different levels of stability relating to attachments to the solid surface as follows: Molecules with three alkoxy groups are highly stable, two alkoxy groups are moderately stable and those with one alkoxy group are the least stable. Trialkoxy silanising agents show enhanced possibilities for being immobilised to the surface due to the maximum number of attachments (three points).[325] Three points of attachments per silane adds rigidity to the molecules to remain anchored to the solid surface, theoretically it would enhance the stability by 3 times relative to those with one alkoxy group. Due to the above reasons trialkoxy silanes were the only choice of silanising agents used within this project.

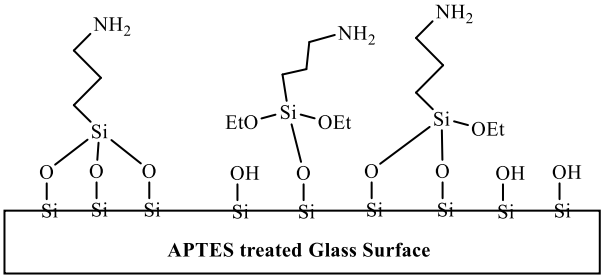

Figure 3.20: *Likely appearance of glass surface treated with 3-aminopropyltriethoxysilane (APTES), where three, two or only one of the alkoxy group could have reacted to form silicon oxide (Si-O) bond(s).*

APTES is a trialkoxy silanising agent and hence provides the highest stability once it has been immobilised. In APTES, the amino group is held only three C-C bonds away from the Si atom of the molecule, thus lowering the chances of the amino group from pointing in multiple directions and enhancing the possibilities of $–NH_2$ groups pointing perpendicular to the surface, where it was immobilised. Furthermore, its chemical reactivity with respect to surface functionalisation has been well studied with an abundance of reports in the literature.[316-318, 325]

The second step was to react isothiocyanate functional group bearing photosensitisers, [**4**] or [**5**], with the amino groups of APTES, leading to the

formation of a covalent thiourea bond as theoretically predicted. Following the immobilisation of photosensitisers [**4**] or [**5**] on to the channel surfaces, the microfluidic glass channels appeared yellow or pink in colours respectively. The pink colour of the channels due to coating with the photosensitiser [**5**] was consistent with the colours observed when the same photosensitiser was in solution or in its crystalline form. The result of yellow colour channels when treated with the photosensitiser [**4**] was in contradiction to the colours observed when the same photosensitiser was in solution (deep red colour) or in its crystal form (purple colour). Hence it was mandatory to verify that the channels contained the photosensitiser [**4**] and not some other substances. It was also essential to verify that they were held by true covalent bonds and not some form of staining on the glass surfaces. These confirmations will be addressed in the following sections. Spectroscopic methods, colorimetric methods and photochemical reactions were used to test for the presence and the covalent immobilisation of photosensitiser [**4**] within the microfluidic channels and were as follows.

3.6.1 UV-Visible measurements

UV-visible absorption spectroscopy was used to confirm the presence of immobilised porphyrin on the microfluidic glass channel surface. It was known that porphyrin derivatives have a strong absorption at around 400 nm called the Soret band. The UV-visible absorption spectrum of photosensitiser [**4**]**,** dissolved in methanol had the Soret band at the wavelength of 418 nm, which was several times stronger than the four Q bands observed at the wavelengths 514, 549, 589 and 647 nm (**Figure 3.21**).

When the UV-visible absorption spectrum of the photosensitiser [**4**] immobilised chip was measured, having methanol filled within the microfluidic channels, only one peak was detectable in the spectrum at a wavelength of 424 nm and this result was consistently reproducible (**Figure 3.22**). In the absence of solvent such as methanol, no peaks or much weaker peaks were observed, this type of behaviour is covered in **Section 3.5.2**. From the comparison of spectra obtained for the same photosensitiser when it was in its solvated form and in its immobilised state, it was deduced that

the peak observed for immobilised photosensitiser [**4**] at 424 nm must be the Soret band, and the four Q-bands were not observable in the spectra produced. It should be noted that the Q-bands for the photosensitiser were only weakly observed even when in its solvated form (**Figure 3.21**), hence in its immobilised state with the increased level of base line these peaks disappeared totally or buried below the base line. In addition to the above reasons, there were possibilities for the spectroscopic characteristics of the sensitiser to be altered. The absorption peak at 424 nm confirmed that the yellow coloured material covering the treated channel surface was the porphyrin and not some other form of contamination (**Figure 3.22**). Microfluidic channel surfaces treated with the photosensitisers [**3**] and [**6**] showed similar spectroscopic properties.

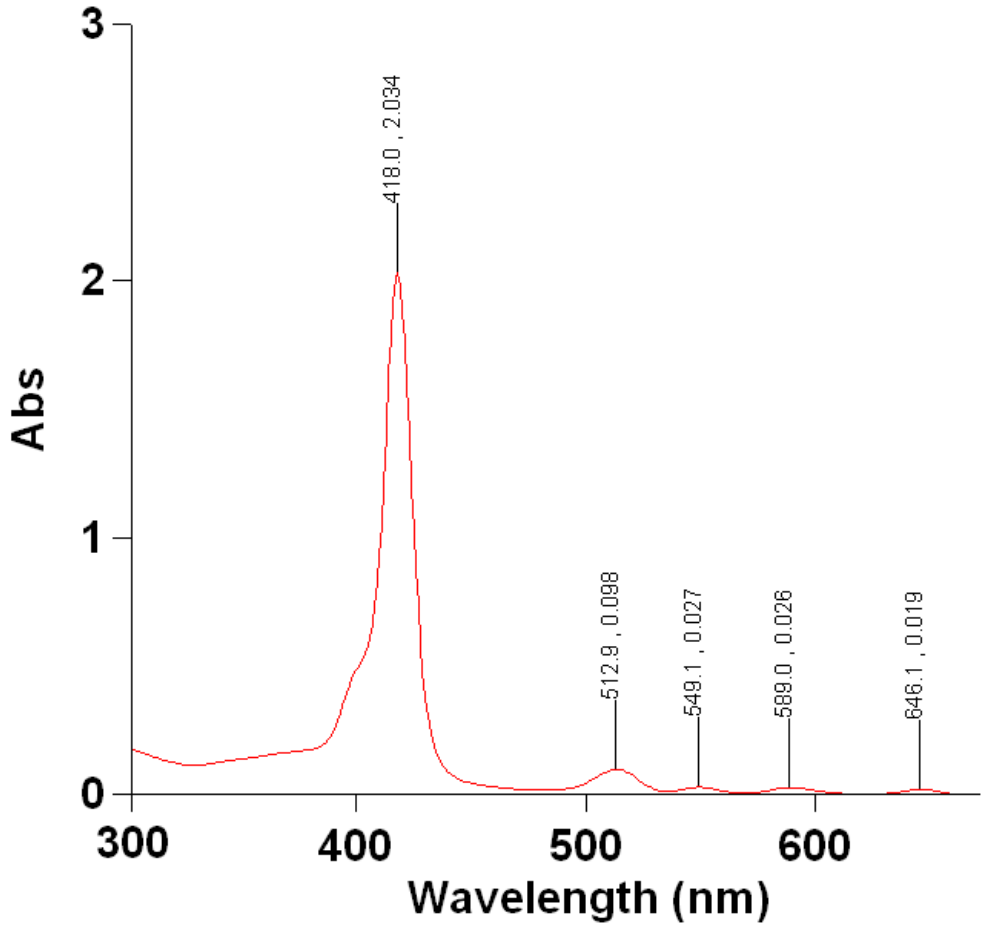

Figure 3.21: *UV-visible absorption spectrum of photosensitiser* [**4**] *hydrolysed off from the surface of immobilised microfluidic channels using aqueous sodium hydroxide*.

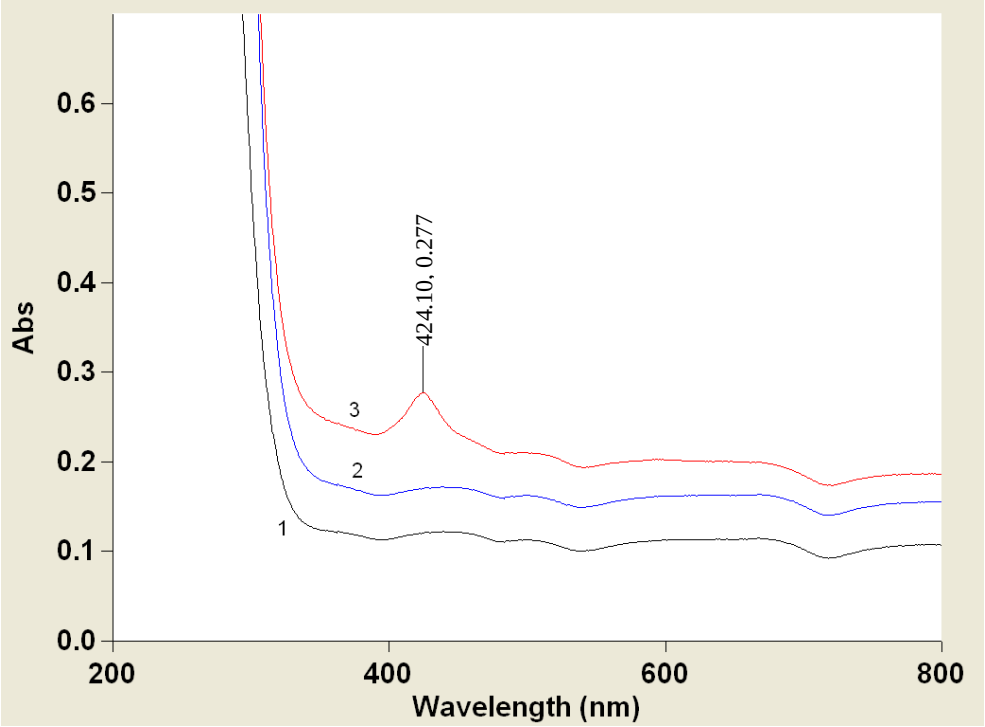

Figure 3.22: *UV-visible absorption spectra of* (1) *non-treated glass slide,* (2) *non-treated microfluidic chip* (**Design 5**) *and* (3) *APTES treatment followed by photosensitiser* [**4**] *immobilised chip* (**Design 5**).

In addition to the reproducibility and the assignment of the peak in the spectrum, four controls were used to verify that the signal at 424 nm was due to the photosensitiser [**4**] and was not an artefact of light reflections from the curvature regions of the channels to the detector. *Control 1*, non-treated glass slide was used to show that just a plain glass slide on its own would not generate any wavelength selective absorption peak(s) (**Figure 3.22**). However, the absorption was not at 0.0 a.u., but there was a constant absorption of about 0.1 to 0.2 a.u., and this was accounted for the amount of light scattered as a result of reflection and refraction processes, and was dependent on the orientation of glass placed against the cuvette holder, the measurement setup provided in **Section 2.4.5** of **Chapter 2**. The variations in the background absorptions were due to imperfections in positioning or orientating the chips or the glass slide between the light source and the detector. Further, the distance between the light source to the chip and the chip to the detector were not precisely (100 %) maintainable between different measurements.

Control 2, non-surface treated microfluidic chip **Design 5** was used as the second control to show that the patterns of the microfluidic channels would not account for any wavelength selective absorption(s) of light, other than the amount of light reflected and refracted as with non-treated glass slide (**Figure 3.22**). *Control 3*, microfluidic glass-surface treated with APTES produced similar spectral output (spectrum not shown) to that of the *controls 1* and *2*, that is, did not contain any wavelength selective absorption peaks. Comparison of the controls against the photosensitiser immobilised chip, favoured the fact that the peak at 424 nm was due to the presence of photosensitiser [**4**].

Control 4, the absorption spectrum was measured having microfluidic channels (**Design 5)** filled with photosensitiser [**4**] (1 mg) dissolved in methanol (3 ml) (**Figure 3.23**). Only three peaks at wavelengths 422, 512 and 592 nm were identifiable in the spectrum, though total of five were expected, that is, one Soret-band and four Q-bands. In addition, the spectrum obtained under these conditions had the Soret-band at 422 nm, while in the case of photosensitiser [**4**] immobilised chip the peak was at 424 nm (**Figure 3.22**). At around 330 nm, the absorption signal increased steeply above the absorption value of 1 a.u., which was the cut-off lower limit wavelength for the borosilicate glasses from which the microfluidic chips were fabricated (**Figures 3.22** and **3.23**).

Using aqueous sodium hydroxide, immobilised photosensitiser [**4**] was hydrolysed off the channel surfaces of chip **Design 5**, and the UV-Visible absorption spectrum was recorded using a 1 cm path-length cuvette. The spectrum produced was similar to the one that was obtained when the same photosensitiser [**4**] was dissolved in methanol (**Figure 3.21**). Using the spectroscopic confirmation of Soret-band signal obtained for immobilised photosensitiser [**4**], and the spectrum obtained for the same sensitiser when hydrolysed off the chip surface, together strongly suggested the presence of the photosensitiser [**4**] covalently bound within the channels.

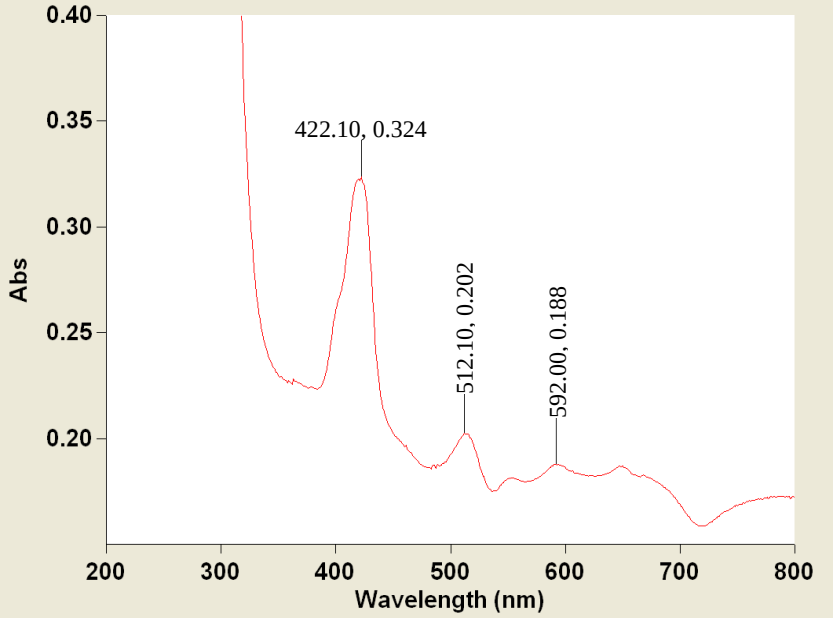

Figure 3.23: *UV-visible absorption spectrum of microfluidic chip* (**Design 5**) *filled with photosensitiser* [**4**] *dissolved in methanol.*

3.6.2 Fluorescence measurements

Using fluorescence spectroscopy, an emission spectrum of photosensitiser [**4**] dissolved in methanol was acquired with an excitation wavelength of 400 nm. The spectrum contained two peaks, one at 655 nm and the other at 719 nm, where each peak corresponded to fluorescence (S_1 – S_0) and phosphorescence (T_1 – T_0) respectively (**Figure 3.24**). When the measurement was repeated for photosensitiser [**4**] hydrolysed off the chip surface using basic condition, a spectrum similar to **Figure 3.24** was recorded, which confirmed that the photosensitiser [**4**] was once contained on the surface.

Fluorescence from photosensitiser [**4**] immobilised on the channel surfaces were measured using fluorescence microscopy and fluorescence spectroscopy. Under a fluorescence microscope, using blue light (Ex 450 - 490 nm, DM 500) as the excitation wavelength led to emission (Em > 515 nm) of green light, and excitation using green light (Ex= 510 – 560 nm, DM 565 nm) produced emission (Em > 590 nm) of red light. The fluorescence results were consistent between the measurements made for different batches of photosensitiser [**4**] immobilised chips, suggesting that the results

were not random. When the same photosensitiser [**4**] was in solution, that is, in its solvated form, excitation using blue light (Ex =450 - 490 nm, DM 500) led to emission (Em > 515 nm) of red light. This difference in observation indicated that the fluorescence behaviour of a macromolecule like porphyrins might show different spectroscopic properties between their solvated forms and when in their immobilised state.

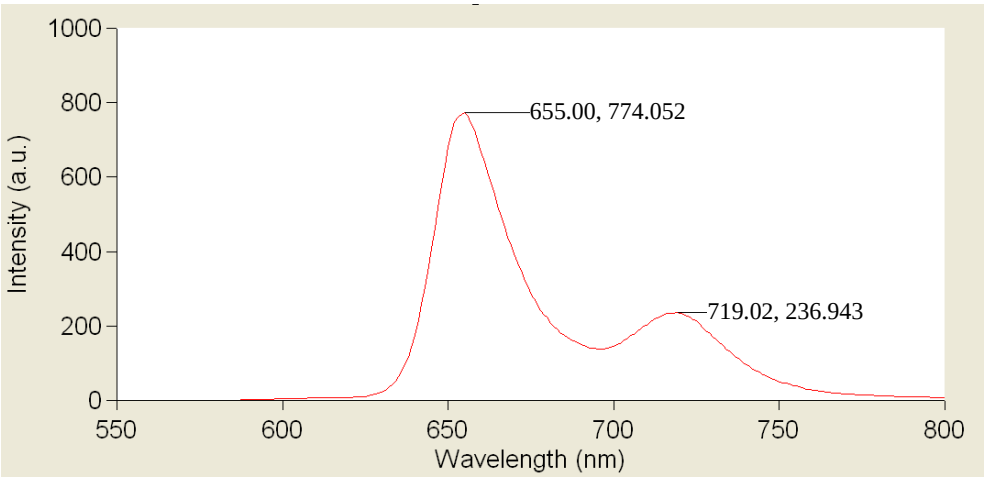

Figure 3.24: *The emission spectrum of photosensitiser* [**4**] *dissolved in methanol, with fluorescence at 655 nm and phosphorescence at 719 nm, using an excitation wavelength of 400 nm.*

It was not always possible to readily observe fluorescence and phosphorescence of immobilised photosensitiser [**4**] under fluorescence microscopy. This could have been due to insufficient number of photosensitisers immobilised per unit surface area, and also could be due to reduced quantum efficiency in their immobilised form. However, under an inverted fluorescence microscope longer acquisition times of about 3 s or higher enabled visualisation and acquisition of emission light from the channels.

Photosensitiser [**4**] immobilised microfluidic chip, filled with methanol was also measured using fluorescence spectroscopy using excitation wavelengths of 400, 418 and 281 nm, which produced the spectra shown in **Figure 3.25**. From the use non-surface treated plain chip as the control, it was known that it would not fluoresce. Hence the spectra obtained must

correspond to the photosensitiser [**4**] present on the surface of the channels. The colours corresponding to the peaks (**Figures 3.25**(**a**) to (**c**)) obtained at 527, 528 or 543 nm and at 594, 596 or 597 nm were similar to those observed under the fluorescent microscope. The main similarity for the photosensitiser [**4**] immobilised chips measurements made with the fluorescent microscope and the fluorescent spectrometer was the observation of two different colours for fluorescence, green (527, 528 or 543 nm) and red (594, 596 or 597 nm) colour lights.

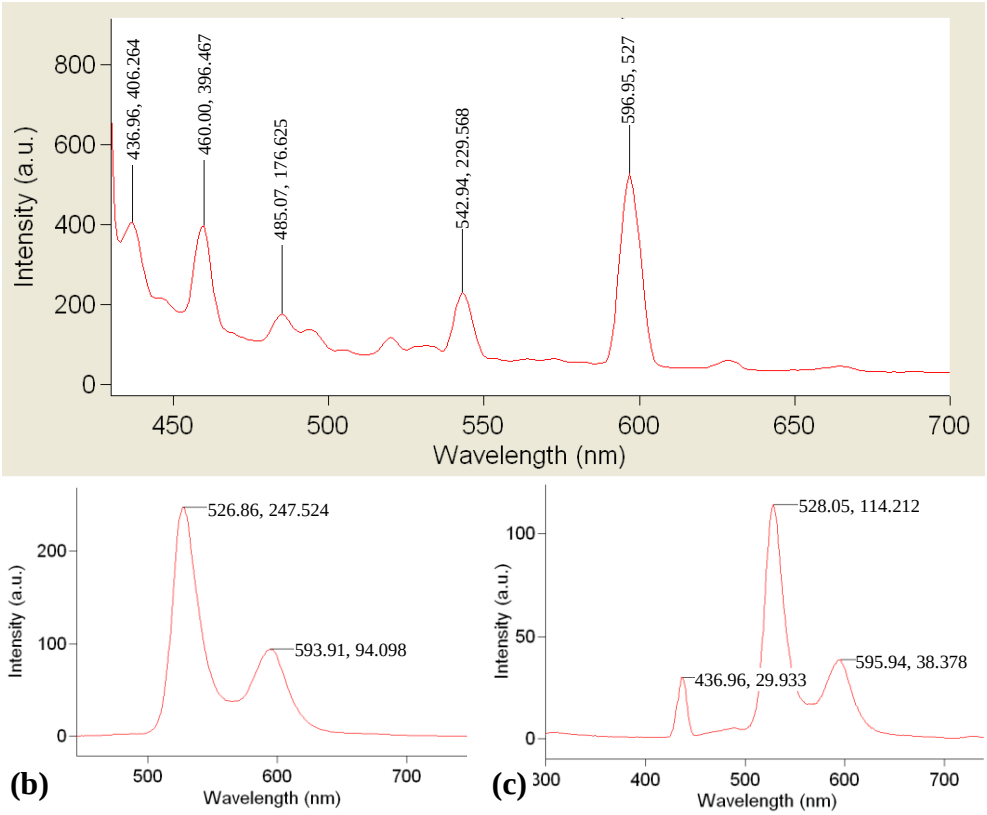

Figure 3.25: *The emission (fluorescence) spectrum of immobilised photosensitiser* [**4**], *using excitation wavelengths of* **(a)** *400 nm,* **(b)** *418 nm and* **(c)** *281 nm.*

3.6.3 Colorimetric confirmation

Porphyrin derivatives are sensitive to changes in pH (**Figure 3.26**). The changes in overall charge of the molecule under different pH conditions are also linked to their colours. Porphyrins appearing red under neutral conditions would exhibit different colours when they are in acidic or in basic medium. Depending on the strength of acidic conditions, two of the four inner nitrogen atoms protonate giving a mono-cationic or di-cationic

porphyrin core which is usually green in colour. Similarly, depending on the strength of basic conditions two of the four inner nitrogen atoms can get singly or doubly deprotonated to give mono- or di-anionic porphyrin core.

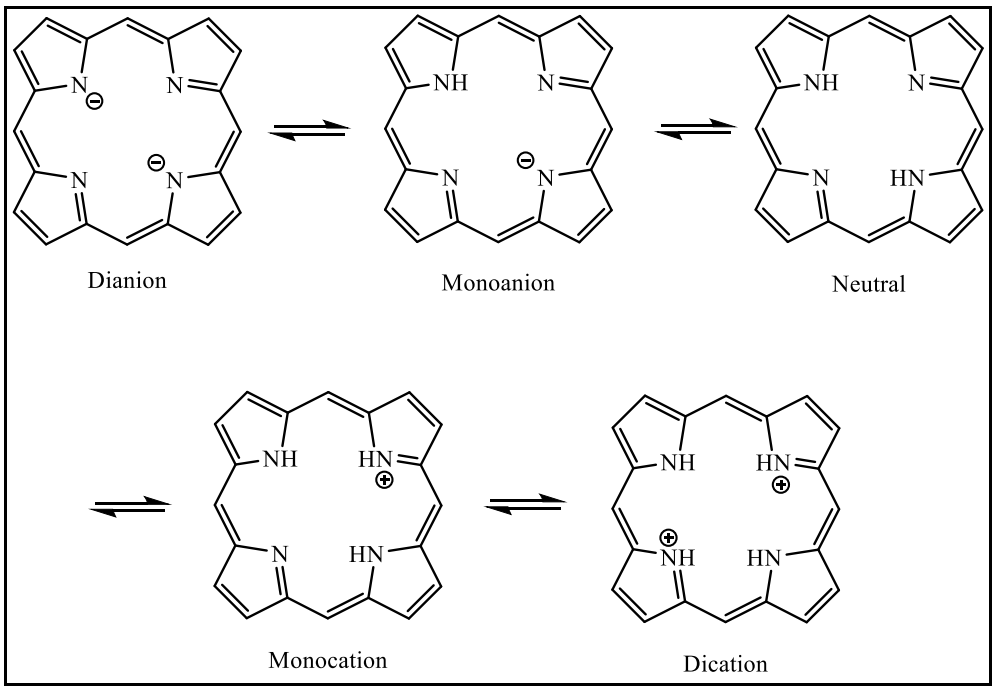

Figure 3.26: *Porphyrin under different pH conditions can give rise to five possible charge states, in the above illustration pH decreases from left to right.*

The above fact was tested by filling the channels containing immobilised photosensitiser [**4**] with 5 % concentrated sulphuric acid in ethanol. In response the colour of the channels changed readily from pale yellow to pale green. When the photosensitiser [**4**] immobilised chip (**Design 5**) was filled with 5 % concentrated sulfuric acid in ethanol and left at RTP for 10 minutes before being flushed with ethanol, at the outlets a green coloured liquid eluted. This observation suggested that the photosensitiser [**4**] had been protonated and the thiourea bonds had been hydrolysed by the acidic condition to release the photosensitiser off the surface.

3.6.4 Cholesterol oxidation

The photo-oxidation of cholesterol was also used as one of the confirmation methods to verify the presence of photosensitiser [**4**] within the microfluidic channels.[346] Initially for comparison, cholesterol oxidation reactions were

carried out under batch conditions as reported in the literature, with certain modifications and adaptations to the method.[75] A cholesterol sample was oxidised as described under the **Section 2.4.6** of **Chapter 2**. Following the oxidation reaction, the product was reduced from its unstable peroxide form to its stable alcohol derivative using $NaBH_4$ as the reducing agent. The resulting mixture was analysed using TLC and reversed-phase HPLC. Through the comparison of areas under the peaks in the chromatograms obtained, the conversion (cholesterol oxidised) was found to be 11.75 % for the batch process.

It was known that macromolecules like porphyrins can aggregate when present in higher concentrations. Aggregation could be due to incomplete solvation or poor solubility in the choice of solvents, thereby eventually leading to precipitating out of the solvent. The aggregation may also be favoured due to effects like π-stacking interactions and poor solubility in the choice of solvent(s). Thus with the use of lower concentrations such as in the micromolar range, the porphyrin derivatives would mostly exists in their monomeric form while being completely solvated.[75] Hence the porphyrins would be free of unfavourable effects such as self-quenching from formation of dimerisation or other higher forms of aggregations.

For the batch cholesterol oxidation reactions, photosensitiser [**4**] solution (1 μmol dm^{-3}) in methanol was used. In order to reduce variability in the spectroscopic properties, solubility, singlet oxygen generation efficiencies (quantum yields); the same porphyrin derivative which was used in immobilisation were used for the batch reactions. Cholesterol was recrystallised from hot methanol, to remove any auto-oxidation products that could have formed during storage, and used in the reactions.[75]

In order to assign the peaks, controls were used as follows; only methanol (HPLC grade, 20 μl) produced a chromatogram with four peaks (between 0 and 6 minutes, **Figure 3.27**). The injection of non-oxidised cholesterol dissolved in methanol (20 μl) using ultra-sonication, produced four peaks for methanol along with an additional large peak at 21.37 minutes

corresponding to the non-oxidised cholesterol. The oxidised cholesterol reaction mixture in methanol (20 µl) produced a total of 6 peaks: four for methanol, a single peak for the non-oxidised cholesterol and an additional small peak at 12.85 minutes corresponding to the oxidised cholesterol as shown in **Figure 3.27**.

Since the oxidised cholesterol being more polar than the non-oxidised (starting) cholesterol, it interacts more with the polar mobile phase and less with the non-polar stationary phase. The opposite is true for the starting cholesterol, which interacts more with the stationary phase and less with the polar mobile phase. Due to the above differences in the interactions, the one which interacts more with the stationary phase elutes at longer retention times or the one which interacts more with the mobile phase gets eluted at shorter retention times.

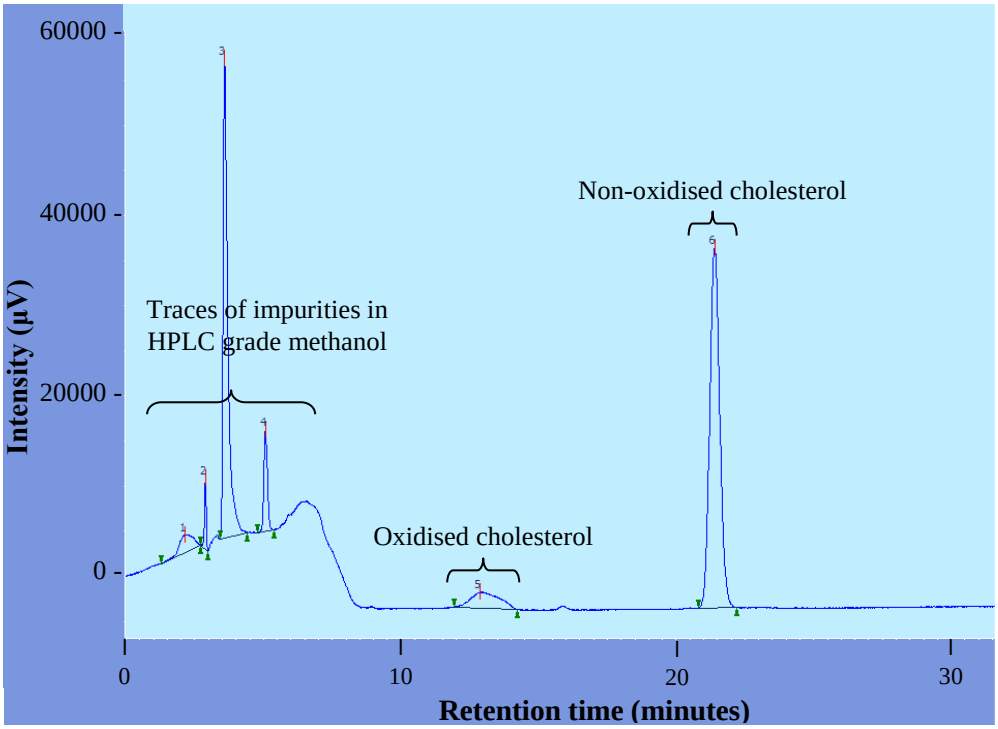

Figure 3.27: *The chromatogram obtained for cholesterol oxidised under batch conditions. The treated cholesterol samples were analysed using a reversed-phase (C_{18}) HPLC along with a polar mobile phase (methanol:acetonitrile, 3:2) and at a flow rate of 1 ml min^{-1}. Purified cholesterol (0.0387 g, recrystallised from methanol) was dissolved in dichloromethane: methanol solvent mixture (9:1, 10 ml) to give a concentration of 10 mM.*

The sum of the areas under the peaks at 12.85 and 21.37 minutes should correspond to 100 % of the cholesterol (oxidised and non-oxidised) present in 20 μl of sample injected, which was a representative portion of the reaction mixture. Hence using the areas under the peaks it was found that 11.75 % of the starting cholesterol (10 mM) was oxidised, that is, 1.18 mM of the starting cholesterol had been oxidised under the batch (off-chip) conditions.

The oxidation reaction of cholesterol was a simple method for identifying the production of singlet oxygen within the reaction setup. Hence this method was used to identify if singlet oxygen was produced within microfluidic channels (**Design 5**) containing immobilised photosensitiser [**4**]. For studying heterogeneous reactions under microfluidic environment, similar to the batch reactions, the starting cholesterol was recrystallised from hot methanol before the preparation of cholesterol solution (10 mM) in the solvent mixture (10 ml) of methanol: dichloromethane (1:9). Cholesterol solution was pumped through microfluidic channels **Design 5**, at fixed flow rates of 0.5, 1, 2.5 and 5 μl min^{-1} for varying lengths of times so that 200 μl of the sample was pumped through, that is, pumped for 400, 200, 80 and 40 minutes, respectively. The collection of 200 μl of treated sample was 10 times excess than what was required (20 μl) for the reverse-phase HPLC analysis. In general with the increase in residence time, the length of the photochemical reaction was also increased hence the total light dose delivered and the amount of oxidised cholesterol.

To the samples (200 μl) collected, excess of reducing agent, $NaBH_4$, was added to reduce the peroxides (5α-OOH) formed into a more stable alcohol product (5α-OH). The presence of organic solvents such as dichloromethane in the sample could eventually cause damages to the reversed-stationary phase HPLC column. Hence following the reduction reactions most of the initial solvents in the samples were vaporised by bubbling nitrogen gas through to ensure dichloromethane was completely removed and was then re-diluted using methanol.

For TLC analysis of the cholesterol sample oxidised under microfluidic conditions using photosensitiser [**4**] immobilised chip, the reaction mixture spots were pre-concentrated onto a normal phase TLC plate and developed twice using 1:1 of hexane: ethyl acetate. The developed TLCs were dipped into 5 % concentrated H_2SO_4 in ethanol before heating on a hot plate until the spots were visible as deep blue coloured for oxidised cholesterol and magenta coloured spots for the starting cholesterol. The presence of blue spots indicated the existence of oxidised cholesterol, TLCs developed for the starting cholesterol was used as a control for comparison. As normal phase TLCs were used, the retention factor (R_f) value of the oxidised cholesterol was higher than the non-oxidised cholesterol.

The cholesterol samples oxidised under microfluidic environment and analysed using TLCs showed presence of oxidised cholesterol. When analysed using reversed-phase HPLC, the peak corresponding to the oxidised cholesterol (5α-OH) was not detected. The inability to detect oxidised cholesterol using HPLC could be due to the low concentration of oxidised cholesterol present in the reaction mixture (200 μl) collected for analysis. While in the analysis using TLCs the spots were concentrated which could have enabled detection. The outcome was similar for all the different flow rates tested. The controlled experiments were carried out using identical conditions but in the absence of photosensitisers. The result from TLC analysis supported the fact that the microfluidic channels contained photosensitisers which was responsible for the oxidation of cholesterol.

3.7 Summary

Immobilisations of photosensitisers [**3**, **4**, **5** and **6**] were possible (related literature work have been reviewed under **Sections 1.3.4.1** and **1.3.4.2** of **Chapter 1**) and their presences within the microfluidic channels were verified using various methods; spectroscopic, colorimetric and photochemical reactions. The introduction of oxygen gas in the form of bubbles within the microfluidic channels was possible, which was utilised for conducting microfluidic photochemical reactions. The production of oxygen gas bubbles within microfluidic environment was not suitable for cell based reactions as it resulted in generation of heterogeneous environment. Hence the cells were suspended in oxygen rich media when conducting the OSR. The chip **Designs 5** and **6** were chosen as the most appropriate types for conducting the MFOSR with immobilised photosensitiser and with photosensitiser in solution, respectively.

This chapter looked at the possibility of immobilising photosensitiser onto glass surface and the possibility of using it for carrying out photosensitisation reactions. In the next chapter, photosensitiser immobilised microfluidic chips were used to study the effects of extracellular oxidative stress on cells.

CHAPTER 4 - Photosensitiser immobilised microfluidic flow oxidative stress reactions

4.1 Introduction

This chapter illustrates the possibility of using surface treated microfluidic chips or magnetic nanoparticles, as the source of extracellular oxidative stress environment generators, for conducting photosensitisation reactions on the flowing cells, that is, PDT-type reactions on cells. The first part of this chapter (**Sections 4.1-4.6**) focuses on the microfluidic flow oxidative stress reactions (MFOSR), carried out using micro-channel surfaces containing the immobilised photosensitiser [**4**]. The second part of this chapter (**Section 4.7**) discusses the hypothesis of immobilising photosensitisers onto magnetic nanoparticles and to use them for the oxidative stress reactions (OSR). The instrument setup details and the type of pumping system tested are discussed in **Chapter 2.** The results corresponding to surface treatment of microfluidic chips including photosensitiser immobilisation and verifications, and the chip designs used were discussed in **Chapter 3**.

In this study, the photosensitisers were localised on the surface of the microfluidic channels, and were not free to interact with the flowing cells as with the solvated photosensitisers, thereby internalisation was prevented. This eliminated any need for considering the amounts and the regions of the internalised photosensitisers within the cells. Hence it was hypothesised that, the method would be useful for cross-comparison of the photosensitisation effects induced by different kinds of photosensitisers on different types of cell lines, while having all other conditions unchanged. The immobilised photosensitisers may be reused, provided that they have not been extensively photobleached, which can be assessed by monitoring the changes in the colour of the photosensitiser and by running a chemical oxidation reaction.

4.2 Cells, conditions and controls used for the reactions

COLO320 was the only cell line model that was used to study the effects of extracellular oxidative stress induced PDT-type reactions. A total of three samples were used for each experiment, two controls and a testing sample. The samples were labelled as *untreated*, *photosensitiser dark-toxicity* and *photodynamically sensitised*. The cells stood in complete RPMI-1640 medium, in the dark at RTP without photosensitiser and treatments were referred to as the *untreated* sample. This was used as the complete control, that is, to act as a reference point for comparing the results from the remaining two samples. The cells flowed through photosensitiser immobilised microfluidic channels at a fixed flow rate for the same length of time as for the *photodynamically sensitised* sample, but without light were referred to as the *photosensitiser dark-toxicity* control. This control was used to account for any changes to the viability of cells, as a result of flowing through the channels containing immobilised photosensitisers. The cells flowed through photosensitiser immobilised microfluidic channels at a fixed flow rate to deliver a light dose of 3.7 J cm^{-2} were referred to as the *photodynamically sensitised* sample, which was the sample under test. Following the treatments the samples were incubated for a fixed length of time (2.5 or 24 hours) at 37 ^{o}C, 5 % CO_2 and 95 % humidity, before being analysed using flow cytometry to assess annexin-V:FITC and propidium iodide levels and determine the ratios of apoptotic and necrotic cells respectively.

The photosensitiser immobilised MFOSR were conducted using the microfluidic chip **Design 5** (page 180). The design contained 3 cm long 16-parallel channels of 300 µm width on the photomask, which was isotropically etched to a depth of 60 µm (**Figures 3.6** and **3.7**). The microfluidic channels were surface treated to attach the immobilised photosensitiser [**4**]. The cells were flowed through microfluidic chips using a peristaltic pump. The use of a peristaltic pump for flowing cells through chip improved both viability and recovery of cells relative to other methods of pumping (**Section 2.3** of **Chapter 2**). The chips were irradiated using two

LED arrays, emitting white light at the total fluence rate of 110 mW cm^{-2}. The flow rate (~21 µl min^{-1}) was set, so that, the residence time of the flowing cells were 34 s, corresponding to the light dose of 3.7 J cm^{-2}. Each set of experiments were repeated minimum of three times and the average number of healthy, apoptosis and necrosis were measured and presented along with their SD error bars.

From the initial experiments it was identified, that the number of cells decreases with time when stored longer than ~1 hour in PBS. Hence the cells were suspended in complete RPMI-1640 medium before, during and after flowing through surface treated or non-surface treated (control) microfluidic chips. The use of complete RPMI-1640 medium was not an issue for the type of OSR considered here, as the immobilised photosensitisers cannot be internalised by the cells. However, the use of complete medium in the presence of freely solvated photosensitisers could lead to enhanced internalisation, as the process is favoured in the presence of serum proteins.[352] Therefore, for the OSR considered in **Chapters 5** and **6**, RPMI free of phenol red, FBS and penicillin-streptomycin was used during the reactions, otherwise stored in complete medium.

4.3 The method used for analysing the treated cells

4.3.1 Flow cytometric analysis

One way of relating the strength of the extracellular oxidative stress induced photosensitisation effects was to measure the changes in cell viability and the associated modes of cell death, for which flow cytometry was used. Flow cytometry gives characteristic information about the cells, such as the types of proteins expressed, in a high-throughput manner with the aid of suitable fluorescent molecules. The method cannot be used for clumped cells, and the simultaneous use of several types of fluorophores could lead to spectral overlap, hence the fluorescent dyes had to be selected appropriately according to their specific emission wavelength to avoid interferences.

The data acquired from flow cytometry were viewed as 2D dot-plot graphs, on which quadrants were placed to extract statistical information about the fractions of cells in healthy-, apoptotic- and necrotic-modes (**Figure 4.1**). The flow cytometer was set to count 1 x 10^4 events, before it stopped sending acquisition data to the storage gate. The samples with less than 1 x 10^4 cells were discarded to maintain consistency within experiments and between different experiments. Hence it was essential to collect a minimum of 1 x 10^4 whole cells per sample; the collected cells may have a status of dead, unhealthy or healthy, but they all must be above the forward scatter (FSC) threshold limit that was set using the subclass controls, in order to be recognised as an event (cell). The FSC threshold level setting was essential to eliminate debris and other background noise from being measured.

In **Figure 4.1**, each axis represents a single parameter and each dot corresponds to an event. The measurements from FL1 detector appeared along the horizontal axis and the measurements from FL3 detector appeared along the vertical axis. The FITC tagged annexin-V was detected in the FL1 PMT detector (optics Ex 488 nm, Em 525 nm), while the PI dye was detected in the FL3 PMT detector (optics Ex 488 nm, Em 620 nm).

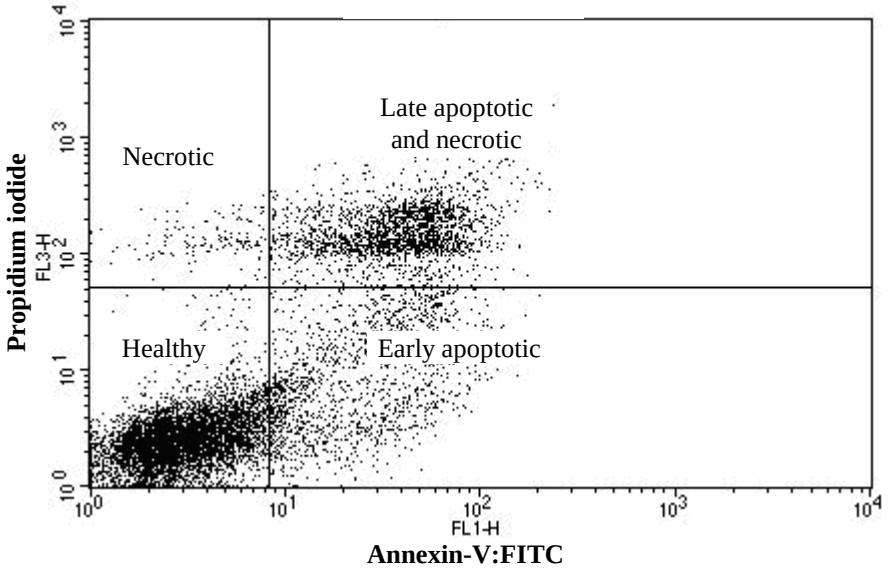

Figure 4.1: *A typical dot-plot from flow cytometry, where a quadrant was placed for distinguishing the cells in different stages of viability. The quadrant was positioned according to the dot-plots obtained for the control samples as the guide.*

The quadrants had four segments, lower left (LL), lower right (LR), upper left (UL) and upper right (UR), each belonged to the status of cells being in healthy-, early apoptotic-, necrotic-, and late apoptotic- and necrotic-modes, respectively. The quadrants were positioned using controls as the guide. The sizes of the quadrants were fixed within the same experimental conditions, and between different experiments their sizes were varied slightly according to the corresponding controls.

The samples were prepared according to the method recommended by the manufacturer (AbD SeroTec) of annexin-V:FITC assay kit (**Section 2.5.6** of **Chapter 2**). For the OSR the cell concentrations were used within the range of $0.5 – 1.5 \times 10^6$ cells ml^{-1}.

4.3.2 Identifying apoptosis and necrosis

Annexin-V protein is one of the five members of the annexin family of proteins. It selectively binds to phosphatidylserine (1,2-diacyl-sn-glycero-3-phospho-L-serine), which is a type of phospholipid found in cells of all classes of organisms.[353, 354] In mammals, phosphatidylserines are usually found attached to the inner cytosolic surface of the cell membranes. Due to its abundance and presence in diverse types of adherent and suspension cells, they can be utilised for identifying cells in their early stages of apoptosis. When severe disturbances causing events strike the cellular structure or their metabolic activities, inversion of phosphatidylserine from inner to outer membrane occurs, which is used as a sign for the early stages of apoptosis.[246, 355] The expression of phosphatidylserine on the extracellular membrane acts as a signal that causes macrophages to engulf these cells.[356] Flippases and scramblases enzymes aid in the transmembrane movement of phospholipids from inner to outer surface of the cell membranes and *vice versa*.[357]

The high binding potential of Annexin-V: protein to phosphatidylserine together with the inversion of phosphatidylserine, were utilised to discriminate apoptotic cells. In order to enable detection using flow cytometry, fluorescein isothiocyanate (FITC) attached annexin-V proteins

were used. The FITC dye was excited by the instrument using a laser wavelength of 488 nm, and the subsequent fluorescence emitted at 525 nm was detected as an event by the FL1 PMT detector.

In order to distinguish necrotic cells from apoptotic cells, propidium iodide (PI) was used as the counter stain. The dye intercalates with DNA, which is possible only when the cellular and the nuclear membranes are damaged. The dye was similarly excited by the flow cytometry using a laser wavelength of 488 nm, and the subsequent fluorescence emitted at 620 nm was detected as an event by the FL3 PMT detector. The main limitation of the assay was that it cannot distinguish the cells that have already died through the apoptotic pathway from that of necrotic pathway, because in either case the dead cells were stained with both annexin-V:FITC and PI.

4.4 Light energy

4.4.1 Light energy delivered

The residence time of cells flowed through the channels (**Design 5**) at a flow rate of 21 μl min^{-1} was 34 s. The maximum fluence rate from one LED array at a distance of 5.4 cm was 34.91 mW cm^{-2}. At the fluence rate of 34.91 mW cm^{-2}, to deliver a light dose of 3.7 J cm^{-2}, the cells had to be irradiated for 106 s. In order to achieve a residence time of 106 s using the chip **Design 5**, it was essential to use a flow rate of about 7 μl min^{-1}, but at reduced flow rates, the number of cells recovered were also decreased. To avoid reducing the flow rate, the fluence rate was increased by incorporating an identical second LED array, thereby the light dose. Having the second LED array at a distance of 3.4 cm, the combined fluence rate was increased to 110 mW cm^{-2}, at this fluence rate irradiation for 34 s delivered 3.7 J cm^{-2} light dose.

With the combined fluence rate of 110 mW cm^{-2}, irradiation for 34, 83 and 106 s delivered the light doses 3.7, 9.1 and 11.6 J cm^{-2} correspondingly. The lengths of irradiations, hence the light doses were decided based on the residence times (34, 83 and 106 s) that were achievable within the parallel

channel regions of the microfluidic chips at the flow rates as follows. The residence times of 34 and 106 s were achievable, when the cells were flowed through the chip **Design 5** of 60 µm depth and at the flow rates of 21 and 7 µl min^{-1}, respectively. The residence times of 83 and 106 s were attainable, when the cells were flowed through the chip **Design 6** (page 180) of 60 µm depth and at the flow rates of 21 and 16.3 µl min^{-1}, respectively. The above reasons formed the basis for the three selected light doses used in **Chapter 5**. For the microfluidic dimensions that were not described here, the flow rates were selected, so that, one of the three residence times, 34, 83 or 106 s was achieved.

4.4.2 Efficiency in using the light energy delivered

In conventional batch PDT reactions, monochromatic light sources are usually employed to excite the photosensitisers, in which the light energy gets used more efficiently than with polychromatic light sources. But all the absorption energy levels for a given photosensitiser would not be utilised for excitation. Conversely, the use of polychromatic (white) light sources enables excitation of photosensitisers using all or most of their absorption wavelengths, where the sensitisers would be used more efficiently, but higher proportion of the light energy would be wasted. In the oxidative stress (PDT-type) reactions considered in this thesis, white light energy was used for the excitation of the photosensitisers thereby the photosensitisers were used more efficiently. Importantly, the use of white light enabled switching between different types of sensitisers without the need for changing the light source.

4.5 Photosensitiser immobilised MFOSR

4.5.1 Using photosensitiser immobilised channels

The changes to the viability of cells and the induction of apoptotic and necrotic pathways after 2.5 hours from the treatment of cells were determined flow cytometrically using annexin-V:FITC and PI. The dot-plot results from the instrument were expressed in terms of percentages and statistically analysed (**Section 2.8**). From the assessment of data in **Figure**

4.2 and the statistical analysis for healthy-, apoptotic- and necrotic-modes, it was found that the *photodynamically sensitised* sample was not significantly different from any of the controls.

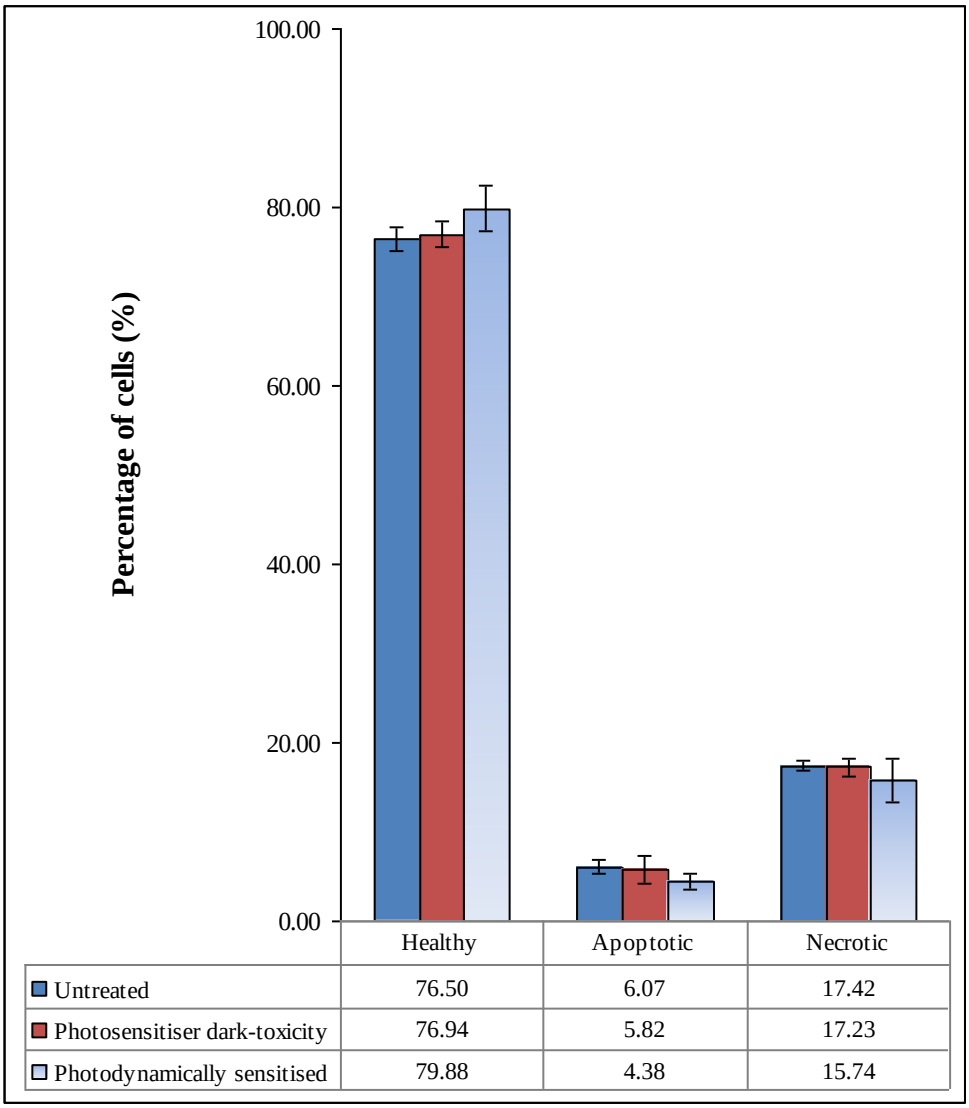

	Healthy	Apoptotic	Necrotic
Untreated	76.50	6.07	17.42
Photosensitiser dark-toxicity	76.94	5.82	17.23
Photodynamically sensitised	79.88	4.38	15.74

Figure 4.2: *The effects of MFOSR on the viability, and the induction of apoptotic and necrotic pathways, compared against two controls under the same conditions; fluence of 3.7 J cm-2 and the cells flowed through photosensitiser* [**4**] *immobilised microfluidic chip (***Design 5***, 60 µm depth) and were analysed after 2.5 hours using flow cytometry. Standard deviation errors of n=3 repeats.*

The changes to the viability of cells and the induction of apoptotic and necrotic pathways following 24 hours of incubation were determined as described for 2.5 hours. The assessment of the data in **Figure 4.3** and statistical analysis revealed that the *photodynamically sensitised* sample was not significantly different from any of the controls. However, in comparison

to the results obtained after 2.5 hours (**Figure 4.2**), in the *photodynamically sensitised* sample the number cells in healthy-mode decreased and the number of cells in apoptotic- and necrotic-modes increased, which showed presence of photosensitisation effects.

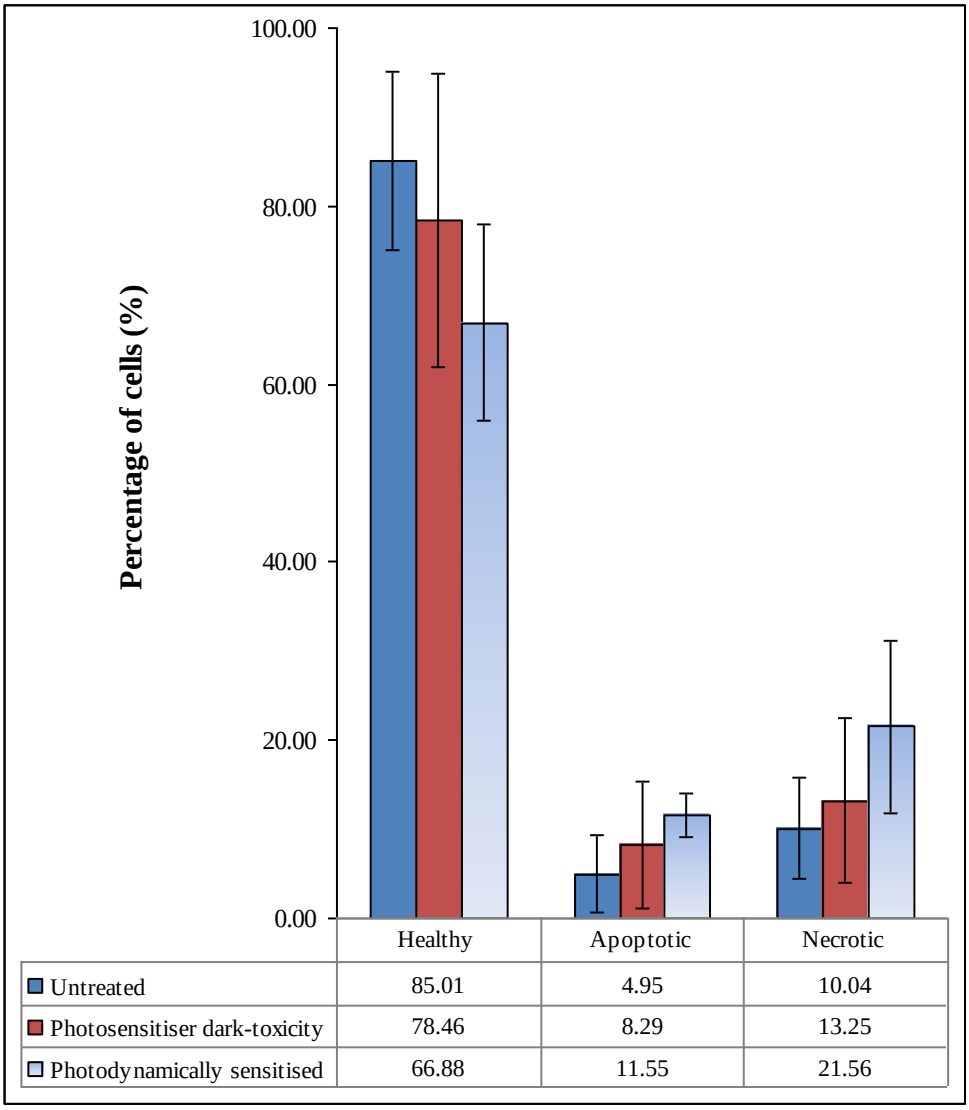

	Healthy	Apoptotic	Necrotic
Untreated	85.01	4.95	10.04
Photosensitiser dark-toxicity	78.46	8.29	13.25
Photodynamically sensitised	66.88	11.55	21.56

Figure 4.3: *The effects of MFOSR on the viability, and the induction of apoptotic and necrotic pathways, compared against two controls under the same conditions; fluence of 3.7 J cm^{-2} and the cells flowed through photosensitiser* [**4**] *immobilised microfluidic chip (***Design 5***, 60 µm depth) and were analysed after 24 hours using flow cytometry. Standard deviation errors of n=3 repeats.*

4.5.2 Using non-surface treated channels

To verify, if the decrease in the number of cells in healthy-mode and increase in the number of cells in apoptotic- and necrotic-modes, for the *photodynamically sensitised* samples analysed after 24 hours (**Figure 4.3**) were due to the photosensitisation effects and not because of incubating for longer time before analysis, control reactions were carried out (**Figure 4.4**). The *light-only toxicity* control was carried out by flowing cells through non-surface treated chips (**Design 5**), while delivering a light dose of 3.7 J cm^{-2} over 34 s. The *light-only toxicity* control was essential to confirm that the light energy on its own without photosensitisers would not induce changes in cell viability. This control would also help in distinguishing the proportion of cells affected, if present, solely by the light energy exciting the natural chromophores present within the cells. The *shear-stress effect* control was carried out by flowing cells through non-surface treated chips (**Design 5**) and without light. The *shear-stress effect* control was used to determine changes in cell viability, due to *shear-stress* force exerted on the cells flowed through the channels.

The changes to the viability of cells and the induction of apoptotic and necrotic pathways following 24 hours of incubation were determined flow cytometrically as before, and the results were statistically analysed. The assessment of the data in **Figure 4.4** and the statistical analysis revealed that there was no significant difference between the three controls. From the results it was clear that the light energy delivered and the shear-stress force exerted, were not too high to induce changes in cell viability. Hence the changes in cell viability observed for the *photodynamically sensitised* samples analysed after 24 hours (**Figure 4.3**) must be due to the photosensitisation effects induced on them.

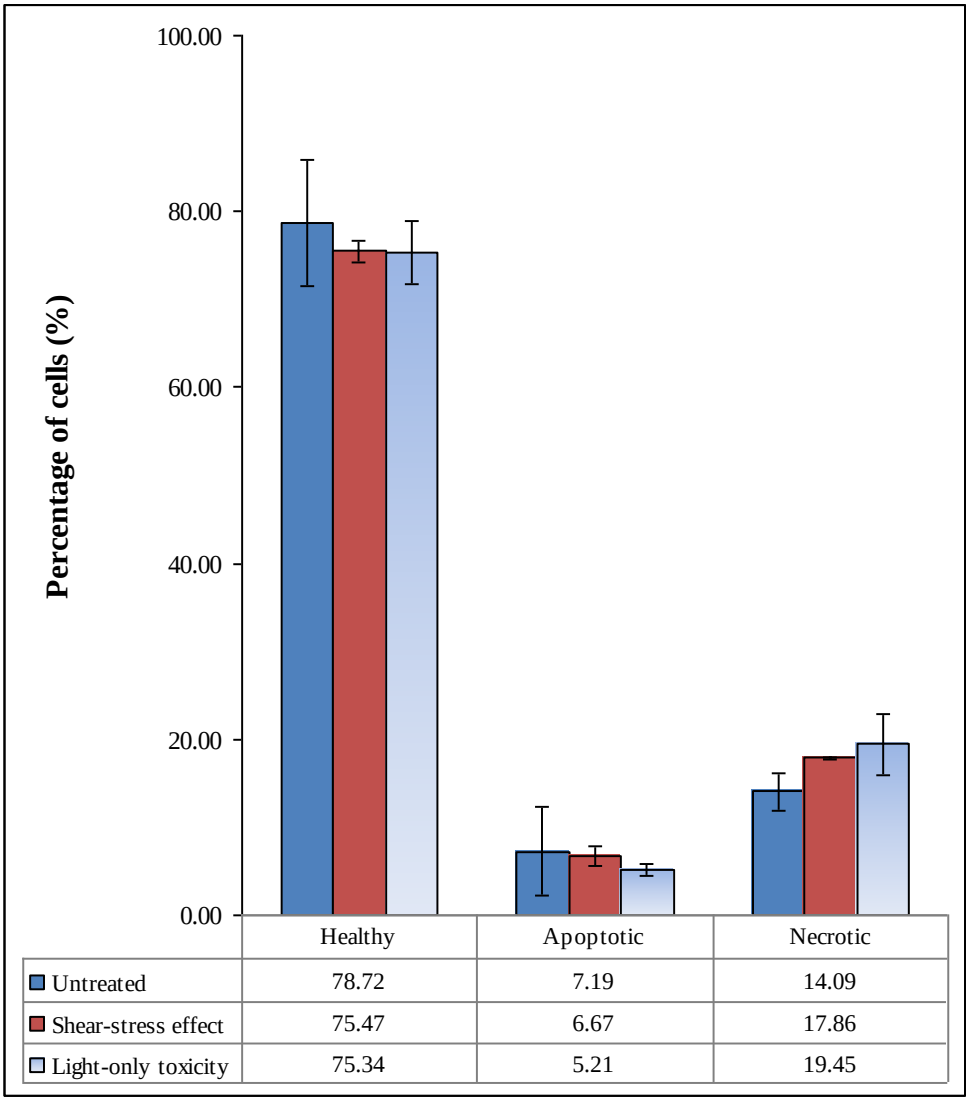

	Healthy	Apoptotic	Necrotic
Untreated	78.72	7.19	14.09
Shear-stress effect	75.47	6.67	17.86
Light-only toxicity	75.34	5.21	19.45

Figure 4.4: *The effects of flowing cells through non-surface treated microfluidic chips (***Design 5***, 60 µm depth) on the viability, and the induction of apoptotic and necrotic pathways; light dose of 3.7 J cm^{-2} and the cells were analysed after 24 hours using flow cytometry. Standard deviation error bars for n=3.*

4.6 Overall observations of the MFOSR

In the photosensitiser immobilised MFOSR, the type of photosensitiser-cell interactions were not important and the photosensitisation effects induced were only dependent on the strength of the oxidative stress environment generated by the immobilised sensitisers in the presence of light. Hence the above approach of exposing cells to extracellular oxidative stress could be adapted to use with any kind of cell lines and photosensitisers. Based on the results in **Section 4.5**, the cell viability for the controls, *untreated* and

photosensitiser dark-toxicity, were similar with no significant differences, thereby suggested no dark toxicity associated with the use of immobilised photosensitiser [**4**]. It was also observed that the *photodynamically sensitised* samples were not significantly different from the controls. This clearly indicated that one or more factors essential to achieve the threshold levels, for the OSR to induce photosensitisation effects, were limited or not provided under the above microfluidic flow conditions used for the reactions, in comparison to the conventional batch reactions.

4.6.1 Factors that limited photosensitisation effects

The numbers of cells recovered at the outlets were typically in the range of 20-70 %, which made it challenging to collect and analyse minimum of 1 x 10^4 cells per sample. The samples with lower recovery (less than 1 x 10^4 cells) were discarded to maintain consistency. The changes in cell viabilities and the number of cells collected were influenced by numerous factors. The reduction in cell recoveries were not only due to photosensitisation associated disintegrations, but were also due to the design of the experimental setup. The widths and depths of the channels were the same across all regions of the chip **Design 5**. Hence, when a single channel divided into two, both flow rates and cell concentrations were reduced by half as before. The reduction in flow speed partly contributed to sedimentation of cells. Cells settled to the surface of the channels developed hindrance to further incoming cells, thereby favoured channel blockages as observed under a light microscope. With the use of higher flow rates, sedimentation of cells reduced at the expense of increased shear-stress force and decreased residence times. In general, it was observed that the use of higher cell concentrations and lower flow rates increased the chances of channel blockages.

In addition, the cells could have also disintegrated due to shear-stress force or from excessive backpressure gradient generated by the blocked channels. In order to avoid rapid blockages and build-up of high backpressure within the microfluidic channels, cell concentrations higher than 1.5 x 10^6 cells ml^{-1} were diluted and were used within the range of 0.5 – 1.5 x 10^6 cells ml^{-1}.

From multiple experiments it was eventually elucidated that the surface roughness, the concentrations of cell suspension, the chip design, the sedimentation within microfluidic channels, the cells being blocked at the capillary connector junctions and the photosensitisation effects, all had different levels of influence on the numbers of cells recovered.

From a chemical point of view, the OSR could have also been limited due to insufficient number of the immobilised photosensitisers per unit surface area, and additionally could be due to changes in quantum efficiencies of the sensitisers, following immobilisation. Further, the use of increased flow rates to improve cell recovery reduced the residence times, as a result the cells would have eluted out of the microfluidic channels without being intensely exposed to ROS.

4.6.2 Cells in the regions of *no-slip condition*

According to the laminar parabolic flow profile (**Figure 1.20**), the velocity of a moving fluid within the channels, ducts or pipes, increases parabolically from their walls to the centre region of the flow. The cells suspended in a flowing fluid would flow at the speed same as that of the fluid. Since the cells were carried along the laminar motion of the fluid (RPMI-1640), their flow velocity patterns would also be similar to the fluid. As a result, the cells in the middle of the channels would have the maximum flow velocity, and the speed would decrease parabolically and reaches zero (minimum) near the surface of the walls, relative to the walls. Because the flow velocity near the surface would be zero, the objects carried along in this region would also come to a halt. This effect is so called the *no-slip condition*, which is a common phenomenon used in fluid dynamics to explain the flow profile of fluids within the channels, ducts or pipes.[297]

Due to the *no-slip condition*, the cells moving near the surface of the channels would have considerably reduced flow rate and could reach zero speed. The cells that were flowing close to the surface of the photosensitiser immobilised channels, and the cells that settled onto it would be affected more by the oxidative stress environment (**Section 4.6.3**), than the ones in

the middle of the channels. With time, the cells on the surface would be affected by more ROS, leading to disintegration of cells. This could also be partly responsible for the reduction in the number of whole cells collected. The disintegrated or the fragmented cells were not accounted by the flow cytometry or the trypan blue assay methods. The cells that have managed to complete the full journey through the channels mostly flowed through the middle regions of the channels, as observed under a light microscope. Hence such cells would have been exposed to significantly reduced concentrations of ROS.

4.6.3 Oxidative stress environment

Several factors influencing the success of the photosensitiser immobilised MFOSR have been considered above. One of the other factors that could have limited the success was the short half-life of $^1O_2$. As a result, the thickness of the oxidative stress environment layer formed by $^1O_2$ would be smaller and closer to the channel surface. $^1O_2$ has a half-life of about ~3.5 µs in water,[63] which is extremely small compared to ROS like H_2O_2 which has a half-life of ~8 hours[62]. The diffusion coefficient of oxygen in water at 20 ^oC is 1.97 x 10^{-5} cm^2 s^{-1}. Using the half-life time for $^1O_2$, the diffusion coefficient of oxygen in water at 20 ^oC, and the **Equations 4.1** and **4.2** corresponding to Fick's *first law of diffusion*, it was calculated that $^1O_2$ can move through a linear distance (*diffusion length*) of 203 nm, provided that it was not quenched by other components present in the medium in which it was generated. At 25 ^oC, the diffusion coefficient of oxygen in water is 2.10 x 10^{-5} cm^2 s^{-1}, consequently $^1O_2$ could have moved through an additional distance of only 7 nm. Therefore $^1O_2$ produced at a distance of about 20-30 nm away from the surface of the channels would have only travelled a distance of 203 or 210 nm. Hence the primary oxidative stress environment would have been established close to the channel surface, approximately within 1 µm from the surface.

This suggested that the distance between the sites of $^1O_2$ production and the cells flowing mostly in the centre regions of 60 µm depth channels were too far from each other for them to interact. Hence, the primary oxidative stress

environment would have not influenced the cells, flowing at least 1 µm away from the surface of the channels. However, the cells that have settled to the surface of the channels would have been affected by the primary oxidative stress environment. Other than the direct effects from singlet oxygen, the side reactions of $^1O_2$ would have generated secondary ROS like H_2O_2. For example, ascorbate generated by glutathione in RPMI-1640 medium can react with $^1O_2$ to generate H_2O_2 in 1:1 ratio.[358] H_2O_2 has a higher half-life, hence is more stable and thus capable of diffusing longer distances. The decrease in the number of cells in healthy-mode observed (**Figure 4.3**), could have been due to the influence of the secondary oxidative stress environment established by the secondary ROS like H_2O_2.

$$J = -D\frac{dc(x)}{dx} \qquad \textbf{Equation 4.1}$$

Where, J is the flux in mol m^{-2} s^{-1}, D is the intrinsic diffusion coefficient in m^2 s^{-1} and $\frac{dc(x)}{dx}$ is the concentration gradient per unit length (mol m^{-3} m^{-1}).

$$r = \sqrt{6Dt} \qquad \textbf{Equation 4.2}$$

Where, r is the diffusion length in m, D is the intrinsic diffusion coefficient in m^2 s^{-1} and t is the time in s.

4.7 Magnetic nanoparticles

The aim of this second approach was to mix cell suspension with photosensitiser immobilised nanoparticles and to flow them through a non-surface treated microfluidic chip, while irradiating. The purpose of this approach was to enable flow OSR, while having photosensitisers immobilised onto a solid support, magnetic nanoparticles. With this method the *no-slip condition* would not significantly affect the recovery of photodynamically treated cells. The main reason behind the use of magnetic nanoparticles was to enable rapid separation[341] of the treated cells from photosensitisers, with the help of an external magnet, a neodymium-iron-boron (NdFeB) magnet (1.0 x 0.5 cm disc shaped) for example.

4.7.1 Immobilisation of sensitisers onto the nanoparticles

Paramagnetic nanoparticles of less than 50 nm were used. They had cobalt (Co) transition metal as their magnetic core with two to four carbon layers (graphene-like) coatings around it, called TurboBeads®.[359] TurboBeads™-Amine with amino group (-Ph-CH_2-NH_2) on their surface were used for the attachment of photosensitisers bearing isothiocyanate or carboxylic acid groups, through the formations of thiourea or amide bonds respectively. RBI with isothiocyanate group and RB with carboxylic group, were covalently attached to the surface of the nanoparticles. Presence of immobilised photosensitisers onto the surface of TurboBeads®, were verified under a fluorescence microscope. The bright-field and the fluorescence images of nanoparticles bearing RBI on their surface are shown in **Figure 4.5**.

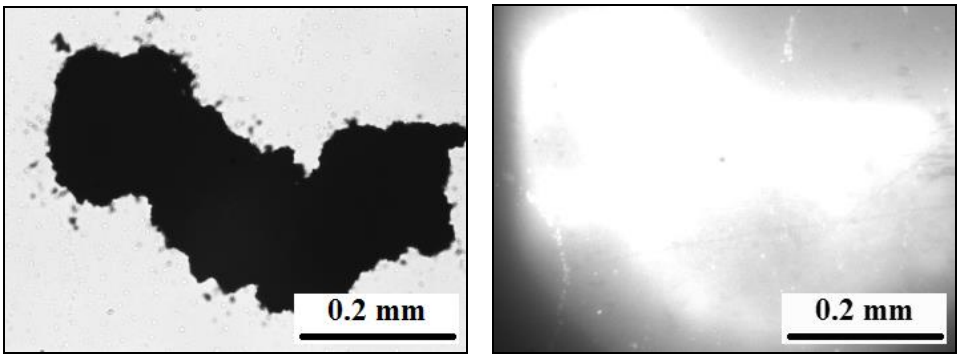

Figure 4.5: *The nanoparticles with immobilised Rhodamine B Isothiocyanate, on left bright-field image and on right viewed under the fluorescence settings, Ex= 510 – 560 nm, DM 565 nm, Em > 590 nm and acquisition time of 700 ms, n = 5.*

4.7.2 Nanoparticles flowed through microfluidic chips

Having the surface treated magnetic nanoparticles suspended in an indicator-free RPMI-1640 medium, they were flowed through non-surface treated microfluidic chips, where the chip **Design 5** and their dimensions were same as that for the first approach (**Section 4.2**). It was found that only trace amounts of nanoparticles eluted at the outlets, while most of them remained within the syringe used to hold the suspension (**Figure 4.6**) and the remaining sedimented within the microfluidic channels (**Figure 4.7**).

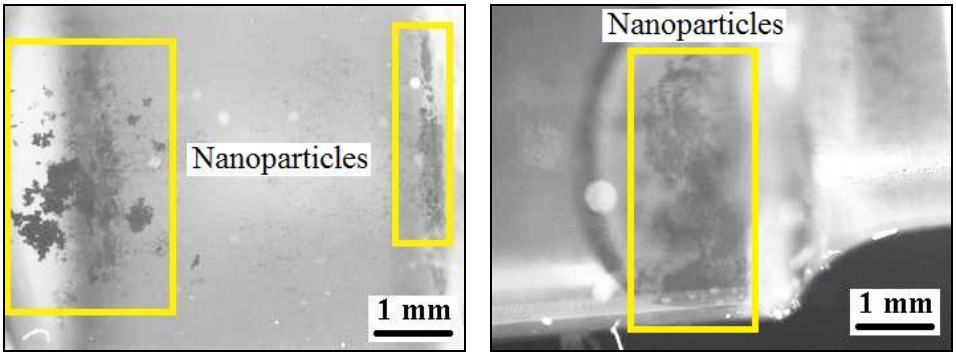

Figure 4.6: *The surface treated nanoparticles that have grouped together within syringe. On left, 3 minutes after loading into syringe and on right, a remaining drop of RPMI containing nanoparticles those have not flowed through the channels, n=3.*

In the case of magnetic nanoparticles, in addition to the force that dragged the nanoparticles along with the laminar flow of the fluid, two other external forces acted on them, gravitational and magnetic. The self-attraction (magnetic-attraction) between the TurboBeads® were much stronger, which led to the formation of larger visible lumps. The larger the sizes of the grouped nanoparticles, the heavier they were, hence sedimentation due to gravitational pull occurred at a faster rate. As a result of greater magnetic attraction, the nanoparticles could not be maintained dispersed equally in an aqueous solution for longer than few minutes (~3 minutes).

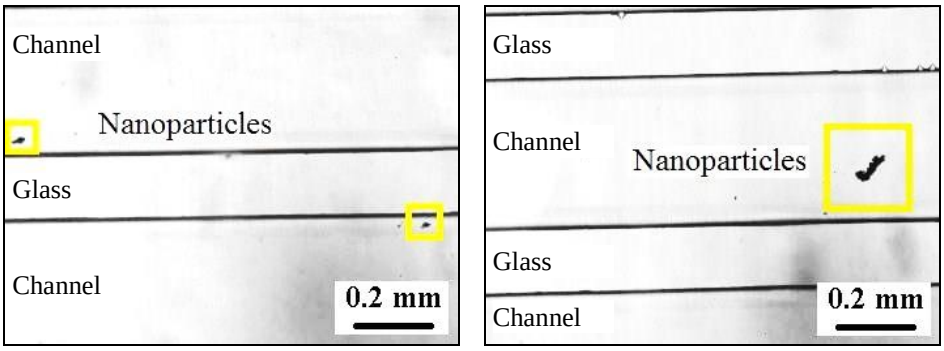

Figure 4.7: *Nanoparticles that have settled to the surface of microfluidic channels.*

The issue faced with the sedimentation of cells left in suspension, was addressed with the use of a peristaltic pump and a magnetic stirrer (**Figure 2.24**). However, the same principles could not be applied for the magnetic nanoparticles to maintain them in suspension, because they were rapidly attracted to the magnetic bar used for stirring. At the start, the magnetic

nanoparticles were dispersed by drawing the suspension into and out of the container using a syringe, before loading into it. The suspended magnetic nanoparticles within syringes, formed significant amount of gathering in 3 minutes, by the time they reached the channels much more of them grouped together and sedimented to the surface of the channels (**Figure 4.7**).

In addition to the use of syringe pump for flowing nanoparticles, peristaltic pumping was also tested without a magnetic stirrer. With the use of peristaltic pumping, the need to flow through 40 cm long peristaltic tubing was a disadvantage, where the nanoparticles grouped before reaching the microfluidic channels. Hence, the use of magnetic nanoparticles with photosensitisers onto their surface was discontinued for further part of the project. The alternative approach to the above two methods of generating extracellular ROS was to use solvated photosensitisers within the medium in which the cells were suspended. The results corresponding to this third approach is discussed in the following two **Chapters 5** and **6**.

4.8 Summary

The possibility of flowing cells through microfluidic chip and collecting enough cells for analysis (more than 10000 cells) had been demonstrated (**Section 4.5**). For the samples analysed after 24 hours, a decrease in the number of cells in healthy-mode and an increase in the number of cells in apoptotic- and necrotic-modes indicated the presence of photosensitisation effects. In this chapter the samples were analysed only using flow cytometry, the method was capable of measuring only the ratios of healthy, apoptotic and necrotic cells, and cells that were above the FSC threshold level set.

Hence, in the photosensitiser immobilised MFOSR, one or more parameters limited the success of inducing significant levels of photosensitisation effects (**Section 4.7**). Further, the amount of photosensitisers immobilised and the number of cells recovered after each reactions varied dramatically. Due to the above factors, a solid conclusion on the success of the approach of using photosensitisers immobilised microfluidic channels could not be established. To get higher controls over the constraints used for the extracellular oxidative stress PDT-type reactions, microbatch oxidative stress reactions were designed and tested (**Chapter 5**). In addition, as the flow cytometry measurements on their own were not adequate; additional methods of analysis had been introduced for measuring the photosensitisation effects (**Chapters 5** and **6**).

In the alternative approach of using photosensitiser immobilised paramagnetic nanoparticles, the sensitisers were successfully covalently immobilised through thiourea and amide bonds, and their presence were verified under a fluorescence microscope. Due to the fact that the magnetic nanoparticles cannot be dispersed homogenously or retained in suspension for longer time, the method was not suitable for conducting the types of OSR considered.

CHAPTER 5 - Microbatch oxidative stress reactions

5.1 Microbatch extracellular oxidative stress reactions

The microbatch oxidative stress reactions (MBOSR) considered within this chapter was designed to look at the effects of extracellular oxidative stress on cells. The importance of the microbatch photosensitisation reactions were to resolve if the conditions employed for the microfluidic photo-oxidation reactions in **Chapter 4**, were adequate enough to induce significant levels of photosensitisation effects, and also to establish the conditions essential for carrying out extracellular oxidative stress under microfluidic flow condition with photosensitisers in solution (**Chapter 6**). In order to determine the parameters, the MBOSR were conducted having photosensitisers in solution. To understand the overview of light, photosensitiser and cell type dependencies, combinations of three levels of light doses (3.7, 9.1 and 11.6 J cm^{-2}) and two different micromolar $AlPcS_4$ concentrations (10 and 100 µM) were tested.

It was found from the early MBOSR that higher the photosensitiser concentration in the medium around the cells, higher the rate and the amount of internalisation occurred. This led to decrease in cell viability from photosensitiser associated dark-toxicity. Though the MBOSR were initially designed to test three different concentrations of $AlPcS_4$ 10, 100 and 500 µM, due to relatively higher level of photosensitiser internalisation observed with the use of 500 µM, it was not used for further testing.

The same cell-line (COLO320), light source and photosensitiser ($AlPcS_4$) were used in all the MBOSR. The dissolved levels of oxygen in the medium were dependent on both the partial pressure of oxygen in the atmosphere and the temperature. The maximum solubility for oxygen in fresh water at room temperature (25 °C) and pressure (1 atm) is 8.9 mg dm^{-3}. Hence it can be approximated that the amount of oxygen dissolved in an indicator-free RPMI-1640 medium would be less than or equal to 8.9 mg dm^{-3}. Further, the dissolved level of oxygen was assumed to be constant and the same for each experiment.

5.1.1 MBOSR using 6-well plates

The initial MBOSR were conducted using multi-well plates (6-well plates). It was observed that, following the photosensitisation reactions all cells from the 6-well plates could not be collected for analysis, but only a fraction of them were gathered and analysed, while most of the cells remained sticking to the surface of the 6-well plates. Counting all the cells within multi-well plates were impossible, and the reduction in the number of cells as a result of being held to the surface hindered determining the absolute percentage of cells that would have disintegrated through necrosis. Hence it was essential to use a suitable container that allowed collection and transfer of all the remaining cells, and their supernatants separately, for which standard 1.5 ml polypropylene tubes were used.

5.1.2 MBOSR using polypropylene tubes

The MBOSR were carried out (**Section 2.6.3** of **Chapter 2**) using standard 1.5 ml polypropylene tubes, while having cells suspended in indicator-free RPMI-1640 medium containing dissolved $AlPcS_4$ (10 or 100 µM). The cell suspension contained within 1.5 ml polypropylene tubes could be considered as immobile cells loaded into a microfluidic chamber for testing. Immediately after the oxidative stress reactions (OSR) it was mandatory to isolate the cells from the medium containing photosensitiser to prevent or reduce occurrence of photosensitiser internalisation. To achieve this, cells were repeatedly (3 times) washed (**Section 2.6.5** of **Chapter 2**) using an indicator-free RPMI until the solution appeared clear and replaced with complete medium.

5.2 Importance of the MBOSR

The MBOSR discussed in this chapter were essential for three important reasons. Firstly it was vital to validate that the instrument (light source) developed can emit sufficient amount of light energy for conducting extracellular PDT-type MFOSR or MBOSR. The results obtained from the MBOSR demonstrated that the LED light setup developed could deliver sufficient amount of light energy to induce photosensitisation effects. The

amount of light dose delivered was controllable either by changing the length of exposure time or by varying the distance between the LED arrays and the samples. For the MBOSR considered within this chapter (**Table 5.1**), the light doses were controlled only by varying the length of exposure, while maintaining the distances to the two LED arrays constant.

Secondly, it was essential to establish that the techniques used for analysing the treated samples were of the appropriate choices. The treated cells were analysed to determine the changes in cell viability (apoptosis and necrosis), the fraction of cells recovered and the fraction of cells underwent necrosis (**Section 2.6.1** of **Chapter 2**). The results of above types were considered to be important for identifying the fraction of cells recovered and their viability status, thereby to study the effects of oxidative stress responses. Thirdly, the results obtained for the MBOSR were essential for comparison against the results obtained under the microfluidic flow oxidative stress reactions (MFOSR) conditions. The comparison enabled differentiating the reactions that were limited by the photosensitisation conditions applied, from the ones that failed to work. The best set of conditions determined from the MBOSR were utilised for conducting MFOSR and the corresponding results are discussed in the following chapter.

Table 5.1: *The twelve possible combinations of microbatch experiment conditions, those were identified as essential to determine the best set of conditions for use in MFOSR.*

Fluence (J cm^{-2})	**Concentration (μM)**	**Time (hours)**
3.7	10	2.5
3.7	10	24.0
3.7	100	2.5
3.7	100	24.0
9.1	10	2.5
9.1	10	24.0
9.1	100	2.5
9.1	100	24.0
11.6	10	2.5
11.6	10	24.0
11.6	100	2.5
11.6	100	24.0

5.2.1 The conditions and the controls used for the reactions

For the MBOSR, a total of four samples were used, three controls and a treatment sample. The four samples were labelled as *untreated*, *photosensitiser dark-toxicity*, *photodynamically sensitised* and *light-only toxicity*. The cells stood in the dark at room temperature (~20ºC) without photosensitiser and treatment was referred to as the *untreated* sample. This was used as the complete control and was used as a reference point to determine the *percentage recovery* of cells in the other three samples. The cells mixed with $AlPcS_4$ containing medium and left at room temperature in the dark for the same length of time as for the *photodynamically sensitised* sample was referred to as the *photosensitiser dark-toxicity* control. This control was used to account for any changes in the numbers of cells or their viability as a result of being in contact with $AlPcS_4$. The cells mixed with $AlPcS_4$ containing medium and exposed to a known level of light dose at room temperature were called the oxidative stress-treated (*photodynamically sensitised)* sample, which was the sample under test. The cells exposed to the same level of light dose as that for the *photodynamically sensitised* sample, but without $AlPcS_4$ in the medium was referred to as the *light-only toxicity* control, which was used to show that the light energy on its own do not induce changes in cell viability.

For the MBOSR, $AlPcS_4$ of concentrations 10 or 100 µM dissolved in an indicator-free RPMI-1640 medium were used. The samples were irradiated using two white light emitting LED arrays, delivering total light doses of 3.7, 9.1 or 11.6 J cm^{-2}, corresponding to the irradiation times 34, 83 and 106 s (**Section 4.4** of **Chapter 4**) at a fluence rate of 110 mW cm^{-2}. The treated cells were incubated for 2.5 or 24 hours, at 37 ºC, 5 % CO_2 and 95 % humidity, before being analysed using haemocytometer coupled with trypan blue assay, to determine percentage recoveries and their cell viabilities (**Section 2.5.3** of **Chapter 2**). The levels of LDH present in the supernatants were also measured to qualitatively estimate the fraction of cells lysed through necrotic pathway (**Section 2.6.5** of **Chapter 2**).[255-260] The ratio of cells in healthy- apoptotic- and necrotic-modes were measured using flow

cytometry coupled with the indicators annexin-V:FITC and propidium iodide (**Section 2.5.6** of **Chapter 2**).

5.3 LDH assay standardisation

To enable direct comparison of results from the MBOSR against the MFOSR, it was essential to calibrate the maximum levels of LDH released against the number of cells lysed (**Section 2.6.4** of **Chapter 2**). For a given cell concentration, two levels of LDH were measurable; spontaneous or naturally releasable level referred to as the *low control* (*LC*), and the total level of LDH that could be released as a result of lysing all the cells to release their cytosolic contents, referred to as the *high control* (*HC*).

For calibration both *HC* and *LC* cells were suspended in RPMI-1640 medium containing phenol red indicator and FBS (1 % v/v). The surfactant Triton X-100 was used for lysing the cells in the *HCs*. Both *HC* and *LC* were incubated at 37 ºC, 5 % CO_2 and 95 % humidity for 2.5 hours, before the absorbance was measured using ELISA reader (BIO-TEK®, Synergy HT). Four different assay development times, 10, 20, 30 and 40 minutes, were tested. For accuracy, reproducibility and to determine the limits of reliability, the assays were performed in triplicates in a 96-well plate.

The levels of LDH released and the numbers of cells were positively correlated for *LC* and *HC*. It was found that 30 and 40 minutes of assay development times had similar net absorbance differences between *LC* and *HC*, and were also higher than after 10 and 20 minutes intervals. Hence 30 minutes was sufficient enough, to clearly distinguish between the populations of *LC* and *HC* samples (**Figure 5.1**). The calibration plots in **Figures 5.1** shows that, above the cell concentration of 25000 cells in 50 µl, a saturation point is reached. Hence the dynamic (sensitive) range was found to be only between 1000 to 25000 cells in 50 µl, that is, the lowest and the highest concentration of LDH from the lysed cells were measurable only within the cell concentration range of 0.02 and 0.5 x 10^6 cells ml^{-1} (**Figure 5.2**).

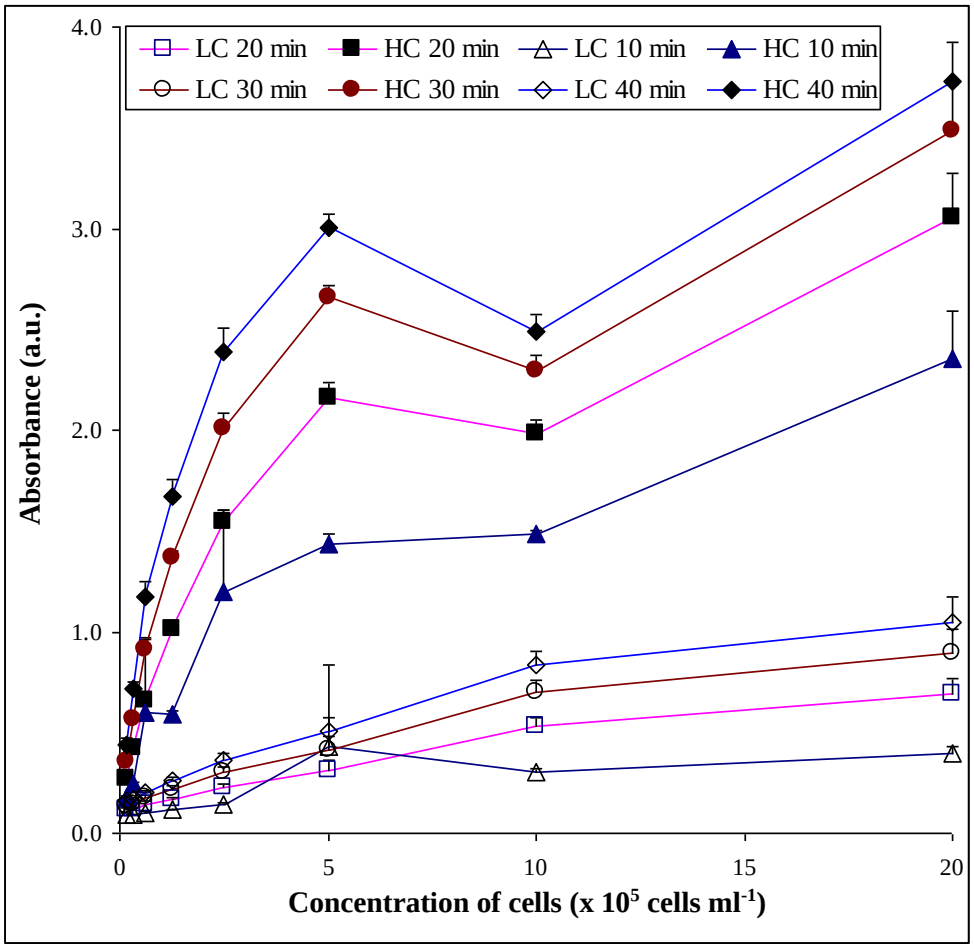

Figure 5.1: *The calibration curves of correlation between LDH levels (absorbance) against concentration of cells, showing the correlation for low controls (LCs, naturally released level in cell culture) and high controls (HCs, when all cells lysed), both measured after four fixed intervals of 10 minutes.*

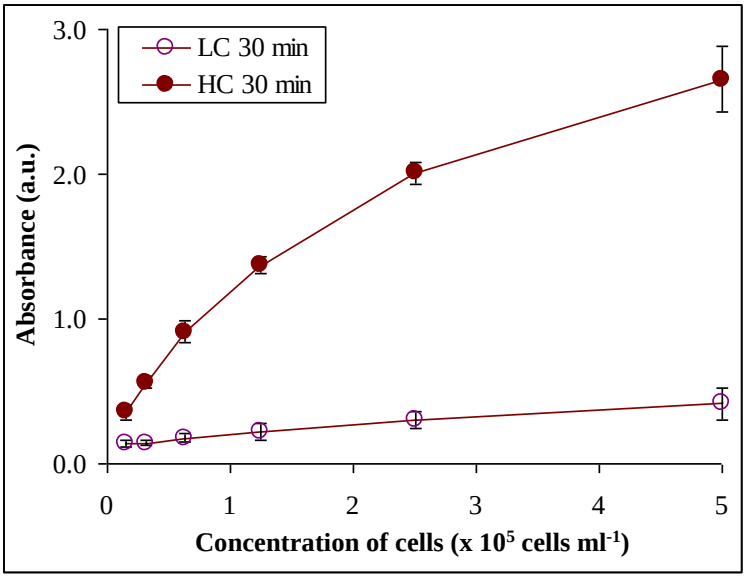

Figure 5.2: *The calibration curves of correlation between LDH levels against concentration of cells, showing the dynamic correlation range expansion for 30 minutes of assay development time.*

5.4 Conditions: Light dose of 3.7 J cm^{-2} and $AlPcS_4$ of 10 μM

The following results correspond to the experimental conditions that utilised $AlPcS_4$ of 10 μM, which was dissolved in an indicator-free RPMI-1640 medium (**Section 2.6.1** of **Chapter 2**), and the samples were irradiated using white light dose of 3.7 J cm^{-2} at a fluence rate of 110 mW cm^{-2}. The samples were analysed using flow cytometry, trypan blue and LDH assays after 2.5 and 24 hours.

The changes to the recovery of cells after 2.5 hours of incubation were determined in terms of percentages (**Figure 5.3**), and the statistical analysis showed no significant difference from any of the controls. Therefore following the OSR, the cells were not highly induced to undergo necrosis or fragmentation, the conclusion was also supported by the LDH assay (**Figure 5.5**) and the flow cytometry results (**Figure 5.6**).

The samples were also measured and analysed after 24 hours. From the assessment of the data in **Figure 5.3**, it was found that the number of cells recovered for the *photodynamically sensitised* samples were relatively lower than in all the controls, and it was only significantly different from the *light-only toxicity* control. The reduction in cell number indicated that following the OSR the cells were induced to undergo necrosis or fragmentation, this conclusion was also supported by the corresponding LDH assay (**Figure 5.5**) and the flow cytometry results (**Figure 5.7**). The strength of the conditions to induce photosensitisation effects was the lowest among the 12 combinations (**Table 5.1**), hence the effects observed were also minimum (**Figures 5.3-5.7**).

The changes to the viability of cells after 2.5 and 24 hours of incubation were determined in terms of percentages (**Figure 5.4**) using trypan blue assay. The statistical analysis showed no significant difference at both time intervals.

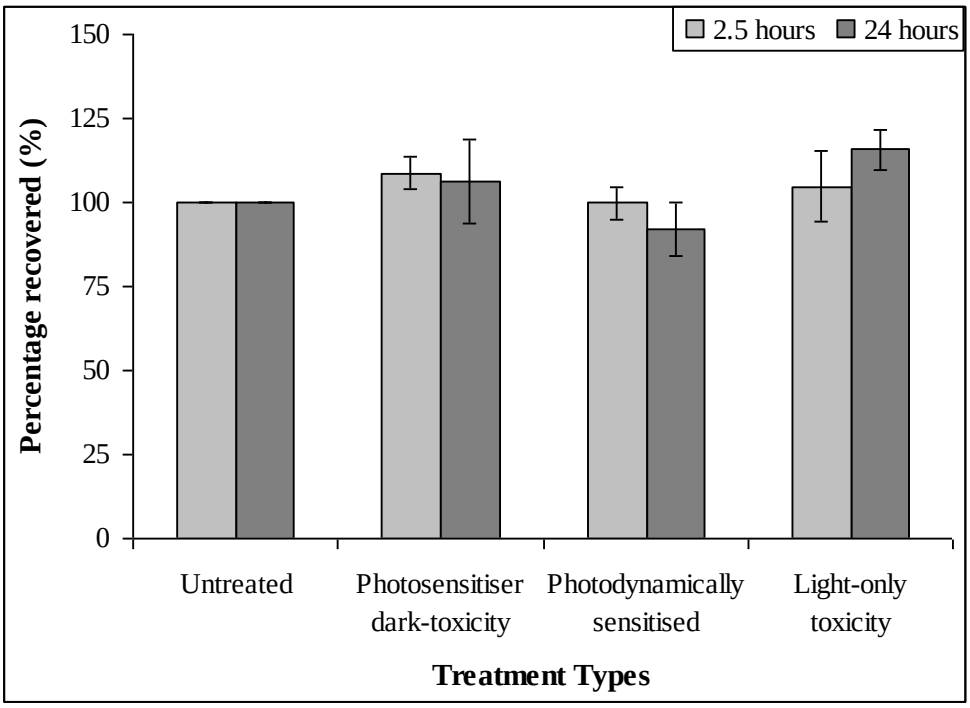

Figure 5.3: *The effects of MBOSR on the total recovery of cells, compared against three controls under the same conditions; 10 μM of $AlPcS_4$, fluence of 3.7 J cm^{-2} and the cells were analysed using haemocytometer after 2.5 and 24 hours. Standard deviation error bars for n=3.*

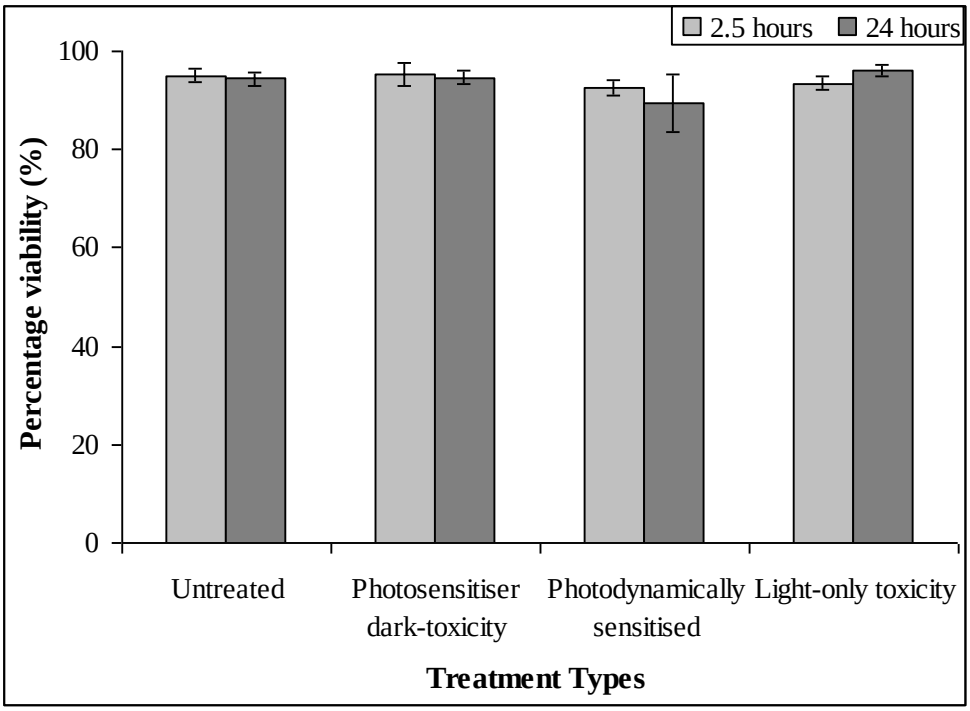

Figure 5.4: *The effects of MBOSR on the total viability of cells, compared against three controls under the same conditions; 10 μM of $AlPcS_4$, fluence of 3.7 J cm^{-2} and the cells were analysed using trypan blue and haemocytometer after 2.5 and 24 hours of incubation. Standard deviation error bars for n=3.*

The levels of LDH released immediately or soon (0 hour) after the OSR was measured, and the statistical analysis showed presence of significant difference ($p < 0.0001$). The assessment of the data for 0 hour in **Figure 5.5** suggested that, the level of LDH released for the samples *photosensitiser dark-toxicity* and *photodynamically sensitised* were similar and relatively lower than in the other two controls. The lower levels of LDH indicated lower number of lysed cells, which was not a reasonable observation, hence the following was proposed. The reduction in the strength of absorbance signals (levels of LDH) could be due to fluorescence of $AlPcS_4$ present in the supernatant, thereby it would have appeared as though the strength of the absorbance had decreased.

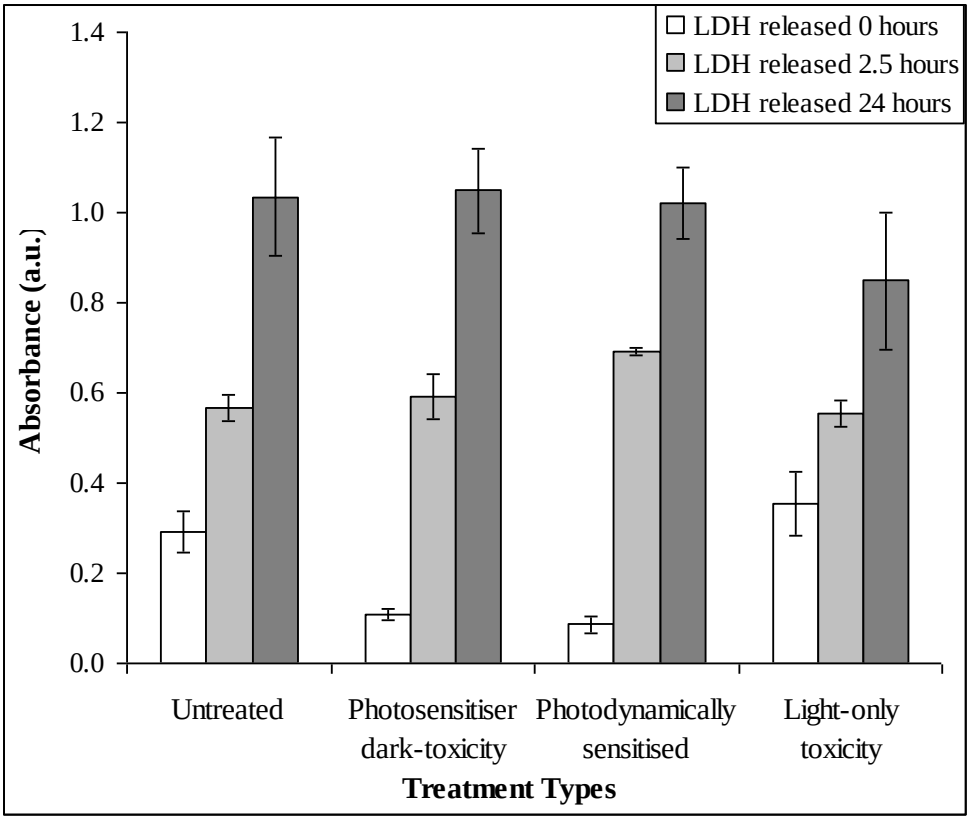

Figure 5.5: *The effects of MBOSR on the levels of LDH released soon after OSR and during 2.5 and 24 hours of incubations, compared against three controls under the same conditions; 10 μM of $AlPcS_4$ and fluence of 3.7 J cm^{-2}. Standard deviation error bars for n=3.*

The levels of LDH released during 2.5 hours of incubation showed significant difference ($p = 3 \times 10^{-3}$). The assessment of the data in **Figure 5.5** showed that the number of cells disintegrated to release their cytosolic

LDH was higher in the *photodynamically sensitised* samples than in the controls. Therefore following the OSR, the numbers of cells maintaining their cytosolic contents intact were significantly reduced, as most of the cells were induced to choose necrotic-pathway or fragmentation as supported by the flow cytometry results (**Figure 5.6**) and the *percentage recovery* measurements (**Figure 5.3**). The levels of LDH released following 24 hours of incubation showed no significant difference and the numbers of fragmented cells were similar in all the samples.

The flow cytometry measurements were targeted only at measuring the proportions of cells in healthy-, apoptotic- and necrotic-modes. It measured only the first 10000 cells from a sample and did not always represent the true nature of the entire sample. Further, only the cells above the FSC threshold limit were measured and the fragmented cells were not detected. Hence the flow cytometry measurements alone could not be used for the conclusions. The measurement principles of flow cytometry analysis and the logics behind identifying the apoptotic and necrotic cells from that of healthy cells, while excluding debris, had been discussed under **Section 4.3** of **Chapter 4**.

The changes to the viability of cells and the induction of apoptotic and necrotic pathways after 2.5 hours from the reactions were determined flow cytometrically using annexin-V:FITC and PI. The dot-plot results from the instrument were expressed in terms of percentages (**Figure 5.6**), and the statistical analysis (**Section 2.8 of Chapter 2**) showed no significant difference from all the controls. The changes to the viability of cells, and the induction of apoptotic and necrotic pathways following 24 hours of incubation, was also measured and expressed as described above (**Figure 5.7**), the statistical analysis showed no significant difference from all the controls.

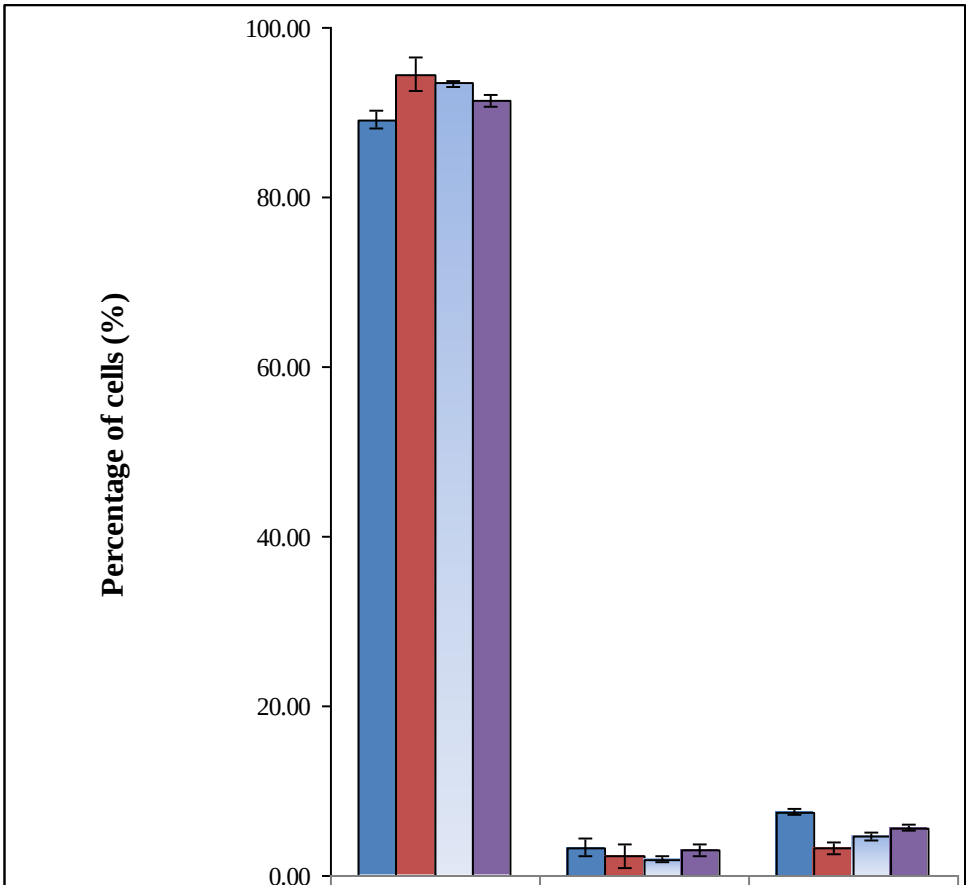

	Healthy	Apoptotic	Necrotic
Untreated	89.18	3.32	7.50
Photosensitiser dark-toxicity	94.48	2.31	3.21
Photodynamically sensitised	93.47	1.96	4.57
Light-only toxicity	91.30	3.02	5.67

Figure 5.6: *The effects of MBOSR on the viability and the induction of apoptotic and necrotic pathways, compared against three controls under the same conditions; 10 μM of $AlPcS_4$, fluence of 3.7 J cm^{-2} and the cells were analysed using flow cytometry after 2.5 hours. Standard deviation error bars for n=3.*

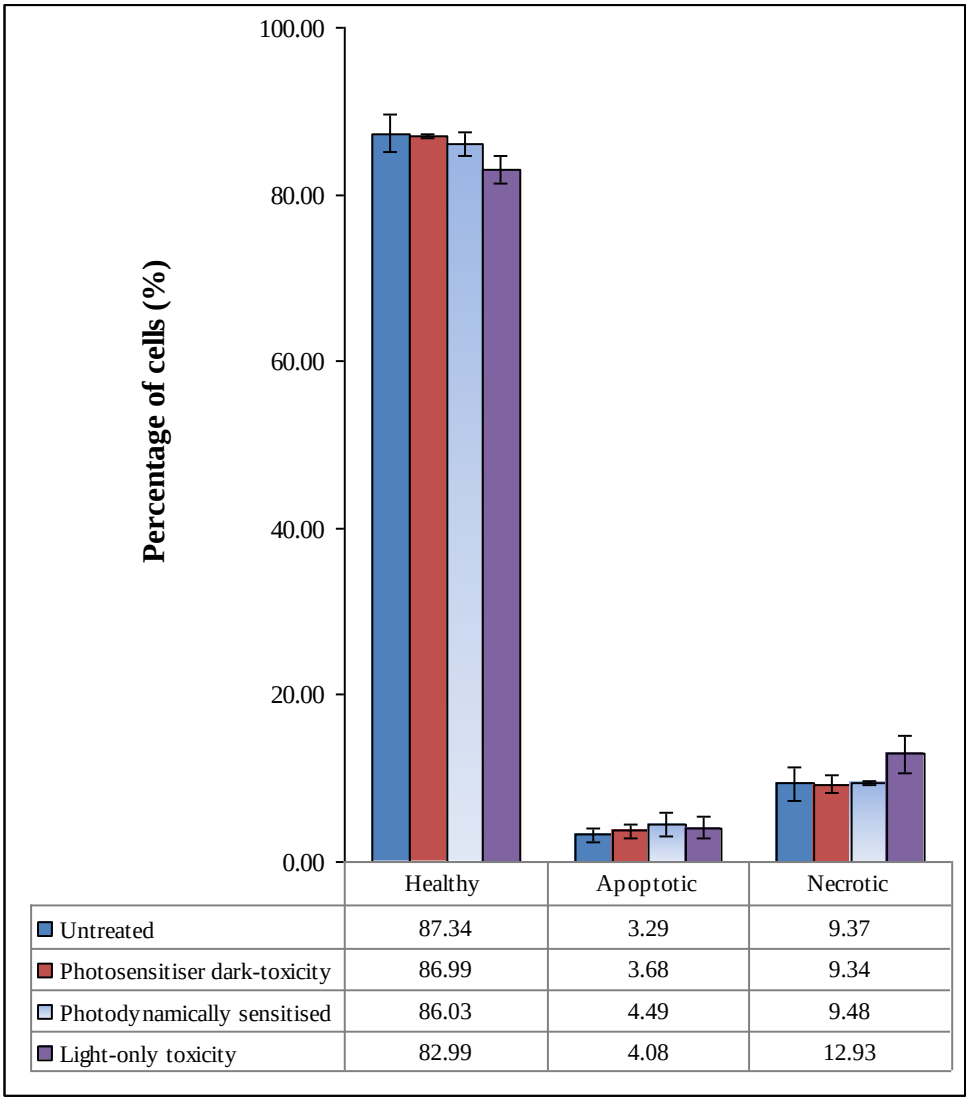

	Healthy	Apoptotic	Necrotic
Untreated	87.34	3.29	9.37
Photosensitiser dark-toxicity	86.99	3.68	9.34
Photodynamically sensitised	86.03	4.49	9.48
Light-only toxicity	82.99	4.08	12.93

Figure 5.7: *The effects of MBOSR on the viability and the induction of apoptotic and necrotic pathways, compared against three controls under the same conditions; 10 μM of $AlPcS_4$, fluence of 3.7 J cm^{-2} and the cells were analysed using flow cytometry after 24 hours. Standard deviation error bars for n=3.*

From all the results (**Figures 5.3** to **5.7**) given under this section, it was clear that one or more parameters were limiting the success of inducing photosensitisation effects, under the conditions of using $AlPcS_4$ of 10 μM together with the light dose of 3.7 J cm^{-2}. Therefore the concentration of $AlPcS_4$ was increased to 100 μM, while maintaining all other parameters constant, the following section discusses their results.

5.5 Conditions: Light dose of 3.7 J cm^{-2} and $AlPcS_4$ of 100 μM

The samples treated under the conditions, a light dose of 3.7 J cm^{-2} and $AlPcS_4$ of 100 μM were measured after 2.5 and 24 hours of incubations, using various methods as in the above section. The changes to the number of cells recovered (**Figure 5.8**) was measured using haemocytometer. The assessment of the data and the statistical analysis showed, the number of cells in the *photodynamically sensitised* samples decreased relative to all the controls, and the changes were significantly different at both time intervals, 2.5 (p = 0.005) and 24 (p = 0.0002) hours. Therefore the results indicated that following the OSR, the cells were significantly induced to undergo necrosis or fragmentation. The conclusion was also supported by the corresponding LDH assay (**Figure 5.10**) and the flow cytometry results (**Figures 5.11** and **5.12**).

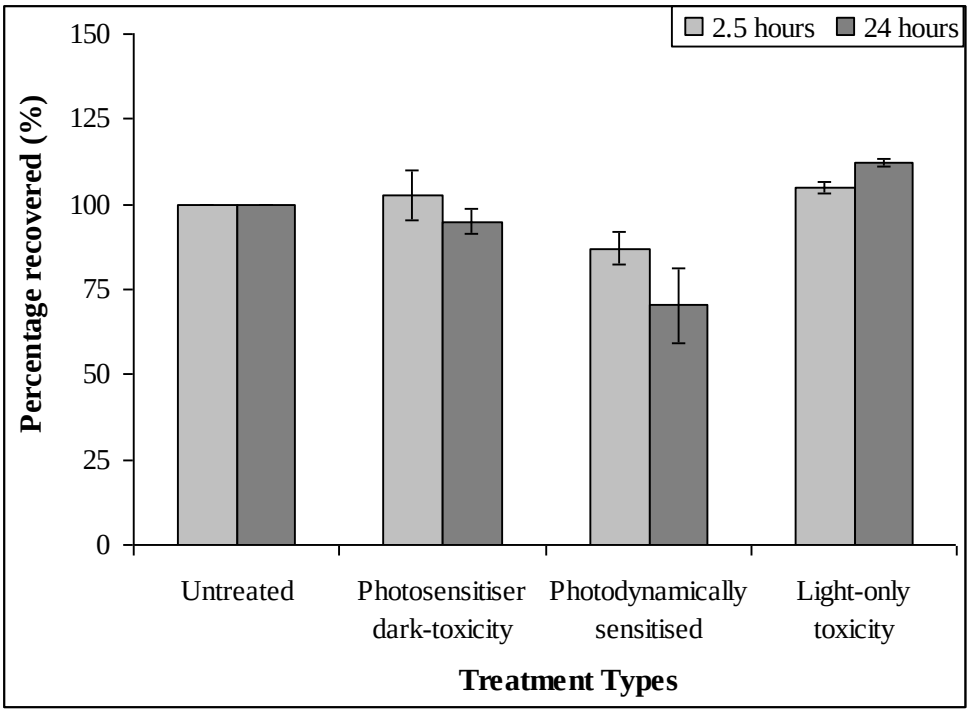

Figure 5.8: *The effects of MBOSR on the total recovery of cells, compared against three controls under the same conditions; 100 μM of $AlPcS_4$, fluence of 3.7 J cm^{-2} and the cells were analysed using haemocytometer after 2.5 and 24 hours. Standard deviation error bars for n=3.*

The changes to the viability of cells after 2.5 and 24 hours of incubation were determined in terms of percentages using trypan blue assay (**Figure 5.9**). The assessment of the data and the statistical analysis showed, the

viability of cells in the *photodynamically sensitised* samples decreased relative to the controls, and the changes were significantly different at both time intervals, 2.5 (p = 0.0002) and 24 (p < 0.0001) hours. Comparison of the *percentage viability* changes (**Figure 5.9**) and the *percentage recovery* (**Figure 5.8**) showed that, the number of cells recovered was higher after 2.5 hours relative to 24 hours, but the *percentage viability* was lower and *vice versa* after 24 hours.

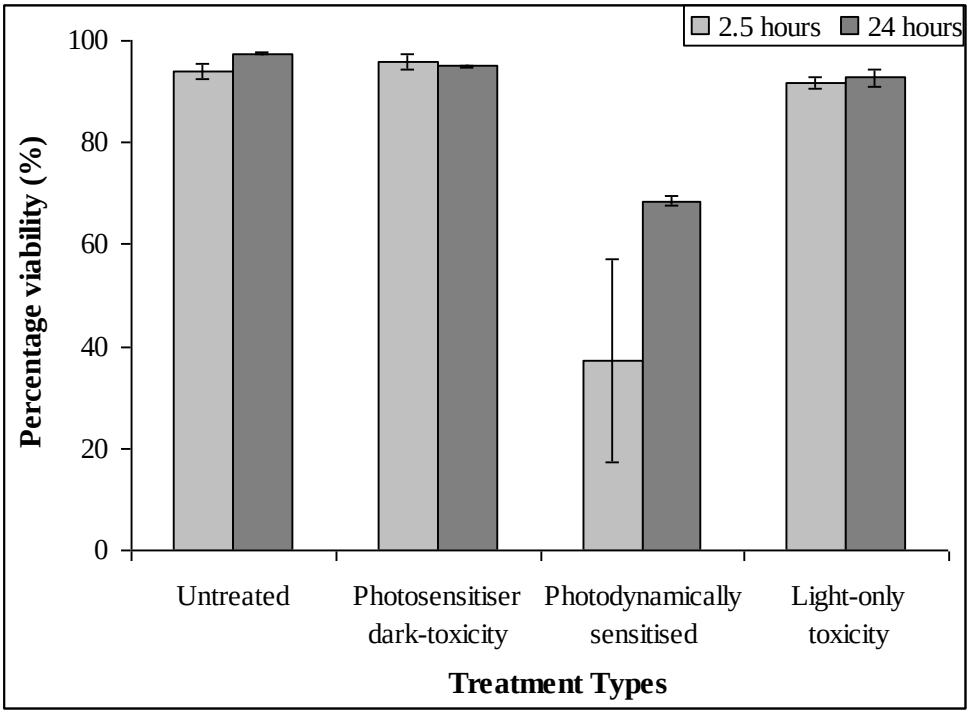

Figure 5.9: *The effects of MBOSR on the total viability of cells, compared against three controls under the same conditions; 100 μM of $AlPcS_4$, fluence of 3.7 J cm^{-2} and the cells were analysed using trypan blue and haemocytometer after 2.5 and 24 hours of incubation. Standard deviation error bars for n=3.*

The levels of LDH released soon (0 hour) after the OSR was measured, and the statistical analysis showed presence of significant difference (p < 0.0001). From the assessment of the data for 0 hour in **Figure 5.10**, it was found that the level of LDH released for the samples *photosensitiser dark-toxicity* and *photodynamically sensitised* were similar and relatively lower than in the other two controls. The reduction in the strength of the signals for the samples, *photosensitiser dark-toxicity* and *photodynamically sensitised*, could be due to fluorescence signal from $AlPcS_4$ contained in the supernatant measured.

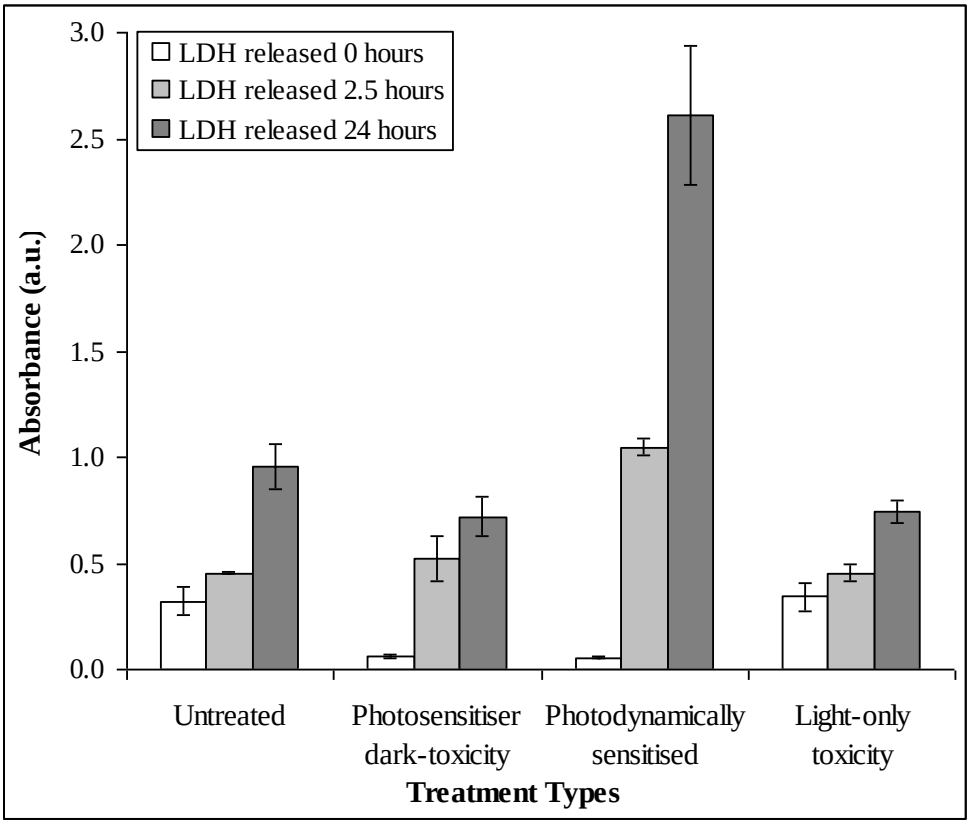

Figure 5.10: *The effects of MBOSR on the levels of LDH released soon after OSR and during 2.5 and 24 hours of incubations, compared against three controls under the same conditions; 100μM of $AlPcS_4$ and fluence of 3.7 J cm^{-2}. Standard deviation error bars for n=3.*

The levels of LDH released during 2.5 hours of incubation (**Figure 5.10**) showed significant difference ($p < 0.0001$). It was identified that the number of disintegrated cells in the *photodynamically sensitised* sample after 2.5 hours was higher than in all the controls, and it was also higher than the level of LDH levels observed after 24 hours for the same controls. Therefore, the results indicated that, following the OSR the cells were disintegrated. The levels of LDH released following 24 hours of incubation was also significantly different ($p < 0.0001$), and the amount of LDH released in the *photodynamically sensitised* sample was about three times higher than in the controls, hence would be the number of cells fragmented. The above interpretations and conclusions were also in agreement with the results in **Figures 5.8**, **5.11** and **5.12**.

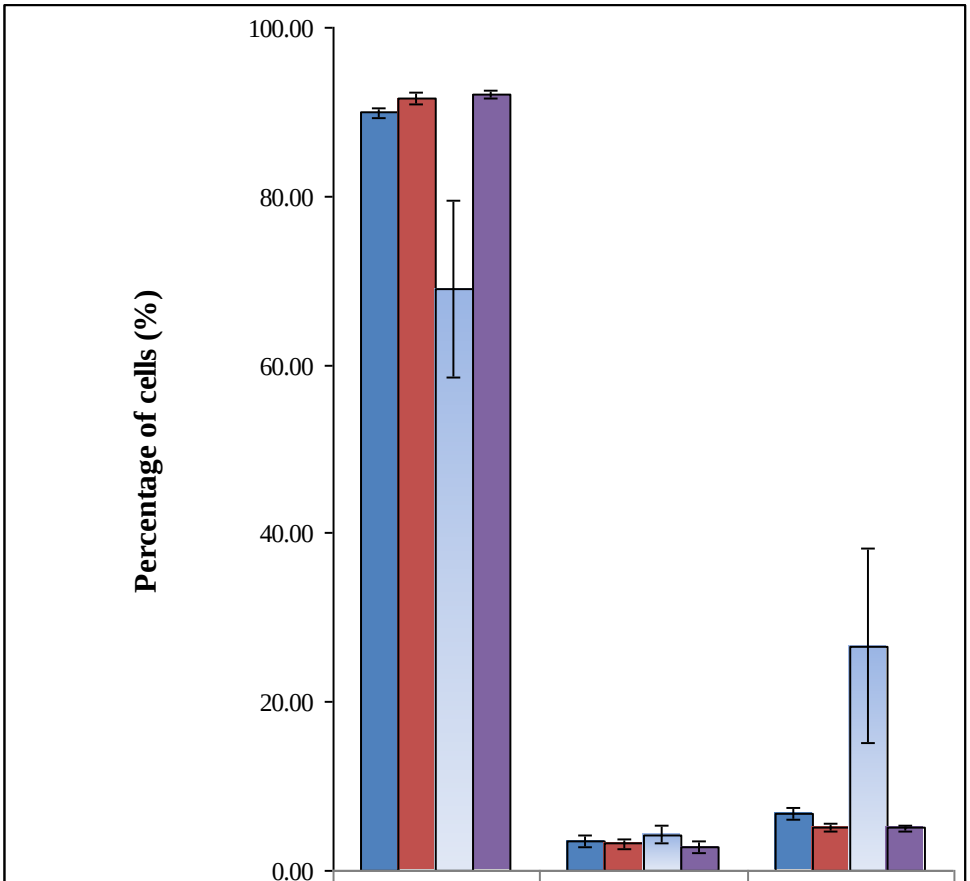

	Healthy	Apoptotic	Necrotic
Untreated	89.87	3.40	6.72
Photosensitiser dark-toxicity	91.64	3.18	5.17
Photodynamically sensitised	69.03	4.30	26.67
Light-only toxicity	92.13	2.82	5.05

Figure 5.11: *The effects of MBOSR on the viability and the induction of apoptotic and necrotic pathways, compared against three controls under the same conditions; 100 μM of $AlPcS_4$, fluence of 3.7 J cm^{-2} and the cells were analysed using flow cytometry after 2.5 hours. Standard deviation error bars for n=3.*

The changes to the viability of cells, and the induction of apoptotic and necrotic pathways after 2.5 hours from the reactions were determined flow cytometrically. The results (**Figure 5.11**) were statistically analysed. The numbers of cells in the healthy-mode decreased (p = 0.002), in the necrotic-mode increased (p = 0.004), and the changes were significantly different from the controls, while no significant difference was observed in the apoptotic-mode. The analysis of the results (**Figure 5.12**) for the samples measured after 24 hours from the reactions showed that, the numbers of cells in the healthy-mode decreased (p = 0.0005), and in the apoptotic- (p =

0.008) and necrotic-modes (p = 0.001) increased, the changes were significantly different from all the controls. Using all the results (**Figures 5.8** to **5.12**) under this section it was noticeable that, without changing the light dose, the use of higher photosensitiser concentration led to improved levels of photosensitisation effects. Further, the conditions predominantly induced necrosis and not apoptosis.

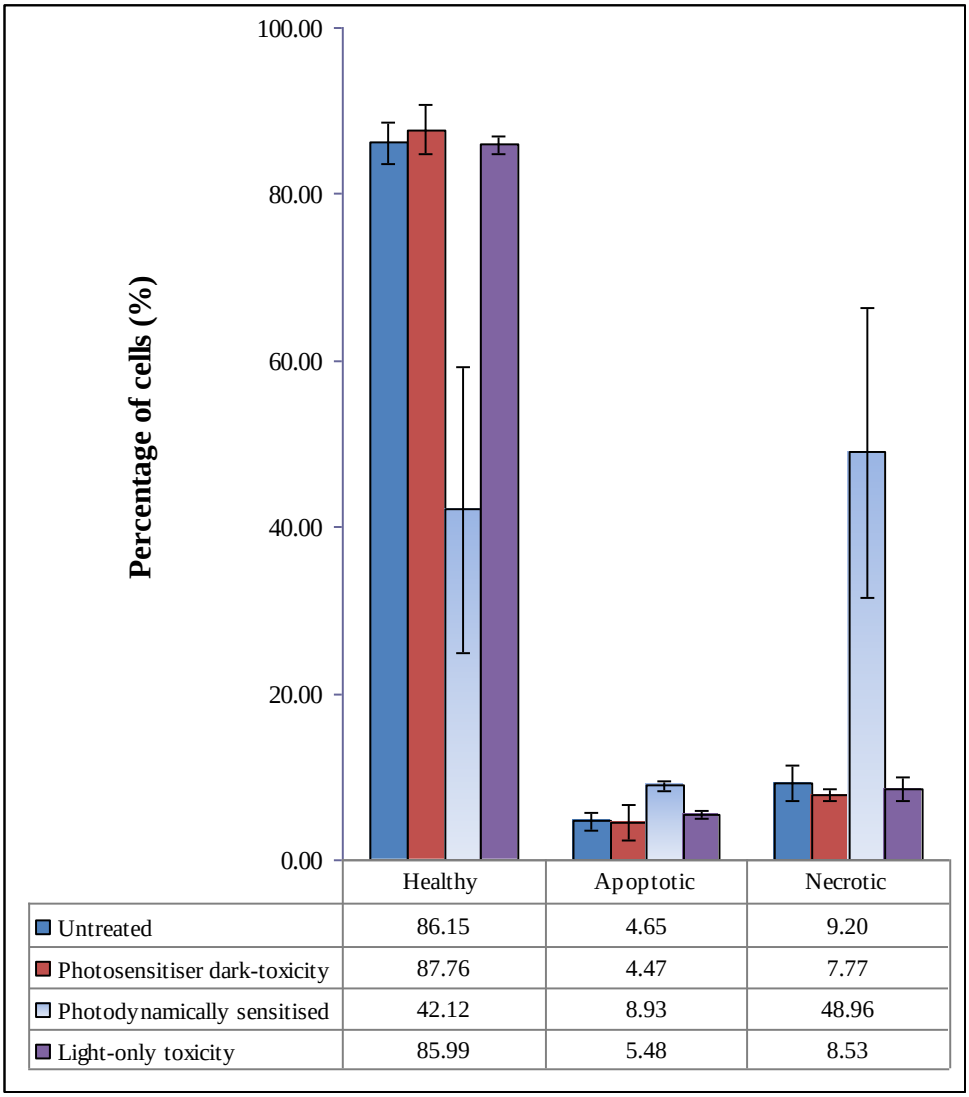

	Healthy	Apoptotic	Necrotic
Untreated	86.15	4.65	9.20
Photosensitiser dark-toxicity	87.76	4.47	7.77
Photodynamically sensitised	42.12	8.93	48.96
Light-only toxicity	85.99	5.48	8.53

Figure 5.12: *The effects of MBOSR on the viability and the induction of apoptotic and necrotic pathways, compared against three controls under the same conditions; 100 μM of $AlPcS_4$, fluence of 3.7 J cm^{-2} and the cells were analysed using flow cytometry after 24 hours. Standard deviation error bars for n=3.*

5.6 Conditions: Light dose of 9.1 J cm^{-2} and $AlPcS_4$ of 10 μM

The samples treated under the conditions, a light dose of 9.1 J cm^{-2} and $AlPcS_4$ of 10 μM was measured after 2.5 and 24 hours of incubations using haemocytometer to determine the changes to the number of cells recovered (**Figure 5.13**). The assessment of the data showed that, the number of cells in the *photodynamically sensitised* samples decreased relative to the controls at both time intervals. However, the statistical analysis revealed that, the changes were significantly different (p = 0.001) from all the controls only after 24 hours. The results indicated that following the OSR, the cells were significantly induced to undergo necrosis or fragmentation. The conclusion was also supported by the corresponding LDH assay (**Figure 5.15**) and the flow cytometry results (**Figures 5.16** and **5.17**).

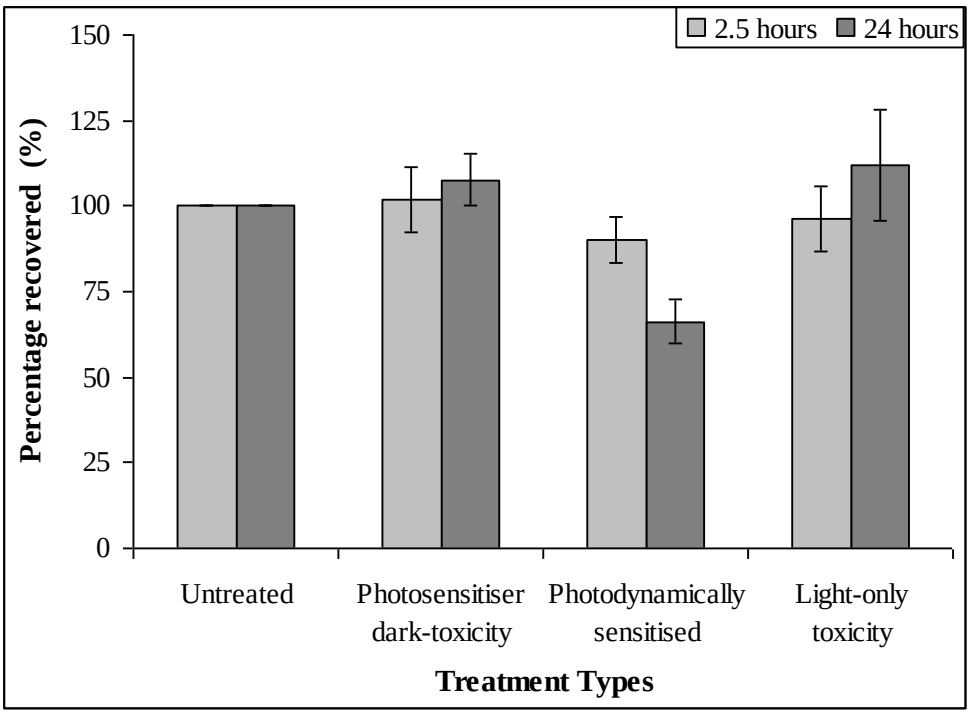

Figure 5.13: *The effects of MBOSR on the total recovery of cells, compared against three controls under the same conditions; 10 μM of $AlPcS_4$, fluence of 9.1 J cm^{-2} and the cells were analysed using haemocytometer after 2.5 and 24 hours. Standard deviation error bars for n=3.*

The changes to the viability of cells after 2.5 and 24 hours of incubation were determined using trypan blue assay (**Figure 5.14**). The assessment of the data and the statistical analysis showed that, the viability of cells in the

photodynamically sensitised samples decreased relative to the controls, and the changes were significantly different at both time intervals, 2.5 (p = 0.007) and 24 (p = 0.02) hours. Comparison of the *percentage viability* changes (**Figure 5.14**) and the *percentage recovery* (**Figure 5.13**) showed that, the number of cells recovered was higher after 2.5 hours, but the viability was lower and *vice versa* after 24 hours.

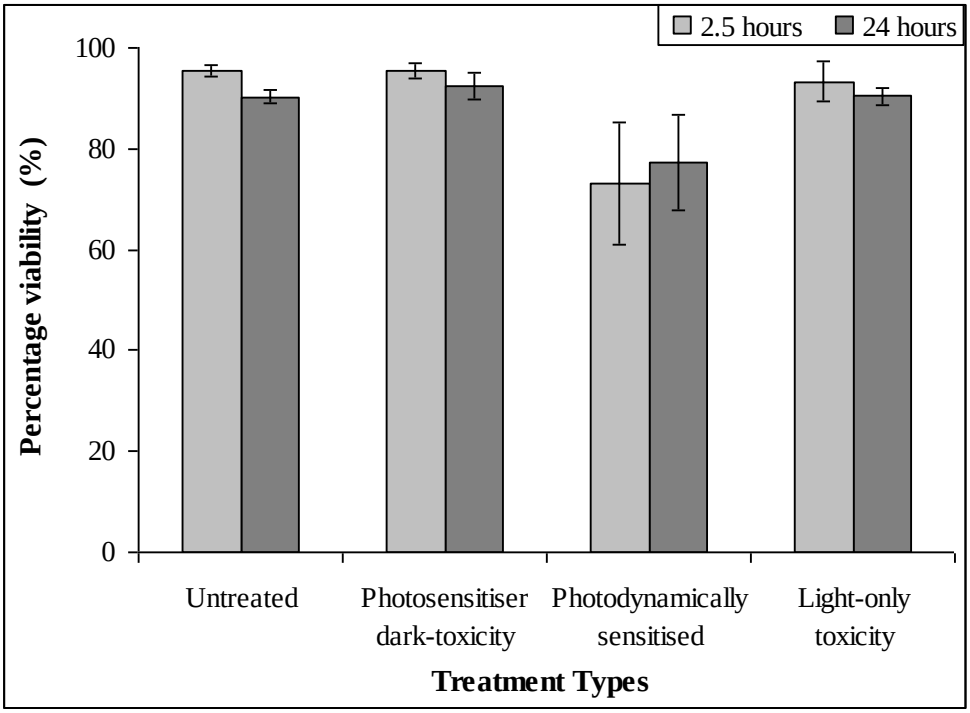

Figure 5.14: *The effects of MBOSR on the total viability of cells, compared against three controls under the same conditions; 10 μM of $AlPcS_4$, fluence of 9.1 J cm^{-2} and the cells were analysed using trypan blue and haemocytometer after 2.5 and 24 hours of incubation. Standard deviation error bars for n=3.*

The levels of LDH released immediately after the OSR was measured (**Figure 5.15**), and the statistical analysis showed presence of significant difference (p = 0.001). From the assessment of the data for 0 hour, it was found that the level of LDH released for the *photodynamically sensitised* sample was lower than in the controls. The levels of LDH released during 2.5 hours of incubation showed significant difference (p = 0.02), and the number of cells disintegrated in the *photodynamically sensitised* sample was higher than in the controls, indicating cellular fragmentation had occurred. The levels of LDH released following 24 hours of incubation was also

significantly different (p = 0.0009), and the level of disintegration (LDH) was about two times higher than in the controls. The above interpretations and conclusions were in agreement with the results in **Figures 5.13**, **5.16** and 5**.17**.

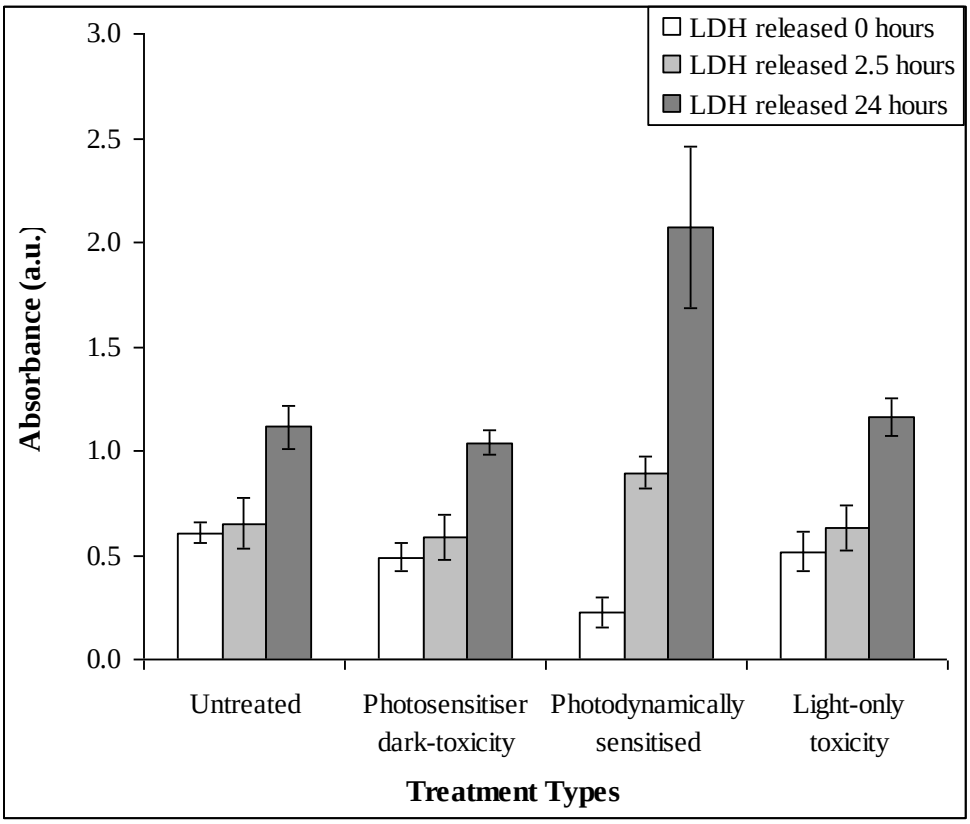

Figure 5.15: *The effects of MBOSR on the levels of LDH released soon after OSR and during 2.5 and 24 hours of incubations, compared against three controls under the same conditions; 10μM of $AlPcS_4$ and fluence of 9.1 J cm^{-2}. Standard deviation error bars for n=3.*

The changes to the viability of cells, and the induction of apoptotic and necrotic pathways after 2.5 from the reactions were determined flow cytometrically (**Figure 5.16**), and the results were statistically analysed. The numbers of cells in the healthy-mode decreased (p = 0.002), in the necrotic-mode increased (p = 0.0006), and the changes were significantly different from all the controls, while in the apoptotic-mode no significant difference was observed. The analysis of the results (**Figure 5.17**) for the samples measured after 24 hours from the reactions showed that, the numbers of cells in the healthy-mode decreased (p = 0.002), in the necrotic-mode (p = 0.0007) increased, and the changes were significantly different from all the

controls, while in the apoptotic-mode no significant difference was observed. Using all the results (**Figures 5.13** to **5.17**) under this section, it was noticeable that, the light dose of 9.1 J cm^{-2} showed improved photosensitisation effects relative 3.7 J cm^{-2} (**Figures 5.3** to **5.7**). Further, the conditions predominantly induced necrosis and not apoptosis.

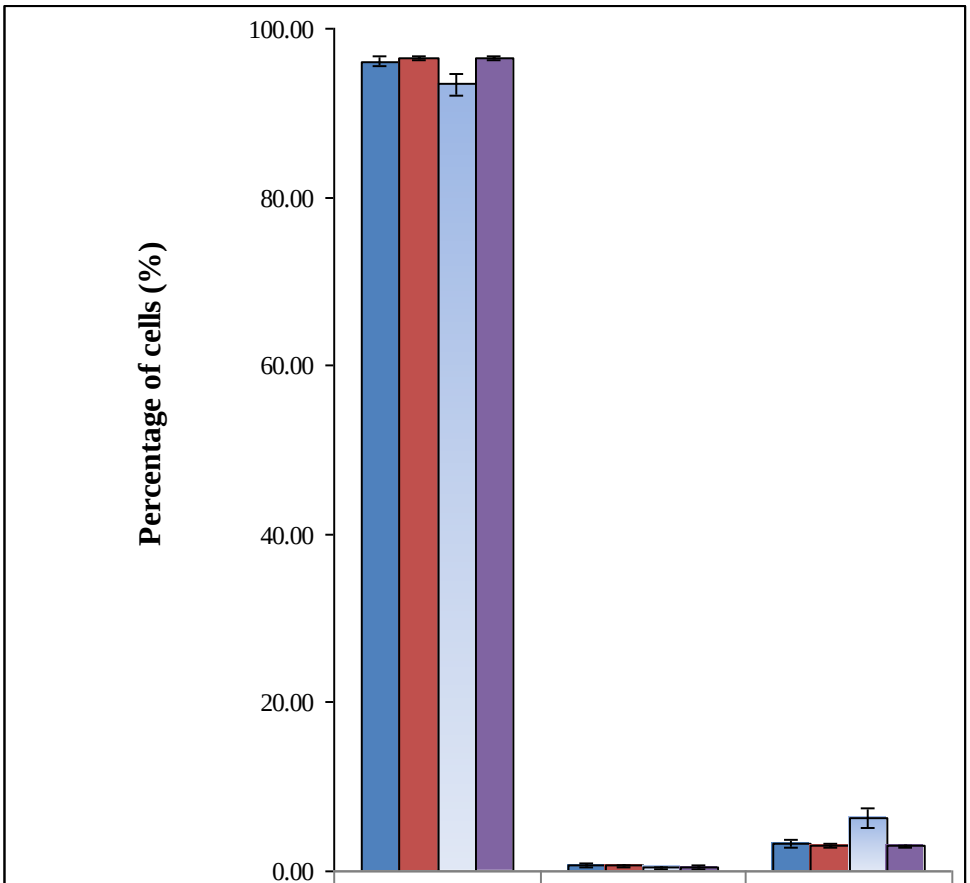

	Healthy	Apoptotic	Necrotic
Untreated	96.07	0.67	3.26
Photosensitiser dark-toxicity	96.41	0.60	2.99
Photodynamically sensitised	93.37	0.36	6.27
Light-only toxicity	96.52	0.50	2.98

Figure 5.16: *The effects of MBOSR on the viability and the induction of apoptotic and necrotic pathways, compared against three controls under the same conditions; 10 μM of $AlPcS_4$, fluence of 9.1 J cm^{-2} and the cells were analysed using flow cytometry after 2.5 hours. Standard deviation error bars for n=3.*

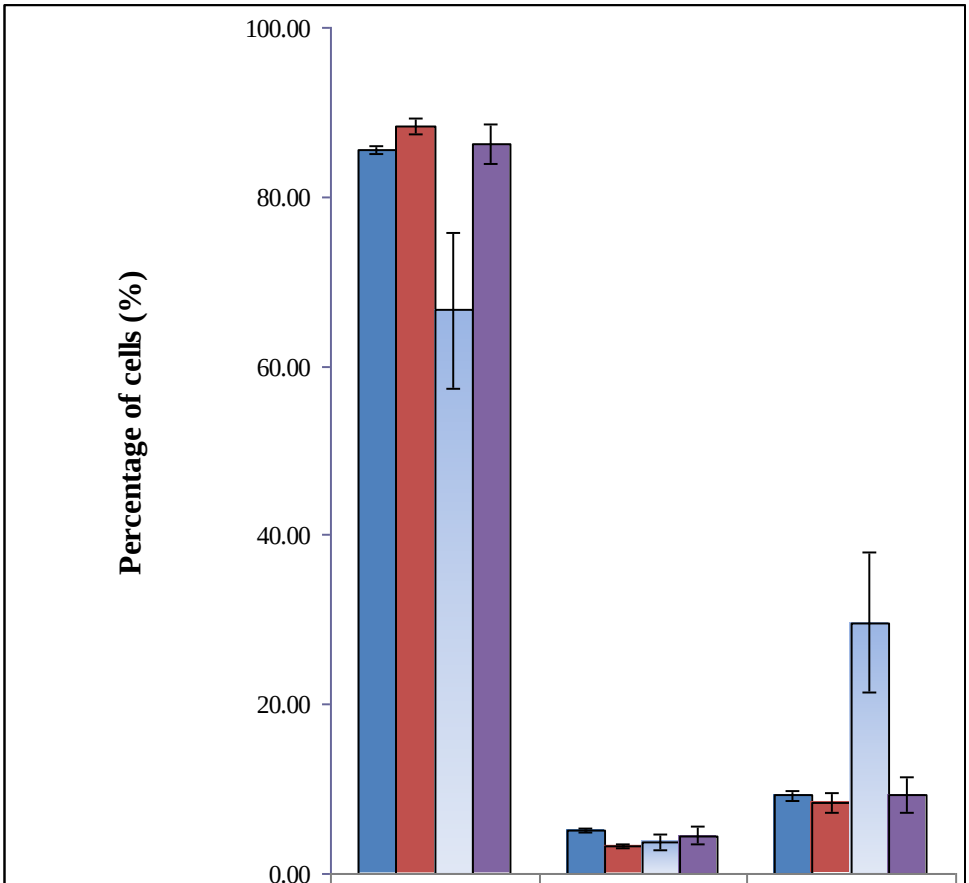

	Healthy	Apoptotic	Necrotic
Untreated	85.56	5.17	9.27
Photosensitiser dark-toxicity	88.32	3.28	8.40
Photodynamically sensitised	66.66	3.64	29.70
Light-only toxicity	86.22	4.47	9.31

Figure 5.17: *The effects of MBOSR on the viability and the induction of apoptotic and necrotic pathways, compared against three controls under the same conditions; 10 μM of $AlPcS_4$, fluence of 9.1 J cm^{-2} and the cells were analysed using flow cytometry after 24 hours. Standard deviation error bars for n=3.*

5.7 Conditions: Light dose of 9.1 J cm^{-2} and $AlPcS_4$ of 100 μM

The samples treated under the conditions, a light dose of 9.1 J cm^{-2} and $AlPcS_4$ of 100 μM was measured after 2.5 and 24 hours of incubations using haemocytometer to determine the number of cells recovered (**Figure 5.18**). The assessment of the data and the statistical analysis showed, the number of cells recovered in the *photodynamically sensitised* samples were lower relative to all the controls, and the changes were significantly different at both time intervals, 2.5 (p = 0.03) and 24 (p < 0.0001) hours. Therefore the

results indicated that following the OSR, the cells were significantly induced to undergo necrosis or fragmentation. The conclusion was also supported by the corresponding LDH assay (**Figure 5.20**) and the flow cytometry results (**Figures 5.21** and **5.22**).

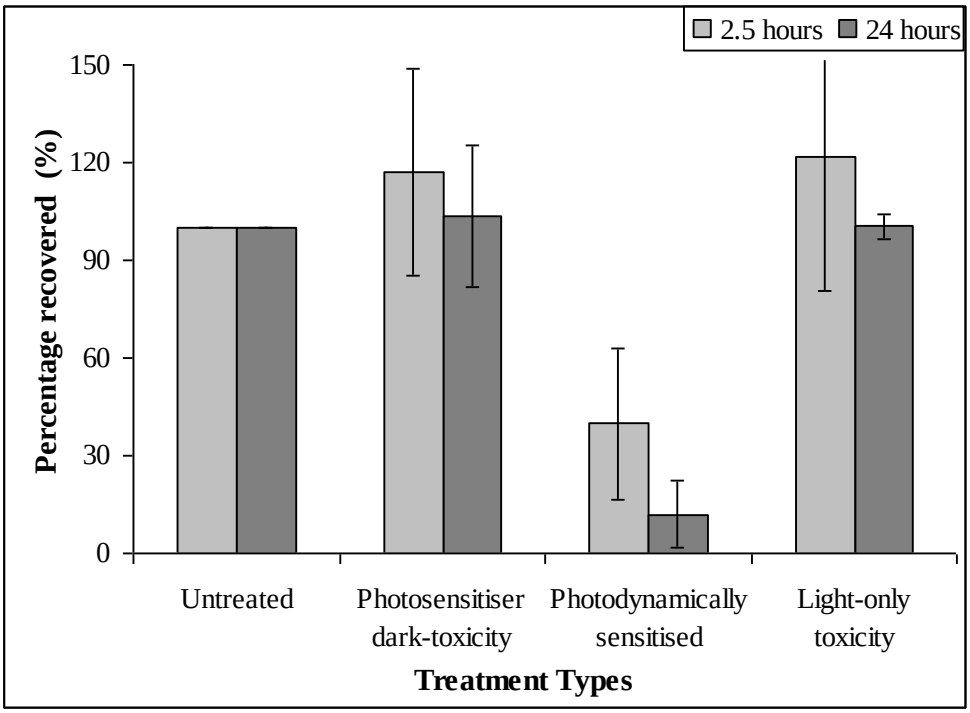

Figure 5.18: *The effects of MBOSR on the total recovery of cells, compared against three controls under the same conditions; 100 μM of $AlPcS_4$, fluence of 9.1 J cm^{-2} and the cells were analysed using haemocytometer after 2.5 and 24 hours. Standard deviation error bars for n=3.*

The changes to the viability of cells after 2.5 and 24 hours of incubation were determined using trypan blue assay (**Figure 5.19**). The assessment of the data and the statistical analysis showed that, the viability of cells in the *photodynamically sensitised* samples decreased close to zero, while the viability of cells in all the controls remained higher than 90 %, and the changes were significantly different at both time intervals, 2.5 ($p < 0.0001$) and 24 ($p < 0.0001$) hours. Comparison of the *percentage viability* changes (**Figure 5.19**) and the *percentage recovery* (**Figure 5.18**) showed that, the number of cells recovered was higher after 2.5 hours relative to 24 hours of incubation, but the viability levels were similar at both time intervals.

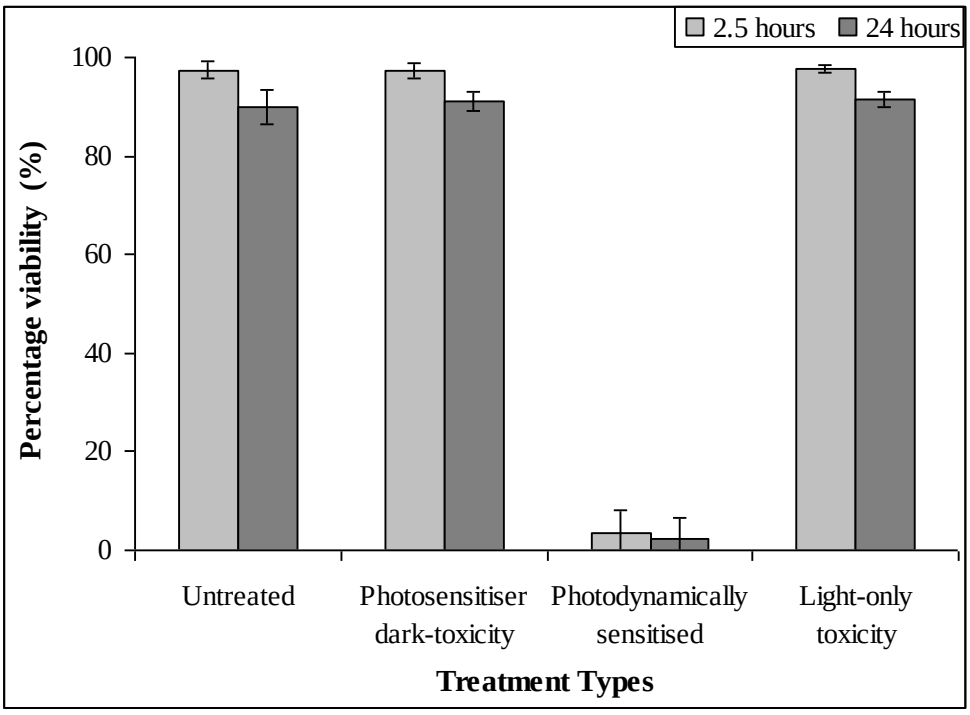

Figure 5.19: *The effects of MBOSR on the total viability of cells, compared against three controls under the same conditions; 100 μM of $AlPcS_4$, fluence of 9.1 J cm^{-2} and the cells were analysed using trypan blue and haemocytometer after 2.5 and 24 hours of incubation. Standard deviation error bars for n=3.*

The levels of LDH released immediately after the OSR was measured, and the statistical analysis showed presence of significant difference ($p < 0.0001$). From the assessment of the data for 0 hour in **Figure 5.20**, it was found that the level of LDH released for the samples *photosensitiser dark-toxicity* and *photodynamically sensitised* were lower than in the other two controls. The lower absorbance signals could be the result of fluorescence from the photosensitiser. The levels of LDH released during 2.5 ($p < 0.0001$) and 24 hours ($p < 0.0001$) of incubation also showed significant differences, and the number of cells disintegrated in the *photodynamically sensitised* sample was higher (about 2 and 2.5 times, respectively) than in all the controls. The above observations were in agreement with the results in **Figures 5.18**, **5.21** and **5.22**.

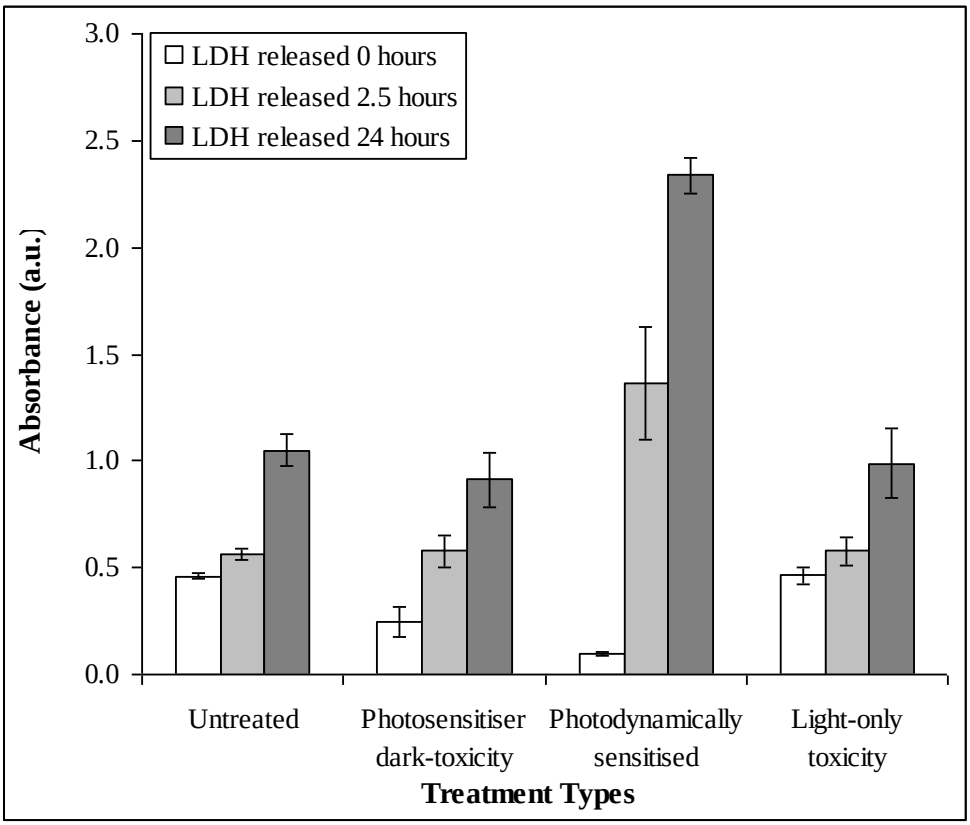

Figure 5.20: *The effects of MBOSR on the levels of LDH released soon after OSR and during 2.5 and 24 hours of incubations, compared against three controls under the same conditions; 100μM of $AlPcS_4$ and fluence of 9.1 J cm^{-2}. Standard deviation error bars for n=3.*

The changes to the viability of cells, and the induction of apoptotic and necrotic pathways after 2.5 hours from the reactions were determined flow cytometrically (**Figure 5.21**), and the results were statistically analysed. The numbers of cells in the healthy- ($p < 0.0001$) and apoptotic-modes ($p = 0.001$) decreased, and in the necrotic- ($p < 0.0001$) mode increased, the above changes were significantly different from all the controls. The analysis of the results (**Figure 5.22**) for the samples measured after 24 hours from the reactions showed that, the numbers of cells in the healthy-mode decreased ($p < 0.0001$), and in the necrotic-mode ($p < 0.0001$) increased, the changes were significantly different from all the controls. The number of cells in the apoptotic-mode increased, but was not significantly different from all the controls. Using all the results (**Figures 5.18** to **5.22**) under this section, it was noticeable that the level of photosensitisation effects increased with the level of light dose, relative to the outcomes in **Figures**

5.8 to **5.12**. As for the other conditions necrosis was predominantly induced and not apoptosis.

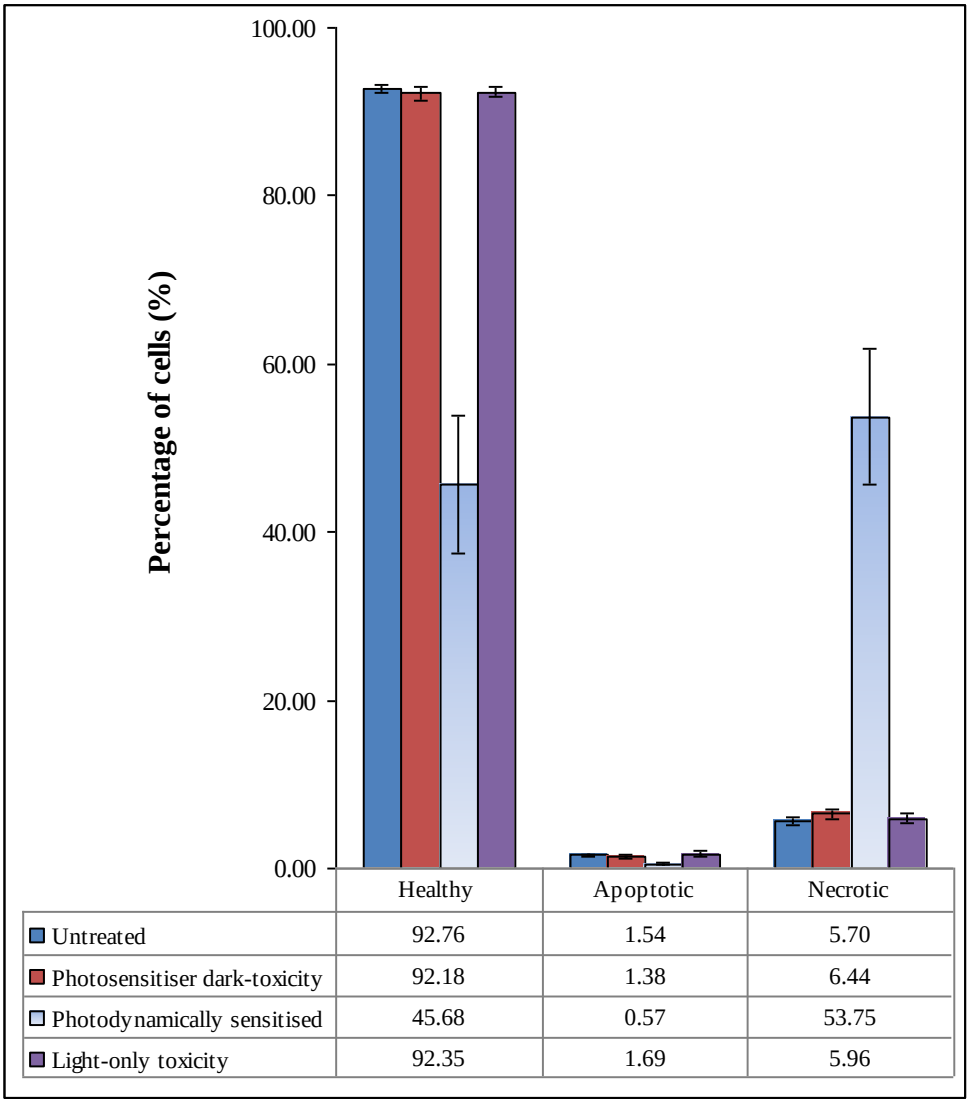

	Healthy	Apoptotic	Necrotic
Untreated	92.76	1.54	5.70
Photosensitiser dark-toxicity	92.18	1.38	6.44
Photodynamically sensitised	45.68	0.57	53.75
Light-only toxicity	92.35	1.69	5.96

Figure 5.21: *The effects of MBOSR on the viability and the induction of apoptotic and necrotic pathways, compared against three controls under the same conditions; 100 μM of $AlPcS_4$, fluence of 9.1 J cm^{-2} and the cells were analysed using flow cytometry after 2.5 hours. Standard deviation error bars for n=3.*

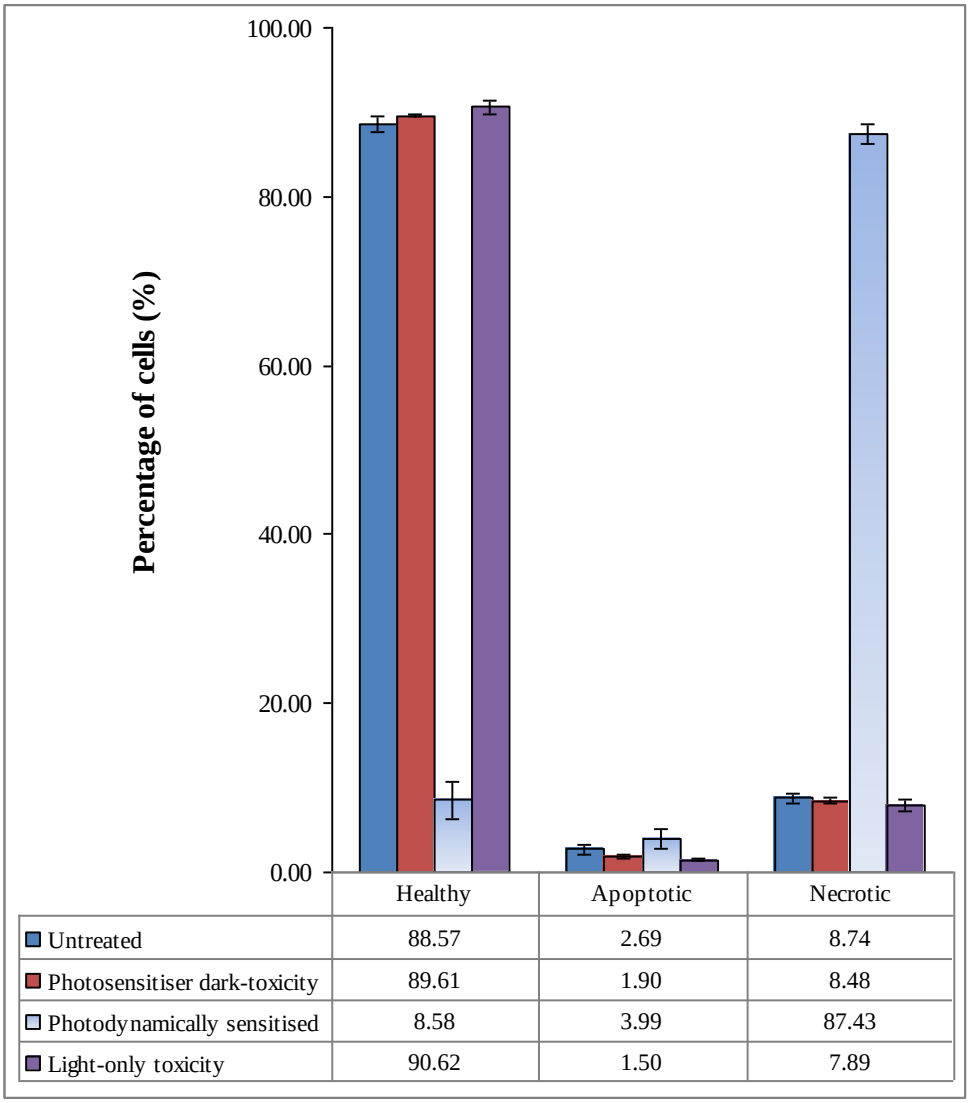

	Healthy	Apoptotic	Necrotic
Untreated	88.57	2.69	8.74
Photosensitiser dark-toxicity	89.61	1.90	8.48
Photodynamically sensitised	8.58	3.99	87.43
Light-only toxicity	90.62	1.50	7.89

Figure 5.22: *The effects of MBOSR on the viability and the induction of apoptotic and necrotic pathways, compared against three controls under the same conditions; 100 μM of $AlPcS_4$, fluence of 9.1 J cm^{-2} and the cells were analysed using flow cytometry after 24 hours. Standard deviation error bars for n=3.*

5.8 Conditions: Light dose of 11.6 J cm^{-2} and $AlPcS_4$ of 10 μM

The samples treated under the conditions, a light dose of 11.6 J cm^{-2} and $AlPcS_4$ of 10 μM was measured after 2.5 and 24 hours of incubations using haemocytometer to determine the number of cells recovered (**Figure 5.23**). The assessment of the data showed that, the number of cells in the *photodynamically sensitised* sample decreased relative to the controls at both time intervals. However, the statistical analysis revealed that, the change was significantly different (p = 0.001) from all the controls only

after 24 hours. Hence, the results indicated that following the OSR, the cells were significantly induced to undergo necrosis or fragmentation. The conclusion was also supported by the corresponding LDH assay (**Figure 5.25**) and the flow cytometry results (**Figures 5.26** and **5.27**).

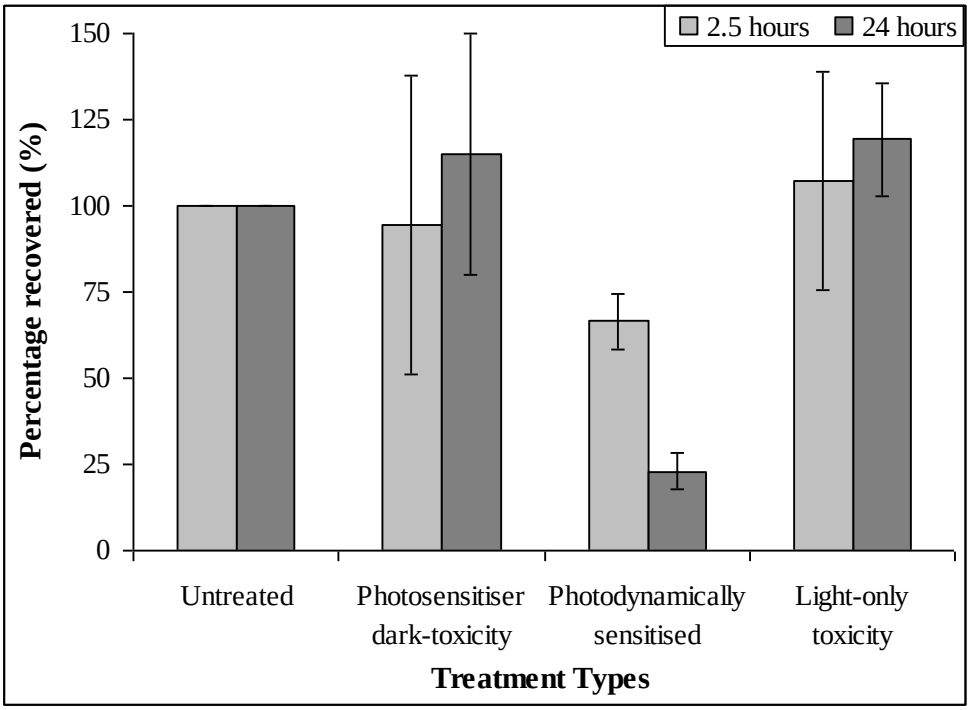

Figure 5.23: *The effects of MBOSR on the total recovery of cells, compared against three controls under the same conditions; 10 μM of $AlPcS_4$, fluence of 11.6 J cm^{-2} and the cells were analysed using haemocytometer after 2.5 and 24 hours. Standard deviation error bars for n=3.*

The changes to the viability of cells after 2.5 and 24 hours of incubation were also determined in terms of percentages using trypan blue assay (**Figure 5.24**). The assessment of the data and the statistical analysis showed that, the viability of cells in the *photodynamically sensitised* sample decreased (~ 50 %) relative to the controls, and the change was significantly different at both time intervals, 2.5 ($p < 0.0001$) and 24 ($p < 0.0001$) hours. Comparison of the data in **Figures 5.23** and **5.24** showed that, the number of cells recovered was higher after 2.5 hours relative to 24 hours, but the viability levels were similar at both time intervals.

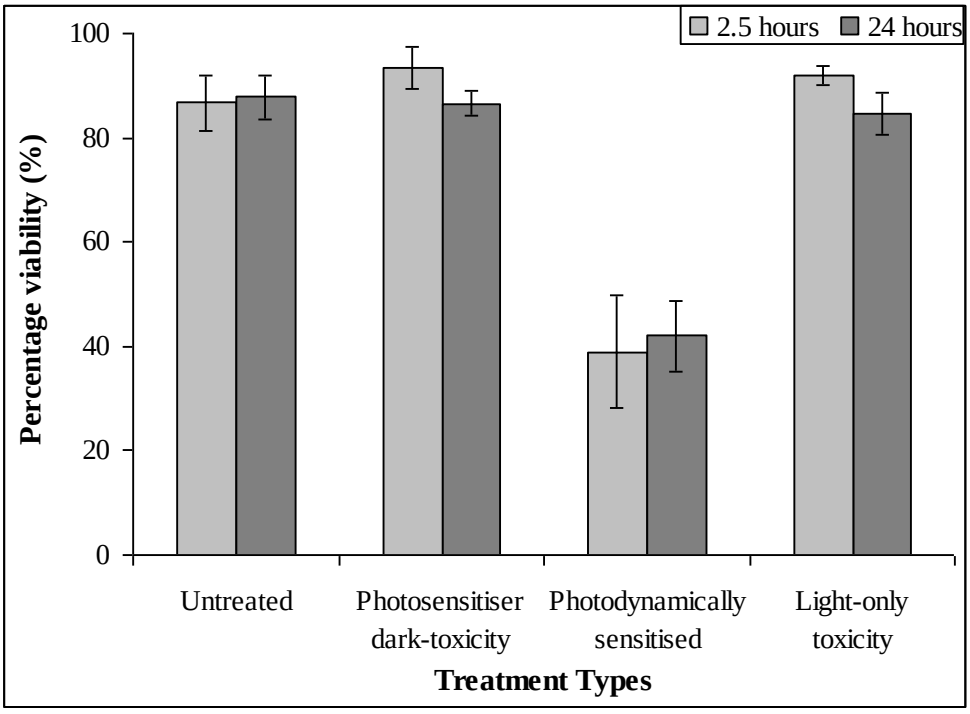

Figure 5.24: *The effects of MBOSR on the total viability of cells, compared against three controls under the same conditions; 10 μM of $AlPcS_4$, fluence of 11.6 J cm^{-2} and the cells were analysed using trypan blue and haemocytometer after 2.5 and 24 hours of incubation. Standard deviation error bars for n=3.*

The levels of LDH released immediately after the OSR was measured, and the statistical analysis showed presence of significant difference (p = 0.005). From the assessment of the data for 0 hour in **Figure 5.25**, it was found that the level of LDH released for the *photodynamically sensitised* sample was relatively lower and significantly different from the controls, *untreated* and *light-only toxicity*. The levels of LDH released during 2.5 (p = 0.0003) and 24 hours (p < 0.0001) of incubation also showed significant differences, and the number of cells disintegrated in the *photodynamically sensitised* sample was higher (about 1.5 and 3 times respectively) than in all the controls. The above observations were in agreement with the results in **Figures 5.23**, **5.26** and **5.27**.

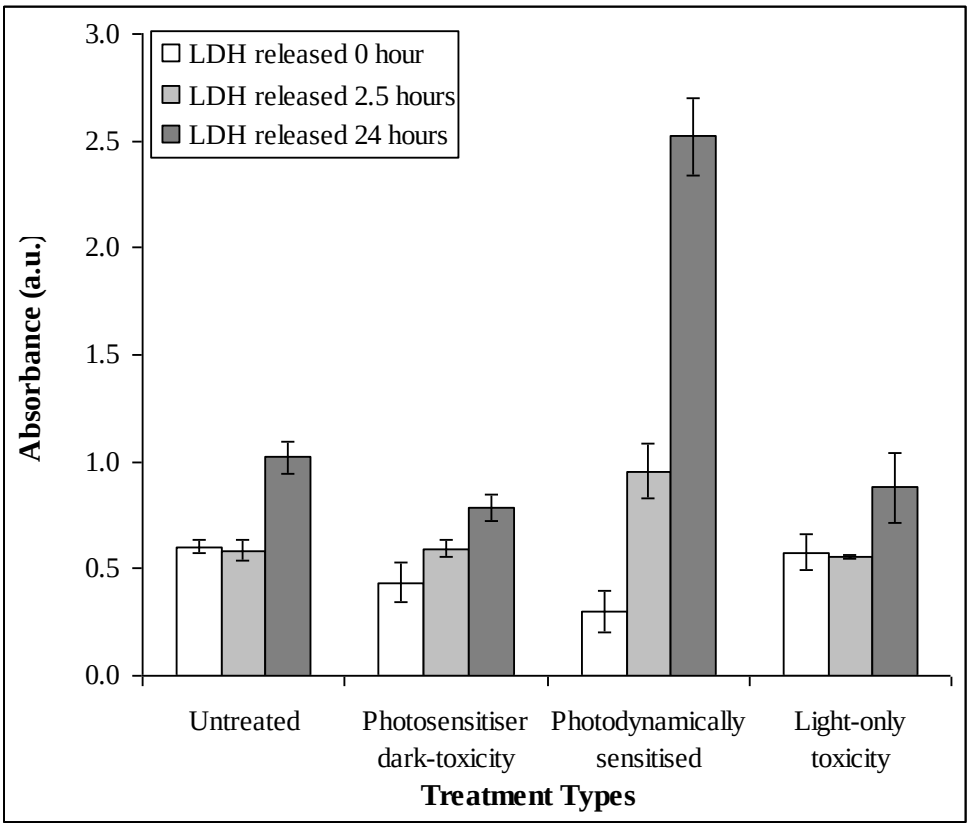

Figure 5.25: *The effects of MBOSR on the levels of LDH released soon after OSR and during 2.5 and 24 hours of incubations, compared against three controls under the same conditions; 10 μM of $AlPcS_4$ and fluence of 11.6 J cm^{-2}. Standard deviation error bars for n=3.*

The changes to the viability of cells, and the induction of apoptotic and necrotic pathways after 2.5 and 24 hours from the reactions were determined flow cytometrically, and the results were statistically analysed. After 2.5 hours (**Figure 5.26**), the numbers of cells in the healthy-mode decreased (p = 0.02), in the necrotic-mode increased (p = 0.02), and the changes were significantly different from all the controls. No significant difference was observed for the number of cells in the apoptotic-mode, and there were less than 1 % cells in all the samples. The analysis of the results (**Figure 5.27**) for the samples measured after 24 hours from the reactions showed that, the numbers of cells in the healthy-mode decreased (p < 0.0001), and in the necrotic-mode increased (p < 0.0001), the changes were significantly different from all the controls. In the apoptotic-mode no change or significant difference was observed, and there were less than 7 % cells in all the samples. Using all the results (**Figures 5.23** to **5.27**) under

this section, it was noticeable that necrosis was predominantly induced, and the level of effects increased with the level of light dose, relative to the outcomes in **Figures 5.3** to **5.7**, and **Figures 5.13** to **5.17**.

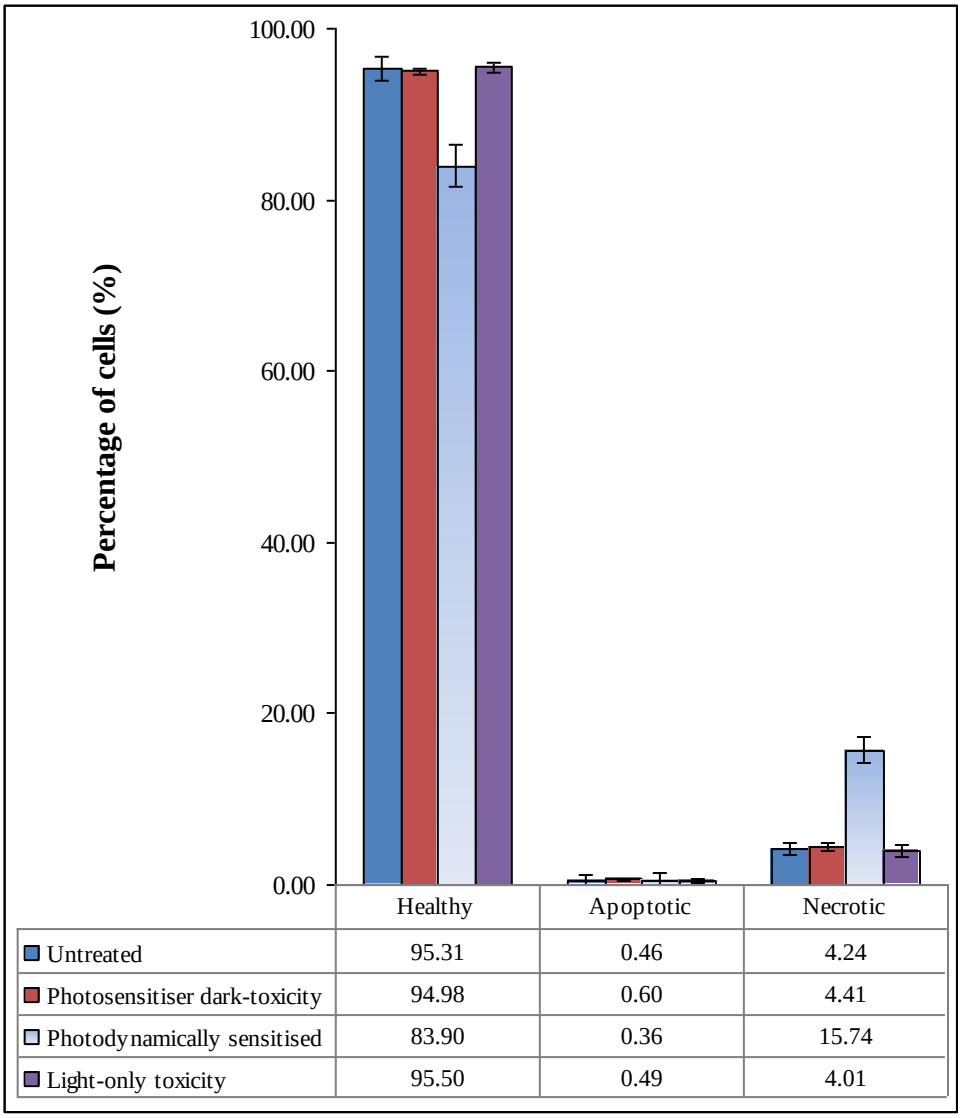

	Healthy	Apoptotic	Necrotic
Untreated	95.31	0.46	4.24
Photosensitiser dark-toxicity	94.98	0.60	4.41
Photodynamically sensitised	83.90	0.36	15.74
Light-only toxicity	95.50	0.49	4.01

Figure 5.26: *The effects of MBOSR on the viability and the induction of apoptotic and necrotic pathways, compared against three controls under the same conditions; 10 μM of $AlPcS_4$, fluence of 11.6 J cm^{-2} and the cells were analysed using flow cytometry after 2.5 hours. Standard deviation error bars for n=3.*

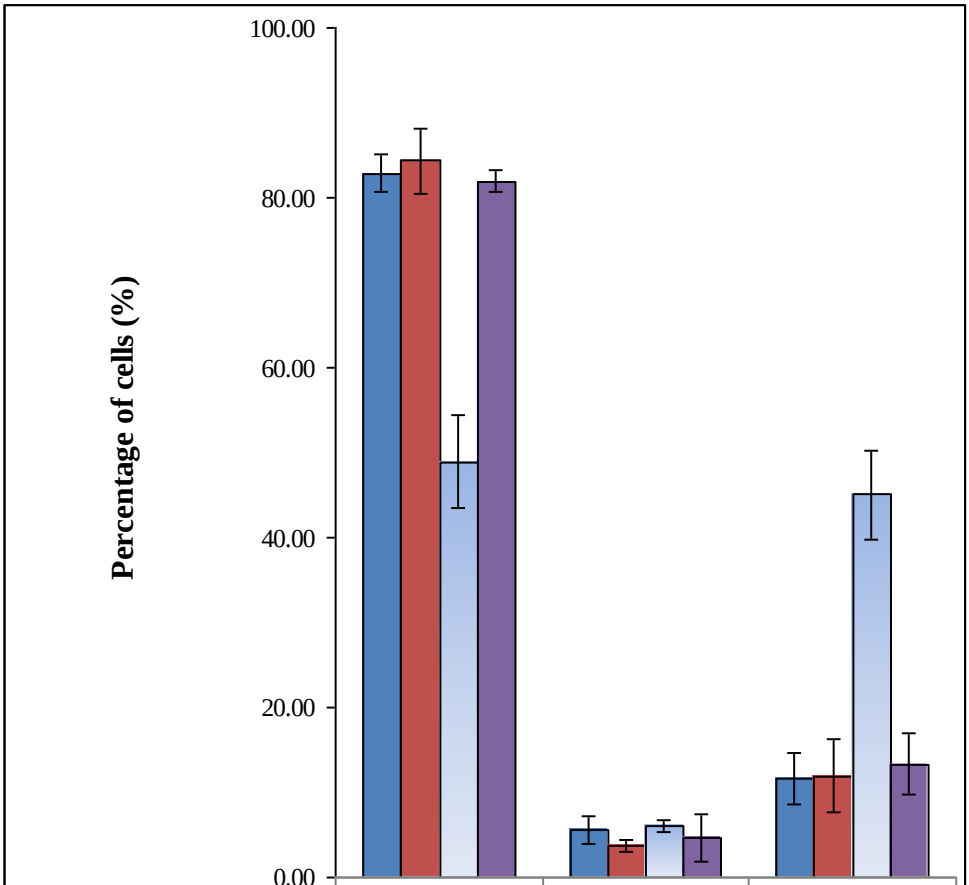

	Healthy	Apoptotic	Necrotic
Untreated	82.83	5.63	11.54
Photosensitiser dark-toxicity	84.37	3.71	11.92
Photodynamically sensitised	48.90	6.02	45.08
Light-only toxicity	81.96	4.70	13.34

Figure 5.27: *The effects of MBOSR on the viability and the induction of apoptotic and necrotic pathways, compared against three controls under the same conditions; 10 μM of $AlPcS_4$, fluence of 11.6 J cm^{-2} and the cells were analysed using flow cytometry after 24 hours. Standard deviation error bars for n=3.*

5.9 Conditions: Light dose of 11.6 J cm^{-2} and $AlPcS_4$ of 100 μM

The samples treated under the conditions, a light dose of 11.6 J cm^{-2} and $AlPcS_4$ of 100 μM was measured after 2.5 and 24 hours of incubations using haemocytometer to determine the number of cells recovered (**Figure 5.28**). The assessment of the data and the statistical analysis showed that the number of cells in the *photodynamically sensitised* sample decreased greater than 50 % relative to all the controls, and the changes were significantly different at both time intervals, 2.5 (p = 0.006) and 24 (p < 0.0001) hours. Therefore the results indicated that, following the OSR the cells were significantly induced to undergo necrosis or fragmentation. The conclusion was also supported by the corresponding LDH assay (**Figure 5.30**) and the flow cytometry results (**Figures 5.31** and **5.32**).

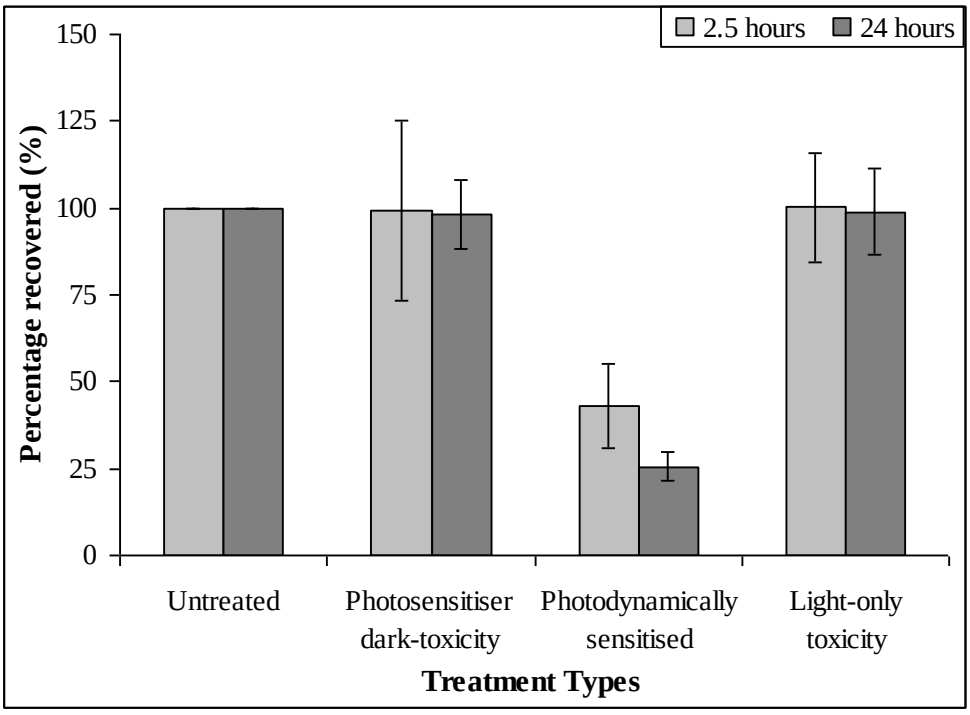

Figure 5.28: *The effects of MBOSR on the total recovery of cells, compared against three controls under the same conditions; 100 μM of $AlPcS_4$, fluence of 11.6 J cm^{-2} and the cells were analysed using haemocytometer after 2.5 and 24 hours. Standard deviation error bars for n=3.*

The changes to the viability of cells after 2.5 and 24 hours of incubation are shown in **Figure 5.29**. The assessment of the data and the statistical analysis showed that, the viability of cells in the *photodynamically sensitised* samples decreased (greater than 70 %) relative to the controls, and the changes were significantly different at both time intervals, 2.5 ($p < 0.0001$) and 24 ($p = 0.0001$) hours. Comparison of **Figures 5.28** and **5.29** showed that the number of cells recovered was higher after 2.5 hours relative to 24 hours, but the viability was similar at both time intervals.

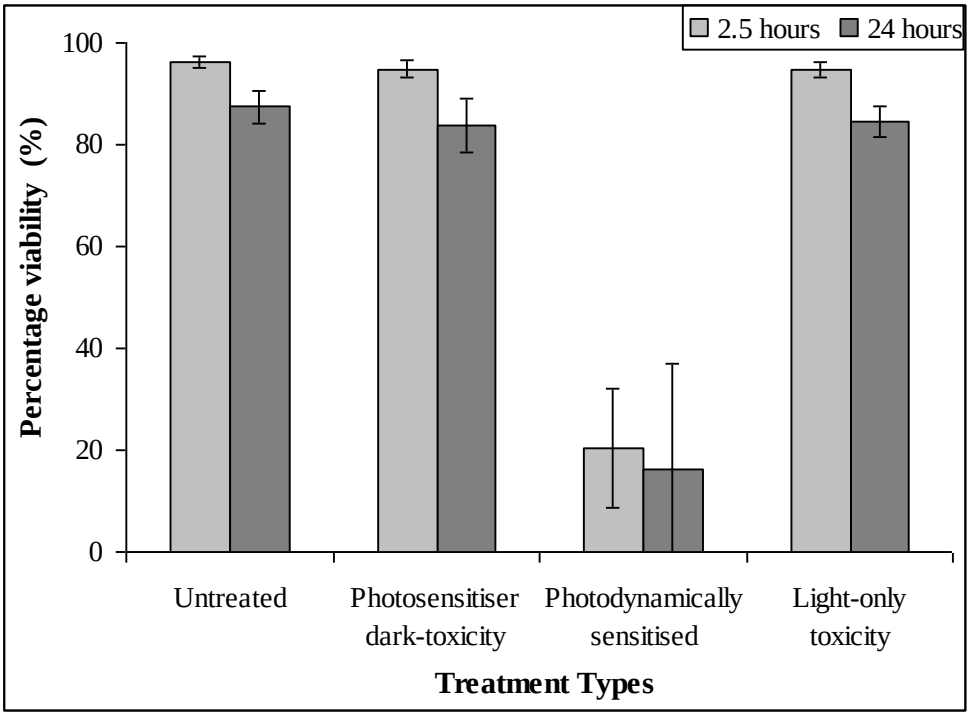

Figure 5.29: *The effects of MBOSR on the total viability of cells, compared against three controls under the same conditions; 100 μM of $AlPcS_4$, fluence of 11.6 J cm^{-2} and the cells were analysed using trypan blue and haemocytometer after 2.5 and 24 hours of incubation. Standard deviation error bars for n=3.*

The levels of LDH released soon after the OSR was measured (**Figure 5.30**), and the statistical analysis showed no significant difference ($p > 0.05$). The levels of LDH released during 2.5 ($p < 0.0001$) and 24 hours ($p = 0.0001$) of incubation showed significant differences, and the number of cells disintegrated in the *photodynamically sensitised* sample was higher (about 1.5 and 2 times respectively) than in the controls. The above

observations were in agreement with the results in **Figures 5.28**, **5.31** and **5.32**.

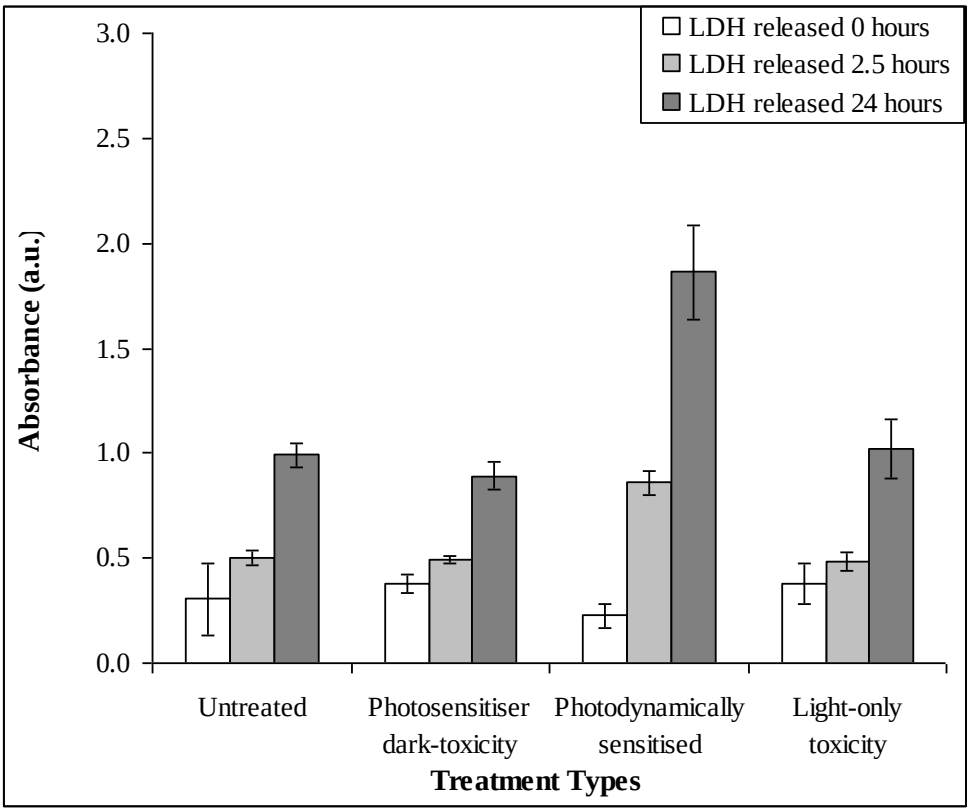

Figure 5.30: *The effects of MBOSR on the levels of LDH released soon after OSR and during 2.5 and 24 hours of incubations, compared against three controls under the same conditions; 100μM of $AlPcS_4$ and fluence of 11.6 J cm^{-2}. Standard deviation error bars for n=3.*

The changes to the viability of cells, and the induction of apoptotic and necrotic pathways after 2.5 hours from the reactions were determined flow cytometrically (**Figure 5.31**), and the results were statistically analysed. The numbers of cells in the healthy-mode decreased ($p < 0.0001$), in the necrotic-mode increased ($p < 0.0001$) and the changes were significantly different from the controls. In the apoptotic-mode, no significant difference was observed, and there were less than 2 % cells in all the samples. The analysis of the results (**Figure 5.32**) for the samples measured after 24 hours from the reactions showed that, the numbers of cells in the healthy-mode decreased ($p < 0.0001$), in the necrotic-mode ($p < 0.0001$) increased, and the changes were significantly different from all the controls. In the apoptotic-

mode there were no significant changes relative to the controls, and all samples had less than 2 % cells in this mode. Using all the results (**Figures 5.28** to **5.32**) in this section, it was noticeable that necrosis was predominantly induced and not apoptosis. Further the levels of photosensitisation effects were higher than in **Figures 5.8** to **5.12**, but similar or lower than in **Figures 5.18** to **5.22**.

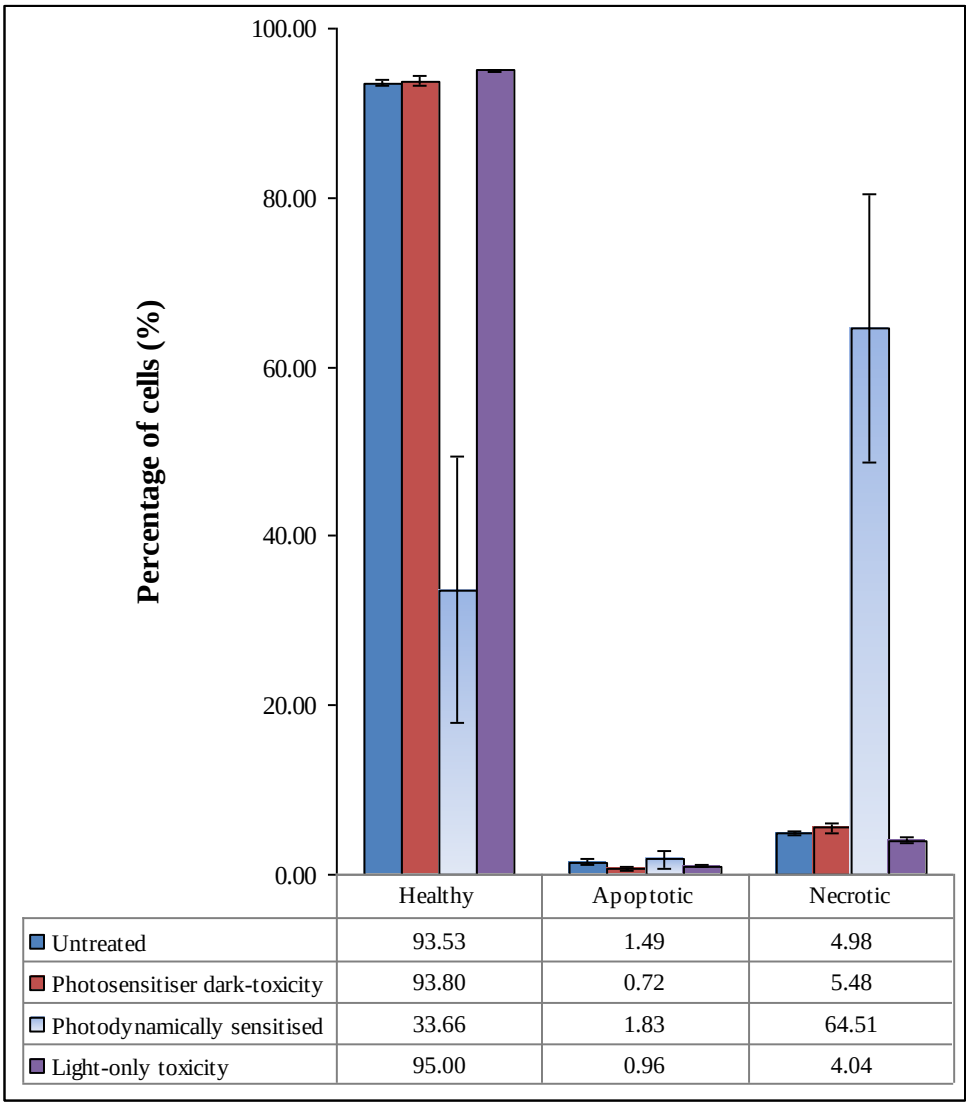

	Healthy	Apoptotic	Necrotic
Untreated	93.53	1.49	4.98
Photosensitiser dark-toxicity	93.80	0.72	5.48
Photodynamically sensitised	33.66	1.83	64.51
Light-only toxicity	95.00	0.96	4.04

Figure 5.31: *The effects of MBOSR on the viability and the induction of apoptotic and necrotic pathways, compared against three controls under the same conditions; 100 μM of $AlPcS_4$, fluence of 11.6 J cm^{-2} and the cells were analysed using flow cytometry after 2.5 hours. Standard deviation error bars for n=3.*

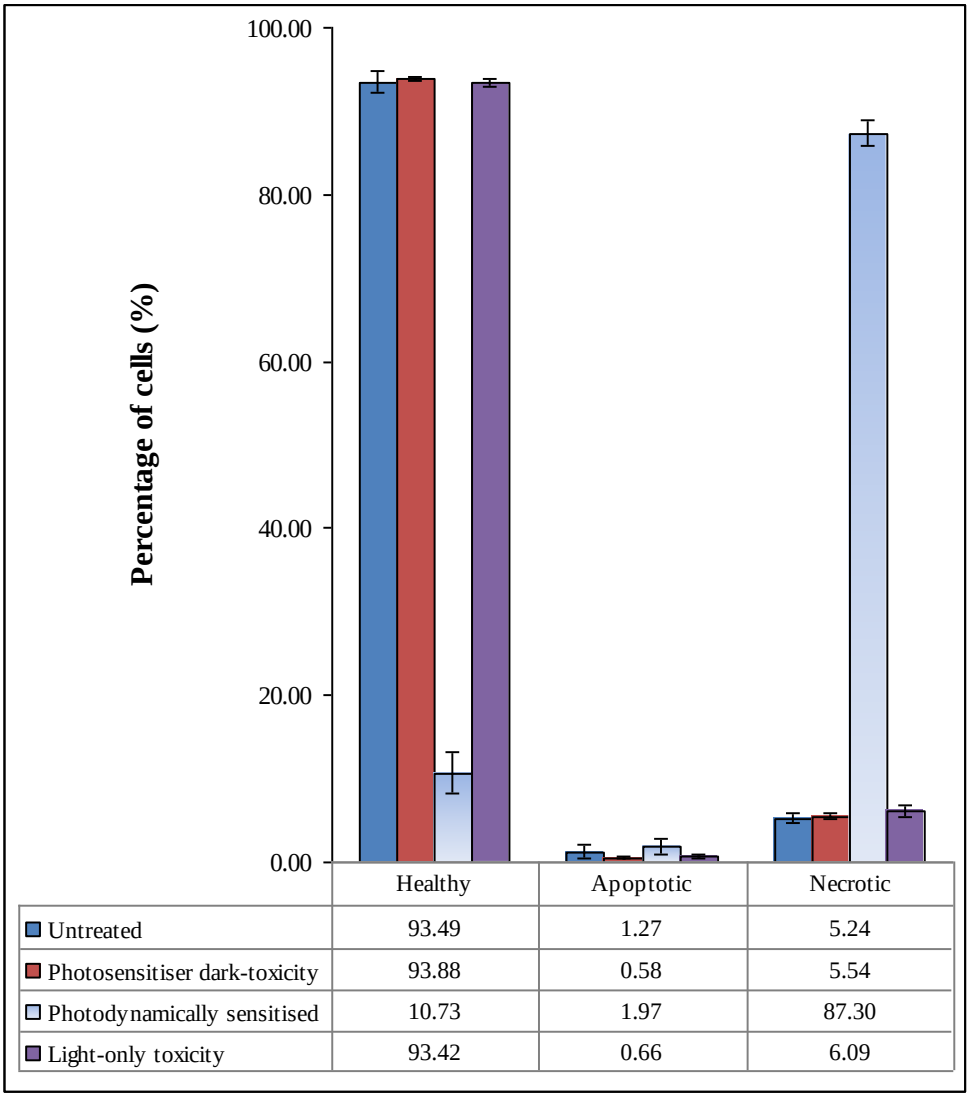

	Healthy	Apoptotic	Necrotic
Untreated	93.49	1.27	5.24
Photosensitiser dark-toxicity	93.88	0.58	5.54
Photodynamically sensitised	10.73	1.97	87.30
Light-only toxicity	93.42	0.66	6.09

Figure 5.32: *The effects of MBOSR on the viability and the induction of apoptotic and necrotic pathways, compared against three controls under the same conditions; 100 μM of $AlPcS_4$, fluence of 11.6 J cm^{-2} and the cells were analysed using flow cytometry after 24 hours. Standard deviation error bars for n=3.*

5.10 Overall conclusion from the trypan blue assays

5.10.1 Recovery of cells

The percentage of cells in the *untreated* control was normalised as 100 %, and all other samples were compared against it for determining their *percentage recoveries*. While maintaining the concentration of $AlPcS_4$ fixed (10 or 100 µM), an increase in light dose (3.7, 9.1 or 11.6 J cm^{-2}) significantly decreased the *percentage recovery* of cells both after 2.5 and 24 hours of incubations.

The number of cells recovered (*percentage recovery*) for all the controls tested under all the conditions (**Table 5.1**) were greater than 95 %. In contrast, the *percentage recovery* of cells in the *photodynamically sensitised* samples decreased in response to the oxidative stress conditions employed. The minimum recorded *percentage recovery* of cells for a *photodynamically sensitised* sample was 12 %, which was obtained under the conditions 100 µM of $AlPcS_4$ and 9.1 J cm^{-2} of light dose, and when the samples were analysed after 24 hours (**Table 5.2**).

Table 5.2: *Recovery and viability of cells, and healthy, apoptotic and necrotic ratios of cells in the photodynamically sensitised samples determined using trypan blue and flow cytometric analyses respectively. SD errors of n=3.*

			Trypan blue assay		Flow cytometric analysis		
Light dose (J cm^{-2})	**$AlPcS_4$ (µM)**	**Time (hours)**	**Recovery (%)**	**Viability (%)**	**Healthy (%)**	**Apoptotic (%)**	**Necrotic (%)**
3.7	10	2.5	100 ± 5	92 ± 2	93.5 ± 0.4	2.0 ± 0.4	5 ± 1
		24	92 ± 8	89 ± 6	86 ± 1	4 ± 2	9.5 ± 0.3
	100	2.5	87 ± 5	37 ± 20	69 ± 10	4 ± 1	27 ± 11
		24	70 ± 11	69 ± 1	42 ± 17	9 ± 1	49 ± 17
9.1	10	2.5	90 ± 7	73 ± 12	93 ± 1	0.4 ± 0.1	6 ± 1
		24	66 ± 6	77 ± 9	67 ± 9	4 ± 1	30 ± 8
	100	2.5	40 ± 23	4 ± 5	46 ± 8	0.6 ± 0.1	54 ± 8
		24	12 ± 10	2 ± 4	9 ± 2	4 ± 1	87 ± 1
11.6	10	2.5	67 ± 8	39 ± 11	84 ± 8	0.4 ± 0.1	16 ± 8
		24	23 ± 6	42 ± 7	49 ± 5	6.0 ± 0.8	45 ± 5
	100	2.5	43 ± 12	20 ± 12	34 ± 16	2 ± 1	65 ± 16
		24	25 ± 4	16 ± 21	11 ± 2	2 ± 1	87 ± 2

Using 10 µM of $AlPcS_4$ together with the light doses 3.7, 9.1 and 11.6 J cm^{-2}, the cell recoveries were 100, 90 and 67 % after 2.5 hours, and the recoveries were 92, 66 and 23 % after 24 hours, respectively. When using

100 µM of $AlPcS_4$ together with the light doses 3.7, 9.1 and 11.6 J cm^{-2}, the cell recoveries were 87, 40 and 43 % after 2.5 hours, and the recoveries were 70, 12 and 26 % after 24 hours, respectively. The *percentage recovery* of cells in the *photodynamically sensitised* samples always decreased when incubated for 24 hours (longer) relative to 2.5 hours. With the use of 10 µM of $AlPcS_4$, an increase in the light dose decreased the numbers of cells recovered, while with the use of 100 µM concentration of $AlPcS_4$, the numbers of cells recovered decreased when the light dose was increased from 3.7 to 9.1 J cm^{-2}, but when the light dose was further increased to 11.6 J cm^{-2}, the recovery was in-between the recovery levels for the light doses 3.7 and 9.1 J cm^{-2}.

5.10.2 Viability of cells

The viability of cells (*percentage viability*) for all the controls tested under all the conditions (**Table 5.1**) were greater than 87 %. In contrast, the *percentage viability* of cells for the *photodynamically sensitised* samples decreased low as 4 and 2 %, under the condition 100 µM of $AlPcS_4$, 9.1 J cm^{-2} of light dose, and when analysed after 2.5 and 24 hours, respectively. When the treated samples were incubated for 24 hours, the *percentage viability* of cells increased or remained similar to that was found after 2.5 hours. For example, under the condition of using a light dose of 3.7 J cm^{-2} and $AlPcS_4$ of 100 µM, when analysed after 2.5 hours the viability was 37 %, and when analysed after 24 hours the viability increased to 69 % (**Table 5.2**). The observations suggested that the healthy cells present within the samples would have proliferated during longer incubation. Alternatively, the non-healthy cells that were detected when analysed after 2.5 hours would have completely disintegrated, thereby it would have relatively appeared as though the viability has increased.

Using 10 µM of $AlPcS_4$ together with the light doses 3.7, 9.1 and 11.6 J cm^{-2}, the cell viabilities were 92, 73 and 39 % after 2.5 hours, and the viabilities were 89, 77 and 42 % after 24 hours, respectively. When using 100 µM of $AlPcS_4$ together with the light doses 3.7, 9.1 and 11.6 J cm^{-2}, the cell viabilities were 37, 4 and 20 % after 2.5 hours, and the viabilities were 69, 2

and 16 % after 24 hours, respectively. Hence with the use of 10 µM concentration of $AlPcS_4$, an increase in the light dose decreased the number of healthy cells, while with the use of 100 µM of $AlPcS_4$, the number of healthy cells decreased when the light dose was increased from 3.7 to 9.1 J cm^{-2}, but when the light dose was increased to 11.6 J cm^{-2}, the number of healthy cells was inbetween the viabilities obtained for the light doses 3.7 and 9.1 J cm^{-2}. These observations were similar to what was observed with the cell recovery measurements (**Table 5.2**). In conclusion, according to the trypan blue assay, except when using a light dose of 3.7 J cm^{-2} and $AlPcS_4$ of 10 µM, all other conditions had significant viability changes at the confidence interval of 95 %. The absence of significant changes to the viabilities could have been due to lack of not generating sufficient oxidative stress environments.

5.11 Overall conclusion from the LDH assay measurements

The cells that were induced to undergo necrosis or fragmentation could not be detected flow cytometrically or using trypan blue assay. Hence LDH assay was used as a complementary technique to measure the levels of LDH present in the supernatants collected, thereby to account for the relative number of cells that would have undergone necrosis to release their cytosolic components, including their LDH enzymes into the suspended medium. The results were used along with the calibration curves in **Figures 5.1** and **5.2** to estimate the numbers of cells that could have possibly be fragmented. For the MBOSR the cell concentrations were maintained within the range of 0.5 - 1.5 x 10^6 cells ml^{-1}, and 1 ml cell suspension was used, following the reactions the supernatants (1 ml) were collected and analysed.

The supernatants collected at 0 hour for the samples *photosensitiser dark-toxicity* and *photodynamically sensitised* contained $AlPcS_4$, while the supernatants of the other two samples did not. All supernatants collected after 2.5 and 24 hours contained complete RPMI-1640 medium. The background absorbance signal for RPMI-1640 medium containing 1 % FBS and phenol red indicator was 0.37 ± 0.02 a.u., for the complete medium

[containing penicillin-streptomycin (final concentration, 100 U ml^{-1}), FBS (10 %) and phenol red indicator] was 0.59 ± 0.05 a.u., and the background absorbance of an indicator-free RPMI-1640 only medium was 0.047 ± 0.001 a.u..

The samples analysed after longer incubation time had higher levels of LDH in their supernatants, which was true for both controls and treated samples. It implied, with time the cells do undergo necrosis even if they were not treated. Under all the conditions tested for the MBOSR, the LDH levels at 0, 2.5 and 24 hours, varied between 0.05 - 0.30, 0.69 - 1.37 and 1.02 - 2.61 a.u., respectively. The higher levels of LDH indicated higher level of ROS generation, and hence the induction of necrosis or fragmentation and *vice versa*. Among all the conditions, the top three higher levels of LDH releases were recorded for the samples analysed after 24 hours of incubation, and were for the samples treated under the conditions; 3.7 J cm^{-2} together with 100 µM, 9.1 J cm^{-2} together with 100 µM, and 11.6 J cm^{-2} together with 10 µM, and their absorbance values were 2.60, 2.34 and 2.50 a.u., respectively (**Table 5.3**). Whereas for the controls, the maximum level of absorbance recorded was 1.200 a.u., even when incubated for 24 hours.

Table 5.3: *Levels of LDH released in the photodynamically sensitised samples, analysed using LDH assay. SD errors of n=3.*

Light dose (J cm^{-2})	**$AlPcS_4$ (µM)**	**Time (hours)**	**LDH levels (a.u.)**
3.7	10	0	0.09 ± 0.02
		2.5	0.69 ± 0.01
		24	1.02 ± 0.08
	100	0	0.056 ± 0.003
		2.5	1.05 ± 0.04
		24	2.60 ± 0.30
9.1	10	0	0.23 ± 0.07
		2.5	0.89 ± 0.08
		24	2.10 ± 0.40
	100	0	0.10 ± 0.01
		2.5	1.40 ± 0.30
		24	2.34 ± 0.08
11.6	10	0	0.30 ± 0.10
		2.5	1.00 ± 0.10
		24	2.50 ± 0.20
	100	0	0.22 ± 0.06
		2.5	0.86 ± 0.06
		24	1.90 ± 0.20

In a photosensitisation reaction, the successful production of ROS depends on the simultaneous interactions between sensitisers, light energy and oxygen. The levels of oxygen present in an indicator-free RPMI-1640 medium used in the reactions were assumed to be constant as discussed earlier. Out of the two remaining variables, the light dose and the concentration of sensitiser were varied to get diverse conditions for the MBOSR. When only one of these two factors was pushed to a higher level, the oxygen concentration in the medium would not be rapidly depleted. If both sensitiser concentration and the light dose were to be maintained at higher levels, the $^3O_2$ content in the medium would be rapidly lowered, following a higher concentration flux of ROS in the medium only for a short time. When all or most of the oxygen in the medium get used, the photosensitisation reactions will not survive only with the remaining two conditions. In other words, when one of the three mandatory variables required for ROS production become limited, hence will be the levels of ROS production and the subsequent effects observed. Therefore the absorbance levels of LDH released corresponded to the success of the balance attained between the three essential parameters to generate ROS for the OSR.

For example, under the condition, a light dose of 3.7 J cm^{-2} together with $AlPcS_4$ of 100 µM, the LDH level was 2.60 a.u., which was the highest level recorded among all the conditions tested. Using the calibration curve in **Figure 5.2**, the absorbance value corresponded to a cell concentration of 0.5 x 10^6 cells ml^{-1}. From the comparison of LDH assay result with the *percentage recovery* of cells, it was found that the reduction of 30 % cell recovery corresponded to approximately 0.5 x 10^6 cells. In the above condition, the photosensitiser concentration was high and the light dose was low. Hence the $^3O_2$ dissolved in the medium would have been consumed at a slower and a balanced rate. Under the condition with higher levels of light dose (9.1 J cm^{-2}) and $AlPcS_4$ (100 µM), the LDH level recorded after 24 hours was 2.34 a.u.. Under such conditions most of the $^3O_2$ in the medium would have been converted into $^1O_2$ at a faster rate, that is, within few

seconds from the start of the reactions, and nothing much would have happened during the remaining length of irradiation.

Under the conditions, a light dose of 11.6 J cm^{-2} together with $AlPcS_4$ of 10 µM, the LDH level was 2.50 a.u., which was the second highest level recorded among all the conditions tested. In which the light dose was high and the photosensitiser concentration was minimum. As the concentration of $AlPcS_4$ was limited to 10 µM, even when all the sensitiser were to be excited, still the maximum rate of ROS production would be maintained lower and relatively uniform throughout the reactions. Hence, it would generate ROS over a longer period to affect many cells, as the concentration of ROS would not be too concentrated at localised regions or only for a shorter time scale. The number of cells corresponding to this level of LDH was also similar to the one obtained for 2.60 a.u. signal.

5.12 Overall conclusion from the flow cytometric analyses

Flow cytometry results represented the first 10000 events recorded. The results would be biased if the samples were to contain heavily fragmented cells or if their sizes were to be below the FSC threshold limit set.

Cells in healthy stage

In general, the number of cells in the healthy-mode was greater than 82 % in all the controls tested under all the conditions (**Table 5.1**). In contrast, for the *photodynamically sensitised* samples the number of cells in the healthy-mode decreased in response to the extracellular oxidative stress conditions employed. When using 10 µM of $AlPcS_4$ together with the light doses 3.7, 9.1 and 11.6 J cm^{-2}, the relative numbers of cells in the healthy-mode were 93, 93 and 84 % after 2.5 hours, and 86, 67 and 49 % after 24 hours, respectively (**Table 5.2**). When using 100 µM of $AlPcS_4$ together with the light doses 3.7, 9.1 and 11.6 J cm^{-2}, the relative numbers of cells in the healthy-mode were 69, 46 and 34 % after 2.5 hours, and 42, 9 and 11 % after 24 hours, respectively. Hence, the highest and the lowest relative number of healthy cells in the treated samples were 93 % and 9 %,

respectively. At both concentrations of $AlPcS_4$, the number of cells in the healthy-mode decreased when incubated for longer, and a simultaneous increase in the numbers of necrotic cells were observed. Two independent trends were observable, the percentage of cells in the healthy-mode decreased either when the concentration of $AlPcS_4$ was increased or when the strength of the light dose was increased.

Cells in apoptotic stage

Under the conditions, 10 μM of $AlPcS_4$ together with the light doses 3.7, 9.1 and 11.6 J cm^{-2}, the relative numbers of apoptotic cells were 2, 0.4 and 0.4 % after 2.5 hours, and 5, 4 and 6 % after 24 hours, respectively (**Table 5.2**). Under the conditions, 100 μM of $AlPcS_4$ together with the light doses 3.7, 9.1 and 11.6 J cm^{-2}, the relative numbers of apoptotic cells were 4, 0.6 and 2 % after 2.5 hours, and 9, 4 and 2 % after 24 hours, respectively. Hence, the highest and the lowest percentages of apoptotic cells recorded for the treated samples were 9 % and 0.4 %, respectively. At both concentrations of $AlPcS_4$, the relative number of cells in the apoptotic-mode increased or remained the similar when incubated for longer. There were no trends observable between changes in the relative number of apoptotic cells and the concentrations of $AlPcS_4$ or the strength of the light doses delivered.

Cells in necrotic stage

Under the conditions, 10 μM of $AlPcS_4$ together with the light doses 3.7, 9.1 and 11.6 J cm^{-2}, the relative numbers of necrotic cells were 5, 6 and 16 % after 2.5 hours, and 9, 30 and 45 % after 24 hours, respectively (**Table 5.2**). Under the conditions, 100 μM of $AlPcS_4$ together with the light doses 3.7, 9.1 and 11.6 J cm^{-2}, the relative numbers of necrotic cells were 27, 54 and 65 % after 2.5 hours, and 49, 87 and 87 % after 24 hours, respectively. Hence the highest and the lowest relative numbers of necrotic cells in the treated samples were 87 % and 5 %, respectively. At both concentrations of $AlPcS_4$, the relative number of cells in the necrotic-mode increased when incubated for longer. Two independent trends were noticeable, the percentage of cells in the necrotic-mode increased either when the concentration of the photosensitiser was increased, or when the strength of

the light dose was increased. These two trends were opposite to what was observed for the cells in healthy-mode, therefore the increase in the numbers of cells in the necrotic-mode were linked with the decrease in the numbers of cells in the healthy-mode.

5.13 Cells with photosensitiser in solution

To verify if photosensitisers had been internalised during the length of conducting the MBOSR, the cells were incubated with a known concentration (10 or 100 µM) of $AlPcS_4$ for a fixed lengths of time (5, 10, 20 or 30 minutes), and the cells were analysed under a fluorescence microscope. Any internalised $AlPcS_4$ within the cells were excited using a monochromatic light source emitting wavelengths of 385 or 430 nm, and the emission wavelengths (fluorescence) above 610 nm were observed (**Figure 5.33**). The acquisition settings of bandwidth 30 nm, maximum gain of 5 and the acquisition time of 5 s were used for recording the fluorescence images.

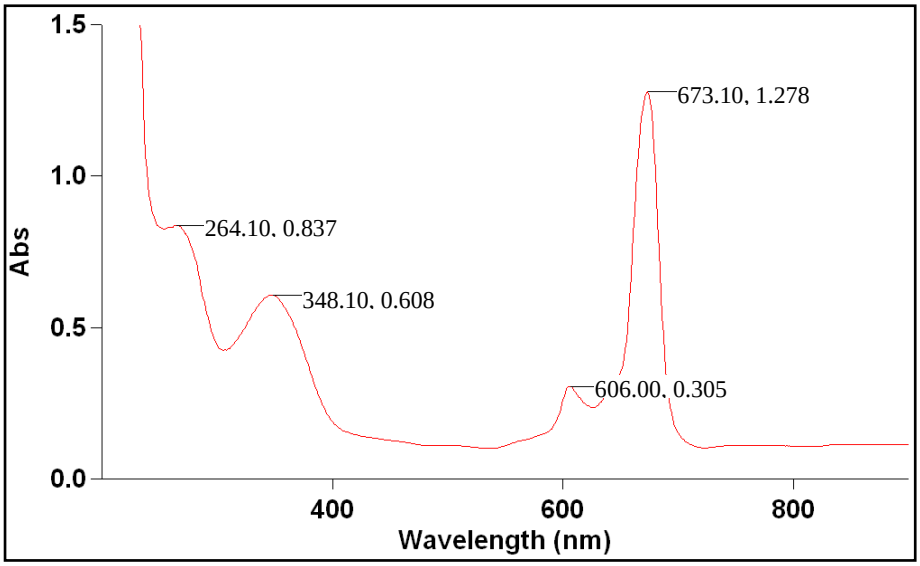

Figure 5.33: *UV-visible absorption spectrum of $AlPcS_4$ dissolved in an indicator-free RPMI-1640 medium.*

No fluorescence were observable from the cells that were incubated with $AlPcS_4$ (10 or 100 µM) for 5, 10 or 20 minutes. The cells incubated with 10 µM of $AlPcS_4$ for 30 minutes also showed no fluorescence, but the cells incubated with 100 µM of $AlPcS_4$ for 30 minutes showed pale fluorescence (hardly detectable), even with the use of 5000 ms of acquisition time. In

other words, the amount of photosensitiser that had been internalised during 20 minutes of contact with $AlPcS_4$ at both concentrations was not sufficient enough to give rise to any detectable fluorescence under the settings specified above. This indicated that adequate amount of $AlPcS_4$ had not been internalised by the cells. Hence it was concluded that, the levels of intracellular oxidative stress environments generated were insufficient to induce photosensitisation effects. Therefore the photosensitisation effects observed during or following the OSR were mainly due to ROS produced extracellular to the cells. A bright field image of COLO320 cells that was captured using acquisition time of only 10 ms is shown in **Figure 5.34**, these cells were previously incubated with $AlPcS_4$ but showed no fluorescence.

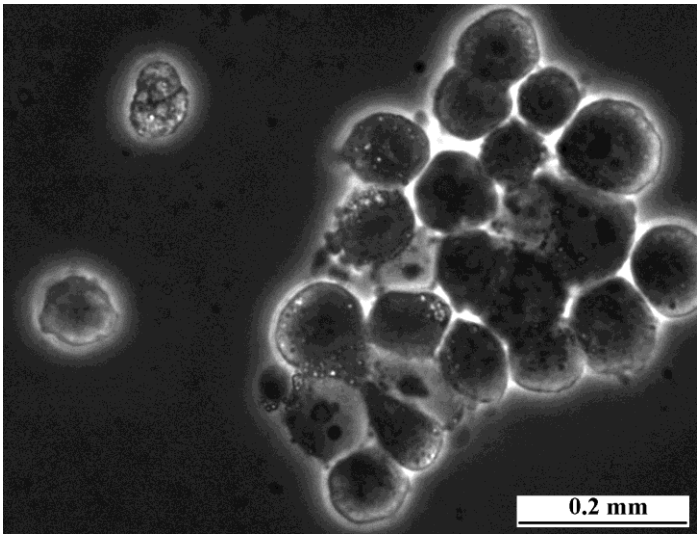

Figure 5.34: *Bright field image of COLO320 cells, using an acquisition time of 10 ms.*

5.14 Summary

The MBOSR were conducted having photosensitiser in solution. Following the reactions, in the *photodynamically sensitised* samples, significant reductions in the total numbers of cells relative to the controls were observed. In addition to minor drop in the number of cells due to unavoidable inefficiencies in replacing the medium (random error), there were some other factor(s) that caused severe reduction in the number of cells. This was studied in detail and was determined to be due to lysis of cells through necrosis as confirmed using haemocytometer, flow cytometry, and LDH assays.

The results also showed that there are links between the modes of cell death, and the conditions and the methods used for the reactions. The cell count measurements using haemocytometer coupled with trypan blue dye, helped in determining decrease in the numbers of cells and their viability. The LDH assays confirmed occurrence of fragmentation associated cellular death, and the flow cytometry measurements were useful in identifying the relative levels of apoptotic and necrotic events induced. The higher levels of necrosis could be due to any of the following reasons. *Firstly*, the concentration of $AlPcS_4$ and the light dose might be equal or higher than what was essential for apoptosis. *Secondly*, the level of ROS produced (oxidative stress generated) extracellular to the cells would have been sufficient, and were in close proximity to the surface of the cells to induce necrosis as the major form of cell death. *Thirdly*, the time points (2.5 or 24 hours) selected for analysis might have been suitable for detecting only necrotic-mode as the major event and not the apoptotic-mode. Hence overall it is an efficient method for the production of extracellular ROS to induce mainly necrotic based cellular disintegrations, as confirmed by the assays. **Section 1.2.2** of **Chapter 1** covers the conventional approach used in photosensitisation reactions, which include localisation of photosensitisers and target of photodamage, the use and effects of PDT on cancer, and discussion on-light (doses) energies used.

Absence of significant differences in-between controls supported the fact that, the effects of oxidative stress observed were due to photosensitisation reactions, and not due to reasons like cytotoxicity of the photosensitiser (*photosensitiser dark-toxicity*), the higher levels of light energy (*light-only toxicity*) or the cells simply disintegrated due to not being at optimum conditions for growth (*untreated*). It was also tested and confirmed that, the amount of extracellular photosensitiser internalised were not sufficient enough to view under a fluorescent microscopy, even with the use of maximum settings together with 5000 ms of acquisition time.

It was also clear from the results that, it would not be possible to measure and confirm all important key effects of extracellular OSR with the use of single type of assay, and multiple methods of analyses were essential to account for at least most of the important effects induced during or following the reactions. Out of all the conditions (**Table 5.1**), $AlPcS_4$ of 10 and 100 μM, analyses times of 2.5 and 24 hours, and the light dose of 9.1 J cm^{-2} corresponding to 83 s of irradiation at the fluence rate of 110 mW cm^{-2}, were selected to test under microfluidic flow settings (**Chapter 6**).

Furthermore, using the results discussed in this chapter for support, it is also emphasized that the use of small clear transparent and completely sealable containers, for example polypropylene tubes like in this chapter, are more efficient for conducting MBOSR in microfluidic styles. It would also enable high throughput screening of many different combinations of conditions required for the generation of various levels of oxidative stress essential for PDT-type reactions.

CHAPTER 6 - Microfluidic flow oxidative stress reactions

6.1 Microfluidic flow oxidative stress reactions

This chapter covers the microfluidic flow oxidative stress reactions (MFOSR) carried out having photosensitiser ($AlPcS_4$) in solution to generate extracellular ROS. The conditions that were recognised as optimum at inducing higher levels of photosensitisation effects in the microbatch oxidative stress reactions (MBOSR, **Chapter 5**) were utilised. Following the reactions, the induced photosensitisation effects were studied by determining the *percentage recoveries*, the *percentage viabilities*, the levels of LDH released and the modes of cellular disintegrations.

6.1.1 The conditions used for the reactions

The use of lower flow rates (**Sections 2.2.1.2** and **2.3.1** of **Chapter 2**) to increase the light dose led to considerable reduction in the number of cells collected for analysis. There were two other possibilities to increase the light dose without reducing the flow rates. One was to increase the fluence rate and the other was to increase the length of the channels thereby the residence time. The fluence rate was increased by incorporating an identical second LED array, where the combined fluence rate from the two LED arrays was 110 mW cm^{-2}. At this fluence rate irradiation for 34 s delivered a total light dose of 3.7 J cm^{-2}, which was achievable with the use of 3 cm long parallel channels and a flow rate of ~21 µl min^{-1}.

It was identified from the MBOSR (**Chapter 5**), with the use of a light dose of 3.7 J cm^{-2}, the strengths of the photosensitisation effects were lower than what was obtained using 9.1 J cm^{-2}. The total light energy delivered was dependent on the length of exposure to irradiation, for microfluidic flow reactions it is dependent on the residence time of cells within the channels. Hence to increase the light dose while maintaining the flow rate (~21 µl min^{-1}) and the fluence rate (110 mW cm^{-2}) constant, the lengths of the parallel channels were increased to 7 cm, thereby the residence time was increased to 83 s, which facilitated delivering light dose of 9.1 J cm^{-2}.

In this chapter, the microfluidic chip **Design 6** (page 180) with 7 cm long 16-parallel channels was used. The chips were fabricated by isotropically etching the **Design 6** to the depths of 60 or 120 µm, where the 60 µm depth channels were made according to the method described under the **Section 2.4.2** of **Chapter 2**, and the 120 µm depth channels were fabricated by bonding two etched slides (each of 60 µm depth) to make the total channel depth of 120 µm. The results corresponding to the use of 60 µm depth are presented in the first half of the chapter and the remaining half discuss the results corresponding to the use of 120 µm depth.

In this chapter three variables were tested, while maintaining six others constant. The three variables were the depth of the channels (60 or 120 µm), the concentration of the photosensitiser (10 or 100 µM), and the time intervals of analysis (2.5 or 25 hours), which made a total of 8 combinations (**Table 6.1**). The six fixed variables were the type of cell line (COLO320), the type of photosensitiser ($AlPcS_4$), the chip design (**Design 6**), the light source (LED array), the level of oxygen concentration (< 8.9 mg dm^{-3}) and the amount of light dose (9.1 J cm^{-2}). Each set of experiments were repeated a minimum of three times and the presented standard deviation error bars correspond to it.

Table 6.1: *The conditions used for the MFOSR with the photosensitiser in solution.*

Fluence (J cm^{-2})	**Channel depth (µm)**	**Concentration (µM)**	**Time (hours)**
9.1	60	10	2.5
			24.0
		100	2.5
			24.0
	120	10	2.5
			24.0
		100	2.5
			24.0

6.1.2 The types of samples used for the reactions

In MFOSR, COLO320 cells were mixed together with 10 or 100 µM of $AlPcS_4$, which was dissolved in an indicator-free RPMI-1640 medium free of phenol red, FBS, and penicillin and streptomycin. The cells were flowed through microfluidic chips and the treated cells were collected at the outlets. Similar to the MBOSR, in the MFOSR a total of four samples were used for each experiment, which included three controls and a treated sample. The samples were labelled as *untreated*, *photosensitiser dark-toxicity*, *photodynamically sensitised* and *light-only toxicity*.

The cells stood in an indicator-free RPMI-1640 medium in the dark at RTP without photosensitiser was referred to as the *untreated* sample. This was used as the complete control, that is, to act as a reference point for comparing the results from the remaining three samples and was highly useful for determining the expected *percentage recovery* of cells. The cells mixed with the photosensitiser containing medium and flowed through microfluidic channels at a fixed flow rate for the same length of time as for the *photodynamically sensitised* sample, but without irradiation was referred as the *photosensitiser dark-toxicity* control. This control was used to account for any changes to the number of cells or their viabilities as a result of flowing through the channels, while being in contact with $AlPcS_4$. The cells mixed with the photosensitiser containing medium and flowed through microfluidic channels at a fixed flow rate (~21 µl min^{-1}) to deliver the intended amount of light dose (9.1 J cm^{-2}) was referred as the *photodynamically sensitised* sample, which was the sample under test. The cells suspended in an indicator-free RPMI-1640 medium and flowed through microfluidic channels at a fixed known flow rate to deliver the same amount of light dose as that for the *photodynamically sensitised* sample was referred as the *light-only toxicity* control, which was used to demonstrate that, flowing cells through microfluidic channels and the light energy on their own would not induce cell death.

Following the reactions, the samples were repeatedly washed using fresh indicator-free RPMI-1640 medium, to isolate the cells from the

photosensitiser containing medium. The cells were incubated for 2.5 or 24 hours at 37 ^{o}C, 5 % CO_2 and 95 % humidity, before being analysed using haemocytometer coupled with trypan blue assay to determine the percentages of cells recovered and their viabilities. The levels of LDH present in the supernatants were measured to estimate the fraction of cells fragmented. The ratio of apoptosis and necrosis were also measured using flow cytometry together with fluorescent indicators, annexin-V:FITC and PI, respectively.

6.2 $AlPcS_4$ of 10 µM and channel depth of 60 µm

The samples treated under the conditions; light dose of 9.1 J cm^{-2}, $AlPcS_4$ of 10 µM and the channel depth of 60 µm, were measured after 2.5 and 24 hours of incubations, using haemocytometer to determine the changes to the number of cells recovered (**Figure 6.1**). The assessment of the data and the statistical analysis, at both time intervals of analysis showed that, the *photodynamically sensitised* sample was not significantly different from any of the controls, and decrease (32 - 72 % and 43 - 63 %, 2.5 and 24 hours, respectively) in the number of cells for all the samples, except the *untreated* control (100 %) was observable. Furthermore, the results were highly variable as indicated by the large error bars. Based on the interpretations of the results in **Figure 6.1**, it was concluded, that there were no significant differences identified under the above conditions. However, it was known from the MBOSR carried out under similar conditions, that the above conditions should have produced significant variation in the *photodynamically sensitised* sample relative to the controls. Flowing cells through chip leads to reduction in the number of cells recovered, and it also gives rise to higher variation in the number of cells collected. Hence it was also clear that the *percentage recovery* of cells in a flow setup influences the interpretation of the results.

The changes to the viability of cells after 2.5 and 24 hours of incubation were determined in terms of percentages using trypan blue assay. The assessment of the data (**Figure 6.2**) and the statistical analysis showed that

there were no significant changes to the viability of cells at both time intervals of analysis, viabilities for the samples were in the ranges of 93 - 95 and 90 - 92 %, after 2.5 and 24 hours, respectively. The comparison of results in **Figures 6.1** and **6.2** show that, the number of cells recovered was highly variable, but not their viability, which was true at both time intervals.

The levels of LDH released immediately (0 hour) after the oxidative stress reactions (OSR), and after 2.5 and 24 hours, were measured. The assessment of the data in **Figure 6.3** showed that the level of LDH released for the *photodynamically sensitised* sample was not significantly different from all the controls, at the time intervals considered.

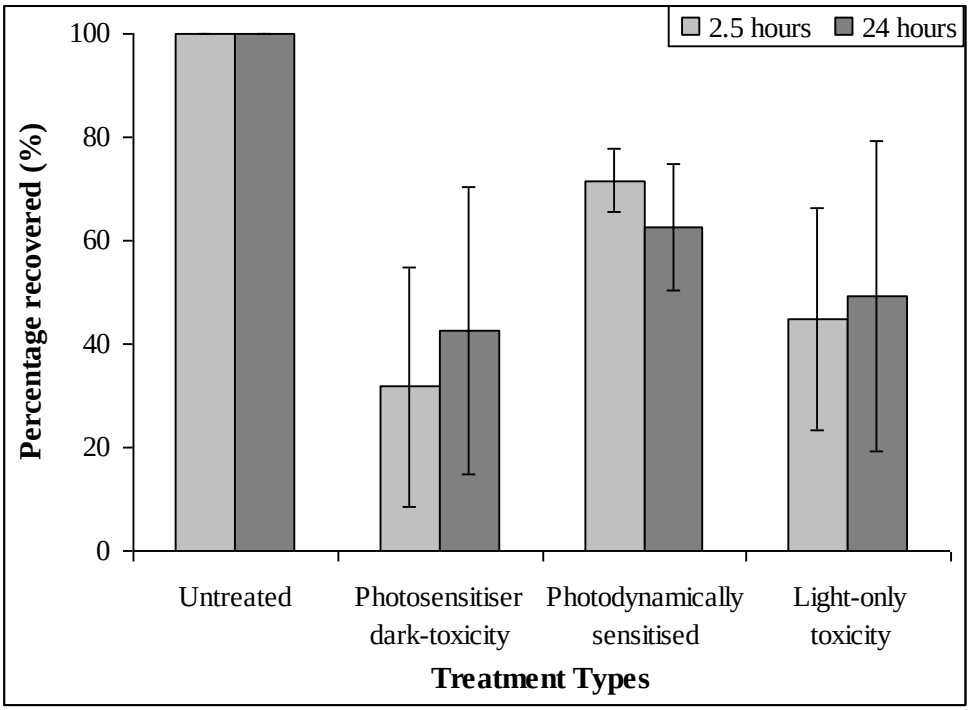

Figure 6.1: *The effects of MFOSR with photosensitiser in solution on the total recovery of cells, compared against three controls under the same conditions; 10 μM of AlPcS$_4$, fluence of 9.1 J cm^{-2}, cells flowed through microfluidic chip (***Design 6***, 60 μm depth) and were analysed using haemocytometer after 2.5 and 24 hours of incubations. Standard deviation error bars with n=3.*

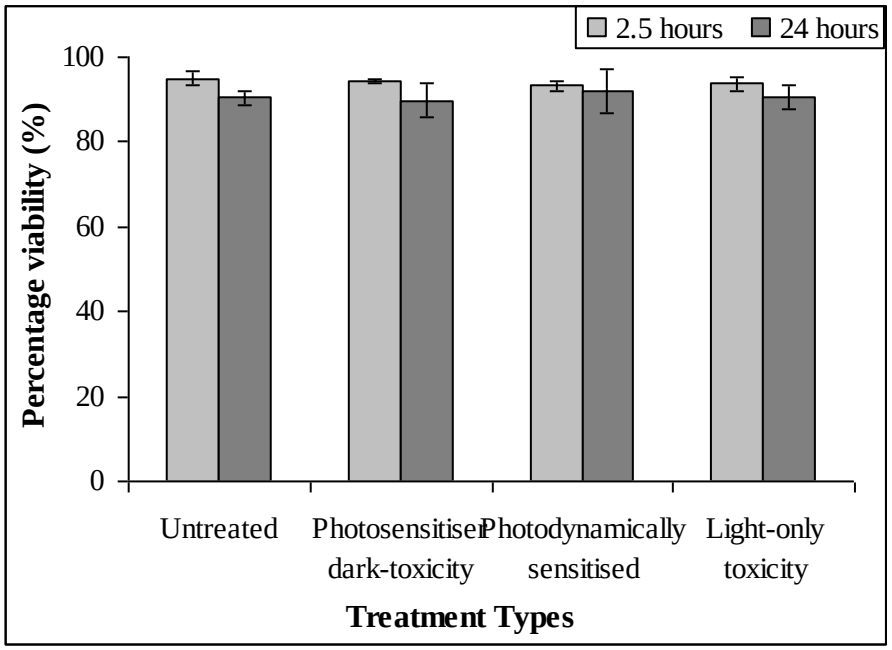

Figure 6.2: *The effects of MFOSR with photosensitiser in solution on the total viability of cells, compared against three controls under the same conditions; 10 μM of $AlPcS_4$, fluence of 9.1 J cm^{-2}, cells flowed through microfluidic chip (***Design 6***, 60 μm depth) and were analysed using trypan blue and haemocytometer after 2.5 and 24 hours of incubations. Standard deviation error bars with n=3.*

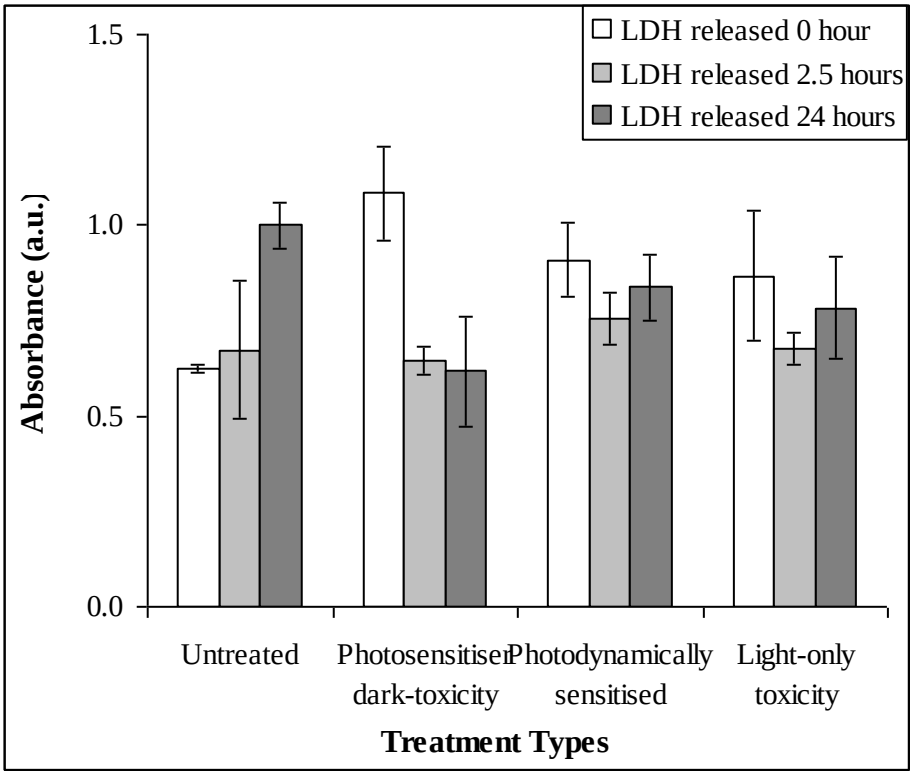

Figure 6.3: *The effects of MFOSR with photosensitiser in solution on the levels of LDH released soon after OSR and during 2.5 and 24 hours of incubations, compared against three controls under the same conditions; 10 μM of $AlPcS_4$, fluence of 9.1 J cm^{-2} and cells flowed through* **Design 6** *chip of 60 μm depth. Standard deviation error bars for n=3.*

The changes to the viability of cells and the induction of apoptotic and necrotic pathways after 2.5 (**Figure 6.4**) and 25 (**Figure 6.5**) hours from the reactions were determined flow cytometrically. Statistical analysis showed no significant difference from all the controls, for the three modes considered in each analysis.

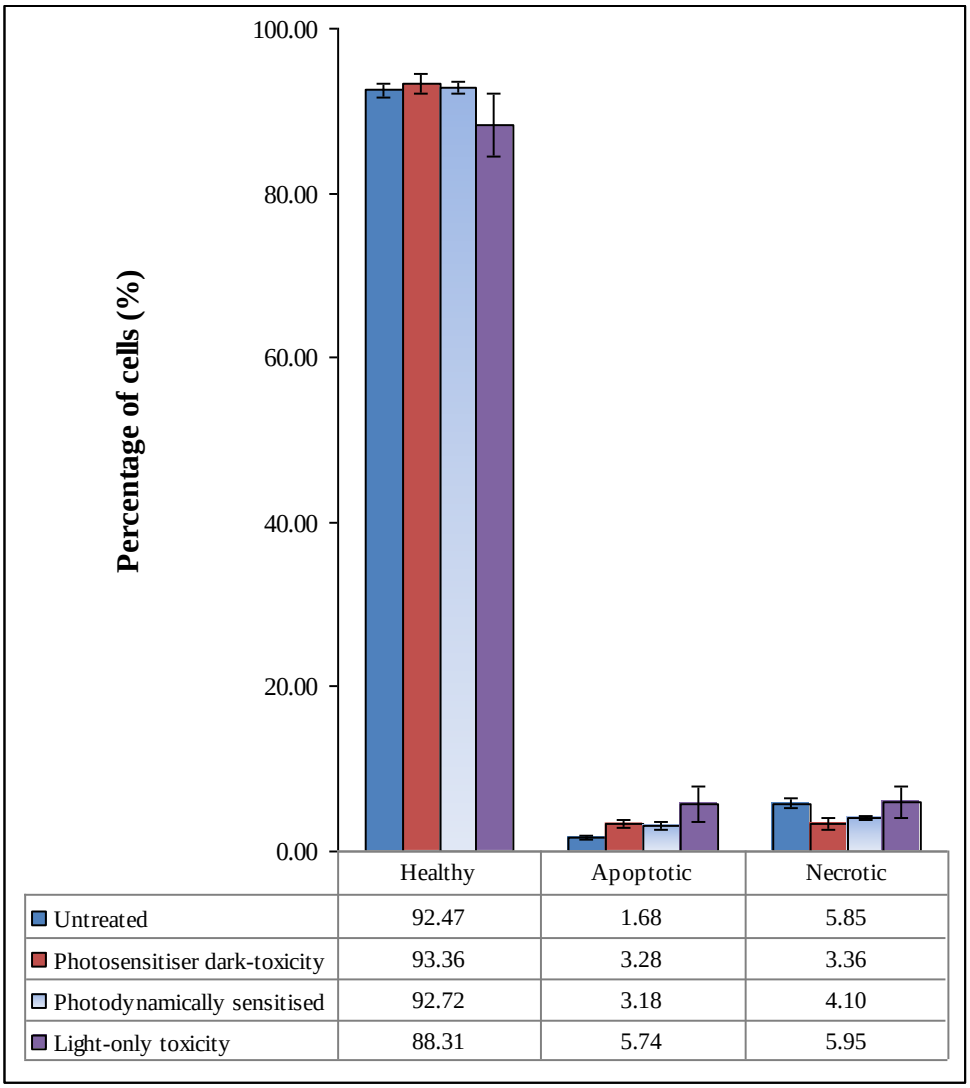

	Healthy	Apoptotic	Necrotic
Untreated	92.47	1.68	5.85
Photosensitiser dark-toxicity	93.36	3.28	3.36
Photodynamically sensitised	92.72	3.18	4.10
Light-only toxicity	88.31	5.74	5.95

Figure 6.4: *The effects of MFOSR with photosensitiser in solution on the viability, and the induction of apoptotic and necrotic pathways, compared against three controls under the same conditions; 10 μM of $AlPcS_4$, fluence of 3.7 J cm^{-2}, cells flowed through microfluidic chip (***Design 6***, 60 μm depth) and were analysed using flow cytometry after 2.5 hours. Standard deviation error bars for n=3.*

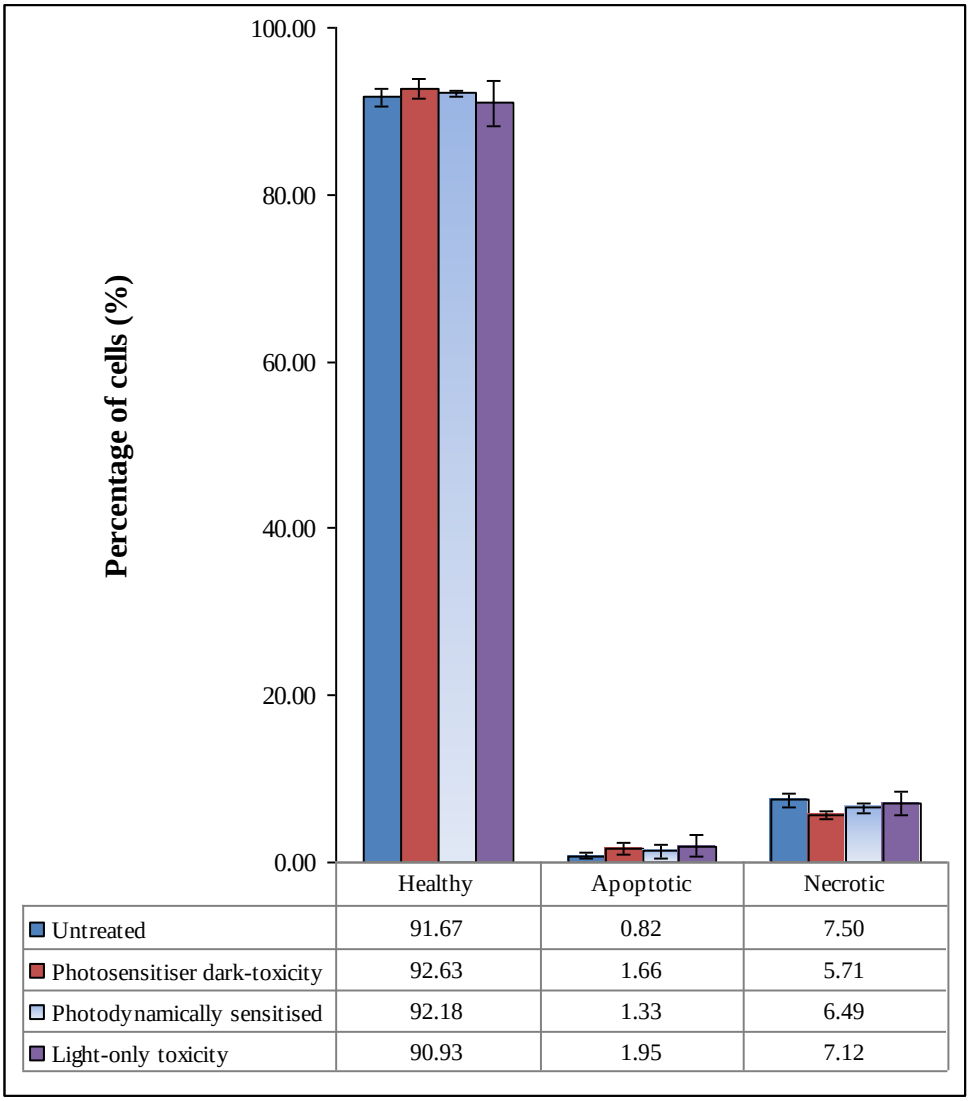

	Healthy	Apoptotic	Necrotic
Untreated	91.67	0.82	7.50
Photosensitiser dark-toxicity	92.63	1.66	5.71
Photodynamically sensitised	92.18	1.33	6.49
Light-only toxicity	90.93	1.95	7.12

Figure 6.5: *The effects of MFOSR with photosensitiser in solution on the viability, and the induction of apoptotic and necrotic pathways, compared against three controls under the same conditions; 10 μM of $AlPcS_4$, fluence of 9.1 J cm^{-2}, cells flowed through microfluidic chip (***Design 6***, 60 μm depth) and were analysed using flow cytometry after 24 hours. Standard deviation error bars for n=3.*

6.3 $AlPcS_4$ of 100 µM and channel depth of 60 µm

The samples treated under the conditions; light dose of 9.1 J cm^{-2}, $AlPcS_4$ of 100 µM and the channel depth of 60 µm, were measured after 2.5 and 24 hours (**Figure 6.6**). At both time intervals of analysis, the number of cells recovered for all the samples flowed through the chip were lower (37 - 77 % and 49 - 85 %, after 2.5 and 24 hours respectively), relative to the *untreated* control (100 %). The results were highly variable with no significant differences. The percentage recovery of 85 %, after 24 hours from the treatment for the *photosensitiser-dark-toxicity* sample was the highest level recorded among all the samples that were flowed through chip.

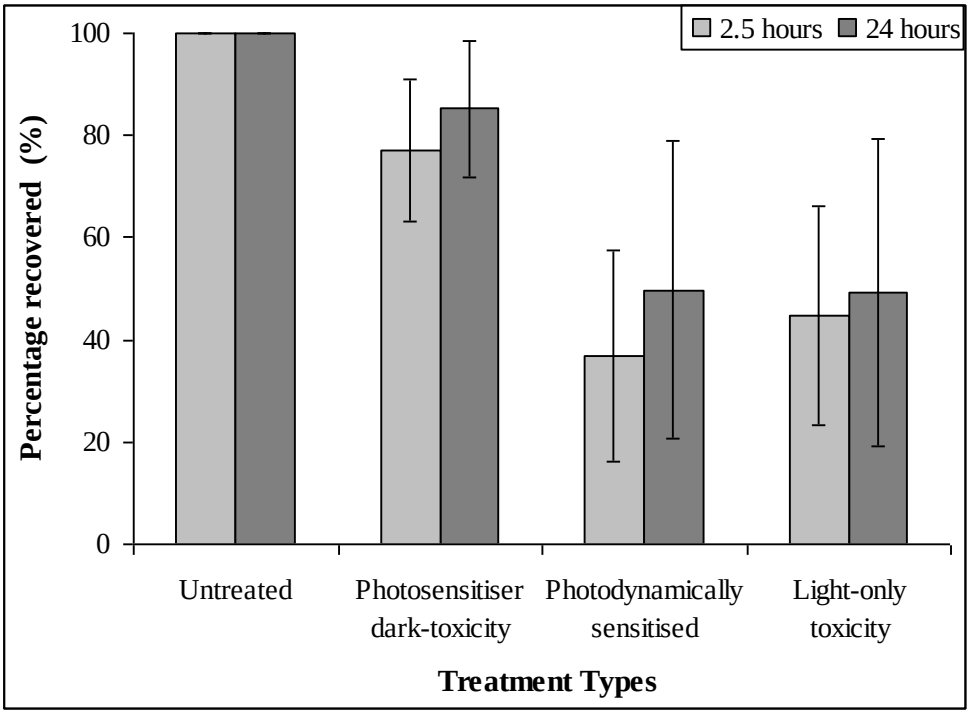

Figure 6.6: *The effects of MFOSR with photosensitiser in solution on the total recovery of cells, compared against three controls under the same conditions; 100 µM of $AlPcS_4$, fluence of 9.1 J cm^{-2}, cells flowed through microfluidic chip (***Design 6***, 60 µm depth) and were analysed using haemocytometer after 2.5 and 24 hours. Standard deviation error bars with n=3.*

The changes to the viability of cells after 2.5 and 24 hours of incubation showed that the number of viable cells varied between 86 - 95 % and 82 - 91 % respectively (**Figure 6.7**), and the statistical analysis showed that there were no significant differences. Further, the *percentage viability* of 82.38 %, was the lowest level of cell viability recorded under tryphan blue assay measurements described in this chapter.

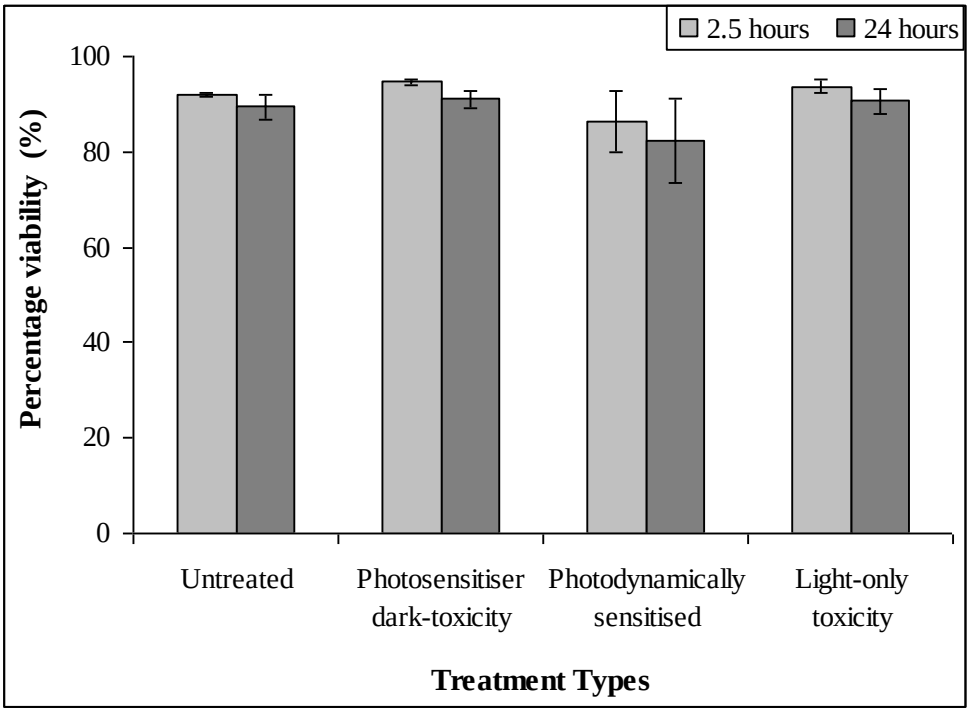

Figure 6.7: *The effects of MFOSR with photosensitiser in solution on the total viability of cells, compared against three controls under the same conditions; 100 μM of $AlPcS_4$, fluence of 9.1 J cm^{-2}, cells flowed through microfluidic chip (***Design 6***, 60 μm depth) and were analysed using trypan blue and haemocytometer after 2.5 and 24 hours of incubation. Standard deviation error bars with n=3.*

The levels of LDH released immediately (0 hour) after the OSR was measured, and the statistical analysis showed presence of significant difference ($p < 0.0001$). From the assessment of the data for 0 hour in **Figure 6.8**, it was found that the significant difference was due to the lower level of LDH released for the *photodynamically sensitised* sample, relative to the controls. In addition to the reduction in the strength of the signal due to fluorescence, the lower number of cells recovered (**Figure 6.6**) was also partly responsible. The levels of LDH released for the *photodynamically*

sensitised sample during 2.5 and 24 hours of incubations, were not significantly different from all the controls.

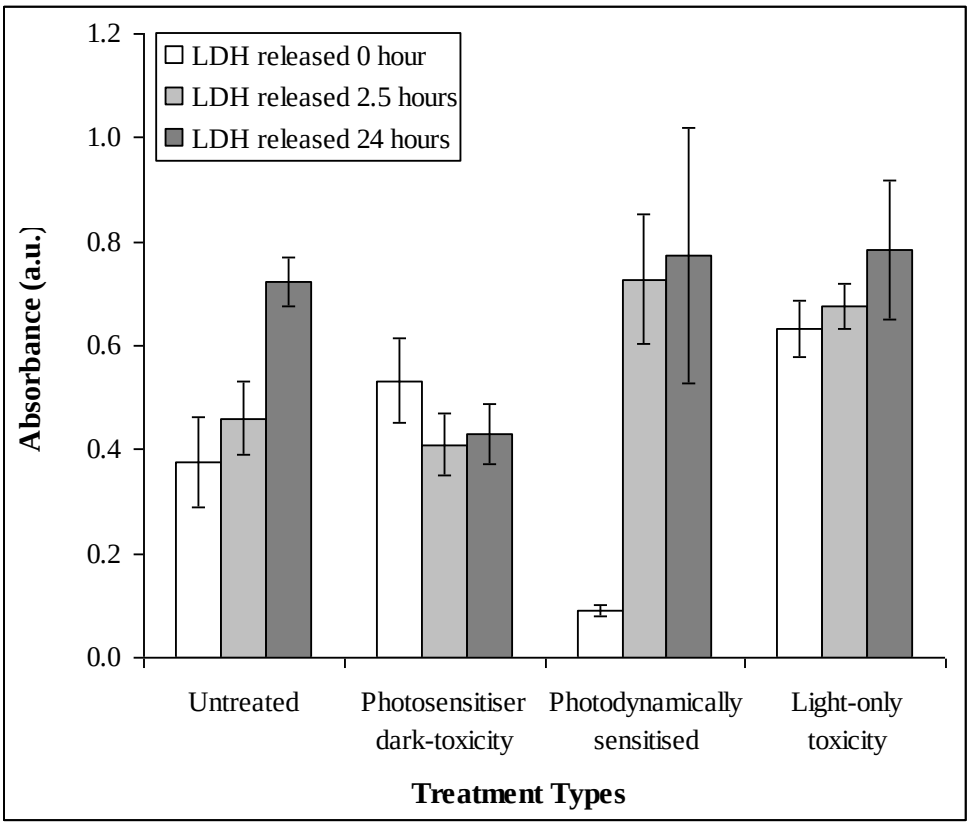

Figure 6.8: *The effects of MFOSR with photosensitiser in solution on the levels of LDH released soon after OSR and during 2.5 and 24 hours of incubations, compared against three controls under the same conditions; 100 μM of $AlPcS_4$, fluence of 9.1 J cm^{-2} and cells flowed through* **Design 6** *chip of 60 μm depth. Standard deviation error bars for n=3.*

The changes to the viability of cells and the induction of apoptotic and necrotic pathways after 2.5 (**Figure 6.9**) and 24 (**Figure 6.10**) hours from the reactions were determined, and the results were statistically analysed. The assessment of the data in **Figure 6.9** showed that, the numbers of cells in the healthy-mode decreased but was not significantly different from all the controls, the number of apoptotic cells were similar in all the samples, and the number of cells in the necrotic-mode increased significantly (p = 0.0007) from the controls.

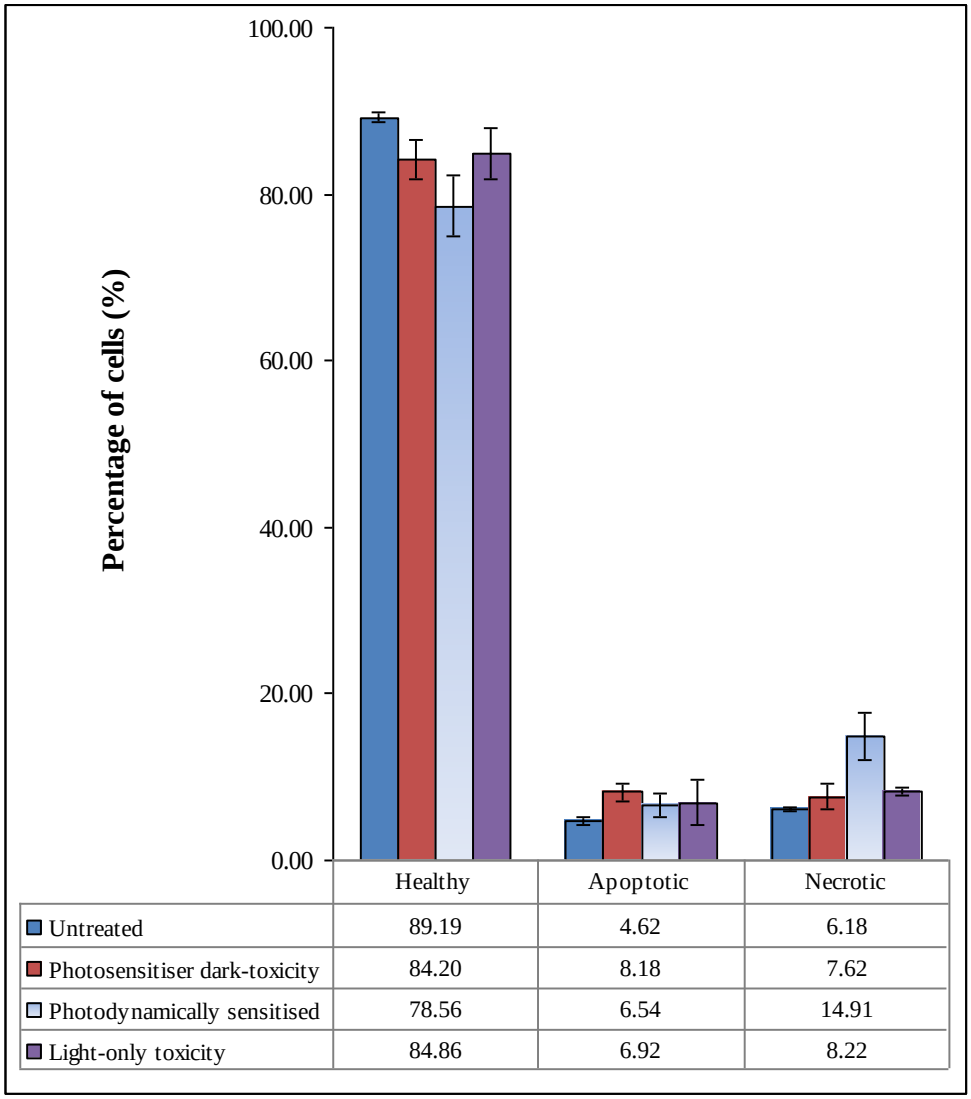

	Healthy	Apoptotic	Necrotic
Untreated	89.19	4.62	6.18
Photosensitiser dark-toxicity	84.20	8.18	7.62
Photodynamically sensitised	78.56	6.54	14.91
Light-only toxicity	84.86	6.92	8.22

Figure 6.9: *The effects of MFOSR with photosensitiser in solution on the viability, and the induction of apoptotic and necrotic pathways, compared against three controls under the same conditions; 100 μM of $AlPcS_4$, fluence of 9.1 J cm^{-2}, cells flowed through microfluidic chip (***Design 6***, 60 μm depth) and were analysed using flow cytometry after 2.5 hours. Standard deviation error bars for n=3.*

The analysis of the data in **Figure 6.10** showed that, the numbers of cells in the healthy-mode decreased significantly ($p < 0.0001$), the number of cells were similar in the apoptotic-mode, and the number of cells in the necrotic-mode increased significantly ($p < 0.0001$). Using the data in **Figures 6.6** to **6.10**, it was noticeable that, the conditions predominantly induced necrosis and not apoptosis. This is consistent with the MBOSR, and illustrates predominant effect of extracellular oxidative stress induced disintegration.

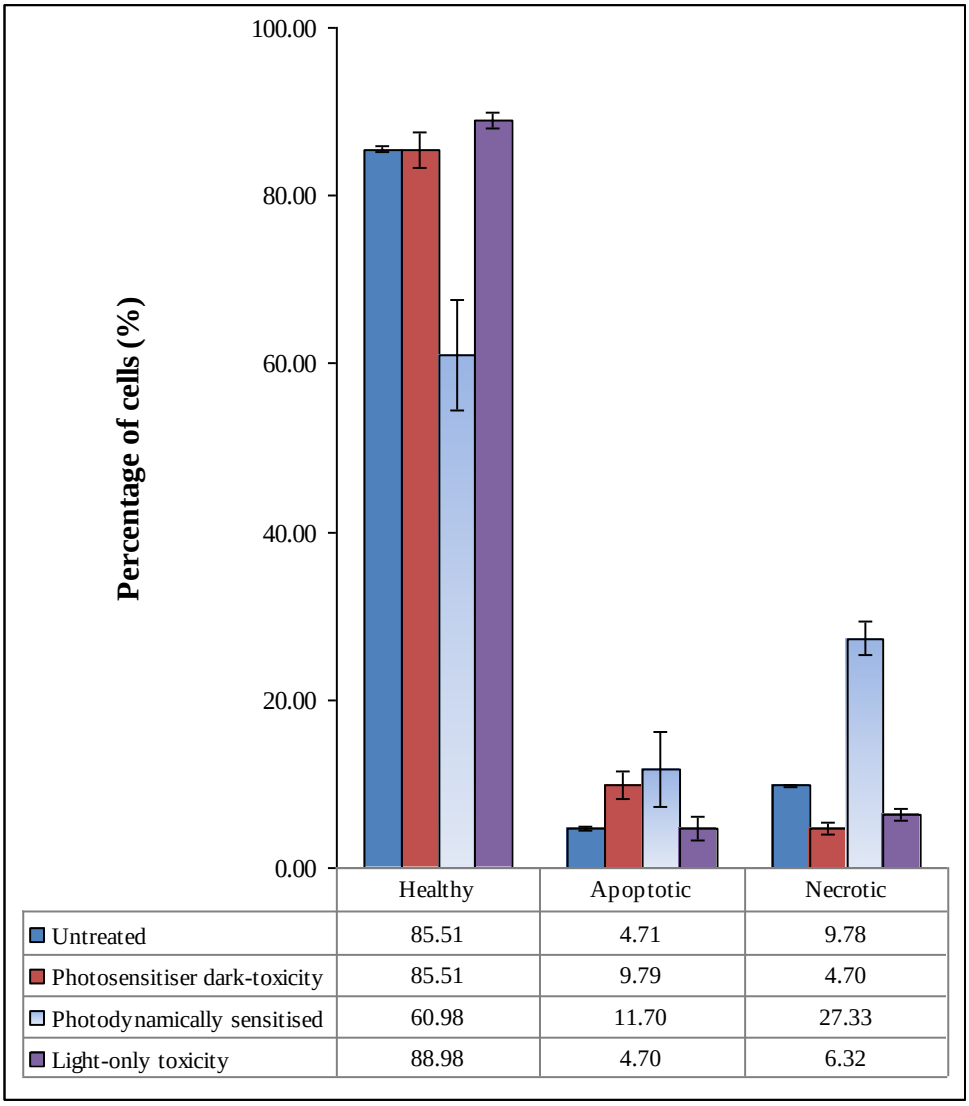

	Healthy	Apoptotic	Necrotic
Untreated	85.51	4.71	9.78
Photosensitiser dark-toxicity	85.51	9.79	4.70
Photodynamically sensitised	60.98	11.70	27.33
Light-only toxicity	88.98	4.70	6.32

Figure 6.10: *The effects of MFOSR with photosensitiser in solution on the viability, and the induction of apoptotic and necrotic pathways, compared against three controls under the same conditions; 100 μM of $AlPcS_4$, fluence of 9.1 J cm^{-2}, cells flowed through microfluidic chip (***Design 6***, 60 μm depth) and were analysed using flow cytometry after24 hours. Standard deviation error bars for n=3.*

6.4 $AlPcS_4$ of 10 µM and channel depth of 120 µm

The samples treated under the conditions; light dose of 9.1 J cm^{-2}, $AlPcS_4$ of 10 µM and the channel depth of 120 µm, were measured after 2.5 and 24 hours of incubations to determine changes to the number of cells recovered (**Figure 6.11**). The assessment of the data and the statistical analysis at both time intervals showed that, there were no significant difference or the significance was only identified against a single control. The number of cells recovered in the samples flowed through the chip were lower (35 - 64 % and 32 - 60 %, after 2.5 and 24 hours, respectively), relative to the *untreated* control (100 %), and the results were highly variable with no significant differences. The results after 24 hours of incubation were also in agreement with the LDH assay (**Figure 6.13**) and the flow cytometry results (**Figure 6.15**).

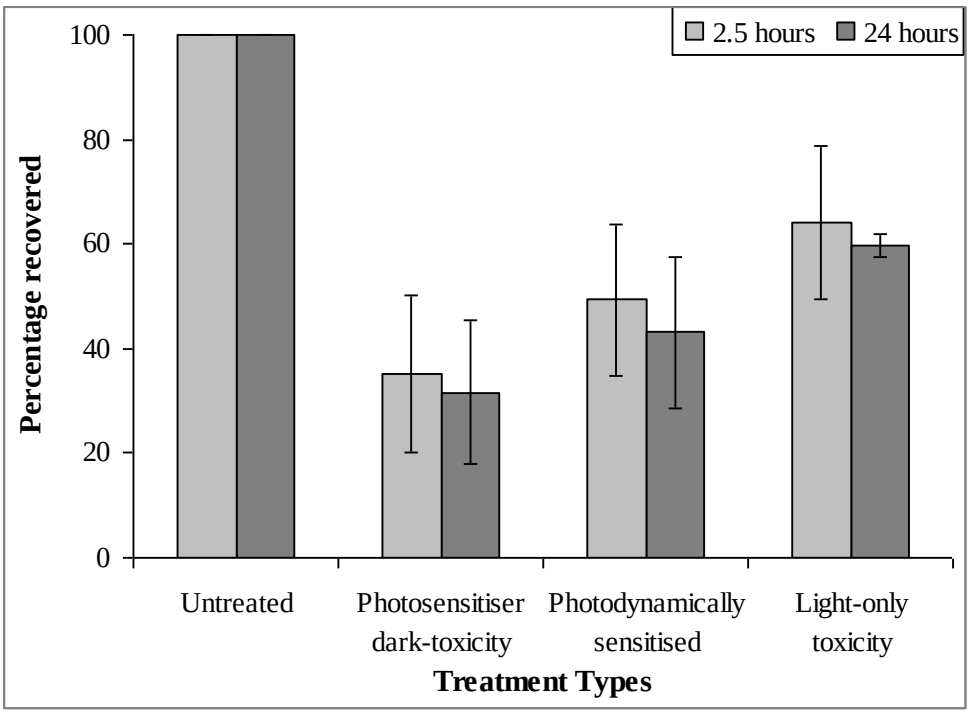

Figure 6.11: *The effects of MFOSR with photosensitiser in solution on the total recovery of cells, compared against three controls under the same conditions; 10 µM of $AlPcS_4$, fluence of 9.1 J cm^{-2}, cells flowed through microfluidic chip (***Design 6***, 120 µm depth) and were analysed using haemocytometer after 2.5 and 24 hours. Standard deviation error bars with n=3.*

The data (**Figure 6.12**) and the statistical analysis for changes to the viability of cells after 2.5 and 24 hours of incubation showed that, the viability was in the range of 94 - 96 and 92 - 94 %, respectively, for all the samples, and there were no significant difference at both time intervals. The data in **Figures 6.11** and **6.12** clearly show that the number of cells recovered and viability both provides different information, that is, though the number of cells recovered were lower and highly variable for all the samples flowed through chips, but their viabilities were similar to the *untreated* sample (healthy cells).

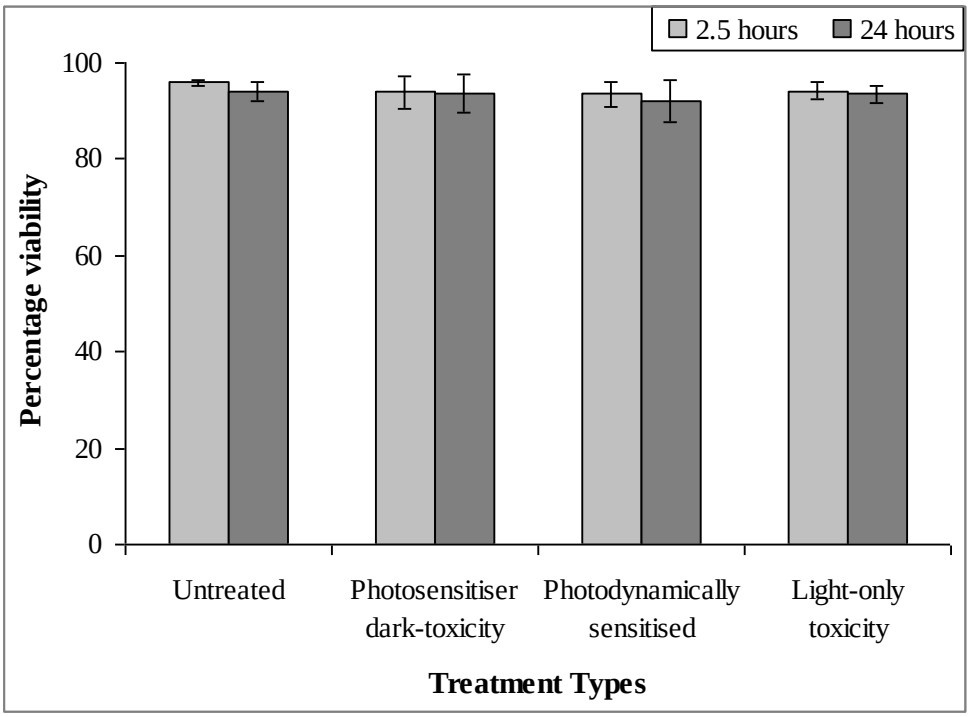

Figure 6.12: *The effects of MFOSR with photosensitiser in solution on the total viability of cells, compared against three controls under the same conditions; 10 μM of $AlPcS_4$, fluence of 9.1 J cm^{-2}, cells flowed through microfluidic chip (***Design 6***, 120 μm depth) and were analysed using trypan blue and haemocytometer after 2.5 and 24 hours of incubation. Standard deviation error bars with n=3.*

The levels of LDH released immediately after the OSR, and after 2.5 and 24 hours were measured. The assessment of the data in **Figure 6.13** showed that, the level of LDH released for the *photodynamically sensitised* sample was not significantly different from all the controls at all three time intervals considered. Similar levels of LDH levels for the controls and the *photodynamically sensitised* samples were the direct consequence of higher variations in the number of cells recovered (**Figure 6.11**).

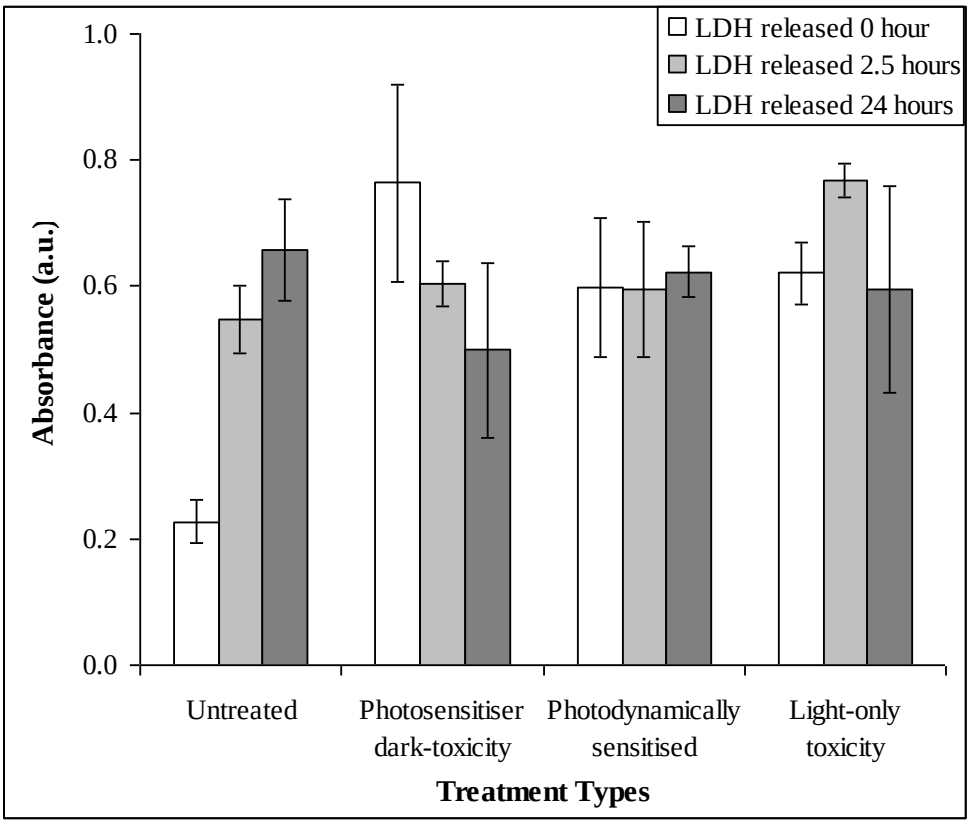

Figure 6.13: *The effects of MFOSR with photosensitiser in solution on the levels of LDH released soon after OSR and during 2.5 and 24 hours of incubations, compared against three controls under the same conditions; 10 μM of $AlPcS_4$, fluence of 9.1 J cm^{-2} and cells flowed through* **Design 6** *chip of 120 μm depth. Standard deviation error bars for n=3.*

The changes to the viability of cells, and the induction of apoptotic and necrotic pathways after 2.5 (**Figure 6.14**) and 25 (**Figure 6.15**) hours from the reactions were determined flow cytometrically. The statistical analysis showed no significant difference from all the controls, for all three modes at each time intervals.

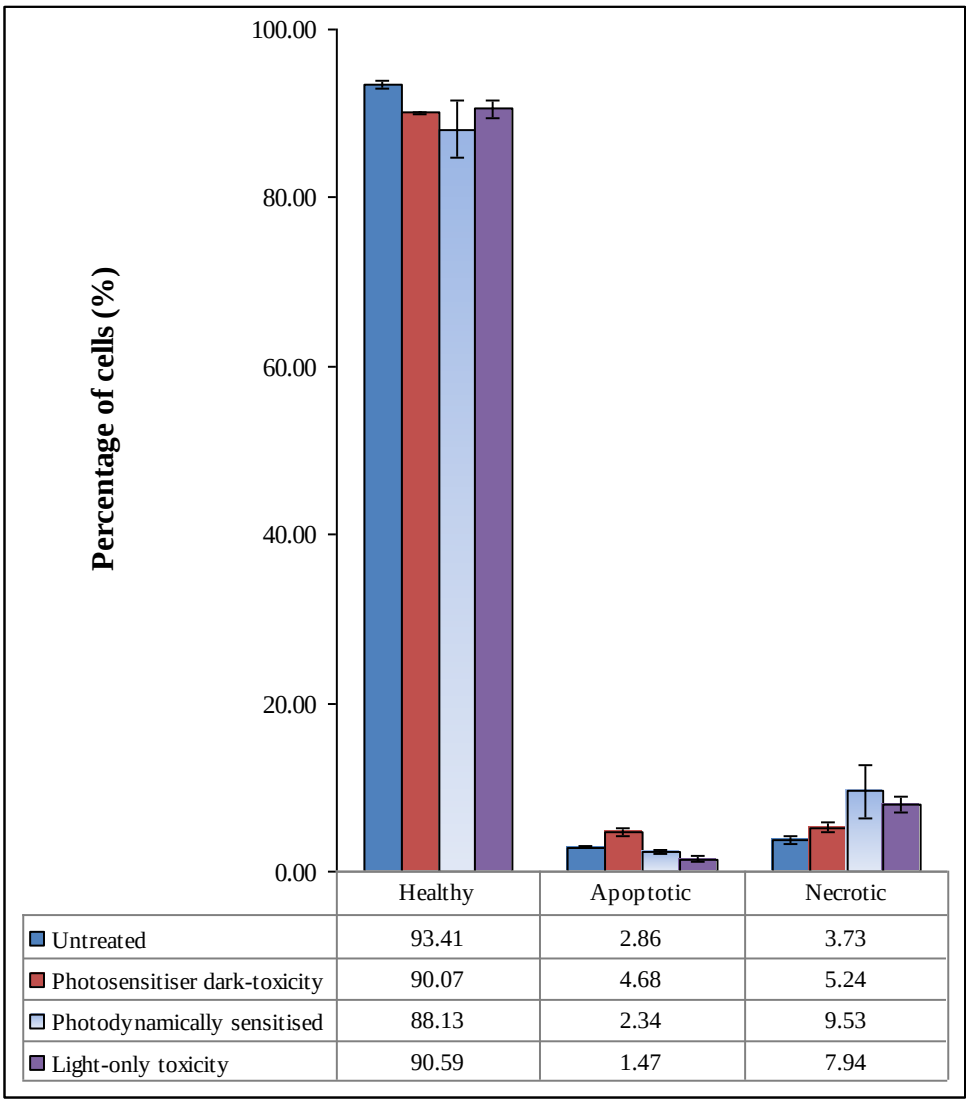

	Healthy	Apoptotic	Necrotic
Untreated	93.41	2.86	3.73
Photosensitiser dark-toxicity	90.07	4.68	5.24
Photodynamically sensitised	88.13	2.34	9.53
Light-only toxicity	90.59	1.47	7.94

Figure 6.14: *The effects of MFOSR with photosensitiser in solution on the viability, and the induction of apoptotic and necrotic pathways, compared against three controls under the same conditions; 10 μM of $AlPcS_4$, fluence of 9.1 J cm^{-2}, cells flowed through microfluidic chip (***Design 6***, 120 μm depth) and were analysed using flow cytometry after 2.5 hours. Standard deviation error bars for n=3.*

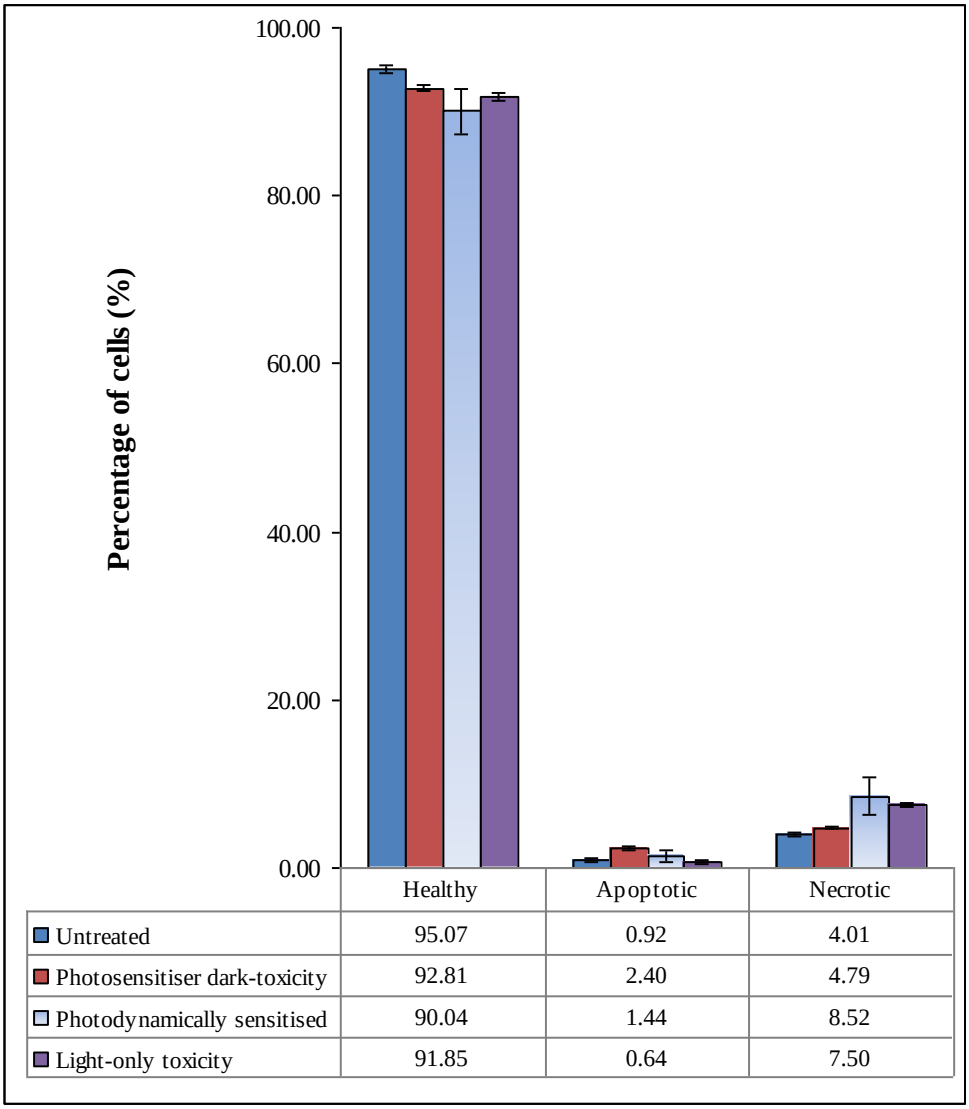

	Healthy	Apoptotic	Necrotic
Untreated	95.07	0.92	4.01
Photosensitiser dark-toxicity	92.81	2.40	4.79
Photodynamically sensitised	90.04	1.44	8.52
Light-only toxicity	91.85	0.64	7.50

Figure 6.15: *The effects of MFOSR with photosensitiser in solution on the viability, and the induction of apoptotic and necrotic pathways, compared against three controls under the same conditions; 10 μM of $AlPcS_4$, fluence of 9.1 J cm^{-2}, cells flowed through microfluidic chip (***Design 6***, 120 μm depth) and were analysed using flow cytometry after 24 hours. Standard deviation error bars for n=3.*

6.5 $AlPcS_4$ of 100 µM and channel depth of 120 µm

The samples treated under the conditions; light dose of 9.1 J cm^{-2}, $AlPcS_4$ of 100 µM and the channel depth of 60 µm, were measured after 2.5 and 24 hours (**Figure 6.16**). At both time intervals of analysis, the number of cells recovered for the samples flowed through the chip were lower (40 - 64 % and 38 - 60 %, after 2.5 and 24 hours, respectively), relative to the *untreated* control (100 %). Furthermore, the results were highly variable and had no significant differences.

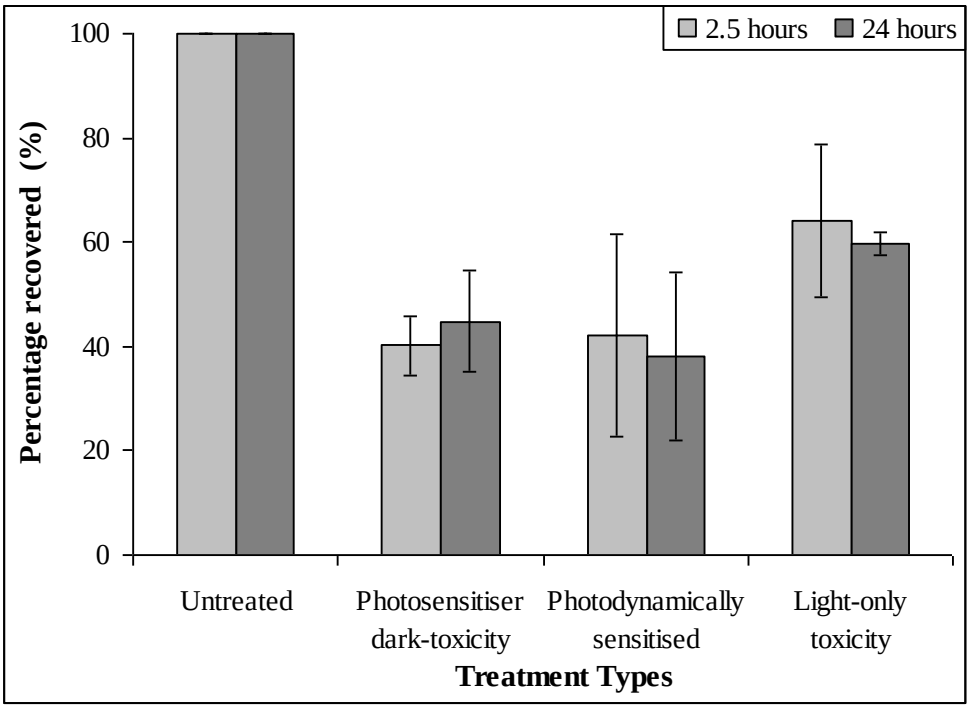

Figure 6.16: *The effects of MFOSR with photosensitiser in solution on the total recovery of cells, compared against three controls under the same conditions; 100 µM of $AlPcS_4$, fluence of 9.1 J cm^{-2}, cells flowed through microfluidic chip (***Design 6***, 120 µm depth) and were analysed using haemocytometer after 2.5 and 24 hours. Standard deviation error bars with n=3.*

The changes to the viability of cells after 2.5 and 24 hours of incubation were measured, the number of viable cells varied between 85 - 96 % and 85 - 95 % respectively (**Figure 6.17**), and the statistical analysis showed that there were no significant differences.

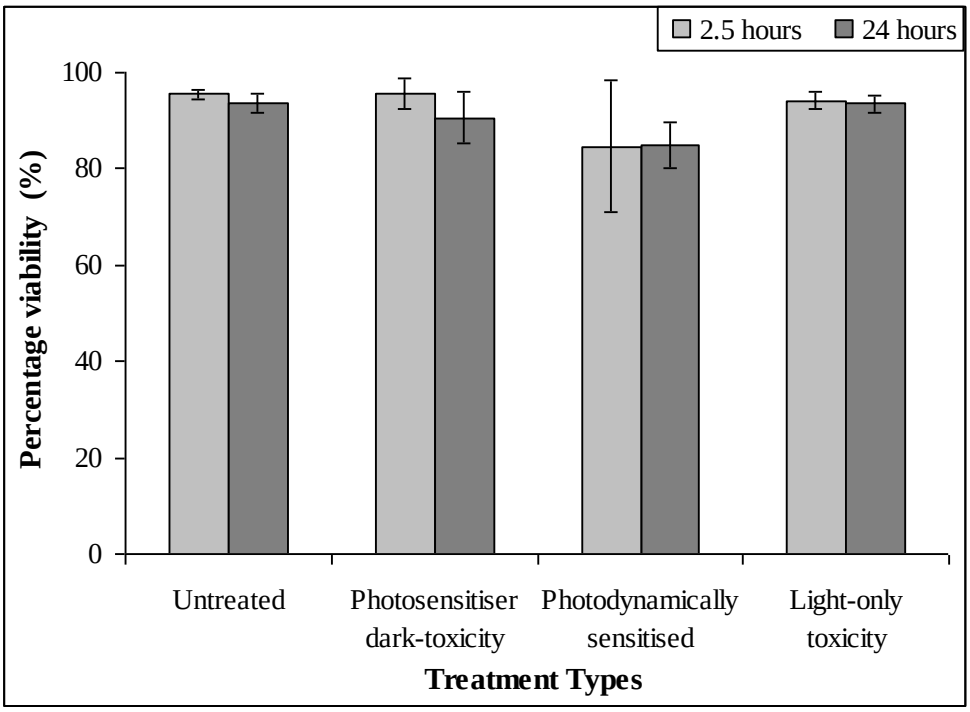

Figure 6.17: *The effects of MFOSR with photosensitiser in solution on the total viability of cells, compared against three controls under the same conditions; 100 μM of $AlPcS_4$, fluence of 9.1 J cm^{-2}, cells flowed through microfluidic chip (***Design 6***, 120 μm depth) and were analysed using trypan blue and haemocytometer after 2.5 and 24 hours of incubation. Standard deviation error bars with n=3.*

The levels of LDH released immediately after the OSR, and after 2.5 and 24 hours were measured. The assessment of the data in **Figure 6.18** showed that, the level of LDH released for the *photodynamically sensitised* sample was not statistically significantly different from all the controls at all the time intervals considered. The similar levels of LDH for the controls and the *photodynamically sensitised* samples were the direct consequence of higher variations in the number of cells recovered (**Figure 6.16**).

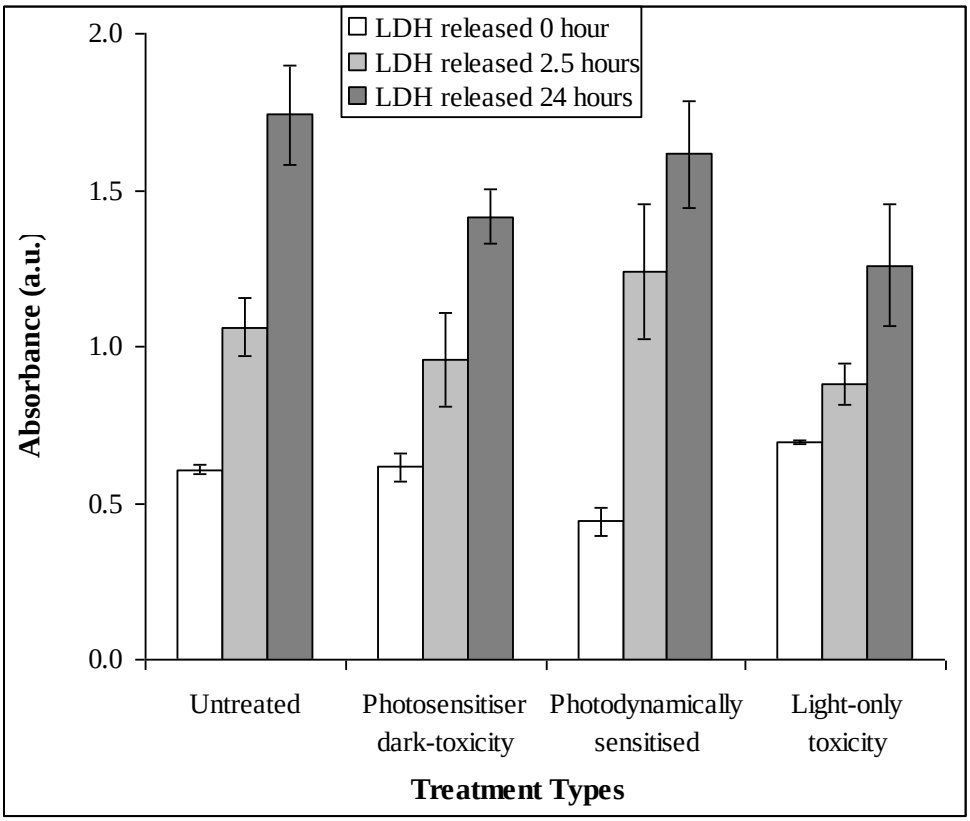

Figure 6.18: *The effects of MFOSR with photosensitiser in solution on the levels of LDH released soon after OSR and during 2.5 and 24 hours of incubations, compared against three controls under the same conditions; 100 μM of $AlPcS_4$, fluence of 9.1 J cm^{-2} and cells flowed through* **Design 6** *chip of 120 μm depth. Standard deviation error bars for n=9.*

The changes to the viability of cells, and the induction of apoptotic and necrotic pathways after 2.5 (**Figure 6.19**) and 24 (**Figure 6.20**) hours were measured. The statistical analysis showed that, following the OSR, at both time intervals of analysis, the number of cells in the healthy-mode decreased (after 2.5 and 24 hours, p = 0.01 and p = 0.006, respectively), and in the necrotic-mode increased (after 2.5 and 24 hours, p = 0.009 and p = 0.006, respectively) significantly from all the controls, while no significant difference was observed in the apoptotic-mode. The conditions predominantly induced necrosis which was consistent with the photosensitisation effect of extracellular oxidative stress induced disintegration.

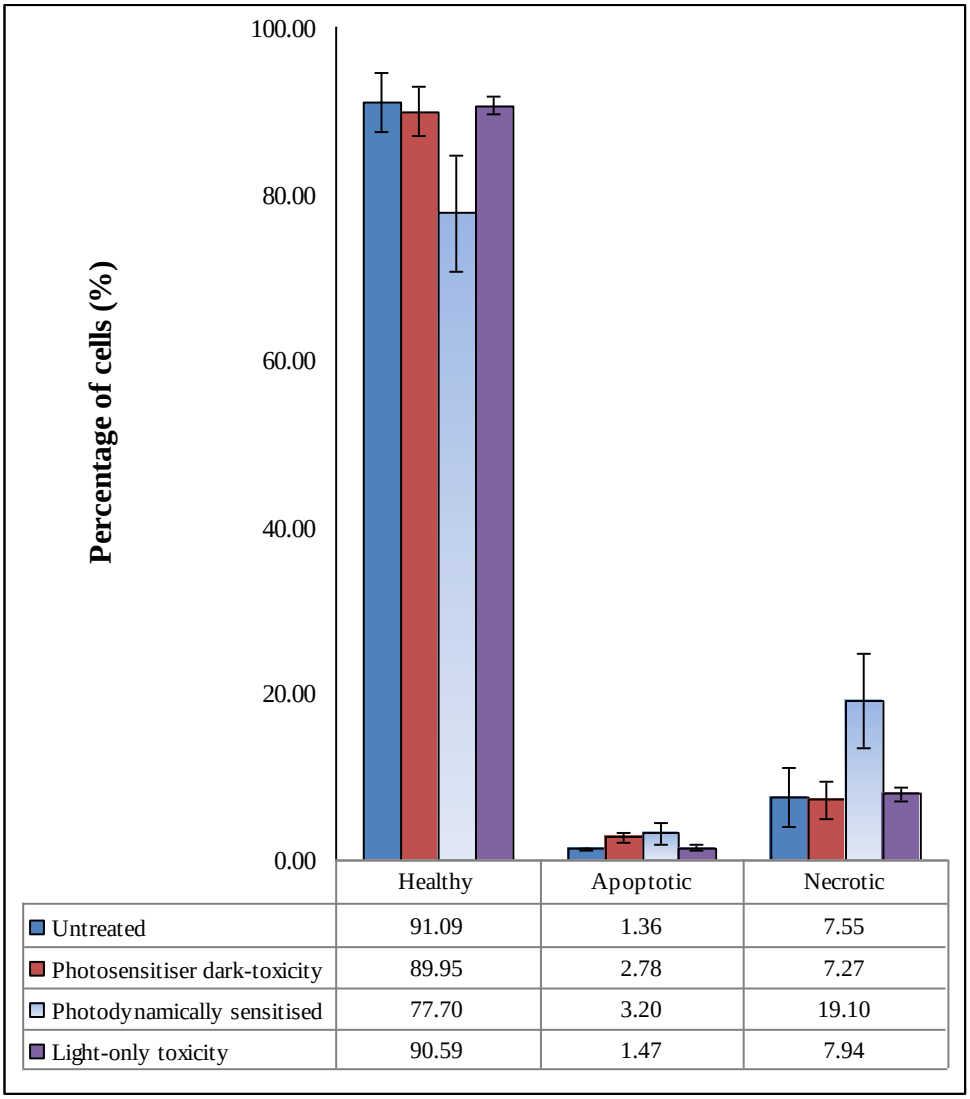

	Healthy	Apoptotic	Necrotic
Untreated	91.09	1.36	7.55
Photosensitiser dark-toxicity	89.95	2.78	7.27
Photodynamically sensitised	77.70	3.20	19.10
Light-only toxicity	90.59	1.47	7.94

Figure 6.19: *The effects of MFOSR with photosensitiser in solution on the viability, and the induction of apoptotic and necrotic pathways, compared against three controls under the same conditions; 100 μM of $AlPcS_4$, fluence of 9.1 J cm^{-2}, cells flowed through microfluidic chip (***Design 6***, 120 μm depth) and were analysed using flow cytometry after 2.5 hours. Standard deviation error bars for n=3.*

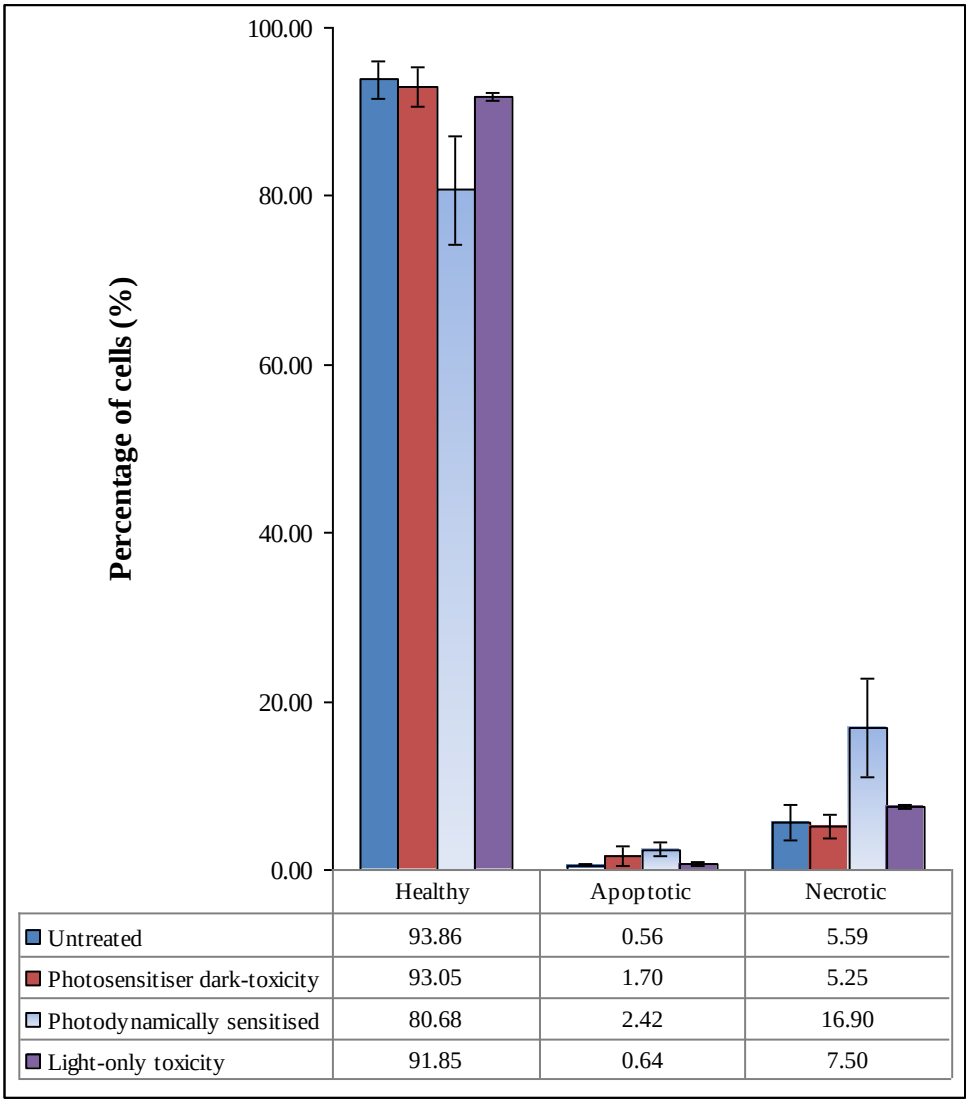

	Healthy	Apoptotic	Necrotic
Untreated	93.86	0.56	5.59
Photosensitiser dark-toxicity	93.05	1.70	5.25
Photodynamically sensitised	80.68	2.42	16.90
Light-only toxicity	91.85	0.64	7.50

Figure 6.20: *The effects of MFOSR with photosensitiser in solution on the viability, and the induction of apoptotic and necrotic pathways, compared against three controls under the same conditions; 100 μM of AlPcS$_4$, fluence of 9.1 J cm^{-2}, cells flowed through microfluidic chip (***Design 6***, 120 μm depth) and were analysed using flow cytometry after 24 hours. Standard deviation error bars for n=3.*

6.6. Overall findings from the trypan blue assays

6.6.1 Recovery of cells

Similar to the previous chapter, the percentage of cells recovered in the *untreated* control was normalised as 100 %, and all other samples were compared against it. The number of cells recovered in the samples flowed through chips were always lower than in the corresponding *untreated* control. The number of cells recovered in the *photodynamically sensitised* samples under the conditions, a light dose of 9.1 J cm^{-2}, $AlPcS_4$ of 10 µM, and flowed through the channel depths of 60 and 120 µm were 72 and 49 % after 2.5 hours, and 62 and 43 % after 24 hours, respectively (**Table 6.2**). When the concentration of $AlPcS_4$ was increased to 100 µM, the numbers of cells recovered were 37 and 42 % after 2.5 hours, and 50 and 38 % after 24 hours, respectively. Hence the highest and the lowest *percentage recoveries* for the *photodynamically sensitised* samples were 72 and 37 %, respectively.

Table 6.2: *Recovery and viability of cells, and healthy, apoptotic and necrotic ratios of cells in the photodynamically sensitised samples determined using trypan blue and flow cytometric analyses respectively. SD errors of n=3.*

			Trypan blue assay		**Flow cytometric analysis**		
Channel depth (µm)	**$AlPcS_4$ (µM)**	**Time (hours)**	**Recovery (%)**	**Viability (%)**	**Healthy (%)**	**Apoptotic (%)**	**Necrotic (%)**
60	10	2.5	72 ± 6	93 ± 1	93 ± 1	3.2 ± 0.5	4.1 ± 0.3
		24	62 ± 12	92 ± 5	92.2 ± 0.4	1 ± 1	6 ± 1
	100	2.5	37 ± 21	86 ± 6	79 ± 4	7 ± 1	15 ± 3
		24	50 ± 29	82 ± 9	61 ± 7	12 ± 5	27 ± 2
120	10	2.5	49 ± 14	94 ± 3	88 ± 3	2.3 ± 0.4	10 ± 3
		24	43 ± 15	92 ± 4	90 ± 3	1 ± 1	9 ± 2
	100	2.5	42 ± 19	85 ± 14	78 ± 7	3 ± 1	19 ± 6
		24	38 ± 16	85 ± 5	81 ± 6	2 ± 1	17 ± 6

In general, the *percentage recoveries* for all the samples flowed through chips (60 and 120 µm) were within the range of 32 – 85 %. For both channel depths, an increase in the concentration of $AlPcS_4$ from 10 to 100 µM decreased the number of cells recovered. The total number of cells collected were always lower than the number of cells flowed in, which was mainly due to the experimental setup alone, as indicated by the controls. As the number of cells recovered varied widely, it interfered with the determination

of the effects induced only by the OSR. This was the case nearly in all the results discussed.

6.6.2 Viability of cells

The changes in the viability of cells were determined using haemocytometer coupled with trypan blue dye. In general, the *percentage viability* was greater than 89 % for all the controls tested under all the conditions (**Table 6.1**). The number of viable cells in the *photodynamically sensitised* samples under the conditions, light dose of 9.1 J cm^{-2}, $AlPcS_4$ of 10 µM, and channel depths of 60 and 120 µm were 93 and 94 % after 2.5 hours, and 92 and 92 % after 24 hours, respectively (**Table 6.2**). When the concentration of $AlPcS_4$ was increased to 100 µM, the number of viable cells were 86 and 85 % after 2.5 hours, and 82 and 85 % after 24 hours, respectively. Hence the highest and the lowest relative numbers of viable cells in the *photodynamically sensitised* samples were 94 % and 82 %. It was observable that for both channel depths, an increase in the concentration of $AlPcS_4$ from 10 to 100 µM decreased the number of viable cells. It was also found that, the number of viable cells decreased or remained similar when stored for 24 hours (longer) relative to 2.5 hours. Further, for both concentrations of $AlPcS_4$, an increase in the depth of the channels did not show any influence on the number of viable cells.

6.7 Overall findings from the LDH assays

In the LDH assay, higher absorption signal indicated presence of higher levels of LDH, which in turn implied that more number of cells had been disintegrated releasing their cytosolic contents. Unlike in the MBOSR, in MFOSR at time 0 hour, the levels of LDH highly varied, which denoted higher difference in the number of cells fragmented. The higher variations in the number of cells disintegrated were mainly attributed to the discrepancies in the levels of blocking, backpressure and shear-stress force, on the cells flowed through the flow system. Under the MFOSR, for the *photodynamically sensitised* samples, at time 0 hour the LDH levels varied between 0.09 - 0.91 a.u. (**Table 6.3**), whereas in the MBOSR carried out under similar conditions, the LDH levels were 0.10 and 0.23 a.u., at 9.1 J

cm^{-2}, and 10 and 100 µM of $AlPcS_4$, respectively. At the time intervals of 2.5 and 24 hours of analyses, in the *photodynamically sensitised* samples of the MFOSR, the LDH levels varied between 0.60 – 1.24 a.u. and 0.62 - 1.62 a.u., respectively (**Table 6.3**), whereas for the *photodynamically sensitised* samples in the MBOSR, the LDH levels were 0.89 and 1.34 a.u., and 2.07 and 2.34 a.u., at 9.1 J cm^{-2}, and 10 and 100 µM of $AlPcS_4$, respectively (**Table 5.3**). Hence, under both microbatch and microfluidic flow OSR, the levels of LDH increased between the incubation times of 2.5 and 24 hours. The maximum level of LDH released under the microfluidic flow reaction condition was 1.62 a.u., which corresponded to about 0.2 x 10^6 cells.

Table 6.3: *Levels of LDH released in the photodynamically sensitised samples, analysed using LDH assay. SD errors of n=3.*

Channel depth (µm)	$AlPcS_4$ (µM)	Time (hours)	LDH levels (a.u.)
60	10	0	0.91 ± 0.10
		2.5	0.76 ± 0.07
		24	0.84 ± 0.09
	100	0	0.09 ± 0.01
		2.5	0.70 ± 0.10
		24	0.80 ± 0.20
120	10	0	0.60 ± 0.10
		2.5	0.60 ± 0.10
		24	0.62 ± 0.04
	100	0	0.44 ± 0.05
		2.5	1.20 ± 0.20
		24	1.60 ± 0.20

6.8 Overall findings from the flow cytometric analysis

Cells in healthy stage - This section summarises the flow cytometry results obtained. For all the controls tested under all the conditions, the number of cells in the healthy-mode was greater than 84 %. In contrast, for the *photodynamically sensitised* samples the number of cells in the healthy-mode decreased up to 61 %, under the conditions, a light dose of 9.1 J cm^{-2}, channel depth of 60 µm, $AlPcS_4$ of 100 µM and analysed after 24 hours. This was the highest reduction in the number of healthy cells recorded out of all the conditions in **Table 6.1**. The number of cells in the healthy-mode under the conditions, a light dose of 9.1 J cm^{-2}, $AlPcS_4$ of 10 µM, and channel depths of 60 and 120 µm were 93 and 88 % after 2.5 hours, and 92 and 49 % after 24 hours, respectively (**Table 6.2**). When the concentration of $AlPcS_4$ was increased to 100 µM, the numbers of cells in the healthy-

mode were 79 and 78 % after 2.5 hours, and 61 and 81 % after 24 hours, respectively. Hence the highest and the lowest number of healthy cells present in the *photodynamically sensitised* samples were 93 % and 61 %, respectively. For both channel depths, an increase in the concentration of $AlPcS_4$ from 10 to 100 µM decreased the number of cells in the healthy-mode. Only for the samples treated using 60 µm depth channels, the number of healthy cells decreased when incubated for longer.

Cells in apoptotic stage - The number of cells in the apoptotic-mode under the conditions, a light dose of 9.1 J cm^{-2}, $AlPcS_4$ of 10 µM, and channel depths of 60 and 120 µm were 3 and 2 % after 2.5 hours, and 1 and 1 % after 24 hours, respectively (**Table 6.2**). When the concentration of $AlPcS_4$ was increased to 100 µM, the numbers of cells in the apoptotic-mode were 7 and 3 % after 2.5 hours, and 12 and 2 % after 24 hours, respectively. Hence the highest and the lowest number of apoptotic cells present in the *photodynamically sensitised* samples were 12 % and 1 %, respectively. For both channel depths, an increase in the concentration of $AlPcS_4$ from 10 to 100 µM increased the number of cells in the apoptotic-mode. It was also found for both channel depths, the number of cells in the apoptotic-mode decreased when incubated for longer, except when using 60 µm depth channels and 100 µM of $AlPcS_4$, where it increased.

Cells in necrotic stage - The number of cells in the necrotic-mode under the conditions, a light dose of 9.1 J cm^{-2}, $AlPcS_4$ of 10 µM, and channel depths of 60 and 120 µm were 4 and 10 % after 2.5 hours, and 7 and 9 % after 24 hours, respectively (**Table 6.2**). When the concentration of $AlPcS_4$ was increased to 100 µM, the numbers of cells in the necrotic-mode were 15 and 19 % after 2.5 hours, and 27 and 17 % after 24 hours, respectively. Hence the highest and the lowest number of necrotic cells present in the treated samples were 27 % and 4 %, respectively. For both channel depths, an increase in the concentration of $AlPcS_4$ from 10 to 100 µM increased the number of cells in the necrotic-mode. It was also found that the number of cells in the necrotic-mode increased when incubated for longer, except when using 120 µm depth channels and 100 µM of $AlPcS_4$, where it decreased.

6.9 Summary

The *percentage recoveries* for all the samples flowed through chips were compared against the *untreated* control, the comparison was useful in determining if the number of cells recovered for the *photodynamically sensitised* samples were significantly lower. The numbers of cells recovered for all the samples flowed through chips were always lower than in the *untreated* control, and on average the *percentage recovery* was around 50 %. In most of the reactions, the number of cells recovered for the *photodynamically sensitised* samples were similar to that for the controls, *photosensitiser dark-toxicity* and *light-only toxicity*, flowed through chips. The higher variations in the number of cells recovered made it challenging to determine the trends in the results. Based on the *percentage recovery* measurements, it was clear that the levels of oxidative stress effects were not much distinct under the microfluidic settings.

According to the flow cytometry results, there were statistically significant ($p < 0.05$) decrease in the numbers of cells in the healthy-mode and statistically significant ($p < 0.05$) increase in the numbers of cells in the necrotic-mode under the conditions; a light dose of 9.1 J cm^{-2}, $AlPcS_4$ of 100 µM, channel depth of 120 µm, and analysed after 2.5 and 24 hours; and also for the light dose of 9.1 J cm^{-2}, $AlPcS_4$ of 100 µM, the channel depth of 60 µm, and when analysed after 24 hours. Similar to the MBOSR, the *photodynamically sensitised* cells were mostly induced to undergo necrosis and not apoptosis.

The results for *percentage viabilities* and LDH assay measurements represented only the fractions of samples collected after flowing through the channels. The effectiveness of the MFOSR could be improved by modifying the flow system. Other than the reduction in cell recovery (~50 %), it was successfully shown (e.g. **Figures 6.10, 6.19** and **6.20**) that the microfluidic flow system could be used for conducting extracellular OSR under the flow conditions.

CHAPTER 7 - Conclusions

Instrument

The instrument and other devices essential for the oxidative stress (PDT-mimicking) reactions were designed and developed successfully. The features of the instrument, like the strength of the light intensity emitted were calibrated as a function of the controller reading and the distance from the light source. The temperature variations due to heat generated by the light source were also recorded as a function of time.

Microfluidic chip designs

Various types of microfluidic chip configurations have been considered, designed, fabricated using glass, and tested to select the most appropriate design for the oxidative stress reactions (OSR). Parallel- and serpentine-channel chip designs were primarily chosen for the microfluidic flow OSR (MFOSR), among which the chip designs with 16-parallel channels having inlets and outlets at the opposite sides were chosen as the most optimum form for the MFOSR. Various dimensions of the latter design were fabricated and used.

Surface treatments

To conduct the novel type of extracellular MFOSR, glass channel surfaces were coated with a layer of photosensitiser (e.g. porphyrin) for the generation of photosensitisation induced oxidative stress environment. Glass surface treatments, silanisation and photosensitiser immobilisation were successful both at 120 °C and at RTP. The latter was chosen as the most optimum condition for immobilisation, as it would reduce limitations like degradation when using thermal sensitive photosensitisers. Silanisation using APTES and triethoxy(ethyl)silane produced hydrophilic and hydrophobic surfaces, which were determined using surface wettability study. Immobilisations of different types of photosensitisers were possible, and their presences within the microfluidic channels were verified using various methods; spectroscopic, colorimetric and photochemical reactions.

Pumping methods and cell recovery

When using syringe pump and a syringe for flowing cell suspension, several initial results corresponding to the MFOSR with immobilised photosensitisers were discarded, as sufficient numbers of cells were not collected for analysis. Following which different types of interfaces were tested for the syringe pump setup to improve the number of cells recovered at the outlets, and two other pumping systems, pressure and peristaltic, were also evaluated. The sedimentation of cells before flowing through the chips was addressed with the use of a magnetic stirrer, and a peristaltic pump was used for flowing cell suspension, thereby the numbers of cells recovered at the outlets were improved.

MFOSR with immobilised photosensitisers

Photosensitiser [**4**] immobilised microfluidic chips were used to carry out photosensitisation induced extracellular MFOSR. The controls and the treated (*photodynamically sensitised*) samples were analysed flow cytometrically, to determine the relative numbers of cells in apoptotic-, necrotic- and healthy-modes. Flow cytometer can detect the intracellular and expressed proteins, or other components on cells of size greater than the forward scatter threshold level, using suitable fluorescent tags, but not the freely released enzyme like LDH contained in the supernatant. Hence the *photodynamically sensitised* cells that have fragmented during or following OSR before being analysed flow cytometrically were not recorded as an event by the flow cytometer. Therefore the flow cytometry results on their own were inadequate, and additional methods of analysis were introduced in the following OSR.

Following the above type of MFOSR, the number of cells in the healthy-mode decreased, while in the apoptotic- and necrotic-modes increased, however the changes were not statistically significant. *Photosensitiser dark-toxicity* control was used to show that, flowing cells through a photosensitiser immobilised channels in the absence of light do not significantly alter the numbers of cells in the three different modes. It was also revealed that pumping cells through chemically non-surface treated

chips (control) do not have any influence on the cells. As another control it was shown that, the fluence rate and the amount of light dose delivered to the cells do not alter the relative numbers of cells in different modes.

In the MFOSR with immobilised photosensitisers, one or more photosensitisation parameters limited the success of inducing significant levels of photosensitisation effects, or the induced effects were not determined with the analysis method. The amount of photosensitisers immobilised and the number of cells recovered after each reaction varied dramatically. Due to the above limitation factors, a solid conclusion on this type of approach could not be made. To get higher control over the constraints used for the OSR, microbatch OSR (MBOSR) were designed and tested. The latter allowed controls over the variables like the concentration of photosensitisers and the amount of light dose delivered, and in determining the absolute number of cells recovered for all the samples. Hence the MBOSR were used for establishing the optimum conditions essential for conducting MFOSR with photosensitiser in solution.

Prior to the MBOSR reactions, immobilisation of photosensitisers onto magnetic nanoparticles was tested and the attachment was successful. However, due to strong magnetic attraction and rapid settling nature of the particles, it was not possible to flow them through the channels, hence was not utilised in the OSR.

MBOSR

It was determined from the initial batch reactions that, the number of cells recovered in the *photodynamically sensitised* samples decreased. Series of MBOSR were carried out using varying concentrations of photosensitisers and light doses. Unlike in MFOSR with immobilised photosensitisers, in MBOSR and in MFOSR with photosensitiser in solution, additional methods of analysis, LDH assay and cell counting coupled with trypan blue assay were incorporated to measure the effects of extracellular OSR. The LDH assay was useful in identifying the proportion of fragmented cells that could not otherwise be determined flow cytometrically or using trypan blue

assay. Trypan blue assay was useful in determining the absolute number of cells present in the samples (*percentage recovery*).

The conditions employed for the MBOSR were effective in producing extracellular oxidative stress environments, which was identified from significant induction of necrosis (fragmentation) under the conditions tested. Alterations to the number of the cells recovered were measured by determining the number of cells left behind (*percentage recovery*) relative to the *untreated* control. The cell count measurements using trypan blue assay have supported decrease in the total number of whole cells. LDH assay have also shown that cellular fragmentations do occur to a significant level both after 2.5 and 24 hours from the reactions. Furthermore flow cytometrically it was revealed that, the relative number of cells in necrotic-mode increases with the decrease in the number of cells in the healthy-mode. Overall there was a linear relationship between the amount of light dose, concentration of $AlPcS_4$ and the induction of photosensitisation effects. In general, the level of necrosis increased with the strength of the extracellular oxidative stress, and the level of induction of apoptosis was relatively lower. Necrosis led to considerable reduction in the number of whole cells recovered following the reactions. Decreases in *percentage recovery* of cells close to 90 % and cell viability close to 100 % were achievable within 24 hours following the photosensitisation reactions under the conditions of 9.1 J cm^{-2} and 100 μM of $AlPcS_4$. The mechanism responsible for cellular fragmentation could be similar to the induction of necrosis by membrane localised photosensitisers, which occurs through damages related to peroxidation of lipids and proteins on the plasma membrane.

$AlPcS_4$ was completely soluble in aqueous medium, which was used for all the extracellular MBOSR and MFOSR with photosensitiser in solution. The use of completely solvated photosensitiser was essential to maximise the interactions between the cells in suspension and the photosensitisers, thereby with the ROS that were produced. It was confirmed using a fluorescence microscopy that, no photosensitiser internalisation had

occurred over the length of the reactions. Hence the photosensitisation effects observed were due to the generation of extracellular OSR.

As described above, the conditions tested under the MBOSR mainly induced necrosis as the major form of cell death and not apoptosis. Necrosis is an important form of cell death during PDT, as it stimulates immune response much more effectively than cells undergoing apoptotic disintegration. Hence, as a further work it would be useful to study multiple ranges of other OSR conditions to confirm or establish the mechanism through which the above occurred, and further the conditions needed for inducing higher level of apoptosis and lower level of necrosis could be determined.

MFOSR with photosensitiser in solution

The numbers of cells recovered for all the samples flowed through chips were compared against the *untreated* control, and they were always lower than in the control and on average the *percentage recovery* was around 50 %. In most of the reactions, the number of cells recovered for the *photodynamically sensitised* samples were similar to that for the controls, *photosensitiser dark-toxicity* and *light-only toxicity*, flowed through chips. The higher variations in the number of cells recovered made it challenging to determine the trends in the results. The flow cytometry results showed that, under certain conditions there were statistically significant decrease and increase in the numbers of cells in the healthy- and necrotic-modes, respectively. Similar to the MBOSR, the *photodynamically sensitised* cells were mostly induced to undergo necrosis and not apoptosis.

It had been demonstrated that flowing cells though microfluidic channels were possible, with the average recovery of about 50 % cells and the reduction in cell recovery was not avoidable under the flow system that was used. As a further work, it would be sensible to modify the flow system to enable higher percentage of cell recovery, thereby the effectiveness of the MFOSR.

Main findings and achievements

The instrument essential for extracellular OSR was built and their features were characterised. The instrument and the extracellular OSR methods developed were capable of allowing control over the levels of oxidative stress generated, which was enabled by controlling the two main parameters, the light dose and the concentration of photosensitisers used for the photosensitisation reactions. Hence the key aim of exposing cells to extracellular OSR without photosensitiser internalisation was achievable with all three types of OSR methods developed; MFOSR with immobilised photosensitises, MBOSR and MFOSR with photosensitiser in solution. The photosensitisation effects of OSR were mainly due to reactive species like ROS.

It was clear from the results that solely flow cytometry measurements on their own or other single form of measurement would not account for all the key effects induced on the photodynamically treated (sensitised) samples. Hence multiple modes of analyses were essential to measure the photosensitisation effects induced by the OSR. The results obtained for all three types of OSR, showed that extracellular oxidative stress primarily induces necrosis and not apoptosis. The mechanism through which it occurred could have been similar to the type of PDT-effects induced by the membrane bound photosensitisers. Hence, overall the study and the latter fact suggest that, during PDT *in vivo*, necrosis could be due to the photosensitisation of photosensitisers that were available in the tissue fluid or that were bound to the membranes of those cells. In overall, the above OSR methods and approaches can be adapted to use in medicine and within various research fields, to study the features such as the effects of oxidative stress on the life cycle of numerous diseases or to understand diseases where oxidative stress is involved.

Further work

The amounts of immobilisable photosensitisers on to a monolayer of amino group formed during silanisation were rather limited, which could be further optimised to improve the loading efficiency. In this thesis the extreme end points of OSR, that is, the changes to the percentage of cells recovered, the viability of remaining cells, the relative levels of fragmented cells, and the modes of cell death were measured. However, it would also be vital to measure and study in great depths the minor changes to the metabolic activities of the OSR treated cells, that is, to move backwards from the extreme end points of outcome for the treated cells to the measurements that looks at subtle but important effects such as expression of certain proteins like heat shock proteins 70 (HSP70), and peroxidation of lipids and proteins. It would also be important to determine the conditions that could lead to apoptosis as the main or only form of cell death. To achieve all the above, it would be essential to study the effects over a wide range of OSR conditions either using MBOSR or MFOSR conditions. When sufficient results have been collected they could be used in determining the strength of the oxidative stress linked with the development of a specific type of disease and its role in the life cycle of that disease, and similarly for all the oxidative stress related diseases in general. Moreover, the components (contents) generated following the direct effects of photosensitisation reactions could be used in immune induction studies (e.g. cancer vaccination) and in clinical treatments.

References

1. Hermes-Lima M. Oxygen in Biology and Biochemistry: Role of Free Radicals. *Functional Metabolism*: John Wiley & Sons, Inc.; 2005. p. 319-68.
2. Reuter S, Gupta SC, Chaturvedi MM, Aggarwal BB. Oxidative stress, inflammation, and cancer: how are they linked? *Free Radic Biol Med*. 2010;49(11):1603-16.
3. Florence TM. The role of free radicals in disease. *Aust N Z J Ophthalmol*. 1995;23(1):3-7.
4. Nair U, Bartsch H, Nair J. Lipid peroxidation-induced DNA damage in cancer-prone inflammatory diseases: a review of published adduct types and levels in humans. *Free Radic Biol Med*. 2007;43(8):1109-20.
5. Wilson JN, Pierce JD, Clancy RL. Reactive oxygen species in acute respiratory distress syndrome. *Heart Lung*. 2001;30(5):370-5.
6. Gill R, Tsung A, Billiar T. Linking oxidative stress to inflammation: Toll-like receptors. *Free Radic Biol Med*. 2010;48(9):1121-32.
7. Doria E, Buonocore D, Focarelli A, Marzatico F. Relationship between human aging muscle and oxidative system pathway. *Oxid Med Cell Longev*. 2012;2012:830257.
8. Liochev SI. Reactive oxygen species and the free radical theory of aging. *Free Radic Biol Med*. 2013;60:1-4.
9. El Assar M, Angulo J, Rodriguez-Manas L. Oxidative stress and vascular inflammation in aging. *Free Radic Biol Med*. 2013;65:380-401.
10. Haigis MC, Yankner BA. The aging stress response. *Mol Cell*. 2010;40(2):333-44.
11. Halliwell B. Oxygen radicals, nitric-oxide and human inflammatory joint disease. *Ann Rheum Dis*. 1995;54(6):505-10.
12. Hensley K, Butterfield DA, Hall N, Cole P, Subramaniam R, Mark R, Mattson MP, Markesbery WR, Harris ME, Aksenov M, Aksenova M, Wu JF, Carney JM. Reactive oxygen species as causal agents in the neurotoxicity of the Alzheimer's disease-associated amyloid beta peptide. In: Kitani K, Aoba A, Goto S, (eds.) *Pharmacological Intervention in Aging and Age-Associated Disorders: Proceedings of the Sixth Congress of the International Association of Biomedical Gerontology*. Annals of the New York Academy of Sciences. 7861996. p. 120-34.
13. Multhaup G, Ruppert T, Schlicksupp A, Hesse L, Beher D, Masters CL, Beyreuther K. Reactive oxygen species and Alzheimer's disease. *Biochem Pharmacol*. 1997;54(5):533-39.
14. Zhu X, Raina AK, Lee HG, Casadesus G, Smith MA, Perry G. Oxidative stress signalling in Alzheimer's disease. *Brain Res*. 2004;1000(1-2):32-9.
15. Ferretti G, Bacchetti T. Peroxidation of lipoproteins in multiple sclerosis. *J Neurol Sci*. 2011;311(1-2):92-7.
16. Bonomini F, Tengattini S, Fabiano A, Bianchi R, Rezzani R. Atherosclerosis and oxidative stress. *Histol Histopathol*. 2008;23(3):381-90.
17. Vogiatzi G, Tousoulis D, Stefanadis C. The Role of Oxidative Stress in Atherosclerosis. *Hellenic J Cardiol*. 2009;50(5):402-09.
18. Stocker R, Keaney JF. Role of oxidative modifications in atherosclerosis. *Physiol Rev*. 2004;84(4):1381-478.
19. Renschler MF. The emerging role of reactive oxygen species in cancer therapy. *Eur J Cancer*. 2004;40(13):1934-40.
20. Weinberg F, Chandel NS. Reactive oxygen species-dependent signaling regulates cancer. *Cell Mol Life Sci*. 2009;66(23):3663-73.
21. Toyokuni S, Okamoto K, Yodoi J, Hiai H. Persistent oxidative stress in cancer. *FEBS Lett*. 1995;358(1):1-3.
22. Valko M, Rhodes CJ, Moncol J, Izakovic M, Mazur M. Free radicals, metals and antioxidants in oxidative stress-induced cancer. *Chem Biol Interact*. 2006;160(1):1-40.
23. Gupte A, Mumper RJ. Elevated copper and oxidative stress in cancer cells as a target for cancer treatment. *Cancer Treat Rev*. 2009;35(1):32-46.
24. Franco R, Schoneveld O, Georgakilas AG, Panayiotidis MI. Oxidative stress, DNA methylation and carcinogenesis. *Cancer Lett*. 2008;266(1):6-11.
25. Pelicano H, Carney D, Huang P. ROS stress in cancer cells and therapeutic implications. *Drug Resist Update*. 2004;7(2):97-110.
26. Costa A, Scholer-Dahirel A, Mechta-Grigoriou F. The role of reactive oxygen species and metabolism on cancer cells and their microenvironment. *Semin Cancer Biol*. 2014;25:23-32.

27. Dreher D, Junod AF. Role of oxygen free radicals in cancer development. *Eur J Cancer*. 1996;32a(1):30-8.
28. Lau ATY, Wang Y, Chiu J-F. Reactive oxygen species: Current knowledge and applications in cancer research and therapeutic. *J Cell Biochem*. 2008;104(2):657-67.
29. Furukawa S, Fujita T, Shimabukuro M, Iwaki M, Yamada Y, Nakajima Y, Nakayama O, Makishima M, Matsuda M, Shimomura I. Increased oxidative stress in obesity and its impact on metabolic syndrome. *J Clin Invest*. 2004;114(12):1752-61.
30. Tsutsui H, Kinugawa S, Matsushima S. Oxidative stress and heart failure. *Am J Physiol Heart Circ Physiol*. 2011;301(6):H2181-90.
31. Tieu K, Ischiropoulos H, Przedborski S. Nitric oxide and reactive oxygen species in Parkinson's disease. *IUBMB Life*. 2003;55(6):329-35.
32. DeMaria N, Colantoni A, Fagiuoli S, Liu GJ, Rogers BK, Farinati F, VanThiel DH, Floyd RA. Association between reactive oxygen species and disease activity in chronic hepatitis C. *Free Radic Biol Med*. 1996;21(3):291-95.
33. Kinnula VL, Fattman CL, Tan RJ, Oury TD. Oxidative stress in pulmonary fibrosis: a possible role for redox modulatory therapy. *Am J Respir Crit Care Med*. 2005;172(4):417-22.
34. Rains JL, Jain SK. Oxidative stress, insulin signaling, and diabetes. *Free Radic Biol Med*. 2011;50(5):567-75.
35. Haurani MJ, Pagano PJ. Adventitial fibroblast reactive oxygen species as autacrine and paracrine mediators of remodeling: bellwether for vascular disease? *Cardiovasc Res*. 2007;75(4):679-89.
36. Chen XQ, Tian XZ, Shin I, Yoon J. Fluorescent and luminescent probes for detection of reactive oxygen and nitrogen species. *Chem Soc Rev*. 2011;40(9):4783-804.
37. Curtin JF, Donovan M, Cotter TG. Regulation and measurement of oxidative stress in apoptosis. *J Immunol Meth*. 2002;265(1-2):49-72.
38. Bergendi L, Benes L, Durackova Z, Ferencik M. Chemistry, physiology and pathology of free radicals. *Life Sci*. 1999;65(18-19):1865-74.
39. Kohen R, Nyska A. Oxidation of Biological Systems: Oxidative Stress Phenomena, Antioxidants, Redox Reactions, and Methods for Their Quantification. *Toxicol Pathol*. 2002;30(6):620-50.
40. Smith LL. Oxygen, oxysterols, ouabain, and ozone: a cautionary tale. *Free Radic Biol Med*. 2004;37(3):318-24.
41. Halliwell B, Whiteman M. Measuring reactive species and oxidative damage in vivo and in cell culture: how should you do it and what do the results mean? *Br J Pharmacol*. 2004;142(2):231-55.
42. Cadet J, Douki T, Ravanat JL, Di Mascio P. Sensitized formation of oxidatively generated damage to cellular DNA by UVA radiation. *Photochem Photobiol Sci*. 2009;8(7):903-11.
43. Mittler R. Oxidative stress, antioxidants and stress tolerance. *Trends in Plant Sci*. 2002;7(9):405-10.
44. Martinez-Cayuela M. Oxygen free radicals and human disease. *Biochimie*. 1995;77(3):147-61.
45. Clennan EL. New Mechanistic and Synthetic Aspects of Singlet Oxygen Chemistry. *Tetrahedron*. 2000;56(47):9151-79.
46. Redmond RW, Kochevar IE. Spatially resolved cellular responses to singlet oxygen. *Photochem Photobiol*. 2006;82(5):1178-86.
47. Ouedraogo GD, Redmond RW. Secondary reactive oxygen species extend the range of photosensitization effects in cells: DNA damage produced via initial membrane photosensitization. *Photochem Photobiol*. 2003;77(2):192-203.
48. Krasnovsky AA. Luminescence and photochemical studies of singlet oxygen photonics. *J Photochem Photobiol, A*. 2008;196(2-3):210-18.
49. Milgrom LR. *The colours of life, An introduction to the chemistry of porphyrins and related compounds* Oxford: Oxford University Press; 1997.
50. Blossey EC, Neckers DC, Thayer AL, Schaap AP. Polymer-based sensitizers for photooxidations. *J Am Chem Soc*. 1973;95(17):5820-22.
51. Ogilby PR. Singlet oxygen: there is still something new under the sun, and it is better than ever. *Photochem Photobiol Sci*. 2010;9(12):1543-60.
52. Wentworth P, Jr., McDunn JE, Wentworth AD, Takeuchi C, Nieva J, Jones T, Bautista C, Ruedi JM, Gutierrez A, Janda KD, Babior BM, Eschenmoser A, Lerner RA. Evidence

for antibody-catalyzed ozone formation in bacterial killing and inflammation. *Science*. 2002;298(5601):2195-9.
53. Babior BM, Takeuchi C, Ruedi J, Gutierrez A, Wentworth P, Jr. Investigating antibody-catalyzed ozone generation by human neutrophils. *Proc Natl Acad Sci U S A*. 2003;100(6):3031-4.
54. Bourne RA, Han X, Poliakoff M, George MW. Cleaner continuous photo-oxidation using singlet oxygen in supercritical carbon dioxide. *Angew Chem Int Ed Engl*. 2009;48(29):5322-5.
55. Wolff CJM, Halmans MTH, van der Heijde HB. The formation of singlet oxygen in surface waters. *Chemosphere*. 1981;10(1):59-62.
56. Kořínek M, Klinger P, Dědic R, Pšenčík J, Svoboda A, Hála J. Delayed fluorescence of meso-tetraphenylporphyrin in acetone and in dimethylsulphoxide. *J Lumin*. 2007;122-123:247-49.
57. Mathews-Roth MM. Photosensitization by porphyrins and prevention of photosensitization by carotenoids. *J Natl Cancer Inst*. 1982;69(1):279-85.
58. Dougherty TJ, Gomer CJ, Henderson BW, Jori G, Kessel D, Korbelik M, Moan J, Peng Q. Photodynamic therapy. *J Natl Cancer Inst*. 1998;90(12):889-905.
59. Changtong C, Carney DW, Luo L, Zoto CA, Lombardi JL, Connors RE. A porphyrin molecule that generates, traps, stores, and releases singlet oxygen. *J Photochem Photobiol, A*. 2013;260:9-13.
60. Rhee SG. Cell signaling. H_2O_2, a necessary evil for cell signaling. *Science*. 2006;312(5782):1882-3.
61. Yan B, Boyd D. Breaking the light and heavy chain linkage of human immunoglobulin G1 (IgG1) by radical reactions. *J Biol Chem*. 2011;286(28):24674-84.
62. Cooper WJ, Lean DRS. Hydrogen peroxide concentration in a northern lake: photochemical formation and diel variability. *Environ Sci Technol*. 1989;23(11):1425-28.
63. Ogilby PR. Singlet oxygen: there is indeed something new under the sun. *Chem Soc Rev*. 2010;39(8):3181-209.
64. Halliwell B. Oxygen radicals, nitric oxide and human inflammatory joint disease. *Ann Rheum Dis*. 1995;54(6):505-10.
65. Wardman P. Fluorescent and luminescent probes for measurement of oxidative and nitrosative species in cells and tissues: progress, pitfalls, and prospects. *Free Radic Biol Med*. 2007;43(7):995-1022.
66. Finkelstein E, Rosen GM, Rauckman EJ. Spin trapping. Kinetics of the reaction of superoxide and hydroxyl radicals with nitrones. *J Am Chem Soc*. 1980;102(15):4994-99.
67. Baumler W, Regensburger J, Knak A, Felgentrager A, Maisch T. UVA and endogenous photosensitizers--the detection of singlet oxygen by its luminescence. *Photochem Photobiol Sci*. 2012;11(1):107-17.
68. Tsay JM, Trzoss M, Shi L, Kong X, Selke M, Jung ME, Weiss S. Singlet oxygen production by Peptide-coated quantum dot-photosensitizer conjugates. *J Am Chem Soc*. 2007;129(21):6865-71.
69. Gorman AA, Rodgers MAJ. Singlet molecular oxygen. *Chem Soc Rev*. 1981;10(2):205-31.
70. Xu K. Cellular responses to UVA as a source of Oxidative Stress. 2007;16:28 to 29.
71. Kruk I, Michalska T, Kladna A. Formation of singlet oxygen during farmorubicin oxidation. *Chemosphere*. 2001;44(7):1565-71.
72. Dědic R, Kořínek M, Molnár A, Svoboda A, Hála J. Singlet oxygen quenching by oxygen in tetraphenyl-porphyrin solutions. *J Lumin*. 2006;119-120:209-13.
73. Mueller S. Sensitive and nonenzymatic measurement of hydrogen peroxide in biological systems. *Free Radic Biol Med*. 2000;29(5):410-5.
74. Harris DC. *Quantitative chemical analysis*. 7th ed. New York, USA: W. H. Freeman and Company; 2007.
75. Van-Lier JE. Photosensitization: Reaction Pathways. In: Valenzeno D, Pottier R, Mathis P, Douglas R, (eds.) *Photobiological Techniques*. NATO ASI Series. 216: Springer US; 1991. p. 85-98.
76. Allison RR, Downie GH, Cuenca R, Hu X-H, Childs CJH, Sibata CH. Photosensitizers in clinical PDT. *Photodiagnosis Photodyn Ther*. 2004;1(1):27-42.
77. Josefsen LB, Boyle RW. Photodynamic therapy and the development of metal-based photosensitisers. *Met Based Drugs*. 2008;2008:276109.

78. Merrit JE, Loening KL. Nomenclature of tetrapyrroles. *Pure Appl Chem*. 1979;51(11):2251-304.
79. Josefsen LB, Boyle RW. Photodynamic therapy: novel third-generation photosensitizers one step closer? *Br J Pharmacol*. 2008;154(1):1-3.
80. Belfield KD, Bondar MV, Przhonska OV. Singlet oxygen quantum yield determination for a fluorene-based two-photon photosensitizer. *J Fluoresc*. 2006;16(1):111-7.
81. Kolarova H, Nevrelova P, Bajgar R, Jirova D, Kejlova K, Strnad M. In vitro photodynamic therapy on melanoma cell lines with phthalocyanine. *Toxicol In Vitro*. 2007;21(2):249-53.
82. Wang Y, Cohen B, Jicsinszky L, Douhal A. Femtosecond to second studies of a water-soluble porphyrin derivative in chemical and biological nanocavities. *Langmuir*. 2012;28(9):4363-72.
83. Castano AP, Mroz P, Hamblin MR. Photodynamic therapy and anti-tumour immunity. *Nat Rev Cancer*. 2006;6(7):535-45.
84. Chavan SA, Maes W, Gevers LE, Wahlen J, Vankelecom IF, Jacobs PA, Dehaen W, De Vos DE. Porphyrin-functionalized dendrimers: synthesis and application as recyclable photocatalysts in a nanofiltration membrane reactor. *Chemistry*. 2005;11(22):6754-62.
85. Oliver IT, Rawlinson WA. The absorption spectra of porphyrin a and derivatives. *Biochem J*. 1955;61(4):641-46.
86. Elgie KJ, Scobie M, Boyle RW. Application of combinatorial techniques in the synthesis of unsymmetrically substituted 5,15-diphenylporphyrins. *Tetrahedron Lett*. 2000;41(15):2753-57.
87. Howe L, Zhang JZ. Ultrafast Studies of Excited-State Dynamics of Phthalocyanine and Zinc Phthalocyanine Tetrasulfonate in Solution. *J Phys Chem A*. 1997;101(18):3207-13.
88. Gijsens A, Derycke A, Missiaen L, De Vos D, Huwyler J, Eberle A, de Witte P. Targeting of the photocytotoxic compound AlPcS4 to Hela cells by transferrin conjugated PEG-liposomes. *Int J Cancer*. 2002;101(1):78-85.
89. Rotomskis R, Streckyte G, Bagdonas S. Phototransformations of sensitizers 1. Significance of the nature of the sensitizer in the photobleaching process and photoproduct formation in aqueous solution. *J Photochem Photobiol, B*. 1997;39(2):167-71.
90. Ogunsipe A, Chen J-Y, Nyokong T. Photophysical and photochemical studies of zinc(II) phthalocyanine derivatives-effects of substituents and solvents. *New J Chem*. 2004;28(7):822-27.
91. Manjon F, Villen L, Garcia-Fresnadillo D, Orellana G. On the factors influencing the performance of solar reactors for water disinfection with photosensitized singlet oxygen. *Environ Sci Technol*. 2008;42(1):301-7.
92. Bullous AJ, Alonso CM, Boyle RW. Photosensitiser-antibody conjugates for photodynamic therapy. *Photochem Photobiol Sci*. 2011;10(5):721-50.
93. Ochsner M. Photophysical and photobiological processes in the photodynamic therapy of tumours. *J Photochem Photobiol B*. 1997;39(1):1-18.
94. Gouterman M, Hanson LK, Khalil GE, Buchler JW, Rohbock K, Dolphin D. Porphyrins. XXXI. Chemical properties and electronic spectra of d0 transition-metal complexes. *J Am Chem Soc*. 1975;97(11):3142-49.
95. Kolarova H, Bajgar R, Tomankova K, Nevrelova P, Mosinger J. Comparison of sensitizers by detecting reactive oxygen species after photodynamic reaction in vitro. *Toxicol In Vitro*. 2007;21(7):1287-91.
96. Ball DJ, Mayhew S, Wood SR, Griffiths J, Vernon DI, Brown SB. A comparative study of the cellular uptake and photodynamic efficacy of three novel zinc phthalocyanines of differing charge. *Photochem Photobiol*. 1999;69(3):390-6.
97. Morgan AR, Garbo GM, Keck RW, Selman SH. New photosensitizers for photodynamic therapy: combined effect of metallopurpurin derivatives and light on transplantable bladder tumors. *Cancer Res*. 1988;48(1):194-8.
98. Samia AC, Dayal S, Burda C. Quantum dot-based energy transfer: perspectives and potential for applications in photodynamic therapy. *Photochem Photobiol*. 2006;82(3):617-25.
99. Meng Y, Zou C, Madiyalakan R, Woo T, Huang M, Yang X, Swanson E, Chen J, Xing JZ. Water-soluble and biocompatible sono/photosensitizer nanoparticles for enhanced cancer therapy. *Nanomed*. 2010;5(10):1559-69.

100. Brasseur N, Ouellet R, La Madeleine C, van Lier JE. Water-soluble aluminium phthalocyanine-polymer conjugates for PDT: photodynamic activities and pharmacokinetics in tumour-bearing mice. *Br J Cancer*. 1999;80(10):1533-41.
101. Wiglusz R, Legendziewicz J, Graczyk A, Radzki S, Gawryszewska P, Sokolnicki J. Spectroscopic properties of porphyrins and effect of lanthanide ions on their luminescence efficiency. *J Alloys Compd*. 2004;380(1-2):396-404.
102. Scholz M, Dedic R, Breitenbach T, Hala J. Singlet oxygen-sensitized delayed fluorescence of common water-soluble photosensitizers. *Photochem Photobiol Sci*. 2013;12(10):1873-84.
103. Gensch T, Braslavsky SE. Volume Changes Related to Triplet Formation of Water-Soluble Porphyrins. A Laser-Induced Optoacoustic Spectroscopy (LIOAS) Study. *J Phys Chem B*. 1997;101(1):101-08.
104. Venkatramaiah N, Ramakrishna B, Venkatesan R, Almeida Paz FA, Tomé JPC. Facile synthesis of highly stable BF3-induced meso-tetrakis (4-sulfonato phenyl) porphyrin (TPPS4)-J-aggregates: structure, photophysical and electrochemical properties. *New J Chem*. 2013;37(11):3745.
105. Brown SB, Shillcock M. Equilibrium and Kinetic Stuies of the Aggregation of Porphyrins in Aqueous Solution. *BiochemJ*. 1976;153:279-85.
106. Udal'tsov AV, Kazarin LA, Sinani VA, Sweshnikov AA. Water–porphyrin interactions and their influence on self assembly of large scale porphyrin aggregates. *J Photochem Photobiol, A*. 2002;151(1–3):105-19.
107. Fagadar-Cosma E, Enachea C, Armeanua I, Fagadar-Cosma G. Comparative investigations of the absorption and fluorescence spectra of tetrapyridylporphyrine and Zn(II) tetrapyridylporphyrine. *Dig J Nanomater Biostruct*. 2007;2(1):175-83.
108. Ribo JM, Crusats J, Farrera J-A, Valero ML. Aggregation in water solutions of tetrasodium diprotonated meso-tetrakis(4-sulfonatophenyl)porphyrin. *J Chem Soc, Chem Commun*. 1994(6):681-82.
109. Bhyrappa P, Wilson SR, Suslick KS. Hydrogen-Bonded Porphyrinic Solids: Supramolecular Networks of Octahydroxy Porphyrins. *J Am Chem Soc*. 1997;119(36):8492-502.
110. Suslick KS, Bhyrappa P, Chou JH, Kosal ME, Nakagaki S, Smithenry DW, Wilson SR. Microporous Porphyrin Solids. *Acc Chem Res*. 2005;38(4):283-91.
111. Li L, Ishdorj G, Gibson SB. Reactive oxygen species regulation of autophagy in cancer: implications for cancer treatment. *Free Radic Biol Med*. 2012;53(7):1399-410.
112. Barth S, Glick D, Macleod KF. Autophagy: assays and artifacts. *J Pathol*. 2010;221(2):117-24.
113. Danial NN, Korsmeyer SJ. Cell death: critical control points. *Cell*. 2004;116(2):205-19.
114. Kreuzaler P, Watson CJ. Killing a cancer: what are the alternatives? *Nat Rev Cancer*. 2012;12(6):411-24.
115. Ryan L, O'Callaghan YC, O'Brien NM. Oxidised Products of Cholesterol: Their Role in Apoptosis. *Curr Nutr Food Sci*. 2005;1(1):41-51.
116. Das UN. Essential fatty acids, lipid peroxidation and apoptosis. *Prostaglandins Leukot Essent Fatty Acids*. 1999;61(3):157-63.
117. Harrington KJ. Biology of cancer. *Medicine*. 2008;36(1):1-4.
118. Niki E, Yoshida Y, Saito Y, Noguchi N. Lipid peroxidation: mechanisms, inhibition, and biological effects. *Biochem Biophys Res Commun*. 2005;338(1):668-76.
119. Porter NA. Mechanisms for the autoxidation of polyunsaturated lipids. *Acc Chem Res*. 1986;19(9):262-68.
120. Schnitzer E, Pinchuk I, Bor A, Leikin-Frenkel A, Lichtenberg D. Oxidation of liposomal cholesterol and its effect on phospholipid peroxidation. *Chem Phys Lipids*. 2007;146(1):43-53.
121. Frankel EN. Lipid oxidation: Mechanisms, products and biological significance. *Journal of the American Oil Chemists' Society*. 1984;61(12):1908-17.
122. Marnett LJ. Lipid peroxidation-DNA damage by malondialdehyde. *Mutat Res*. 1999;424(1-2):83-95.
123. Valenzuela A, Sanhueza J, Nieto S. Cholesterol oxidized products in foods: potential health hazards and the role of antioxidants in prevention. *Grasas Y Aceites*. 2004;55(3):312-20.

124. Catala A. Lipid peroxidation modifies the picture of membranes from the "Fluid Mosaic Model" to the "Lipid Whisker Model". *Biochimie*. 2012;94(1):101-9.
125. Jacob RF, Mason RP. Lipid peroxidation induces cholesterol domain formation in model membranes. *J Biol Chem*. 2005;280(47):39380-7.
126. Galeotti T, Borrello S, Palombini G, Masotti L, Ferrari MB, Cavatorta P, Arcioni A, Stremmenos C, Zannoni C. Lipid peroxidation and fluidity of plasma membranes from rat liver and Morris hepatoma 3924A. *FEBS Lett*. 1984;169(2):169-73.
127. Courtois F, Seidman EG, Delvin E, Asselin C, Bernotti S, Ledoux M, Levy E. Membrane peroxidation by lipopolysaccharide and iron-ascorbate adversely affects Caco-2 cell function: beneficial role of butyric acid. *Am J Clin Nutr*. 2003;77(3):744-50.
128. Boselli E, Cardenia V, Rodriguez-Estrada MT. Cholesterol photosensitized oxidation in muscle foods. *Eur J Lipid Sci Technol*. 2012;114(6):644-55.
129. Sieber R. Oxidised cholesterol in milk and dairy products. *Int Dairy J*. 2005;15(3):191-206.
130. Morales-Aizpurúa IC, Tenuta-Filho A. Oxidation of cholesterol in mayonnaise during storage. *Food Chem*. 2005;89(4):611-15.
131. Kanofsky JR, Sima PD, Richter C. Singlet-oxygen generation from A2E. *Photochem Photobiol*. 2003;77(3):235-42.
132. Korytowski W, Girotti AW. Singlet oxygen adducts of cholesterol: photogeneration and reductive turnover in membrane systems. *Photochem Photobiol*. 1999;70(4):484-9.
133. McNulty HP, Byun J, Lockwood SF, Jacob RF, Mason RP. Differential effects of carotenoids on lipid peroxidation due to membrane interactions: X-ray diffraction analysis. *Biochim Biophys Acta*. 2007;1768(1):167-74.
134. Hawkins CL, Morgan PE, Davies MJ. Quantification of protein modification by oxidants. *Free Radic Biol Med*. 2009;46(8):965-88.
135. Gracanin M, Hawkins CL, Pattison DI, Davies MJ. Singlet-oxygen-mediated amino acid and protein oxidation: formation of tryptophan peroxides and decomposition products. *Free Radic Biol Med*. 2009;47(1):92-102.
136. Davies MJ. Singlet oxygen-mediated damage to proteins and its consequences. *Biochem Biophys Res Commun*. 2003;305(3):761-70.
137. Wright A. Photo-oxidation of cells generates long-lived intracellular protein peroxides. *Free Radic Biol Med*. 2003;34(6):637-47.
138. Kim J, Rodriguez ME, Guo M, Kenney ME, Oleinick NL, Anderson VE. Oxidative modification of cytochrome c by singlet oxygen. *Free Radic Biol Med*. 2008;44(9):1700-11.
139. Jung T, Bader N, Grune T. Oxidized proteins: intracellular distribution and recognition by the proteasome. *Arch Biochem Biophys*. 2007;462(2):231-7.
140. Davies MJ. The oxidative environment and protein damage. *Biochim Biophys Acta*. 2005;1703(2):93-109.
141. Kim J, Rodriguez ME, Oleinick NL, Anderson VE. Photo-oxidation of cardiolipin and cytochrome c with bilayer-embedded Pc 4. *Free Radic Biol Med*. 2010;49(5):718-25.
142. Cardoso DR, Libardi SH, Skibsted LH. Riboflavin as a photosensitizer. Effects on human health and food quality. *Food Funct*. 2012;3(5):487-502.
143. Shacter E. Quantification and significance of protein oxidation in biological samples. *Drug Metab Rev*. 2000;32(3-4):307-26.
144. Pattison DI, Rahmanto AS, Davies MJ. Photo-oxidation of proteins. *Photochem Photobiol Sci*. 2012;11(1):38-53.
145. Morgan PE, Dean RT, Davies MJ. Protective mechanisms against peptide and protein peroxides generated by singlet oxygen. *Free Radic Biol Med*. 2004;36(4):484-96.
146. Davies MJ. Reactive species formed on proteins exposed to singlet oxygen. *Photochem & Photobiol Sci*. 2004;3(1):17-25.
147. Haag WR, Hoigne´ Jr, Gassman E, Braun AM. Singlet oxygen in surface waters — Part I: Furfuryl alcohol as a trapping agent. *Chemosphere*. 1984;13(5):631-40.
148. Allen JM, Gossett CJ, Allen SF. Photochemical formation of singlet molecular oxygen ($^1O_2$) in illuminated aqueous solutions of p-aminobenzoic acid (PABA). *J Photochem Photobiol B*. 1996;32(1-2):33-7.
149. Sies H. Strategies of antioxidant defense. *Eur J Biochem*. 1993;215(2):213-9.
150. Brigelius-Flohe R, Kipp A. Glutathione peroxidases in different stages of carcinogenesis. *Biochim Biophys Acta*. 2009;1790(11):1555-68.

151. Orellana M, Guajardo V, Araya J, Thieleman L, Rodrigo R. Oxidative stress, microsomal and peroxisomal fatty acid oxidation in the liver of rats treated with acetone. *Comparative Biochem and Phys C-Tox & Pharm*. 2001;128(4):503-09.
152. Droge W. Free radicals in the physiological control of cell function. *Physiol Rev*. 2002;82(1):47-95.
153. DeYulia GJ, Cárcamo JM, Bórquez-Ojeda O, Shelton CC, Golde DW. Hydrogen peroxide generated extracellularly by receptor–ligand interaction facilitates cell signaling. *Proc Natl Acad Sci U S A*. 2005;102(14):5044-49.
154. Miyajima A, Nakashima J, Yoshioka K, Tachibana M, Tazaki H, Murai M. Role of reactive oxygen species in cis-dichlorodiammineplatinum-induced cytotoxicity on bladder cancer cells. *Br J Cancer*. 1997;76(2):206-10.
155. Salganik RI, Albright CD, Rodgers J, Kim J, Zeisel SH, Sivashinskiy MS, Van Dyke TA. Dietary antioxidant depletion: enhancement of tumor apoptosis and inhibition of brain tumor growth in transgenic mice. *Carcinogenesis*. 2000;21(5):909-14.
156. Bhatti P, Stewart PA, Hutchinson A, Rothman N, Linet MS, Inskip PD, Rajaraman P. Lead exposure, polymorphisms in genes related to oxidative stress, and risk of adult brain tumors. *Cancer Epidemiol Biomarkers Prev*. 2009;18(6):1841-8.
157. Brown NS, Bicknell R. Hypoxia and oxidative stress in breast cancer - Oxidative stress: its effects on the growth, metastatic potential and response to therapy of breast cancer. *Breast Cancer Res*. 2001;3(5):323-27.
158. Lakshmi A, Subramanian SP. Tangeretin ameliorates oxidative stress in the renal tissues of rats with experimental breast cancer induced by 7,12-dimethylbenz[a]anthracene. *Toxicol Lett*. 2014;229(2):333-48.
159. Guo CH, Hsia S, Chen PC. Distribution of selenium and oxidative stress in breast tumor-bearing mice. *Nutrients*. 2013;5(2):594-607.
160. Leung T, Rajendran R, Singh S, Garva R, Krstic-Demonacos M, Demonacos C. Cytochrome P450 2E1 (CYP2E1) regulates the response to oxidative stress and migration of breast cancer cells. *Breast Cancer Res*. 2013;15(6).
161. Vieira FGK, Di Pietro PF, Boaventura BCB, Ambrosi C, Rockenbach G, Fausto MA, Crippa CG, Da Silva EL. Factors associated with oxidative stress in women with breast cancer. *Nutr Hosp*. 2011;26(3):528-36.
162. Sharma A, Rajappa M, Satyam A, Sharma M. Oxidant/anti-oxidant dynamics in patients with advanced cervical cancer: correlation with treatment response. *Mol Cell Biochem*. 2010;341(1-2):65-72.
163. Oliveira C, Kassab P, Lopasso FP, Souza HP, Janiszewski M, Laurindo FRM, Iriya K, Laudanna AA. Protective effect of ascorbic acid in experimental gastric cancer: reduction of oxidative stress. *World J Gastroenterol*. 2003;9(3):446-48.
164. Borrego S, Vazquez A, Dasi F, Cerda C, Iradi A, Tormos C, Sanchez JM, Bagan L, Boix J, Zaragoza C, Camps J, Saez G. Oxidative Stress and DNA Damage in Human Gastric Carcinoma: 8-Oxo-7 ' 8-dihydro-2 '-deoxyguanosine (8-oxo-dG) as a Possible Tumor Marker. *Int J Mol Sci*. 2013;14(2):3467-86.
165. Calvisi DF, Ladu S, Hironaka K, Factor VM, Thorgeirsson SS. Vitamin E down-modulates iNOS and NADPH oxidase in c-Myc/TGF-alpha transgenic mouse model of liver cancer. *J Hepatol*. 2004;41(5):815-22.
166. Azad N, Rojanasakul Y, Vallyathan V. Inflammation and lung cancer: roles of reactive oxygen/nitrogen species. *J Toxicol Environ Health B Crit Rev*. 2008;11(1):1-15.
167. Lawless MW, O'Byrne KJ, Gray SG. Oxidative stress induced lung cancer and COPD: opportunities for epigenetic therapy. *J Cell Mol Med*. 2009;13(9A):2800-21.
168. Fruehauf JP, Trapp V. Reactive oxygen species: an Achilles' heel of melanoma? *Expert Rev Anticancer Ther*. 2008;8(11):1751-57.
169. Meierjohann S. Oxidative stress in melanocyte senescence and melanoma transformation. *Eur J Cell Biol*. 2014;93(1-2):36-41.
170. Anasagasti MJ, Martin JJ, Mendoza L, Obrador E, Estrela JM, McCuskey RS, Vidal-Vanaclocha F. Glutathione protects metastatic melanoma cells against oxidative stress in the murine hepatic microvasculature. *Hepatology*. 1998;27(5):1249-56.
171. Lodh M, Goswami B, Gupta N, Patra SK, Saxena A. Assessment of oxidative stress and inflammatory process in patients of multiple myeloma. *Indian J Clin Biochem*. 2012;27(4):410-3.
172. Hole PS, Darley RL, Tonks A. Do reactive oxygen species play a role in myeloid leukemias? *Blood*. 2011;117(22):5816-26.

173. Winter JL, Barber LG, Freeman L, Griessmayr PC, Milbury PE, Blumberg JB. Antioxidant Status and Biomarkers of Oxidative Stress in Dogs with Lymphoma. *J Vet Intern Med*. 2009;23(2):311-16.
174. Wilkinson ST, Tome ME, Briehl MM. Mitochondrial adaptations to oxidative stress confer resistance to apoptosis in lymphoma cells. *Int J Mol Sci*. 2012;13(8):10212-28.
175. Bahar G, Feinmesser R, Shpitzer T, Popovtzer A, Nagler RM. Salivary analysis in oral cancer patients: DNA and protein oxidation, reactive nitrogen species, and antioxidant profile. *Cancer*. 2007;109(1):54-9.
176. Chan DW, Liu VW, Tsao GS, Yao KM, Furukawa T, Chan KK, Ngan HY. Loss of MKP3 mediated by oxidative stress enhances tumorigenicity and chemoresistance of ovarian cancer cells. *Carcinogenesis*. 2008;29(9):1742-50.
177. Edderkaoui M, Hong P, Vaquero EC, Lee JK, Fischer L, Friess H, Buchler MW, Lerch MM, Pandol SJ, Gukovskaya AS. Extracellular matrix stimulates reactive oxygen species production and increases pancreatic cancer cell survival through 5-lipoxygenase and NADPH oxidase. *Am J Physiol Gastrointest Liver Physiol*. 2005;289(6):G1137-47.
178. Teoh ML, Sun W, Smith BJ, Oberley LW, Cullen JJ. Modulation of reactive oxygen species in pancreatic cancer. *Clin Cancer Res*. 2007;13(24):7441-50.
179. Freitas M, Baldeiras I, Proenca T, Alves V, Mota-Pinto A, Sarmento-Ribeiro A. Oxidative stress adaptation in aggressive prostate cancer may be counteracted by the reduction of glutathione reductase. *FEBS Open Bio*. 2012;2:119-28.
180. Khandrika L, Kumar B, Koul S, Maroni P, Koul HK. Oxidative stress in prostate cancer. *Cancer Lett*. 2009;282(2):125-36.
181. Ma Q, Cavallin LE, Yan B, Zhu S, Duran EM, Wang H, Hale LP, Dong C, Cesarman E, Mesri EA, Goldschmidt-Clermont PJ. Antitumorigenesis of antioxidants in a transgenic Rac1 model of Kaposi's sarcoma. *Proc Natl Acad Sci U S A*. 2009;106(21):8683-8.
182. Fuchs-Tarlovsky V. Role of antioxidants in cancer therapy. *Nutrition*. 2013;29(1):15-21.
183. Klaunig JE, Wang Z, Pu X, Zhou S. Oxidative stress and oxidative damage in chemical carcinogenesis. *Toxicol Appl Pharmacol*. 2011;254(2):86-99.
184. Foster I. Cancer: A cell cycle defect. *Radiography*. 2008;14(2):144-49.
185. Folkman J, Merler E, Abernathy C, Williams G. Isolation of a tumor factor responsible for angiogenesis. *J Exp Med*. 1971;133(2):275-88.
186. Folkman J. Tumor Angiogenesis: Therapeutic Implications. *N Engl J Med*. 1971;285(21):1182-86.
187. Valastyan S, Weinberg RA. Tumor metastasis: molecular insights and evolving paradigms. *Cell*. 2011;147(2):275-92.
188. Massagué J. TGFβ in Cancer. *Cell*. 2008;134(2):215-30.
189. Reddy RD, Yao JK. Free radical pathology in schizophrenia: a review. *Prostaglandins Leukot Essent Fatty Acids*. 1996;55(1-2):33-43.
190. Aggarwal BB, Shishodia S, Sandur SK, Pandey MK, Sethi G. Inflammation and cancer: how hot is the link? *Biochem Pharmacol*. 2006;72(11):1605-21.
191. Aggarwal BB, Gehlot P. Inflammation and cancer: how friendly is the relationship for cancer patients? *Curr Opin Pharmacol*. 2009;9(4):351-69.
192. Allavena P, Garlanda C, Borrello MG, Sica A, Mantovani A. Pathways connecting inflammation and cancer. *Curr Opin Genet Dev*. 2008;18(1):3-10.
193. Lesterhuis WJ, Haanen JB, Punt CJ. Cancer immunotherapy--revisited. *Nat Rev Drug Discov*. 2011;10(8):591-600.
194. Hanahan D, Weinberg RA. The hallmarks of cancer. *Cell*. 2000;100(1):57-70.
195. Hanahan D, Weinberg RA. Hallmarks of cancer: the next generation. *Cell*. 2011;144(5):646-74.
196. Cramer T, Yamanishi Y, Clausen BE, Forster I, Pawlinski R, Mackman N, Haase VH, Jaenisch R, Corr M, Nizet V, Firestein GS, Gerber HP, Ferrara N, Johnson RS. HIF-1alpha is essential for myeloid cell-mediated inflammation. *Cell*. 2003;112(5):645-57.
197. Nathan C. Immunology: Oxygen and the inflammatory cell. *Nature*. 2003;422(6933):675-6.
198. Sherr CJ. Principles of tumor suppression. *Cell*. 2004;116(2):235-46.
199. Block K, Gorin Y. Aiding and abetting roles of NOX oxidases in cellular transformation. *Nat Rev Cancer*. 2012;12(9):627-37.
200. Sherr CJ, McCormick F. The RB and p53 pathways in cancer. *Cancer Cell*. 2002;2(2):103-12.

201. Borrello MG, Degl'Innocenti D, Pierotti MA. Inflammation and cancer: the oncogene-driven connection. *Cancer Lett*. 2008;267(2):262-70.
202. Ding XZ, Flatt PR, Permert J, Adrian TE. Pancreatic cancer cells selectively stimulate islet beta cells to secrete amylin. *Gastroenterol*. 1998;114(1):130-38.
203. Biasutto L, Dong LF, Zoratti M, Neuzil J. Mitochondrially targeted anti-cancer agents. *Mitochondrion*. 2010;10(6):670-81.
204. O'Hayre M, Vazquez-Prado J, Kufareva I, Stawiski EW, Handel TM, Seshagiri S, Gutkind JS. The emerging mutational landscape of G proteins and G-protein-coupled receptors in cancer. *Nat Rev Cancer*. 2013;13(6):412-24.
205. Spiegel D. Minding the body: psychotherapy and cancer survival. *Br J Health Psychol*. 2014;19(3):465-85.
206. Firczuk M, Nowis D, Golab J. PDT-induced inflammatory and host responses. *Photochem Photobiol Sci*. 2011;10(5):653-63.
207. Stamati I, Kuimova MK, Lion M, Yahioglu G, Phillips D, Deonarain MP. Novel photosensitisers derived from pyropheophorbide-a: uptake by cells and photodynamic efficiency in vitro. *Photochem Photobiol Sci*. 2010;9(7):1033-41.
208. Green B, Cobb AR, Hopper C. Photodynamic therapy in the management of lesions of the head and neck. *Br J Oral Maxillofac Surg*. 2013;51(4):283-7.
209. Ferreira SD, Tedesco AC, Sousa G, Zangaro RA, Silva NS, Pacheco MT, Pacheco-Soares C. Analysis of mitochondria, endoplasmic reticulum and actin filaments after PDT with AlPcS(4). *Lasers Med Sci*. 2004;18(4):207-12.
210. Vollet-Filho JD, Menezes PFC, Moriyama LT, Grecco C, Sibata C, Allison RR, Castro e Silva O, Bagnato VS. Possibility for a full optical determination of photodynamic therapy outcome. *J Appl Phys*. 2009;105(10):102038.
211. Cottrell WJ, Paquette AD, Keymel KR, Foster TH, Oseroff AR. Irradiance-dependent photobleaching and pain in delta-aminolevulinic acid-photodynamic therapy of superficial basal cell carcinomas. *Clin Cancer Res*. 2008;14(14):4475-83.
212. Kuimova MK, Botchway SW, Parker AW, Balaz M, Collins HA, Anderson HL, Suhling K, Ogilby PR. Imaging intracellular viscosity of a single cell during photoinduced cell death. *Nat Chem*. 2009;1(1):69-73.
213. Andersson H, van den Berg A. Microfluidic devices for cellomics: a review. *Sens Actuators, B*. 2003;92(3):315-25.
214. Smith K, Malatesti N, Cauchon N, Hunting D, Lecomte R, van Lier JE, Greenman J, Boyle RW. Mono- and tri-cationic porphyrin-monoclonal antibody conjugates: photodynamic activity and mechanism of action. *Immunology*. 2011;132(2):256-65.
215. Giuntini F, Alonso CM, Boyle RW. Synthetic approaches for the conjugation of porphyrins and related macrocycles to peptides and proteins. *Photochem Photobiol Sci*. 2011;10(5):759-91.
216. Derycke AS, Kamuhabwa A, Gijsens A, Roskams T, De Vos D, Kasran A, Huwyler J, Missiaen L, de Witte PA. Transferrin-conjugated liposome targeting of photosensitizer AlPcS4 to rat bladder carcinoma cells. *J Natl Cancer Inst*. 2004;96(21):1620-30.
217. Westerman P, Glanzmann T, Andrejevic S, Braichotte DR, Forrer M, Wagnieres GA, Monnier P, van den Bergh H, Mach JP, Folli S. Long circulating half-life and high tumor selectivity of the photosensitizer meta-tetrahydroxyphenylchlorin conjugated to polyethylene glycol in nude mice grafted with a human colon carcinoma. *Int J Cancer*. 1998;76(6):842-50.
218. Vrouenraets MB, Visser GW, Stigter M, Oppelaar H, Snow GB, van Dongen GA. Comparison of aluminium (III) phthalocyanine tetrasulfonate- and meta-tetrahydroxyphenylchlorin-monoclonal antibody conjugates for their efficacy in photodynamic therapy in vitro. *Int J Cancer*. 2002;98(5):793-8.
219. van Dongen GA, Visser GW, Vrouenraets MB. Photosensitizer-antibody conjugates for detection and therapy of cancer. *Adv Drug Deliv Rev*. 2004;56(1):31-52.
220. Sitnik TM, Henderson BW. The effect of fluence rate on tumor and normal tissue responses to photodynamic therapy. *Photochem Photobiol*. 1998;67(4):462-6.
221. Henderson BW, Busch TM, Snyder JW. Fluence rate as a modulator of PDT mechanisms. *Lasers Surg Med*. 2006;38(5):489-93.
222. Jarvi MT, Patterson MS, Wilson BC. Insights into photodynamic therapy dosimetry: simultaneous singlet oxygen luminescence and photosensitizer photobleaching measurements. *Biophys J*. 2012;102(3):661-71.

223. Sitnik TM, Hampton JA, Henderson BW. Reduction of tumour oxygenation during and after photodynamic therapy in vivo: effects of fluence rate. *Br J Cancer*. 1998;77(9):1386-94.
224. Cottrell WJ, Paquette AD, Keymel KR, Foster TH, Oseroff AR. Irradiance-dependent photobleaching and pain in δ-aminolevulinic acid-photodynamic therapy of superficial basal cell carcinomas. *Clin Cancer Res*. 2008;14(14):4475-83.
225. Wang HW, Rickter E, Yuan M, Wileyto EP, Glatstein E, Yodh A, Busch TM. Effect of photosensitizer dose on fluence rate responses to photodynamic therapy. *Photochem Photobiol*. 2007;83(5):1040-8.
226. Muncaster R. *Advanced level Physics*. 4th ed. Cheltenham, UK: Nelson Thornes Ltd; 1993.
227. Moseley H. Light distribution and calibration of commercial PDT LED arrays. *Photochem Photobiol Sci*. 2005;4(11):911-4.
228. Brackett CM, Gollnick SO. Photodynamic therapy enhancement of anti-tumor immunity. *Photochem Photobiol Sci*. 2011;10(5):649-52.
229. Kammerer R, Palluch P, Oboukhovskij K, Toelge M, Pongratz T, Beyer W, Buchner A, Baumgartner R, Zimmermann W. The molecular basis of prostate cancer cell escape from protoporphyrin IX-based photodynamic therapy. *Med Laser Appl*. 2009;24(4):237-46.
230. Zeina B, Greenman J, Purcell WM, Das B. Killing of cutaneous microbial species by photodynamic therapy. *Br J Dermatol*. 2001;144(2):274-8.
231. Korbelik M, Dougherty GJ. Photodynamic therapy-mediated immune response against subcutaneous mouse tumors. *Cancer Res*. 1999;59(8):1941-6.
232. Mroz P, Szokalska A, Wu MX, Hamblin MR. Photodynamic therapy of tumors can lead to development of systemic antigen-specific immune response. *PLoS One*. 2010;5(12):e15194.
233. Kwitniewski M, Juzeniene A, Glosnicka R, Moan J. Immunotherapy: a way to improve the therapeutic outcome of photodynamic therapy? *Photochem Photobiol Sci*. 2008;7(9):1011-7.
234. Banchereau J, Steinman RM. Dendritic cells and the control of immunity. *Nature*. 1998;392(6673):245-52.
235. Steinman RM, Banchereau J. Taking dendritic cells into medicine. *Nature*. 2007;449(7161):419-26.
236. Krysko DV, Garg AD, Kaczmarek A, Krysko O, Agostinis P, Vandenabeele P. Immunogenic cell death and DAMPs in cancer therapy. *Nat Rev Cancer*. 2012;12(12):860-75.
237. Gollnick SO, Owczarczak B, Maier P. Photodynamic therapy and anti-tumor immunity. *Lasers Surg Med*. 2006;38(5):509-15.
238. Castano AP, Liu Q, Hamblin MR. A green fluorescent protein-expressing murine tumour but not its wild-type counterpart is cured by photodynamic therapy. *Br J Cancer*. 2006;94(3):391-7.
239. Fleming M, Ravula S, Tatishchev SF, Wang HL. Colorectal carcinoma: Pathologic aspects. *J Gastrointest Oncol*. 2012;3(3):153-73.
240. Quinn LA, Moore GE, Morgan RT, Woods LK. Cell lines from human colon carcinoma with unusual cell products, double minutes, and homogeneously staining regions. *Cancer Res*. 1979;39(12):4914-24.
241. Collins JF, Herman P, Schuch C, Bagby GC, Jr. c-myc antisense oligonucleotides inhibit the colony-forming capacity of Colo 320 colonic carcinoma cells. *J Clin Invest*. 1992;89(5):1523-7.
242. Boersma HH, Kietselaer BL, Stolk LM, Bennaghmouch A, Hofstra L, Narula J, Heidendal GA, Reutelingsperger CP. Past, present, and future of annexin A5: from protein discovery to clinical applications. *J Nucl Med*. 2005;46(12):2035-50.
243. Christie WW. *Phosphatidylserine* [online]. AOCS Lipid Library; 2013 [December 21 2013]. Available from: http://lipidlibrary.aocs.org/Primer/content.cfm?ItemNumber=39360.
244. Vance JE. Phosphatidylserine and phosphatidylethanolamine in mammalian cells: two metabolically related aminophospholipids. *J Lipid Res*. 2008;49(7):1377-87.
245. Verhoven B, Schlegel RA, Williamson P. Mechanisms of phosphatidylserine exposure, a phagocyte recognition signal, on apoptotic T lymphocytes. *J Exp Med*. 1995;182(5):1597-601.

246. Tyurina YY, Shvedova AA, Kawai K, Tyurin VA, Kommineni C, Quinn PJ, Schor NF, Fabisiak JP, Kagan VE. Phospholipid signaling in apoptosis: peroxidation and externalization of phosphatidylserine. *Toxicology*. 2000;148(2-3):93-101.
247. Kay JG, Grinstein S. Sensing phosphatidylserine in cellular membranes. *Sensors (Basel)*. 2011;11(2):1744-55.
248. Bigl M, Bruckner MK, Arendt T, Bigl V, Eschrich K. Activities of key glycolytic enzymes in the brains of patients with Alzheimer's disease. *J Neural Transm*. 1999;106(5-6):499-511.
249. Starkweather WH, Cousineau L, Schoch HK, Zarafonetis CJ. Alterations of Erythrocyte Lactate Dehydrogenase in Man. *Blood*. 1965;26(1):63-73.
250. Lossos IS. Differential Diagnosis of Pleural Effusion by Lactate Dehydrogenase Isoenzyme Analysis. *CHEST*. 1997;111(3):648.
251. Lubrano T, Dietz AA, Rubinstein HM. Extra lactate dehydrogenase isoenzyme band in serum of patients with severe liver disease. *Clin Chem*. 1971;17(9):882-5.
252. Bishop MJ, Everse J, Kaplan NO. Identification of Lactate Dehydrogenase Isoenzymes by Rapid Kinetics. *Proc Natl Acad Sci U S A*. 1972;69(7):1761-65.
253. Emerson PM, Wilkinson JH. Urea and oxalate inhibition of the serum lactate dehydrogenase. *J Clin Pathol*. 1965;18(6):803-07.
254. Shaw CR, Barto E. Genetic evidence for the subunit structure of lactate dehydrogenase isozymes. *Proc Natl Acad Sci U S A*. 1963;50(2):211-14.
255. Bacci G, Longhi A, Ferrari S, Briccoli A, Donati D, De Paolis M, Versari M. Prognostic significance of serum lactate dehydrogenase in osteosarcoma of the extremity: experience at Rizzoli on 1421 patients treated over the last 30 years. *Tumori*. 2004;90(5):478-84.
256. Arditi M, Zhou J, Dorio R, Rong GW, Goyert SM, Kim KS. Endotoxin-mediated endothelial cell injury and activation: role of soluble CD14. *Infect Immun*. 1993;61(8):3149-56.
257. Madara JL, Stafford J. Interferon-gamma directly affects barrier function of cultured intestinal epithelial monolayers. *J Clin Invest*. 1989;83(2):724-27.
258. Loo DT, Copani A, Pike CJ, Whittemore ER, Walencewicz AJ, Cotman CW. Apoptosis is induced by beta-amyloid in cultured central nervous system neurons. *Proc Natl Acad Sci U S A*. 1993;90(17):7951-55.
259. Johnston RB, Lehmeyer JE. Elaboration of toxic oxygen by-products by neutrophils in a model of immune complex disease. *J Clin Invest*. 1976;57(4):836-41.
260. Martin KR, Failla ML, Smith JC, Jr. Beta-carotene and lutein protect HepG2 human liver cells against oxidant-induced damage. *J Nutr*. 1996;126(9):2098-106.
261. Jähnisch K, Dingerdissen U. Photochemical Generation and [4+2]-Cycloaddition of Singlet Oxygen in a Falling-Film Micro Reactor. *Chem Eng Technol*. 2005;28(4):426-27.
262. Wlodkowic D, Cooper JM. Tumors on chips: oncology meets microfluidics. *Curr Opin Chem Biol*. 2010;14(5):556-67.
263. Wang N, Lei L, Zhang XM, Tsang YH, Chen Y, Chan HLW. A comparative study of preparation methods of nanoporous TiO2 films for microfluidic photocatalysis. *Microelectronic Engineering*. 2011;88(8):2797-99.
264. Tucker JW, Zhang Y, Jamison TF, Stephenson CR. Visible-light photoredox catalysis in flow. *Angew Chem Int Ed Engl*. 2012;51(17):4144-7.
265. Oelgemoller M, Shvydkiv O. Recent advances in microflow photochemistry. *Molecules*. 2011;16(9):7522-50.
266. Meyer S, Tietze D, Rau S, Schäfer B, Kreisel G. Photosensitized oxidation of citronellol in microreactors. *J Photochem Photobiol, A*. 2007;186(2-3):248-53.
267. Gorges R, Meyer S, Kreisel G. Photocatalysis in microreactors. *J Photochem Photobiol, A*. 2004;167(2-3):95-99.
268. Vesborg PCK, Olsen JL, Henriksen TR, Chorkendorff I, Hansen O. Gas-phase photocatalysis in µ-reactors. *Chem Eng J*. 2010;160(2):738-41.
269. Knowles JP, Elliott LD, Booker-Milburn KI. Flow photochemistry: Old light through new windows. *Beilstein J Org Chem*. 2012;8:2025-52.
270. Wootton RCR, Fortt R, de Mello AJ. A Microfabricated Nanoreactor for Safe, Continuous Generation and Use of Singlet Oxygen. *Org Process Res Dev*. 2002;6(2):187-89.
271. Lévesque F, Seeberger PH. Highly Efficient Continuous Flow Reactions Using Singlet Oxygen as a "Green" Reagent. *Org Lett*. 2011;13(19):5008-11.

272. Dugan CE, Cawthorn WP, MacDougald OA, Kennedy RT. Multiplexed microfluidic enzyme assays for simultaneous detection of lipolysis products from adipocytes. *Anal Bioanal Chem*. 2014;406(20):4851-9.
273. Barteneva NS, Ketman K, Fasler-Kan E, Potashnikova D, Vorobjev IA. Cell sorting in cancer research--diminishing degree of cell heterogeneity. *Biochim Biophys Acta*. 2013;1836(1):105-22.
274. Kotz KT, Xiao W, Miller-Graziano C, Qian WJ, Russom A, Warner EA, Moldawer LL, De A, Bankey PE, Petritis BO, Camp DG, 2nd, Rosenbach AE, Goverman J, Fagan SP, Brownstein BH, Irimia D, Xu W, Wilhelmy J, Mindrinos MN, Smith RD, Davis RW, Tompkins RG, Toner M, Inflammation, the Host Response to Injury Collaborative Research P. Clinical microfluidics for neutrophil genomics and proteomics. *Nat Med*. 2010;16(9):1042-7.
275. Lee J, Soper SA, Murray KK. Microfluidics with MALDI analysis for proteomics--a review. *Anal Chim Acta*. 2009;649(2):180-90.
276. Wheeler AR, Moon H, Bird CA, Loo RR, Kim CJ, Loo JA, Garrell RL. Digital microfluidics with in-line sample purification for proteomics analyses with MALDI-MS. *Anal Chem*. 2005;77(2):534-40.
277. Lion N, Rohner TC, Dayon L, Arnaud IL, Damoc E, Youhnovski N, Wu ZY, Roussel C, Josserand J, Jensen H, Rossier JS, Przybylski M, Girault HH. Microfluidic systems in proteomics. *Electrophoresis*. 2003;24(21):3533-62.
278. Sorribas H, Padeste C, Tiefenauer L. Photolithographic generation of protein micropatterns for neuron culture applications. *Biomaterials*. 2002;23(3):893-900.
279. Gross PG, Kartalov EP, Scherer A, Weiner LP. Applications of microfluidics for neuronal studies. *J Neurol Sci*. 2007;252(2):135-43.
280. Sylvester DC, Hattersley SM, Haswell SJ, Stafford ND, Greenman J. Development of microfluidic based devices for studying tumour biology and evaluating treatment response in head and neck cancer biopsies. *14th International Conference on Miniaturized Systems for Chemistry and Life Sciences*; 3 - 7 October 2010; Groningen, The Netherlands2010. p. 1472-74.
281. Sylvester D, Hattersley SM, Stafford ND, Haswell SJ, Greenman J. Development of Microfluidic-based Analytical Methodology for Studying the Effects of Chemotherapy Agents on Cancer Tissue. *Curr Anal Chem*. 2013;9(1):2-8.
282. Chou H-P, Spence C, Scherer A, Quake S. A microfabricated device for sizing and sorting DNA molecules. *Proc Natl Acad Sci*. 1999;96(1):11-13.
283. Abate AR, Hung T, Sperling RA, Mary P, Rotem A, Agresti JJ, Weiner MA, Weitz DA. DNA sequence analysis with droplet-based microfluidics. *Lab Chip*. 2013;13(24):4864-9.
284. Erickson D, Li D. Integrated microfluidic devices. *Anal Chim Acta*. 2004;507(1):11-26.
285. Harris LF, Rainey P, Castro-Lopez V, O'Donnell JS, Killard AJ. A microfluidic anti-Factor Xa assay device for point of care monitoring of anticoagulation therapy. *Analyst*. 2013;138(17):4769-76.
286. Craw P, Balachandran W. Isothermal nucleic acid amplification technologies for point-of-care diagnostics: a critical review. *Lab Chip*. 2012;12(14):2469-86.
287. Bissonnette L, Bergeron MG. Diagnosing infections--current and anticipated technologies for point-of-care diagnostics and home-based testing. *Clin Microbiol Infect*. 2010;16(8):1044-53.
288. Fiorini GS, Chiu DT. Disposable microfluidic devices: fabrication, function, and application. *Biotechniques*. 2005;38(3):429-46.
289. Barnes JM, Nauseef JT, Henry MD. Resistance to fluid shear stress is a conserved biophysical property of malignant cells. *PLoS One*. 2012;7(12):e50973.
290. Sud D, Mehta G, Mehta K, Linderman J, Takayama S, Mycek MA. Optical imaging in microfluidic bioreactors enables oxygen monitoring for continuous cell culture. *J Biomed Opt*. 2006;11(5):050504.
291. Wilding P, Kricka LJ, Cheng J, Hvichia G, Shoffner MA, Fortina P. Integrated cell isolation and polymerase chain reaction analysis using silicon microfilter chambers. *Anal Biochem*. 1998;257(2):95-100.
292. Rusconi R, Garren M, Stocker R. Microfluidics expanding the frontiers of microbial ecology. *Annu Rev Biophys*. 2014;43:65-91.

293. Bridle H, Miller B, Desmulliez MP. Application of microfluidics in waterborne pathogen monitoring: a review. *Water Res*. 2014;55:256-71.
294. Huh D, Hamilton GA, Ingber DE. From 3D cell culture to organs-on-chips. *Trends Cell Biol*. 2011;21(12):745-54.
295. Jedrych E, Chudy M, Dybko A, Brzozka Z. The microfluidic system for studies of carcinoma and normal cells interactions after photodynamic therapy (PDT) procedures. *Biomicrofluidics*. 2011;5(4):41101-411016.
296. Lou X, Kim G, Lee YK, Kopelman R, Yoon E. Investigating photodynamic efficiency of tumour targetted nanoparticluar photosensitizer using microfluidic chips. *15th International Conference on Miniaturized Systems for Chemistry and Life Sciences* October 2-6, 2011; Seattle, Washington, USA 2011. p. 2058-60.
297. White FM. *Fluid Mechanics*. 4th ed. Holman JP, Lloyd J, editors. Boston: McGraw-Hill Higher Education; 1998.
298. Kestin J, Sokolov M, Wakeham WA. Viscosity of liquid water in the range -8 ºC to 150 ºC. *J Phy Chem Ref Data*. 1978;7(3):941-48.
299. Hinderliter PM, Minard KR, Orr G, Chrisler WB, Thrall BD, Pounds JG, Teeguarden JG. ISDD: A computational model of particle sedimentation, diffusion and target cell dosimetry for in vitro toxicity studies. *Part Fibre Toxicol*. 2010;7(1):36.
300. Wootton RC, deMello AJ. A one-step protocol for the chemical derivatisation of glass microfluidic devices. *Lab Chip*. 2006;6(4):471-3.
301. Kim D, Herr AE. Protein immobilization techniques for microfluidic assays. *Biomicrofluidics*. 2013;7(4):41501.
302. Prakash S, Long TM, Selby JC, Moore JS, Shannon MA. "Click" Modification of Silica Surfaces and Glass Microfluidic Channels. *Anal Chem*. 2007;79(4):1661-67.
303. Müller RH, Clegg DL. Automatic Paper Chromatography. *Anal Chem*. 1949;21(9):1123-25.
304. Reyes DR, Iossifidis D, Auroux PA, Manz A. Micro total analysis systems. 1. Introduction, theory, and technology. *Anal Chem*. 2002;74(12):2623-36.
305. van Laar FMPR, Holsteyns F, Vankelecom IFJ, Smeets S, Dehaen W, Jacobs PA. Singlet oxygen generation using PDMS occluded dyes. *J Photochem Photobiol, A*. 2001;144(2–3):141-51.
306. Xia Y, Whitesides GM. Soft lithography. *Annu Rev Mater Sci*. 1998;28(1):153-84.
307. Gomez FA. *Biological Applications of Microfluidics*. Hoboken, New Jersey and Canada: John Wiley & Sons, Inc.; 2008.
308. Pallandre A, de Lambert B, Attia R, Jonas AM, Viovy JL. Surface treatment and characterization: perspectives to electrophoresis and lab-on-chips. *Electrophoresis*. 2006;27(3):584-610.
309. Costantini F, Tiggelaar R, Sennato S, Mura F, Schlautmann S, Bordi F, Gardeniers H, Manetti C. Glucose level determination with a multi-enzymatic cascade reaction in a functionalized glass chip. *Analyst*. 2013;138(17):5019-24.
310. Mahadevan TS, Garofalini SH. Dissociative Chemisorption of Water onto Silica Surfaces and Formation of Hydronium Ions. *J Phys Chem C*. 2008;112(5):1507-15.
311. Arkles B. *Techniques for Silylation* [online]. United Chemical Technologies, Inc.; [August 20 2014]. Available from: https://www.unitedchem.com/sites/default/files/posters-and-papers/SPEC-Techniques%20for%20Silylation.pdf.
312. Haensch C, Hoeppener S, Schubert US. Chemical modification of self-assembled silane based monolayers by surface reactions. *Chem Soc Rev*. 2010;39(6):2323-34.
313. Glass NR, Tjeung R, Chan P, Yeo LY, Friend JR. Organosilane deposition for microfluidic applications. *Biomicrofluidics*. 2011;5(3):36501-365017.
314. Hoffmann H, Mayer U, Brunner H, Krischanitz A. Reflection-absorption infrared spectroscopy of self-assembled monolayers on gold and silicon surfaces. *Vib Spectrosc*. 1995;8(2):151-57.
315. Netzer L, Sagiv J. A new approach to construction of artificial monolayer assemblies. *J Am Chem Soc*. 1983;105(3):674-76.
316. Sharma M, Dube A, Engstrom JR. Growth of first generation dendrons on SiO_2: controlling chemisorption of transition metal coordination complexes. *J Am Chem Soc*. 2007;129(48):15022-33.
317. Zhang F, Srinivasan MP. Self-Assembled Molecular Films of Aminosilanes and Their Immobilization Capacities. *Langmuir*. 2004;20(6):2309-14.

318. Vandenberg ET, Bertilsson L, Liedberg B, Uvdal K, Erlandsson R, Elwing H, Lundström I. Structure of 3-aminopropyl triethoxy silane on silicon oxide. *J Colloid Interface Sci*. 1991;147(1):103-18.
319. Razumovitch J, Meier W, Vebert C. A microcontact printing approach to the immobilization of oligonucleotide brushes. *Biophys Chem*. 2009;139(1):70-4.
320. Pereira C, Patricio S, Silva AR, Magalhaes AL, Carvalho AP, Pires J, Freire C. Copper acetylacetonate anchored onto amine-functionalised clays. *J Colloid Interface Sci*. 2007;316(2):570-9.
321. Howarter JA, Youngblood JP. Surface Modification of Polymers with 3-Aminopropyltriethoxysilane as a General Pretreatment for Controlled Wettability. *Macromolecules*. 2007;40(4):1128-32.
322. Caravajal GS, Leyden DE, Quinting GR, Maciel GE. Structural characterization of (3-aminopropyl)triethoxysilane-modified silicas by silicon-29 and carbon-13 nuclear magnetic resonance. *Anal Chem*. 1988;60(17):1776-86.
323. White LD, Tripp CP. Reaction of (3-Aminopropyl)dimethylethoxysilane with Amine Catalysts on Silica Surfaces. *J Colloid Interface Sci*. 2000;232(2):400-07.
324. Kim J, Seidler P, Wan LS, Fill C. Formation, structure, and reactivity of amino-terminated organic films on silicon substrates. *J Colloid Interface Sci*. 2009;329(1):114-9.
325. Waddell TG, Leyden DE, DeBello MT. The nature of organosilane to silica-surface bonding. *J Am Chem Soc*. 1981;103(18):5303-07.
326. Ribeiro SM, Serra AC, Rocha Gonsalves AMdA. Covalently immobilized porphyrins as photooxidation catalysts. *Tetrahedron*. 2007;63(33):7885-91.
327. Ribeiro S, Serra A, Rocha Gonsalves AMdA. Immobilised porphyrins in monoterpene photooxidations. *J Catal*. 2008;256(2):331-37.
328. Kitamura N, Yamada K, Ueno K, Iwata S. Photodecomposition of phenol by silica-supported porphyrin derivative in polymer microchannel chips. *J Photochem Photobiol, A*. 2006;184(1-2):170-76.
329. Ribeiro SM, Serra AC, Rocha Gonsalves AMdA. Covalently immobilized porphyrins on silica modified structures as photooxidation catalysts. *J Mol Catal A: Chem*. 2010;326(1-2):121-27.
330. Savenije TJ, Marée CHM, Habraken FHPM, Koehorst RBM, Schaafsma TJ. Deposition of watersoluble porphyrins on solid substrates. *Thin Solid Films*. 1995;265(1–2):84-88.
331. Giaimuccio J, Zamadar M, Aebisher D, Meyer GJ, Greer A. Singlet oxygen chemistry in water. 2. Photoexcited sensitizer quenching by O_2 at the water-porous glass interface. *J Phys Chem B*. 2008;112(49):15646-50.
332. Aebisher D, Azar NS, Zamadar M, Gandra N, Gafney HD, Gao R, Greer A. Singlet Oxygen Chemistry in Water: A Porous Vycor GlassSupported Photosensitizer. *J Phys Chem B*. 2008;112(7):1913-17.
333. Da Cruz F, Driaf K, Berthier C, Lameille JM, Armand F. Study of a self-assembled porphyrin monomolecular layer obtained by metal complexation. *Thin Solid Films*. 1999;349(1–2):155-61.
334. Zhang X, Gao M, Kong X, Sun Y, Shen J. Build-up of a new type of ultrathin film of porphyrin and phthalocyanine based on cationic and anionic electrostatic attraction. *J Chem Soc, Chem Commun*. 1994(9):1055.
335. Gryglik D, Miller JS, Ledakowicz S. Solar energy utilization in degradation of 2-chlorophenol by immobilized photosensitizers. *Sol Energy*. 2004;77(5):615-23.
336. Schaap AP, Thayer AL, Blossey EC, Neckers DC. Polymer-based sensitizers for photooxidations. II. *J Am Chem Soc*. 1975;97(13):3741-45.
337. Tamagaki S, Liesner CE, Neckers DC. Polymer-based sensitizers for photochemical reactions. Silica gel as a support. *J Org Chem*. 1980;45(9):1573-76.
338. Janssen D, De Palma R, Verlaak S, Heremans P, Dehaen W. Static solvent contact angle measurements, surface free energy and wettability determination of various self-assembled monolayers on silicon dioxide. *Thin Solid Films*. 2006;515(4):1433-38.
339. Krishnan A, Liu YH, Cha P, Woodward R, Allara D, Vogler EA, Hematology at Biomaterial Interfaces Research G. An evaluation of methods for contact angle measurement. *Colloids Surf B Biointerfaces*. 2005;43(2):95-8.
340. Sridharan A, Muthuswamy J, Labelle JT, Pizziconi VB. Immobilization of functional light antenna structures derived from the filamentous green bacterium Chloroflexus aurantiacus. *Langmuir*. 2008;24(15):8078-89.

341. Grass RN, Athanassiou EK, Stark WJ. Covalently functionalized cobalt nanoparticles as a platform for magnetic separations in organic synthesis. *Angew Chem Int Ed Engl*. 2007;46(26):4909-12.
342. Tassa C, Shaw SY, Weissleder R. Dextran-coated iron oxide nanoparticles: a versatile platform for targeted molecular imaging, molecular diagnostics, and therapy. *Acc Chem Res*. 2011;44(10):842-52.
343. Schätz A, Grass RN, Kainz Q, Stark WJ, Reiser O. Cu(II)−Azabis(oxazoline) Complexes Immobilized on Magnetic Co/C Nanoparticles: Kinetic Resolution of 1,2-Diphenylethane-1,2-diol under Batch and Continuous-Flow Conditions. *Chem Mater*. 2010;22(2):305-10.
344. Sutton JM, Clarke OJ, Fernandez N, Boyle RW. Porphyrin, chlorin, and bacteriochlorin isothiocyanates: useful reagents for the synthesis of photoactive bioconjugates. *Bioconjug Chem*. 2002;13(2):249-63.
345. Tarn MD. *Continuous flow process on single magnetic and diamagnetic particles in microfluidic devices* [PhD thesis]: The University of Hull; 2011.
346. Lumley EK. *Development of a microfluidic device for the in situ production of singlet oxygen for chemical and biological applications* [PhD thesis]: The University of Hull; 2012.
347. Strober W. Trypan blue exclusion test of cell viability. *Curr Protoc Immunol*. 2001;Appendix 3:Appendix 3B.
348. *Cytotoxicity detection KitPLUS (LDH)* [online]. Roche Applied Science; 2005 [August 30 2013]. Available from: https://pim-eservices.roche.com/LifeScience/Document/d5f8384f-92ed-e311-98a1-00215a9b0ba8.
349. Kolb HC, Finn MG, Sharpless KB. Click Chemistry: Diverse Chemical Function from a Few Good Reactions. *Angew Chem Int Ed Engl*. 2001;40(11):2004-21.
350. Choi S-H, Zhang Newby B-m. Suppress polystyrene thin film dewetting by modifying substrate surface with aminopropyltriethoxysilane. *Surf Sci*. 2006;600(6):1391-404.
351. Wang W, Vaughn MW. Morphology and amine accessibility of (3-aminopropyl) triethoxysilane films on glass surfaces. *Scanning*. 2008;30(2):65-77.
352. Rosenkranz AA, Jans DA, Sobolev AS. Targeted intracellular delivery of photosensitizers to enhance photodynamic efficiency. *Immunol Cell Biol*. 2000;78(4):452-64.
353. Vermes I, Haanen C, Steffens-Nakken H, Reutelingsperger C. A novel assay for apoptosis. Flow cytometric detection of phosphatidylserine expression on early apoptotic cells using fluorescein labelled Annexin V. *J Immunol Methods*. 1995;184(1):39-51.
354. Chaurio RA, Janko C, Munoz LE, Frey B, Herrmann M, Gaipl US. Phospholipids: key players in apoptosis and immune regulation. *Molecules*. 2009;14(12):4892-914.
355. Callahan MK, Williamson P, Schlegel RA. Surface expression of phosphatidylserine on macrophages is required for phagocytosis of apoptotic thymocytes. *Cell Death Differ*. 2000;7(7):645-53.
356. Brouckaert G, Kalai M, Krysko DV, Saelens X, Vercammen D, Ndlovu M, Haegeman G, D'Herde K, Vandenabeele P. Phagocytosis of Necrotic Cells by Macrophages Is Phosphatidylserine Dependent and Does Not Induce Inflammatory Cytokine Production. *Mol Biol Cell*. 2004;15(3):1089-100.
357. Daleke DL. Phospholipid flippases. *J Biol Chem*. 2007;282(2):821-5.
358. *Glutathione in Cell Culture* [online]. Sigma-Aldrich; 2015 [September 13 2015]. Available from: http://www.sigmaaldrich.com/life-science/cell-culture/learning-center/media-expert/glutathione.html#Primary_Functions.
359. *Turbobeads* [online]. TurboBeads®; 2013 [July 09 2013]. Available from: http://www.turbobeads.com/.